SISSA
Scuola Internazionale Superiore di Studi Avanzati

**Neuroscience Area – PhD course in Neurobiology**

# Exosomes: unconventional players in spinal cord neuroinflammation

Candidate:
**Christian Memo**

Supervisors:
**Prof. Laura Ballerini**
**Prof. Loredana Casalis**

Academic Year: 2021/2022

# Table of contents

## Abstract

Neuroinflammation is a common underlying event in all central nervous system diseases, essentially based on altered communication patterns between resident cells (neurons and glia), which finally leads to detrimental functional alteration and potentially irreversible cell damage. Extracellular vesicles (EVs) are a recently discovered intercellular delivery system secreted by cells for specific intercellular communication. They are composed by a lipid bilayer containing a wide range of molecular signals like cytokines, microRNA, receptors and enzymes able to modify the phenotype of the recipient cells, integrating coordinated physiological response to environmental stimuli. Given their pivotal role in conveying key regulatory molecules, EVs are now intensively studied as novel fundamental players in many pathological processes, including neuroinflammation. Here, we studied the dysfunctional glial cells behaviour induced by EVs in the context of spinal cord neuroinflammation. Particularly, we focused on dissecting the role of exosomes, the smaller class of EVs originated by the endolysosomal secretory pathway, in promoting a proinflammatory phenotype in astrocytes and microglia, in organotypic spinal cord slices. We first realized an efficient protocol to isolate small extracellular vesicle (sEVs), primarily constituted by exosomes, to our knowledge for the first time, from spinal slices after LPS-induced neuroinflammation. We then used such vesicles (from here on referred to as exosomes or EXO) isolated from the inflammatory microenvironment to treat naïve slices and characterize their impact on healthy spinal tissue. Our results showed that upon inflammatory stimulation with LPS, EXOs secretion significantly increase compared to control condition. Interestingly, EXOs isolated from LPS treated slices were able to induce microglia activation and proliferation comparably to LPS. Furthermore, live calcium imaging recordings using GCaMP6f expressed only in GFAP+ cells showed that inflammatory EXOs can disrupt astrocytic physiological calcium dynamics increasing the frequency of $Ca^{2+}$ events. In order to obtain novel mechanistic cues about the ability of inflammatory EXOs in modulating glial calcium dynamics we focused on connexin 43 (Cx43) hemichannels. Cx43 is the main component of astrocytic gap junctions and uncoupled hemichannels, key macromolecular structures in the regulation of intra- and intercellular $Ca^{2+}$ signalling. Interestingly, inflammatory EXOs treatment was able to promote Cx43 hemichannel opening in GFAP+ cells, as revealed by Lucifer Yellow (LY) permeability assay. Our previous experiments showed that gap27, a Cx43 inhibitor peptide, was able to restore physiological calcium signals in spinal slices challenged with diverse danger stimuli, including LPS. Interestingly, inflammatory EXOs preincubated with gap27, didn't affect astrocytic calcium dynamics suggesting a pivotal role for exosomal Cx43 hemichannels in transfer danger signals to the recipient cells. All these evidences suggest that exosomes play an active role in mediating and spreading neuroinflammatory events, modulating glial cells reactivity through a Cx43-mediated mechanism.

# -1-
# Neuroinflammation: an overview

Mammalian central nervous system (CNS) is characterized by a high level of structural and functional organization that allows the fine control of voluntary tasks and homeostatic functions essentials for adaptating to a dynamic environment. In this framework, the development of efficient strategies to ensure neural tissue protection against noxious stimuli has been a biological imperative through animal evolution.

Neuroinflammation can be defined as the response of CNS reactive cellular and molecular components (i.e. neurons and glial cells) to an alteration of the homeostatic state due to endogenous or exogenous noxious stimuli [Kölliker-Frers et al., 2021]. This concept has evolved during the last decades: once thought to be an immune-privileged district of the body, intrinsically incapable of an efficient immune response, it's now clear that, the CNS is constantly involved in an extensive interplay with the immune system to ensure a good degree of protection. In addition, CNS inflammatory processes are a common pathological hallmark in many neurological diseases ranging from infection, to trauma, neurodegeneration and even psychiatric diseases [Najjar et al., 2013; Kölliker-Frers et al., 2021].

## 1.1. CNS: between immune privilege and immune competence

Inflammation is an evolutionary conserved phenomenon across both invertebrates and vertebrates. It has an essential role in maintaining tissues homeostasis in response to diverse physiological processes (like cell turnover) and pathological damages [Ashley et al., 2012]. The basic event in all inflammatory reactions is the activation of the immune system to remove the triggering stimulus while promoting the healing of the damaged tissue [Carson et al., 2006]. However, immune cells activation in itself often involves cellular and molecular pathways that can lead to tissue damage. For example, the production of reactive oxygen and nitrogen species (ROS and RNS respectively), essential for microbes killing, is associated to structural damages to cell membranes, proteins and nucleic acids [Abe et al., 2020], while the secretion of proinflammatory cytokines and chemokines can promotes apoptotic cascades in recipient cells [Ferro et al., 2021]. Thus, given the post-mitotic nature of neurons, which leads to poor recovery outcomes after brain and spinal cord damage, the CNS results particularly vulnerable to inflammatory responses [Carson et al., 2006] giving rise to the notion that it had to be a "privileged" system form an immunological point of view.

Historically, early experimental observations made in the mid 20$^{th}$ century highlighted the fact that heterologous tissue grafts transplanted on mammal brain parenchyma resist to rejection much longer than those transplanted on peripheral tissues [Shiray Y., 1921]. Furthermore, it was noted that co-

transplantation with autologous spleen tissue, transplantation close to the brain ventricles [Murphy J. B. et al., 1923] and prior immune priming by peripheral transplantation [Medawar P. B., 1948] favoured the rejection of the graft from the brain parenchyma, suggesting that a strong immune response could be obtained only when the interaction with peripheral immune cells was facilitated. All these observations led the immunologist and neuroscientist P. B. Medawar to coin the concept of "immune-privilege", which define all the body's districts (e.g. the eye, the placenta and the CNS) in which the immune inflammatory response is tightly regulated.
This theoretical construct was originally based on the following three assumptions [Louveau A. et al, 2015]:

- The CNS is structurally separated from the periphery by the blood-brain barrier (BBB) which interfere with immune surveillance
- The CNS lacks resident efficient professional antigen presenting cells (APCs) like dendritic cells and it's characterized by a low major histocompatibility complex (MHC) expression profile
- The CNS lacks a diffuse lymphatic system that allows an immune cells trafficking and antigen drainage to the lymph nodes

This radical view of immune-privilege as "immune-isolation", biologically justified as a mechanism to protect the CNS from inflammatory reaction's collateral damages, has been recently challenged and refined by experimental and clinical observation [Engelhardt B. et al., 2017] that can be resumed as follow:

- In physiological condition the BBB restricts leukocyte migration thanks to various mechanism including [Shechter et al., 2013]:

  - the production of sonic hedgehog protein and the endothelial expression of its receptor that suppresses T cell migration and production of pro-inflammatory mediators
  - the endothelial expression of interleukin-25 (IL-25) that prevents the BBB collapse due to proinflammatory cytokines and increases the expression of tight junction proteins
  - the lack of selectin ligands that prevents T cell adhesion and diapedesis

  However, this barrier function is not absolute and can be modulated (and even disrupted) during systemic and CNS inflammation allowing peripheral immune cells infiltration (see Fig. 1). This highly regulated modulation of the barrier function consists in various mechanisms stimulated by

circulating proinflammatory cytokines that facilitates the adhesion, rolling and diapedesis of immune cells [Galea I., 2021]:

- the degradation of the endothelial glycocalyx which expose the surface adhesion molecules
- the endothelial upregulation of E/P-selectins which mediates rolling
- chemokines such as CCL2 and integrin ligands such as ICAM-1 which mediates adhesion

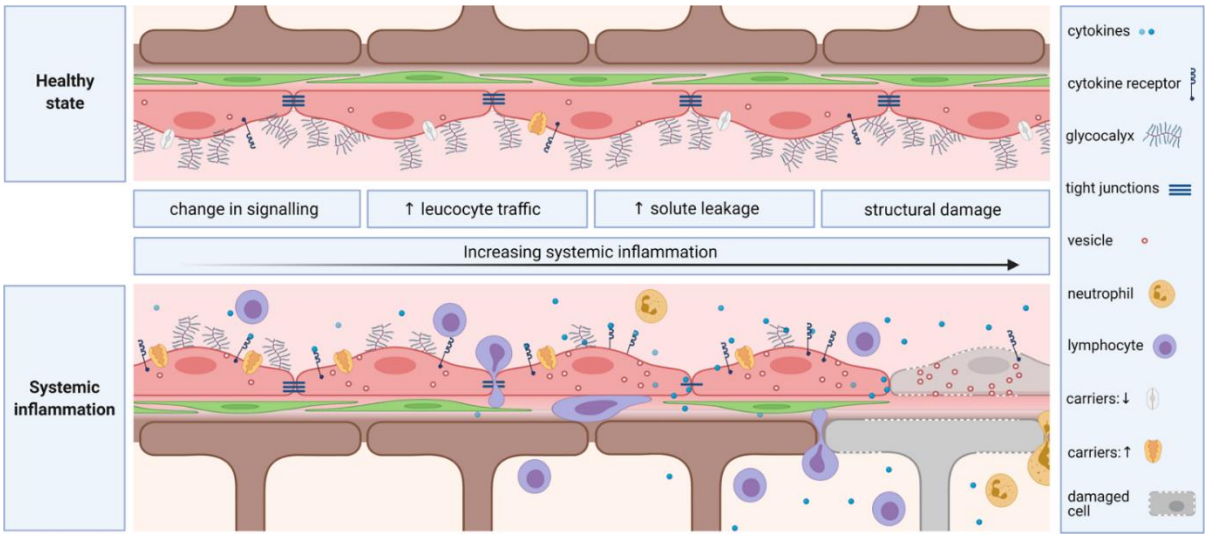


**Fig 1. Permeability modulation and disruption of the BBB during inflammation (brown: astrocytic endfeet, green: pericytes, light red: endothelial cells) [Galea I., 2021]**

- The precise cell phenotyping of the subarachnoid space, of the Virchow-Robin perivascular space and of the cerebral ventricles, showed that the cerebrospinal fluid (which lays at the CNS-periphery interfaces) is enriched in immunocompetent cells like perivascular macrophages, dendritic cells, epiplexus Kolmer cells (residing in the choroid plexus), innate lymphoid cells, T cells, monocytes, and granulocytes (i.e., neutrophils, eosinophils and mast cells) [Mundt S. et al., 2019] with various functions including the sampling of the macromolecules and antigens that exit the brain parenchyma via perivascular efflux into the CSF [Louveau et al., 2018]
- Two seminal studies published in 2015 demonstrated the presence of lymphatic vessels in the mouse dura mater venous sinuses [Aspelund et al., 2015; Louveau et al., 2015]. These vessels are directly connected with the deep cervical lymph nodes and adsorb the cerebrospinal fluid from the subarachnoid space and the brain interstitial fluid from the perivascular glymphatic network allowing an efficient drainage of antigens and other molecules from the brain parenchyma [Aspelund et al., 2015]. Furthermore, these discoveries provided new anatomical foundations for the study of lymphocytic CNS surveillance and infiltration in health and diseases (see Fig. 2).

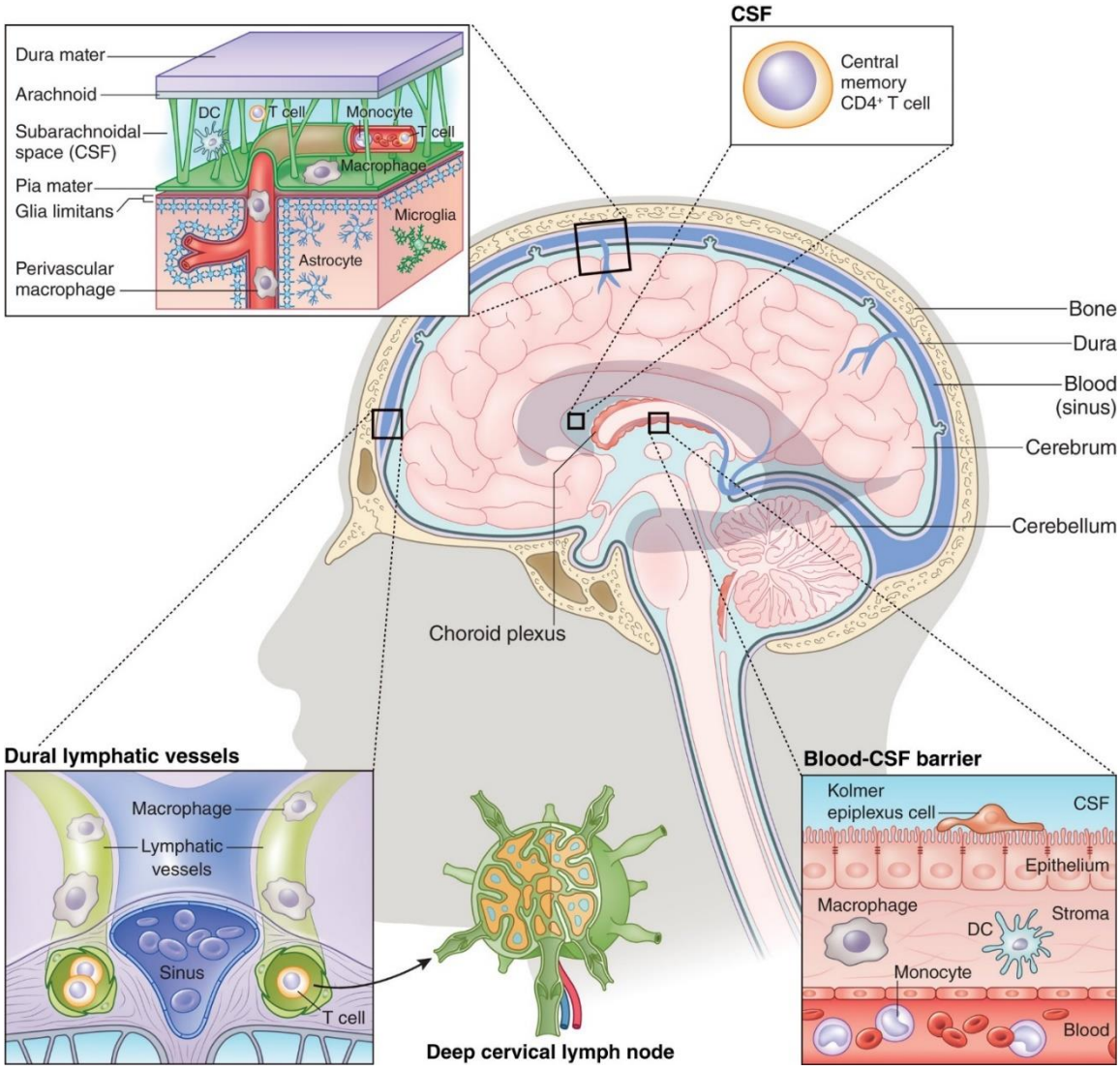


**Fig. 2: anatomical and cellular correlates of immune competence at the CNS-periphery interface [Prinz M. et al. 2017]**

While all these evidences explain the modality of intervention of peripheral immune cells in neuroinflammatory processes like CNS infections or autoimmune diseases (e.g. multiple sclerosis), they do not fully contribute to our understanding of neurodegenerative processes in which the role of peripheral immune cells is limited [Becher et al., 2016; Ranshoff, 2016].

## 1.2. Neuroinflammation: a non-cell autonomous approach

The idea that all the CNS's resident cells (i.e. neurons, microglia, astrocytes and oligodendrocytes) actively participate to neuroinflammatory processes in health and disease is relatively recent, and have invaluably enriched our view of brain and spinal cord disorders [Lobsiger C. et al., 2007; Ranshoff, 2016].

Indeed, for over a century, the study of neurodegenerative diseases has been heavily influenced by the work of the great pathologist Rudolf Virchow that, in the mid 19$^{th}$ century, inspired by the "cell theory", proposed a cell autonomous view of these disorders in which the damage of a precise population of affected neurons alone suffices to produce the clinical outcome [Ilieva H. et al., 2009]. Furthermore, his histological studies on neural tissue led him initially to consider glial cells as a mere connective tissue that structurally support neurons (coining in 1856 the term neuroglia, i.e. nerve glue) excluding them from any relevant physiopathological role [Kettenmann H. et al., 2008].

Our current understanding of neuroinflammation relies instead on a non-cell autonomous view, supported by many experimental evidences that, during the last decades, uncovered the pivotal role of glial cells in these processes in the contest of neurodegenerative diseases models [Chai M. et al. 2019; Kim C. et al 2021; Van Harten A. C. M. et al., 2021]. Furthermore, glial contribution to neuroinflammation goes beyond the more obvious role of microglia, the resident immune cell of the CNS, involving also astrocytes and oligodendrocytes.

For example, several studies modelling amyotrophic lateral sclerosis (ALS) using selective mutant superoxide dismutase (mSOD1) silencing, have revealed different roles for affected neurons and glial cells in governing the course of the pathogenesis of this disease. Particularly, it has been observed that while the mutation within motor neurons drives the disease initiation, mSOD1 expression in microglia and astrocytes underlies rapid disease progression. More importantly, selective mSOD1 expression in motor neurons, or in microglia or in astrocytes alone was not sufficient to induce motor neuron degeneration [Lobsiger C. et al. 2007] (see Fig. 3).

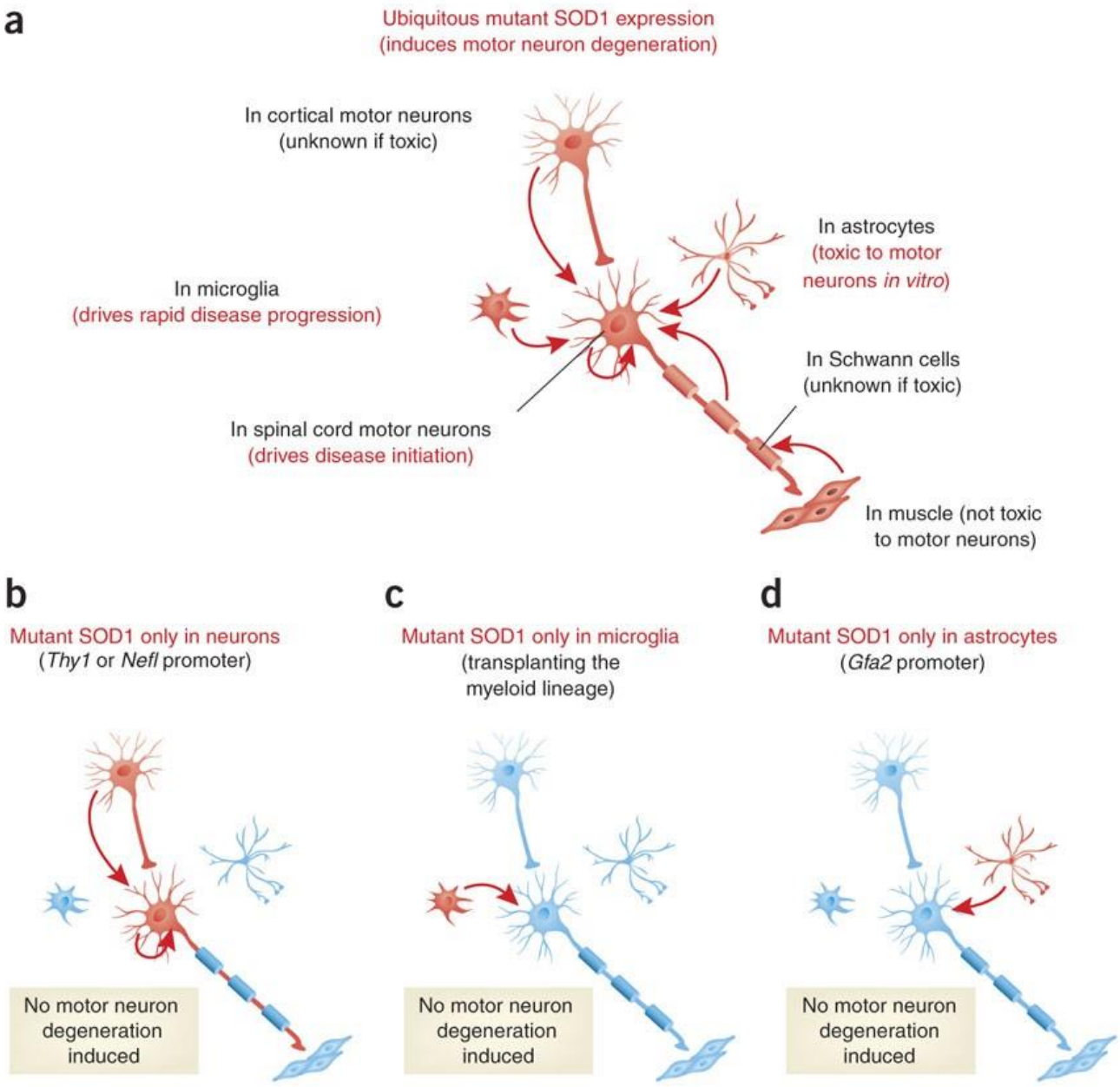


**Fig. 3: non-cell autonomous pathogenesis in ALS [Lobsiger C. et al. 2007]**

Furthermore, the potential role of oligodendrocytes in the pathogenesis of these diseases can be instead well exemplified by a mouse model of multiple system atrophy (MSA), in which the overexpression of α-synuclein in this glial lineage is sufficient to cause secondary axonal degeneration and reactive gliosis producing the characteristic histopathological feature and symptomatology of the disease [Yazawa I. et al. 2005].

Similar results have been obtained from other models of neurodegeneration aiming to elucidate the pathophysiological mechanisms that characterize Parkinson's disease (PD), Alzheimer's disease (AD) and Huntington's disease (HD), suggesting that the detrimental processes which underlies these

disorders derive from a well-orchestrated chain reaction that involve all the CNS resident cells [Glass C. K. et al., 2010; Crotti A. et al., 2015].

Interestingly, the active role of glial cells in neuroinflammatory processes has been widely demonstrated also in clinical condition where genetic factors are not directly involved, like ischaemic stroke, brain tumours and spinal cord injury, suggesting that their ability to participate to sterile inflammatory processes is an intrinsic property of those cell types due to the constitutive and inducible expression of dedicated molecular machineries.

Together, all these evidences underlie the importance of considering CNS diseases as non-cell autonomous diseases allowing a full comprehension of these phenomena while offering the opportunity to find novel therapeutic approaches.

## 1.3. Pattern recognition receptors in the CNS: the danger theory effectors

Despite the study of neurodegenerative diseases gave us fundamental hints about the role of glial cells in neuroinflammatory processes, it's important to consider that their involvement goes far beyond the accumulation and spreading of pathologic misfolded proteins, relying instead on the expression of a wide range of germline-encoded receptors including pattern recognition receptors (PRRs) [Antel J. P. et al., 2020].

The term PRRs was coined in 1989 by the immunologist C. A. Janeway who theorized their existence before their discovery, as potential evolutionary precursors of the more specific receptors expressed by lymphocytes [Janeway C. A., 1989]. Nowadays, this term defines a variegated class of receptors widely expressed in in many types of cells, originally discovered for their role in recognizing pathogens through the binding of pathogen-associated molecular patterns (PAMPs): highly conserved structures (e.g. nucleic acids, bacterial wall components, lipopolysaccharide, flagellin, etc.) which are not susceptible of immune escaping through antigenic mutations [Kigerl K. A. et al., 2014].

Interestingly, from the late 90's, an increasing number of studies have uncovered the ability of PRRs to bind even endogenous molecules released in the extracellular environment by dying cells during tissue damage [Takeuchi O. et al., 2012]. These molecules, collectively called damage (or danger) associated molecular patterns (DAMPs or alarmins), have been found to be able to elicit a strong inflammatory response defined as sterile inflammation [Schaefer L., 2014]. Despite this fundamental double-edged process is highly conserved through animal evolution, aiming to promote tissue healing and physiological cell turnover through a beneficial immune activation, it seems that excessive or chronic release of DAMPs, and the consequent abnormal activation of PRRs, has a pivotal role in driving the evolution of many non-infectious pathological processes including many CNS's diseases [Gadani S. P., 2015].

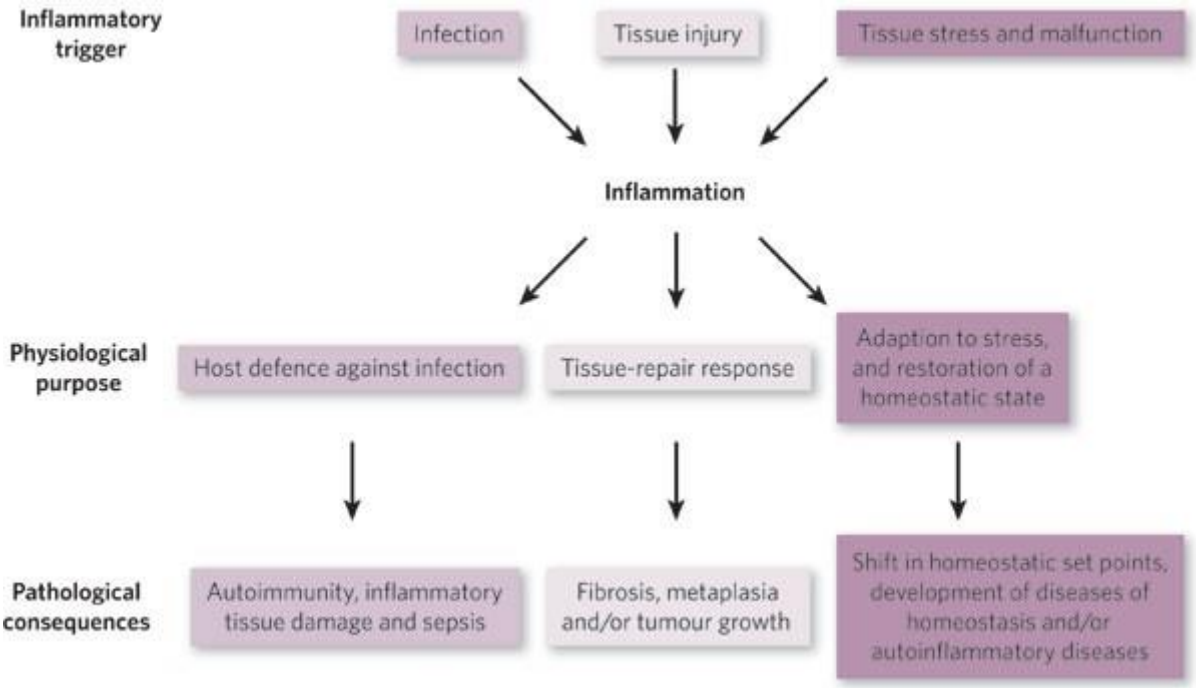


**Fig. 4: Causes and possible outcomes of inflammation [Medzhitov R., 2008]**

All these findings finally gave rise to the "danger hypothesis". Proposed for the first time in 1994 by the immunologist Polly Matzinger, this theory states that the immune system has evolved to respond to any type of danger rather than to react exclusively to objects not considered as part of the body (i.e. non-self) [Matzinger P., 1994]. This theory has been widely supported by many experimental evidences, expanding the classical self/non-self paradigm proposed by Frank Macfarlane Burnet in 1949 which dominated the immunological research landscape of the twentieth century [Tauber A. I., 2000], and offering a valid theoretical framework to approach the study of neuroinflammatory phenomena linked to non-infectious diseases and putting PRRs at the centre of the debate [Amarante-Mendes et al., 2018].

Mammal cells express several distinct families of PRRs including Toll-like receptors (TLRs), Nod-like receptors (NLRs), RIG-I-like receptors (RLRs), AIM2-like receptors (ALRs), C-type lectin receptors (CLRs), intracellular DNA sensors such as cGAS, and many others, able to bind various classes of molecules and all of them are widely expressed in the neural tissue [Kigerl K. A. et al. 2014].

***Toll-like receptors***: the first protein of this family was discovered in 1985 in *Drosophila melanogaster*, where it was found to control the embryos' dorso-ventral development [Anderson K. V. et al., 1985], and it was named Toll (from the German word which means weird, fantastic), given

the strange appearance of the *Toll* gene knock-out fly embryos. Many years later, further knock-out experiments linked the same protein to *D. melanogaster* adults' resistance to *fungi* infection, providing the first evidence of its involvement in immune response [Lemaitre B. et al., 1996].

In 1997 a mammalian Toll homologue named TLR-4 (the protein product of the correspondent knock-out gene *Tlr4*) was the first PRR to be discovered in humans [Medzhitov R. et al., 1997], and the same receptor was later found in mice to be able to recognize bacterial lipopolysaccharide (LPS), a major component of gram-negative bacteria cell wall, providing the first evidence of the involvement of this receptor class in regulating innate immunity also in vertebrates [Poltorak A. et al., 1998]. Subsequently, many additional homologues have been identified across diverse species, counting to date 13 subtypes in mammals among which TLRs 1-10 are expressed in humans while rodents' cells express also 11-13 [Moresco et al., 2011; Nie L. et al., 2018].

Interestingly, despite initial controversies, it's now well assessed that TLRs are widely expressed in all the mammals CNS' cell types (cell expression patterns resumed in Tab.1) in health and disease [Bsibsi M. et al., 2002; Lee S. J., 2013], accounting for their demonstrated involvement in regulating also physiological functions like neural tissue development, synaptic pruning, cognitive functions (like memory and learning), as well as in neuroinflammatory processes and neuropathology, further supporting the non-cell autonomous view of neurological disorders [Okun E. et al., 2011].

| Cells | TLRs | Species |
|---|---|---|
| Neuron | TLR3, 4, 7, 9 | H |
| | TLR2–4, 6–8, 11–13 | M |
| Astrocytes | TLR3, 4 | H |
| | TLR2–5, 9 | M |
| Microglia | TLR1–4 | H |
| | TLR2, 4, 9 | M |
| Oligodendrocytes | TLR2 | H |
| | TLR2–4 | M, R |
| Schwann cells | TLR2 | H |
| | TLR3, 4 | R |

H: human, M: mouse, R: rat

**Tab 1: TLRs expression in CNS cell types [Lee S. J., 2013]**

Structurally, TLRs are type I transmembrane glycoproteins (i.e. constituted by a single α-helix transmembrane domain with an extracellular N-terminus and an intracellular C-terminus),

characterized by an extracellular leucine-rich repeat (LRR) domain, which contains the ligand binding site and gives them the characteristic horseshoe shape, and an intracellular Toll/IL-1 receptor (TIR) domain which is linked to the transduction molecular machinery whose main convergence endpoint is the activation of the proinflammatory transcription factor NF-κB which leads to the synthesis and secretion of proinflammatory cytokines and interferons. Furthermore, it's of note that, given the structural variety and complexity of their ligands, TLRs activation often requires homo or heterodimerization and different combinations of co-receptors and accessory molecules which allow them to expand the range of their binding affinity [Mogensen T. H., 2009; Piccinini A. M. et al., 2010; Gao W. et al., 2017].

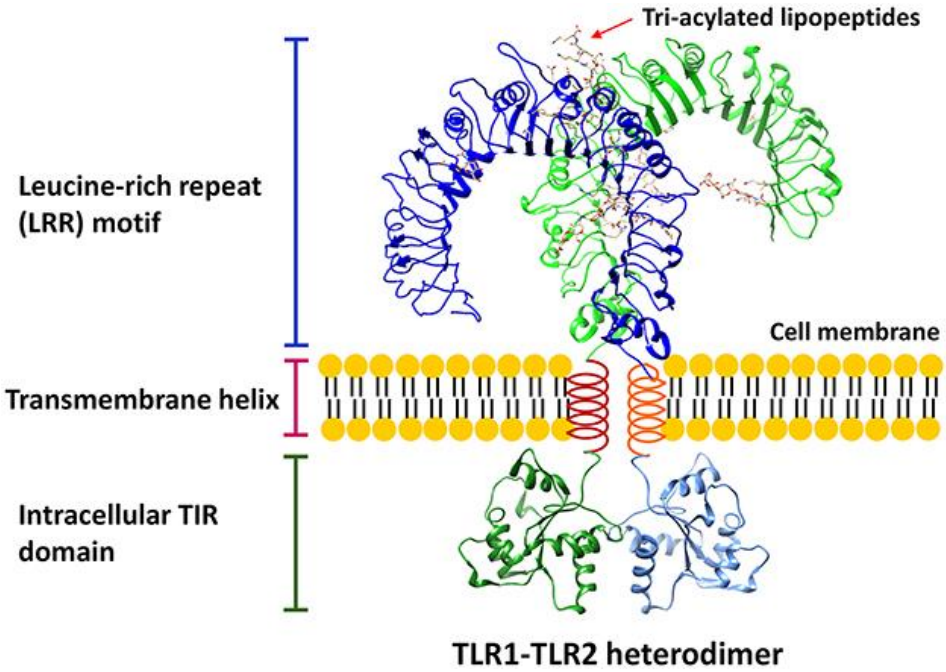


**Fig. 5: example of typical TLRs structure [Gao W. et al., 2017]**

Indeed, beside their classical role in binding PAMPs, TLRs have been found to bind efficiently a wide range of DAMPs (resumed below in Tab. 2), a fact that fully reflect the complexity and versatility of their extracellular domain and their well-established role in promoting sterile inflammation [Piccinini A. M. et al., 2010].

The first report of an endogenous ligand of TLRs dates back to 2000, when heat shock protein 60 (HSP60) was shown to activate TLR-4, inducing cytokine synthesis [Ohashi K. et al., 2000]. Since then, more and more endogenous TLRs ligands have been found (resumed in Tab. 2) and correlated with CNS' pathologies [Piccinini A. M. et al., 2010; S. P. Gadani et al., 2016].

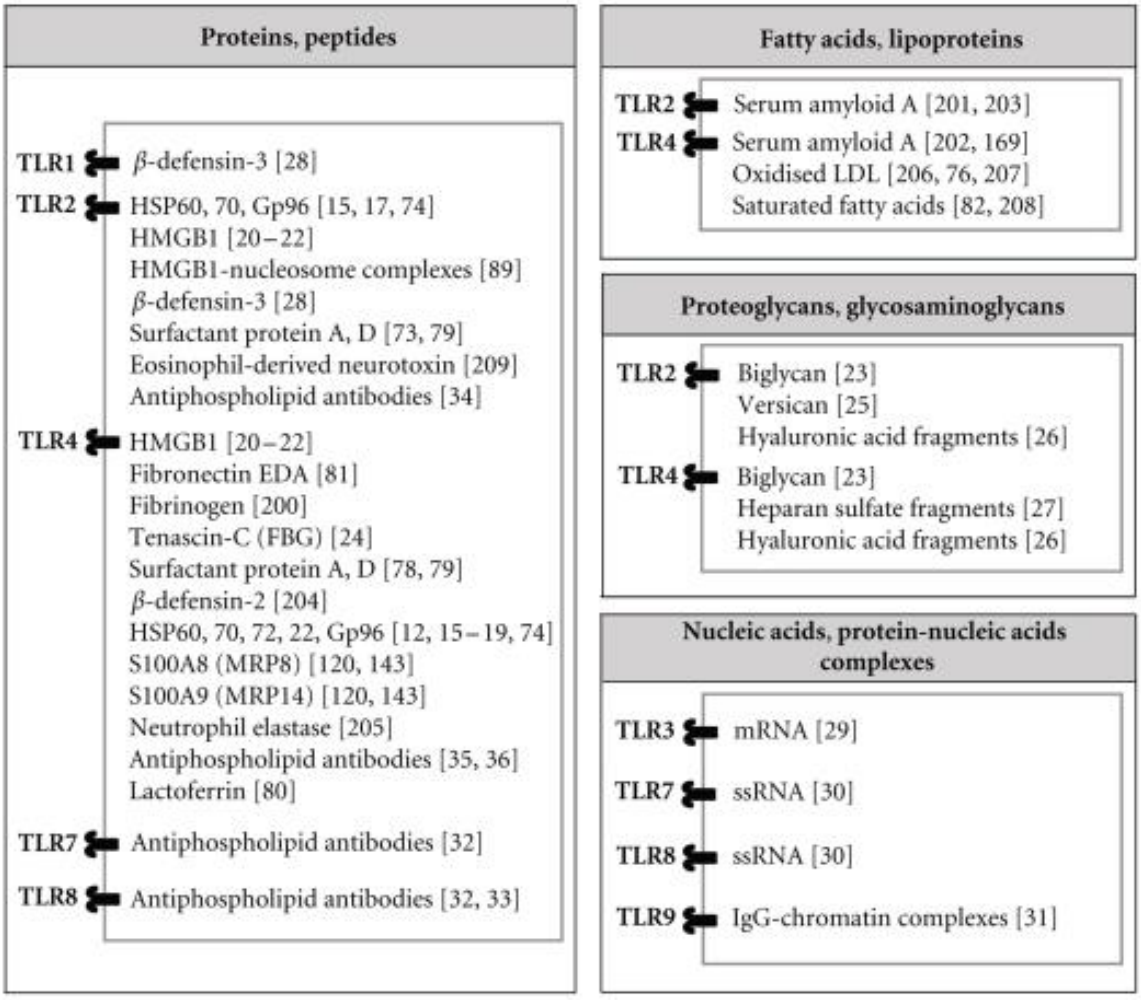


**Tab 2: confirmed TLRs endogenous ligands [Piccinini A. M. et al., 2010]**

Surely, the most studied receptor of this family is TLR-4. Its unique mechanism of activation (TLR-4 intercellular signalling cascade resumed in Fig. 6) involves homodimerization and the presence of the co-receptor CD14 and the accessory protein MD2 which are essential for the ligand binding. Its involvement in CNS' disorders has been initially deduced from the experimental evidence of the neurotoxic potential of its activation which can lead to neuronal death and oligodendrocytes damage [Lehnardt S. et al., 2002; Lehnardt S. et al., 2003]. Interestigly, its increased expression and function has been detected in neural tissue samples from animal models and patients affected by many types of CNS' disorders such as ALS [Casula M. et al., 2011], PD and MSA [Panaro M. A. et al., 2008], AD [Calvo-Rodriguez M. et al., 2020; Huges C. et al., 2020], or brain trauma and spinal cord injury [Kigerl K. A. et al., 2007; Zhang Y.K. et al., 2013]. Furthermore, TLR-4 knock-out or the pharmacological inhibition of this receptor, has been found to exert a significant neuroprotective action in many animal models of neuroinflammatory diseases [De Paola et al., 2012; Lee J. Y., 2015; De Paola et al., 2016; Campolo M. et al., 2019; Cui W. et al., 2020].

All these evidences, in addition to a well characterized kinetics and experimental reproducibility, make LPS-induced neuroinflammation through the activation of TLR-4, one of the most widely used experimental paradigm in this field [Ribeiro Alvares Batista C. et al., 2019]

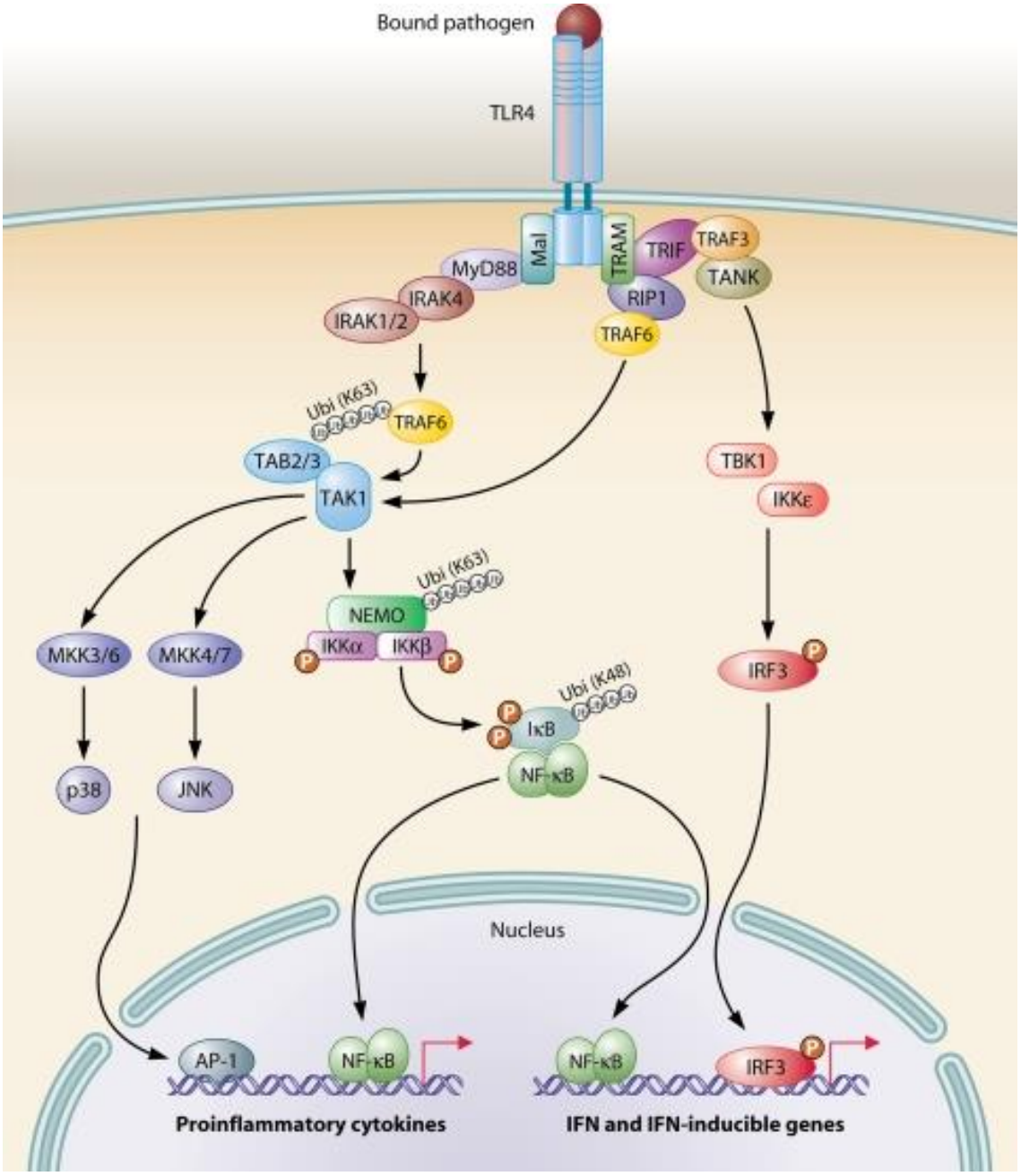


**Fig. 6: TLR-4 classical transduction cascade [Mogensen T. H., 2009]**

***NOD-like receptors and the inflammasome*:** the secretion of the mature and fully active form of IL-1β following PRRs activation is considered a pivotal event in the induction of a functional inflammatory response to danger. NOD-like receptors belong to a class of intracellular PRRs, that to date consists of 22 members in humans, which exerts a fundamental role in ensuring this response [Lopez-Castejon G. et al., 2011].

From a structural point of view, NOD-like receptors are multi-domain proteins characterized by a tripartite architecture in which a central nucleotide-binding domain, termed NOD domain, lays between a C-terminal receptor domain, characterized by (similarly to TLRs) a series of LRRs and a N-terminal effector domain often referred as caspase recruitment domain (CARD) which is able to bind and activate the proinflammatory protein caspase 1 [Proell M. et al., 2008]. One of the more studied NOD-like receptors in the context of neuroinflammation is NLRP3 (NOD-, LRR- and pyrin domain-containing 3), originally found in myeloid lineage cells, such as microglia and macrophages, recent studies confirm its expression also in astrocytes and oligodendrocytes, while neurons seems to express predominantly NLRP1 [Heneka M. T. et al., 2018].

NLRP3 activation is a tightly regulated process and requires multiple steps. Indeed, while it's usually expressed at low levels in a constitutive manner, its massive expression can be induced after TLRs or cytokine receptors activation, through the NF-κB pathway as a response to an explicit proinflammatory microenvironment (priming step). After this priming, a second stimulus is required to induce NLRP3 multimerization and the consequent formation of the so called inflammasome (see Fig. 7). Such secondary stimuli include glutamate, pannexin 1 channel opening, ATP via triggering of the P2X7 receptor, changes in the extracellular concentration of potassium, mitochondrial dysfunction and many types of neurodegeneration-associated misfolded proteins like oligomeric and fibrillar forms of amyloid-β, α-synuclein and transactive response (TAR) DNA-binding protein 43 (TDP43) [Freeman L. C. et al., 2016; Heneka M. T. et al., 2018]. The multimerization occurs via CARD-CARD-PYD-PYD domains interaction which lead to the formation of a molecular scaffold able to recruit and activate procaspase-1 through enzymatic cleavage. Active caspase-1 is essential for the cleavage of pro–interleukin 1β (pro-IL-1β) and pro-IL-18 into their mature and biologically active forms [Franchi L. et al., 2009].

Interestingly, the pharmacological inhibition of TLR-4 has been shown to exert a neuroprotective activity through a down-regulation of NLRP3 [Cui W. et al., 2020].

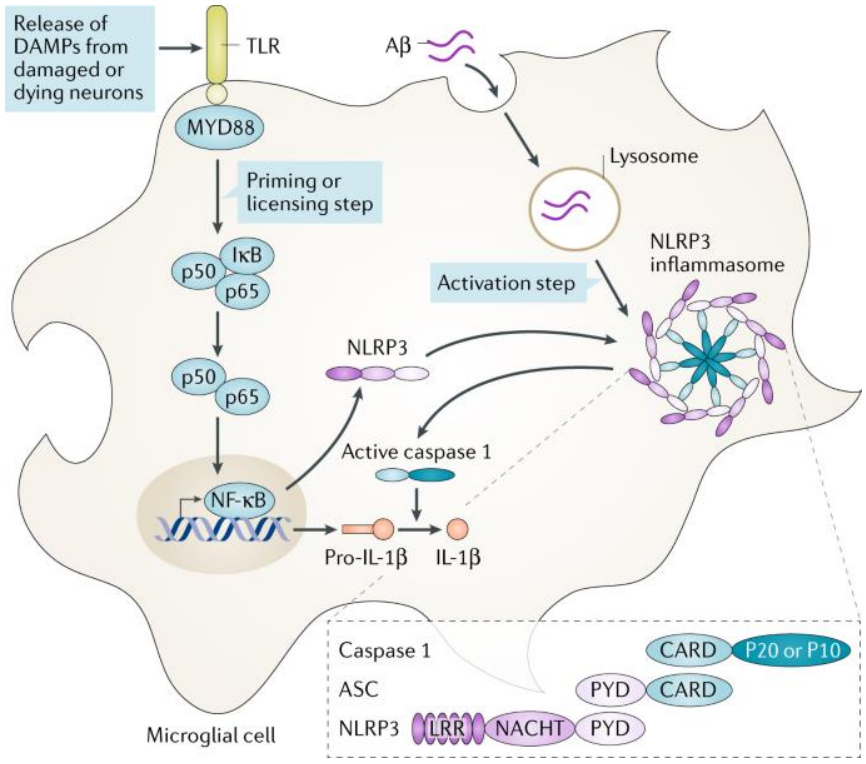


**Fig. 7: IL-1β maturation through TLRs – Inflammasome interplay [Heneka M. T. et al., 2018]**

***ATP as a danger signal*:** beside its fundamental role as the main intracellular energy source, adenosine 5′-triphosphate (ATP) acts also as an extracellular signalling molecule through the activation of the so-called purinergic receptors, firstly described by Geoffrey Burnstock in 1976 [Burnstock G., 1976]. This receptor family comprise nowadays nearly twenty subtypes, involved in a wide range of physiological functions including neurotransmission, neuromodulation, secretion, chemoattraction, acute inflammation, cell proliferation, differentiation, motility and death [Burnstock G., 2018].

Those receptors are generally classified in three main families according to their ligand specificity: P0 receptors activated by adenine, P1 receptors activated by adenosine and P2 receptors activated by ATP or ADP. Moreover, the latters are further classified into two subfamilies: P2X and P2Y (see Fig. 8) [Kaebisch C. et al., 2015]. While the majority of them are G protein-coupled metabotropic receptors, only P2X are ligand-gated ion channels preferably permeable to sodium, potassium and calcium [North R. A., 2016]. They are expressed in many types of excitatory and non-excitatory cells like neurons, glial cells, platelet, epithelia and immune cells, where they ensure a fast signal transduction upon ligand binding, regulating many essential physiological processes including synaptic transmission, inflammation, cardiovascular function and immunomodulation [Wang J. et al., 2016].

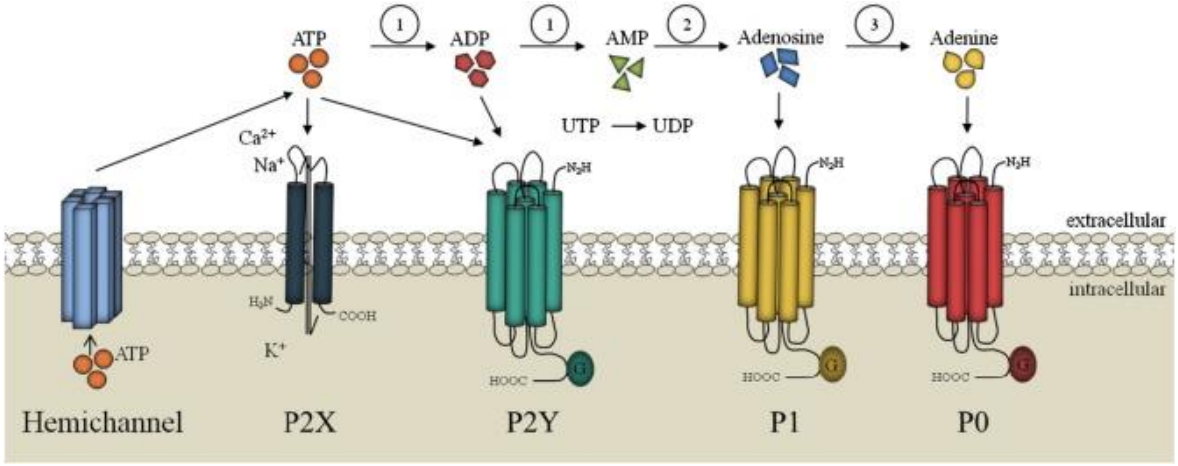


**Fig. 8: purinergic receptors families and their ligands [Kaebisch C. et al., 2015]**

Interestingly, this receptor subfamily is gaining attention in relation to its role in regulating inflammatory phenomena including neurodegenerative disorders. Indeed, there is growing body of evidence confirming a rapid increase of the extracellular ATP (eATP) levels in many pathological CNS conditions, due to structural cell damages or regulated secretion mechanisms including vesicular release from neurons, astrocytes and microglia, and pannexin and/or connexin uncoupled hemichannels opening [Rodrigues R. J. et al., 2015].

In this context, P2X7, and in a lesser extent P2X1 and P2X4, seems to act as PPRs [Burnstock G., 2016]. Particularly, P2X7R have shown a lower binding affinity for ATP (EC50 = 0.1–1 mM) when compared to other P2X receptors (EC50 = 1–10 μM) suggesting that its activation mostly occurs in pathological conditions associated to enhanced eATP levels. Interestingly, many experimental observations carried out from the late ’90, revealed that a massive release of eATP can occur upon TLR-4 activation by LPS through a calcium dependent mechanism and that LPS-dependent IL-1β release involves activation of this purinergic receptor [Ferrari et al., 1997]. Indeed, the release of eATP and the consequent potassium efflux due to P2X7 opening has been confirmed to be essential for the inflammasome activation and the consequent secretion of the mature form of IL-1β [Fiebich B. L. et al., 2014]. The uncovering of the pivotal role of eATP as a permissive second signal for the regulation of the TLR-4/P2X7 axis and the consequent secretion of mature IL-1β, which allow a functional neuroinflammatory response, led finally to the so called “two hit hypothesis” of neuroinflammation making P2X7 an attractive therapeutic target [De Marchi E. et al., 2016].

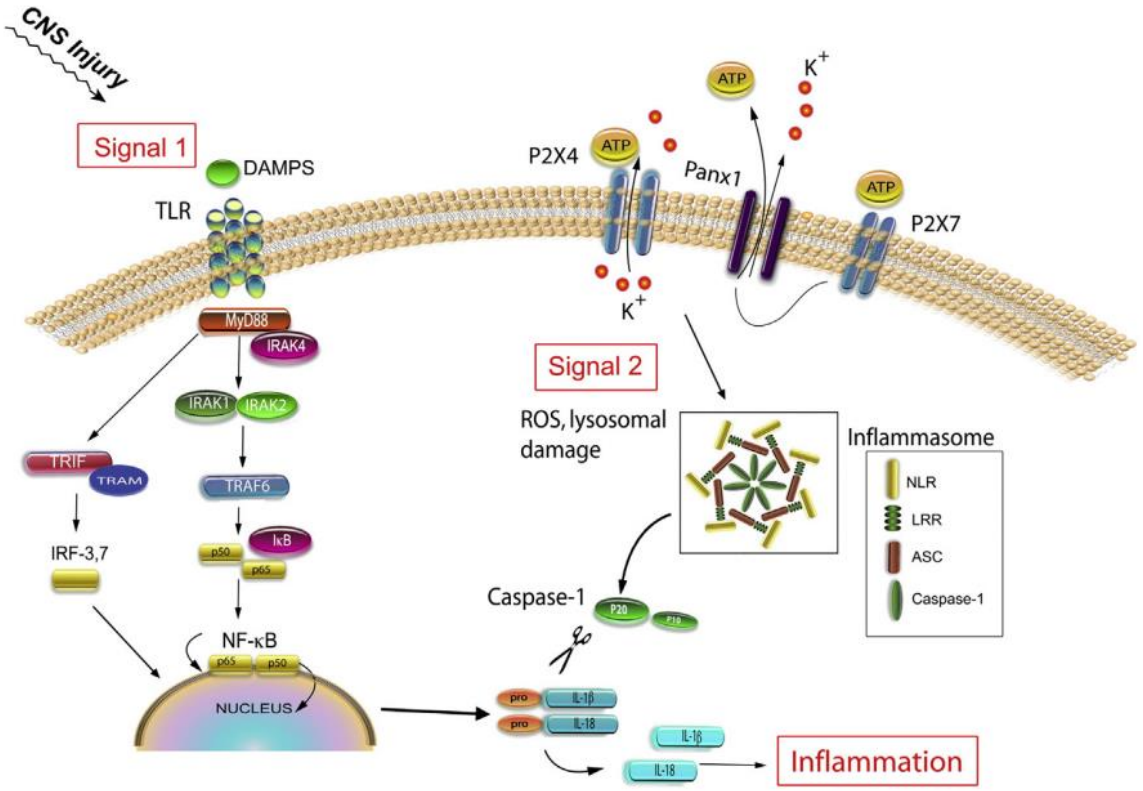


**Fig. 9: the two-hit hypothesis of neuroinflammatin [Kigerl K. A. et al., 2014]**

***The role of hemichannels in neuroinflammation***: hemichannels (HC) are transmembrane hexameric protein complexes which act as mediators in intercellular communication. Despite not belonging to the PRRs family they recently gain attention for their role in mediating neuroinflammatory events consequently to PRRs activation [Xing LY et al., 2019]. HCs can be coupled, bridging one cell with another one, forming the so called gap junctions (GJ) which allow the intercytoplasmatic transfer of macromolecules and ions with signalling or metabolic functions like $Ca^{2+}$, $IP_3$, cAMP, glutamate, glucose, glutathione, ATP, ADP, and RNA, or uncoupled allowing the transfer of small hydrophilic molecules and ions from the cytoplasm to the extracellular environment where they can act as autocrine or paracrine signals. Interestingly, while GJs are usually open allowing the physiological communication between adjacent cells, uncoupled HCs are typically closed, but they can be activated by various pathological triggers, such as increased membrane depolarization, changings in intracellular or extracellular calcium homeostasis, mechanical stimulation, oxidative stress, ischemic events and inflammatory conditions [Willebrords et al., 2016].

HCs are composed of six transmembrane monomers called connexins (Cxs) belonging to a heterogeneous protein class which consists of various isoforms (21 identified in humans which share 19 orthologs with mice) named based on their predicted molecular weight expressed in KDa, which can be variously assembled to form homomeric or heteromeric HCs [Takeuchi et al., 2014].

CNS cells express a wide range of Cxs with a certain degree of isoform preference among cell types. Surely, one of the most intensively studied isoforms in this context is Cx43, which tends to form coupled and uncoupled homomeric HCs expressed prevalently by neurons and astrocytes ensuring fast and efficient communication between those cell types. Astrocytes represent the largest gap junction coupled network in the CNS, forming a functional syncytium which provides efficiently coordinated homeostatic functions [Kielian T., 2008; Takeuchi et al., 2014]. Several knockout studies have in fact uncovered the fundamental role of Cx43 in regulating intracellular and intercellular free calcium $[Ca^{2+}]_i$ signalling in astrocytes in health and disease. In *in-vitro* settings, proinflammatory treatments with LPS or cytokines cocktail are able to reduce gap junction expression and coupling, reducing long distance cell signal synchronization, while increases uncoupled Cx43 hemichannel opening and activity allowing the efflux of ATP and the influx of $Ca^{2+}$ ions altering the dynamics of astrocytic calcium signals and further stimulating microglia to produce proinflammatory cytokines [De Vuyst E. et al., 2007; Retamal M.A. et al., 2007; Yin X. et al., 2018; Panattoni et al 2021].
Abnormal Cx43 HC expression and opening has been observed in several CNS' pathological conditions like AD, PD, ALS, ischemia, SCI and neuropathic pain (see Fig. 10) suggesting an important role of this channel in the pathogenesis of these diseases and making it an attractive therapeutic target [Xing LY et al., 2019].

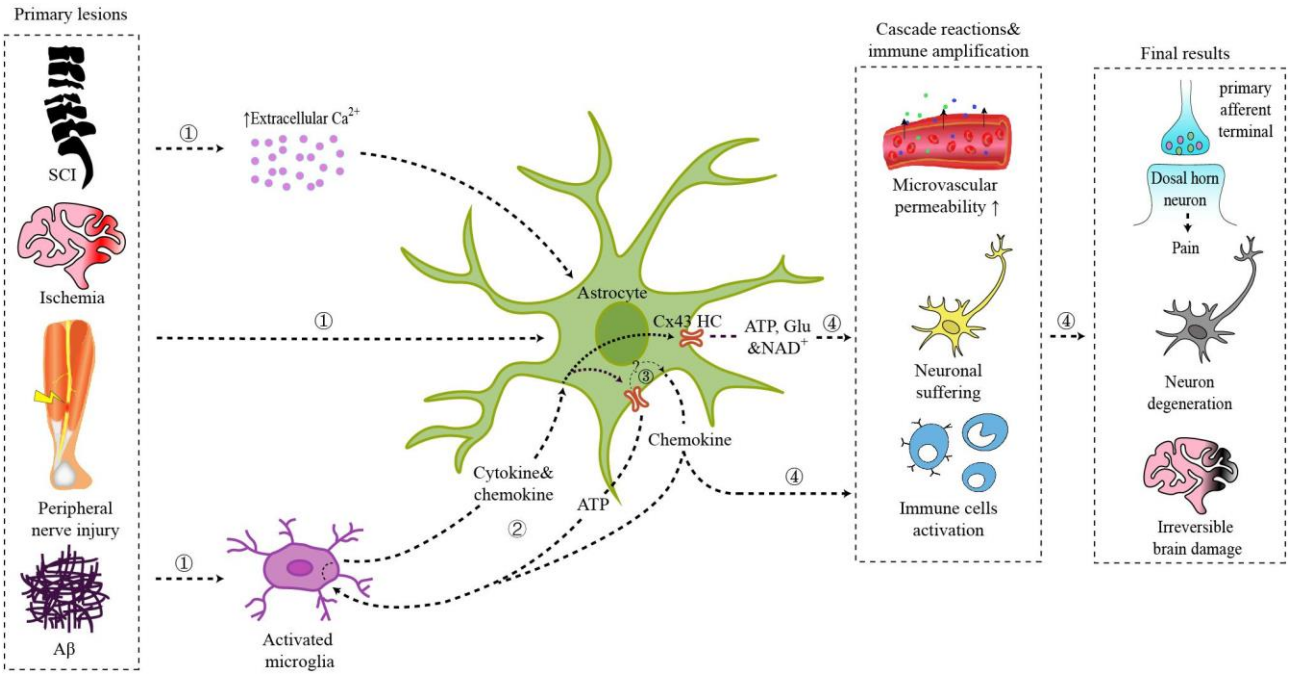


**Fig. 10: astrocytic Cx43 and neuroinflammation [Xing L. Y. et al., 2019]**

## 1.4. Cytokines, chemokines and their receptors

A striking effect of PRRs activation is the induction of the of gene expression encoding for cytokines and their receptors [Zhou et al., 2015]. Indeed, this variegated and pleiotropic protein class is the major orchestrator of inflammation and its resolution, a fact that led, in the last two decades, to the fast growth and development of anti-cytokines therapies, now the cornerstone of the clinical management of many chronic inflammatory disorders [Ratsimandresey et al., 2009].

The word "cytokines" is an umbrella term that covers over 300 small polypeptides grouped into families based upon their structural homology or that of their receptors [Ramesh G. et al., 2013; Becher B. et al. 2016] even if, because of their enormous variety, a simple and precise classification system for cytokines is not feasible [Rothwell et al., 1996]. The most important and best characterized families include interleukins (IL), chemokines (C, CC, CXC and CX3C depending on the spacing of their first two cysteine residues), interferons (IFN), tumour necrosis factors (TNF), transforming growth factors (TGF) and colony stimulating factors (CSF) [Allan S. M. et al., 2001].

Despite initially characterized as immune-modulating agents, it is now clear that cytokines exert a wide range of physiological functions including the regulation of CNS development and its functions during adulthood [Deverman B. E. et al., 2009]. Some of these functions includes: the self-renewal of the neuroepithelial/radial glia cells (RGC), the differentiation and induction of primitive neural stem cells (NSC) [Tropepe V. et al., 2001], the maintaining of the neural progenitor pool in the adult brain [Carpentier P. A et al. 2009], neuronal differentiation, axon pathfinding and synaptic pruning [Deverman B. E. et al., 2009] and the modulation of long-term potentiation [Aleph Prieto G. et al., 2017]. This huge range of functions is due to the fact that, by activating their cognate receptors in target cells, cytokines are able to induce intracellular pathways which differ among cell types, often resulting in divergent pathophysiologic outcomes [Vezzani A. et al., 2015]. Indeed, all the CNS cell types, including neurons, express a wide range of cytokines and cytokines receptors in health and disease and, given the complexity of their physiological functions, is not surprising that a local or systemic perturbation in cytokines homeostasis has a profound impact on CNS' functions possibly leading to a plethora of symptoms including complex ones such as depression, seizures, neuropathy and neurodegeneration (see Fig. 11)) [Szelenyi J., 2001; Sankowsky R. et al., 2015].

As resident macrophage in the CNS, microglia has been traditionally thought to be the major source of cytokines during neuroinflammatory processes, however, in the last two decades many researchers have uncovered the immunologic functions of astrocytes [Dong Y. et al., 2001]. Upon pathogenic stimuli, those cells produce large amounts of IL-1β, IL-6, IFN-γ, TGF-β and TNF-α which result in rapid and persistent modifications in neuron-glia and vascular communication. Such phenomena include increased BBB permeability and expression of adhesion molecules, increased microglia and

astrocytes proliferation, alterations in synaptic transmission and the induction of cell death machinery [Vezzani A. et al., 2015]. Those effects are mainly due to the activation of transcription factors that induce the expression of genes that lead to the synthesis of more cytokines and enzymes like inducible nitric oxide synthase (iNOS) and cyclooxygenase 2 (COX-2), which promote the production of other proinflammatory mediators [Garcia-Bonilla L. et al., 2014].

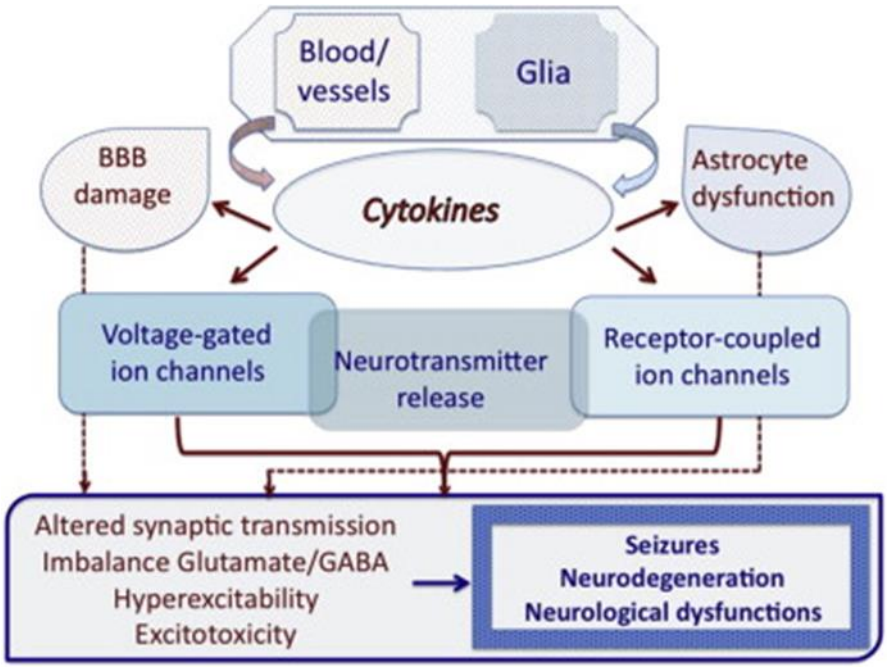


**Fig. 11: cytokine-induced CNS microenvironment alterations [Vezzani A. et al., 2015]**

In this context, TNF-α is surely one of the most complex players. Elevated levels of TNF-α is an evident feature in patients as well as in animal models of a wide range of CNS disorders including MS, ALS, AD, PD, HIV-induced encephalopathy, meningitis stroke and SCI. Furthermore, circulating TNF-α, as seen in many systemic autoimmune disorders, can easily reach the CNS crossing the BBB [Probert L. et al., 1997; Yune T. Y. et al., 2003; Probert L., 2015].

Interestingly, despite TNF-α represents a prototypical proinflammatory cytokine and its role in many inflammatory and autoimmune diseases is well recognized, it can exert pleiotropic functions *via* complex signalling mechanisms. TNF-α is produced in two bioactive forms: transmembrane (tmTNF), acting by cell-to-cell contact, and soluble (solTNF), released following regulated cleavage by a dedicated converting enzyme (TACE/ADAM17) and acting as autocrine or paracrine signal. solTNF can act by binding two distinct receptors: TNFR1, which has a central role in the propagation of the inflammatory milieu, and the induction of cell death through its intracellular caspase-recruiting death domain, and TNFR2, linked to the induction of pro-survival pathways. One of the most striking consequences of this Janus-like properties emerged in 1999 during the lenercept phase II randomized,

multi-centre, placebo-controlled trial in MS patients [The Lenercept Multiple Sclerosis Study Group and The University of British Columbia, MS/MRI Analysis Group, 1999]. Lenercept, a dimeric TNFR1 receptor extracellular domain fused to a human IgG1heavy chain fragment, acting as a decoy receptor for circulating TNF-α, induced a dose-dependent increase in MS attack frequency, duration and severity. Subsequently TNFR1 signaling has been demonstrated to mediate demyelination through the induction of oligodendrocytes apoptosis, whereas TNFR2 signalling has been shown to be crucial for remyelination [McCoy M. K. et al., 2008].

# -2-

# Neuron-glia interaction in neuroinflammation

Glial cells are the major components of the neural tissue [Jäkel S. et al., 2017]. Despite that, the idea that they may be fundamental active players in physiological as well as pathological processes in the CNS is relatively recent. This huge delay in acknowledge their complex roles derives from the late discovery of these cell lineages that results in the prior formulation of the "neuron doctrine" by Christian Ehrenberg, Jan Evangelista Purkinje and Robert Remak, in the 30s of the 19$^{th}$ century. Indeed, thanks to the first available microscopes, they provided the first description of nerve cells, recognizing them as the individual cellular elements that constitute the genetic, anatomic, functional and trophic units of the neural tissue. This idea was further reinforced a decade later by the histopathologic works of Rudolf Virchow that led him to propose a cell autonomous (i.e. neuronocentric) view of CNS disorders [Fodstad H., 2001]. Despite Virchow itself coined the term "glia" to define an amorphous connective tissue structurally supporting nerve cells, the recognition of glial cells as defined cellular elements occurs later at the turn of the 19$^{th}$ and the 20$^{th}$ century through the work of various authors. Among others, Rudolf Albert von Kölliker and William Lloyd Andriezen, in 1893, identified fibrous glial cells and protoplasmic glial cells, Santiago Ramon y Cajal who, in his seminal work on the histology of the nervous system published in 1904, adopted the term astrocyte for both those cell populations and Pio Del Rio-Hortega who, in 1920, identified oligodendrocytes and microglia [Somjen G. G., 1988]. Since then, the introduction of more sensitive tissue staining techniques, molecular biology approaches and new functional investigative methods has progressively dissected the diversity of those cell types and the complexity of their functions.

Despite, the neuron doctrine has served for decades as an invaluable theoretical framework for the great advances in our comprehension of the cellular basis of the CNS functions, it's now clear that a broader view is needed and that neurons and glial cells cannot be studied in isolation.

## 2.1 Neurons in inflammation

Neurons are highly specialized cells considered the fundamental effector units of the CNS whose functions depend largely on their peculiar electric and secretory activity [Hof P. R. et al., 2014]. Those functions arise from interrelations between neurons and glial cells, rather than from neuronal activity alone, however, the loss of neuronal functionality, through pathologic modulation or even cell death, is still considered the critical event in all neurologic and psychiatric disorders [Bernaus A. et al., 2020]. Given their postmitotic nature, neurons are often seen as passive "victims" of neuroinflammatory events, even though they can actively regulate the CNS immune

microenvironment. Indeed, neurons can maintain their own synaptic connectivity, survival and metabolic activity, regulating glial cells functions through the secretion of various immunolmodulatory molecules including TGF-β, which maintains neuronal differentiation and regulates synaptic plasticity, and CD22, CD200 and fractalkine, which suppress microglia activation promoting the secretion of anti-inflammatory cytokines [Mizuno T., 2013]. Nevertheless, a proinflammatory cytokines imbalance, as seen in neuroinflammatory conditions, can overcome these regulatory systems potentially inducing profound alterations in neuronal electric activity. In 1991, Lawrence Miller and colleagues reported the first evidence of cytokine alteration of neuronal ion channels studying the effect of high levels of IL-1β on GABA currents in dissociated chick neuronal culture [Miller L. G. et al., 1991]. Since then, a growing body of evidences confirmed cytokines ability to perturb neuronal excitability in many pathological conditions like epilepsy, hyperalgesia and injury [Bodnar C. N. et al., 2018; Chavan S. S. et al., 2017; Vezzani A. et al., 2015]. For example, in the spinal cord there is an association between TNF-α levels, neuronal sensitization and pain. Particularly, intrathecal administration of TNF-α has been shown to enhance C fibres activity, increasing the response of dorsal horn neurons. Importantly, these phenomena seem due to a decreased expression and activity of glutamate transporters EAAT and GLAST, resulting in a decreased glutamate uptake and a consequent increase in neuronal activity and pain behaviour due to changes in spinal processing [Schäfers M. et al., 2008]. Interestingly, similar cytokines effects are implicated in the excitotoxic phenomena that characterize ALS pathogenesis, where motoneurons are more susceptible to glutamate induced cell death [Van Den Bosch L. et al., 2006].

In addition to this indirect mechanism, IL-1β, TNF-α and IL-6 were described to directly modulate the major classes of voltage gated ion channels. As an example, in spinal cord neurons, IL-6 is able to suppresses depolarization-evoked $Na^+$ currents, an effect prevented by IL-6R antagonist. IL-1β reduces voltage gated $K^+$ currents *in vivo* in trigeminal ganglion nociceptive neurons and inhibits voltage-gated $Ca^{2+}$ channels in dissociated primary cultures of hippocampal and cortical neurons. Furthermore, IL-1R1 is enriched at postsynaptic sites where it co-localizes with NMDA receptors (NMDAR), while TNF-α modulates specifically AMPA receptors (AMPAR) through their association with TNF-R1. Such interactions occur via the induction of cytosolic kinase proteins following cytokines receptors activation, which modulate neurotransmitter receptors activity through phosphorylation. Particularly, IL-1R1 activation induce NMDAR phosphorylation via Src tyrosine kinase through a MyDD88 mediated pathway, while TNF-R1 induces AMPAR phosphorylation via p38 MAPK (see Fig. 12) [Vezzani A. et al., 2015].

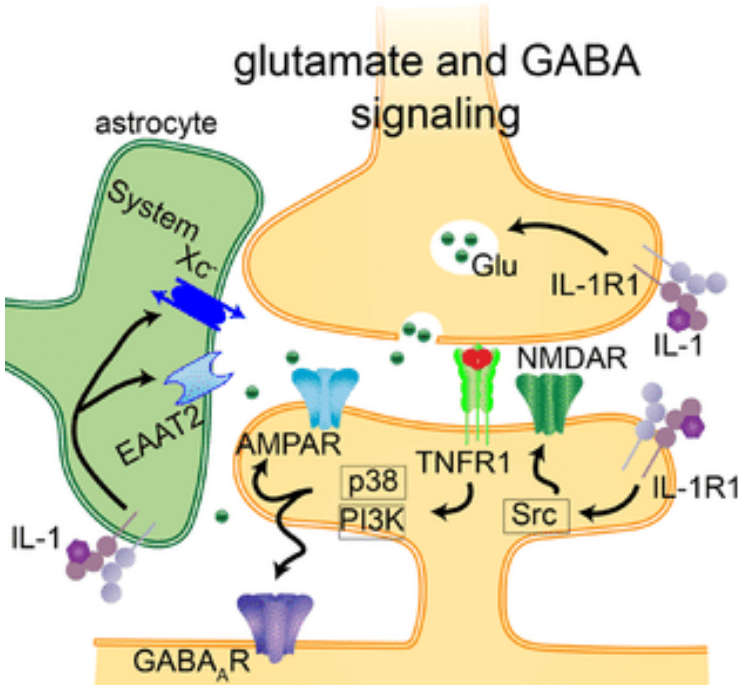


**Fig. 12: Cytokines network at synaptic level [mod. from Bodnar C. N. et al., 2018]**

While cytokines play a major role in neuronal dysregulation and damage, also purinergic signalling seems to be involved in the detrimental effects of neuroinflammatory processes. Indeed, despite initial controversies, many studies have confirmed that P2X7R is expressed by neurons in many areas of the CNS including the spinal cord, and that its activation can mediates pathological events [Miras-Portugal M. T. et al., 2017]. Particularly, in 2012, Kentaro Nishida and colleagues observed that acute P2X7R activation by high concentrations of eATP can induce neuronal death in rodent dissociated cortical neuron cultures, through mitochondrial dysfunction and activation of caspase-3, an effect prevented by selective P2X7R antagonists [Nishida K. et al., 2012].

Furthermore, as mentioned above, neurons can express various types of PRRs including TLR-4. In neural precursor cells TLR-4 signalling regulates cell proliferation and differetiation, while during adulthood seems to be involved in axonal growth and maintenance, synaptic plasticity and neurogenesis [Rolls A. et al., 2007]. Despite less is known about the role of neuronal TLR-4 in CNS innate immunity, in 2012, Sophie Leow-Dyke and colleagues demonstrate for the first time that the activation of this receptor in neurons through LPS stimulation, promotes the release of the chemokines CXCL1 and CCL5 while, interestingly, failed to induce the synthesis of IL-1β, TNF-α and IL-6 [Leow-Dyke, S. et al., 2012].

## 2.2. Microglia in neuroinflammation

Microglial cells are the resident macrophages of the neural tissue, ontogenetically distinct from the other CNS cell types for their mesodermal origin. Despite originally it was speculated that they originate from precursors in the bone marrow [Kettenmann H. et al., 2010], only recently, *in vivo* lineage tracing studies showed that microglia arise early in mouse development (E8) deriving from primitive myeloid progenitors in the yolk sac [Ginhoux F. et al., 2010].

Unlike "classical" macrophages, in the healthy CNS microglial cells display a peculiar resting state feature characterized by a mildly ramified morphology with a small soma and fine cellular processes that constantly monitor the surrounding environment [Hristovska I. et al., 2016]. The motility of those processes is intended to fulfil microglial immune surveillance functions and to constantly monitor neuronal activity through the establishment of transient activity-dependent contact with synapses [Wake H. et al., 2009]. This cell type is also characterized by a significant morphological plasticity that reflects its degree of activation, a fact that can be used to quantify microglia reactivity in experimental settings. Generally, mildly activated microglia is known to display a larger cell body and elongated processes with higher motility, while strongly activated microglia is characterized by an amoeboid feature that indicate an increased phagocytic activity (see Fig.13) [Hof P. R. et al., 2014].

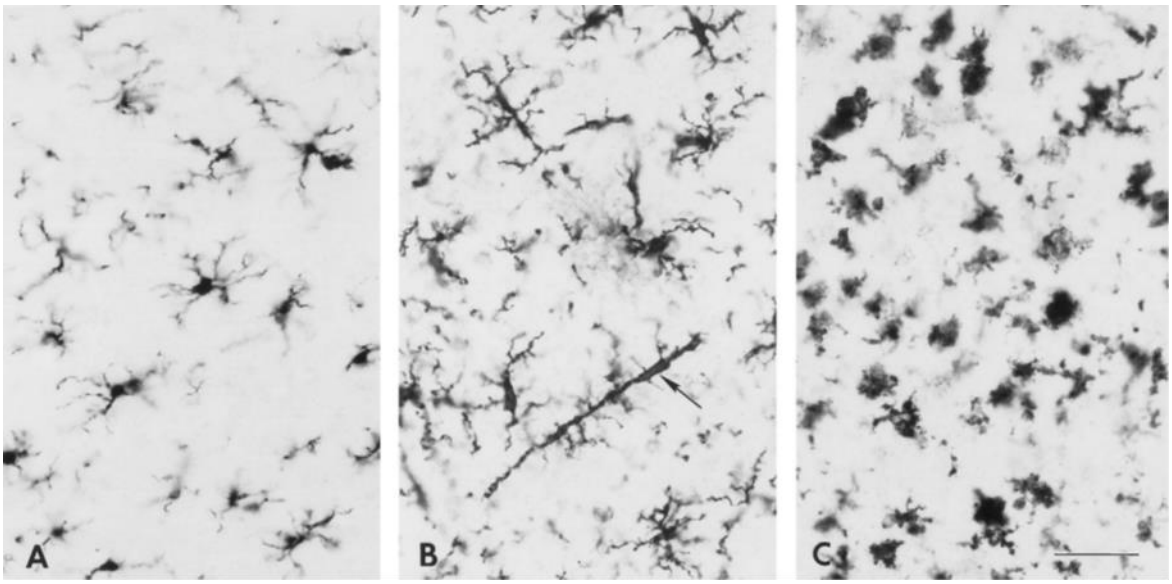


**Fig. 13: microglia morphology in different activation states. A. resting state B. activated microglia C. amoeboid phagocytic microglia [Hof P. R. et al., 2014]**

As an immune cell, microglia express a wide range of PRRs (including TLR-4), purinergic receptors (including P2X7R) and MHC class I and II that make it the most competent APC in the CNS. Microglia also express neurotransmitter receptors for glutamate, γ-aminobutyric acid (GABA),

norepinephrine, cannabinoid and acetylcholine, which enable the synchronization with neuronal activity [Liu H. et al., 2016]. In addition to their well establish immune function, microglial cells are involved in other fundamental homeostatic processes such as synaptic pruning, especially during development [Paolicelli R. C. et al., 2011], neuronal differentiation and maintenance through interactions with neuronal precursor cells [Wolf S. A. et al., 2017], cell debris removal and myelin recycling through phagocytosis [Berghoff S. A. et al., 2021]. All these complex functions are tightly regulated by the local molecular milieu, which includes cytokines and chemokines, which can drive microglia reactivity to two possible main activation states: the so called M1 and M2, both characterized by distinct functions, markers expression profiles and cytokines secretion patterns (see Fig. 14) [Guo S. et al., 2022]. M1 microglia is a common feature in all neuroinflammatory diseases and is considered the classical proinflammatory activation state. The transition from the resting state to M1 is mainly triggered by the activation of PRRs by PAMPs and DAMPs derived from infective pathogens and tissue damages respectively. It's characterized by the sustained secretion of proinflammatory cytokines through the activation of the inflammasome/caspase-3 pathway, and reactive oxygen and nitrogen species, aimed at the removal of the noxious stimulus. As an example, the activation of TLR-4 by bacterial product like LPS or by proteins released from dying neurons, like HMGB1, induce microglial transition to M1 stimulating the secretion of IL-1β, TNF-α and GM-CSF that promote its reactivity, replication and the proinflammatory activation of the surrounding cells, including astrocytes [Liddelow S. A. et al., 2017]. Similarly, an increase in eATP as a result of tissue damage, is known to stimulate M1 state through the activation of P2X7R/inflammasome axis and promotes process motility and elongation through the ATP gradient, driving microglial cell to reach the damaged area in order to ensure the phagocytosis of debris, facilitating the restoration of the homeostatic state [Hristovska I. et al., 2016].

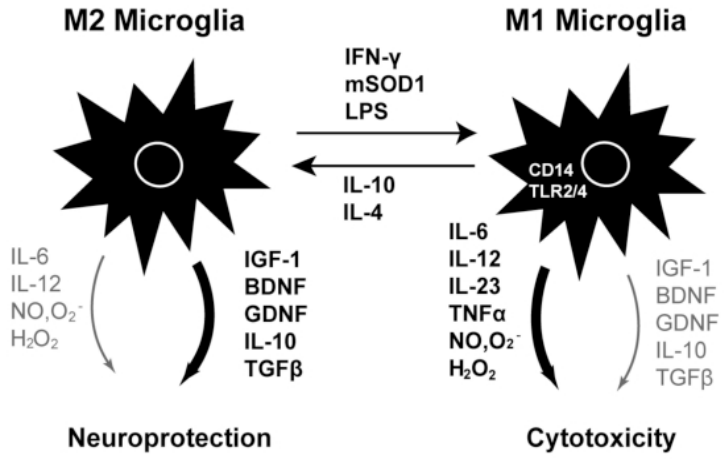


**Fig. 14: microglia activation states [mod. from Appel S. H. et al., 2011]**

In physiological condition, after the treat removal, M1 state is followed by M2 state that drives the resolution of the neuroinflammatory process through the secretion of anti-inflammatory cytokines, and the repair of tissue damages through the secretion of trophic factors like brain derived neurotrophic factor (BDNF), insulin-like growth factor 1 (IGF-1) and TGF-β [Appel S. H. et al., 2011]. In pathological conditions, like neurodegenerative diseases, the M1-M2 transition results impaired by the sustained neuronal death and the production and accumulation of misfolded proteins, leading to a chronic M1 state that results neurotoxic. Furthermore, long term exposure to a proinflammatory microenvironment not only affect neurons but can also cause detrimental effects on microglial functions inhibiting the phagocytosis of pathologic protein aggregates [Heneka M. T. et al., 2014]. Microglia are key elements in modulating neuroinflammatory processes favouring the progression of neurodegeneration (see Fig. 15), however, the clinical use of anti-inflammatory drugs or of other therapeutic molecules able to modulate the degree of microglial activation is still controversial. Indeed, clinical trials aimed reducing neuroinflammation to treat neurodegenerative disorders have always failed to produce significant clinical outcomes, even reporting, in some cases, the worsening of the course of the disease probably by the inhibition of the initial positive effect of neuroinflammation [Esposito E. et al., 2007; Howard R. et al., 2019].

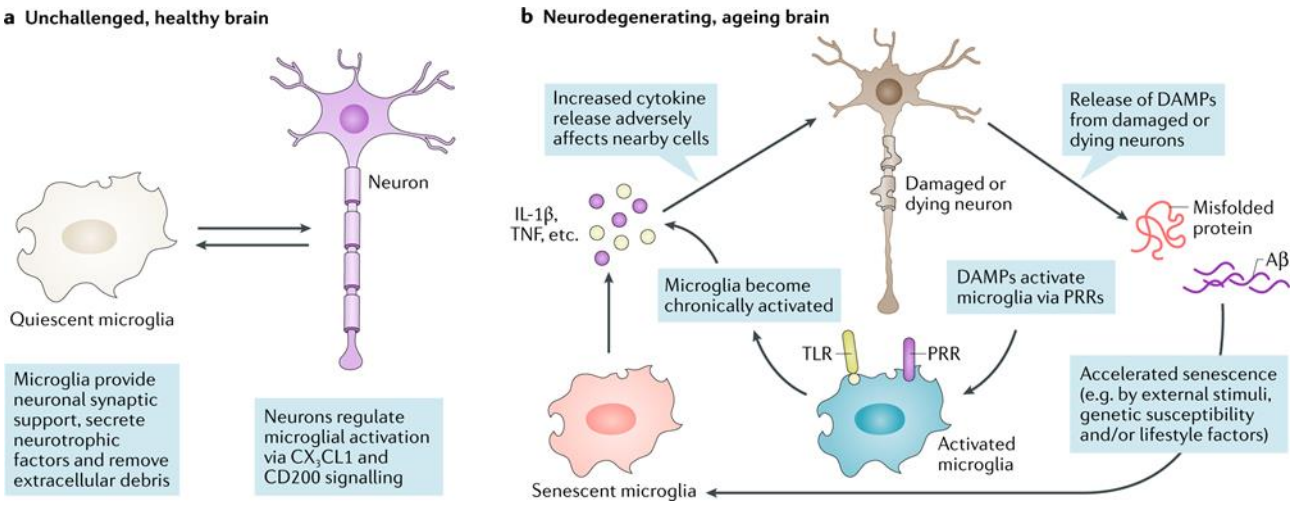


**Fig. 15: microglia-neuron crosstalk in health and disease [Heneka M. T. et al., 2018]**

## 2.3. Astrocytes in neuroinflammation

Astrocytes are the major resident glial cell population of the CNS. They are a fundamental component of the BBB, contributing to the neuro-vascular coupling, the selective transfer of nutrients and metabolites between the blood and neurons and they are involved in a continuous interplay with the other CNS cells through direct connections (i.e. GJs) or *via* the release a wide array of signalling molecules including neurotransmitters, hormones, metabolic and trophic factors [Verkhratsky A. et

al., 2016]. Astrocytes are integral elements involved in synaptic function as a part of the so called "tripartite synapse", constituted by an interneuronal synapse enwrapped by an astrocytic process. The intimate connection of astrocytes with the synaptic cleft allows them to sense the release of neurotransmitters, buffering the excess of glutamate and ions avoiding excitotoxic neuronal damage, and modulate neuronal signalling through the release of gliotransmitters [Allen N. J. et al., 2017].

Given the complexity of those functions, their involvement in neuroinflammatory processes can consequently have a profound impact on CNS homeostasis. One of the most common hallmark of astrocyte reactivity to an inflammatory environment is astrogliosis, defined as an hyperproliferation of these cells at the level of the injured area, experimentally revealed by the local increased expression of glial fibrillary acidic protein (GFAP), a cytoskeletal protein commonly used as astrocytic marker. Despite astrogliosis is an adaptive process with protective functions essential for tissue repair, it can also have detrimental effects when driven by context-inappropriate signalling interactions [Sofroniew M. V., 2018]. As an example, despite the formation of the astrocytic scar in SCI is essential for restricting the infiltration of inflammatory cells at the site of damage, limiting an uncontrolled diffusion of the inflammatory process, it also represent a physical barrier to axonal regeneration [Yang T. et al., 2020].

Inflammatory and immune responses in the CNS are commonly attributed to microglia, but they have been recognized as important functional properties of astrocytes [Quincozes-Santos A. et al., 2021] which express PRRs, including TLR-4 and NOD-like receptors 1-2 [Farina C. et al., 2007], MHC class II and the adhesion molecule ICAM-1 necessary for the antigen presentation to T lymphocytes [Dong Y. et al., 2001]. In addition, astrocytes secrete a wide range of cytokines and chemokines. In fact, they are characterized by distinct cytokine secretomic profiles in control condition and upon proinflammatory stimulation *in vitro* and *in vivo*. As an example, purified human unstimulated astrocytes tend to secrete G-CSF, GM-CSF, CCL2, IL-6, CXCL8, CXCL1, Serpin E1 and MIF, while the stimulation with IL-1β and TNF-α can induce them to secrete IL-1β, IL-1ra, TNF-α, CXCL10, CCL5, CCL3 through the activation of the NF-κB pathway, and increases the expression of ICAM1 and several complement proteins [Choi S. S. et al., 2014].

Recently, pioneering studies conducted by Ben Barres and colleagues revealed that, similarly to what happens with microglia, the inflammatory molecular milieu can drive astrocyte reactivity to two possible main activation states: the so called A1 and A2, both characterized by distinct functions, profiles of markers expression and patterns of cytokines secretion (see Fig. 16). Particularly, while A2 astrocytes display a neuroprotective phenotype upregulating many neurotrophic factors, A1 astrocytes are induced by LPS-activated microglia through the secretion of IL-1α, TNF-α and C1q and exert a strong toxic effect for neurons and oligodendrocytes [Liddelow S. A. et al., 2017].

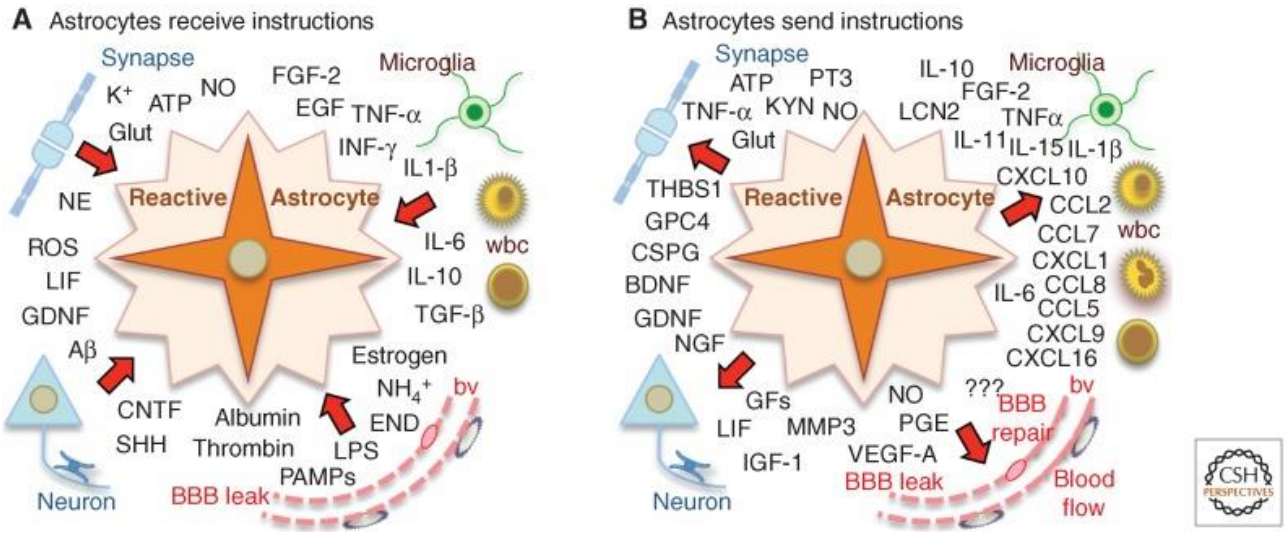


**Fig. 16: received and sent molecular signals that characterize reactive astrocytes activity and their relation with the other CNS cells [Sofroniew M. V., 2014]**

One of the more relevant approaches in the study of astrocytes biology is the advent of calcium imaging techniques in the 1990s, which challenged the view that neurons are the only active cells in CNS information/integration tasks, revealing that astrocytes can respond to environmental and neuronal stimuli with intracellular $Ca^{2+}$ oscillation [Durkee C. A. et al., 2020]. In 1990, Ann Cornell-Bell and colleagues, using the fluorescent calcium indicator fluo-3, provide first evidence of this process revealing that cultured hippocampal astrocytes can respond to glutamate with an elevation of intracellular $Ca^{2+}$, hypothesizing that propagating calcium waves through an astrocytes network could serves as a long-range signalling system in the CNS [Cornell-Bell A. H. et al., 1990]. Since then, accumulating evidence have linked astrocytic calcium activity with neural information integration, synaptic modulation, plasticity and metabolic functions in physiological conditions. The mechanisms underlying the generation and propagation of calcium signals are very complex and, yet, not completely understood. These signals emerge from the fine tuning of the mobilization of intracellular $Ca^{2+}$ stores (endoplasmic reticulum and mitochondria) through the activation of several types of Gq-protein coupled receptors (GqPCRs) via IP3Rs pathway, as well as the contribution of extracellular $Ca^{2+}$, whose influx is regulated by the opening of several types of channels including glutamate receptors, GABA receptors, TRP channels and P2X purinergic receptors [Shigetomi E. et al., 2019]. Furthermore, it seems that propagation of astrocyte $Ca^{2+}$ waves be mediated by Cx43 GJs while the synchronization with distal cell is mediated by eATP released from volume-regulated anion channels and acting on P2 receptors (see Fig. 17) [Scemes E. et al., 2000; Fujii Y. et al., 2017].

Interestingly, reactive astrocytes are characterized by anomalous $Ca^{2+}$ signals that, in most cases, show increased amplitude, duration and frequency [Shigetomi E. et al., 2019] a fact due to the modulatory effect of cytokines and chemokines on key $Ca^{2+}$ signalling-related proteins.

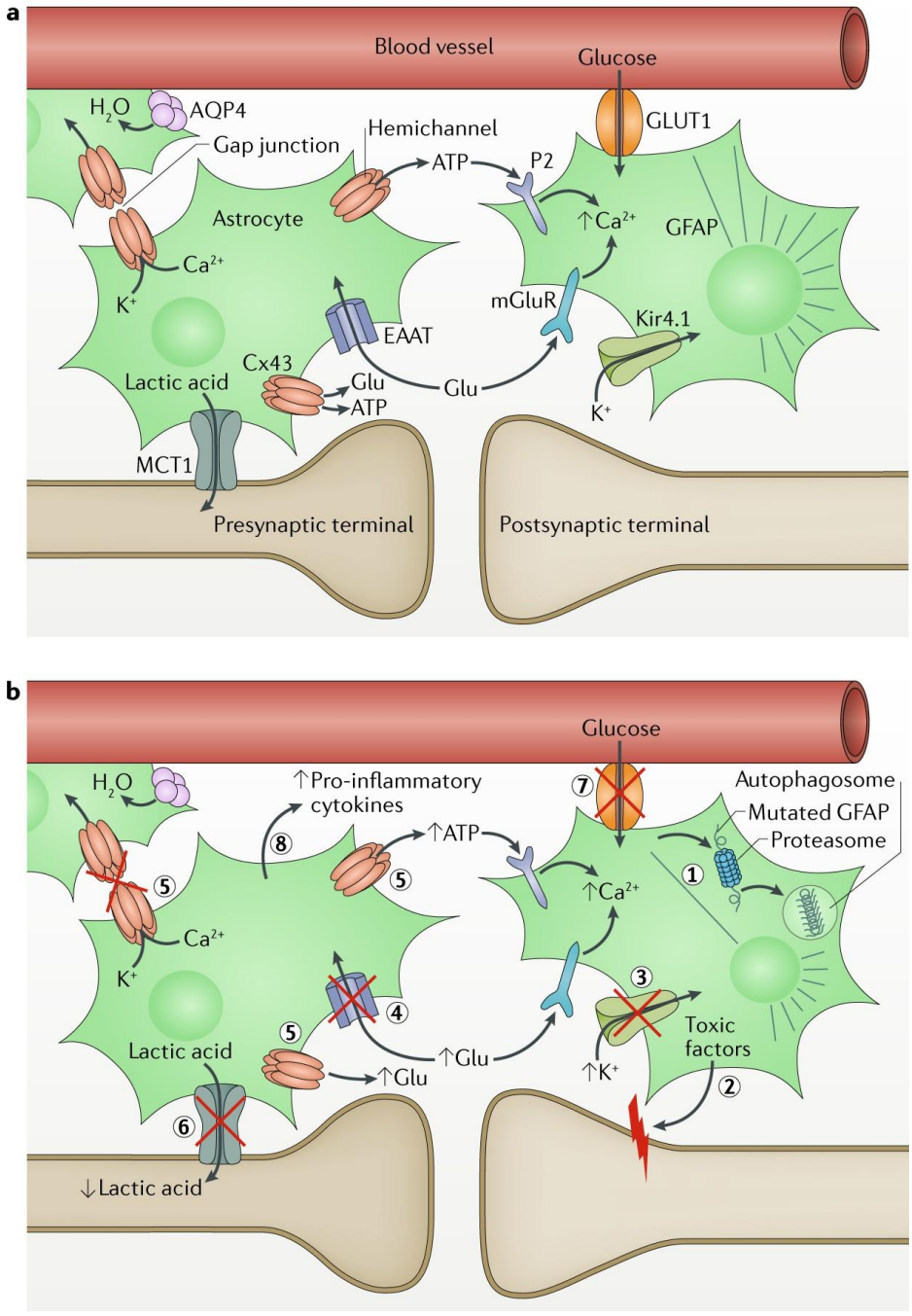


**Fig. 17: astrocytic $Ca^{2+}$ signals modulation in health and disease [Almad A. et al., 2018]**

Indeed, IL-1β decreases Cx43 junctional conductance through GJs uncoupling, down-regulates Cx43 mRNA expression while potentiating calcium waves via the purinergic-mediated pathway through the increase of eATP and P2 receptor expression [John G. R. et al., 1999] and the stimulation of astrocytic P2Y1 receptor by ATP (released by LPS-stimulated microglia) increases excitatory

postsynaptic current frequency in acute hippocampal slices, through a metabotropic glutamate receptor 5-dependent mechanism [Pascual O. et al., 2012] suggesting a role of $Ca^{2+}$ oscillation-dependent gliotransmitters release in the synaptopathy associated with neuroinflammatory diseases. In fact, one of our recent work documents an increase in the frequency and a decrease in the synchronization of astrocytic $Ca^{2+}$ events associated with augmented frequency of postsynaptic currents in mouse spinal cord organotypic slices when stimulated with LPS or with a cytokines cocktail containing IL-1β, TNF-α and GM-CSF. Interestingly, such phenomena seem to be linked to an impairment in Cx43 GJs function and to the opening of membrane uncoupled Cx43 hemichannels, suggesting differential roles for connexin-based protein structures during neuroinflammation [Panattoni G. et al., 2021].

## 2.4. Oligodendrocytes in neuroinflammation

Oligodendrocytes are the myelinating cells of the CNS. Myelin consist in multiple oligodendrocyte membrane wrapping around the axons, which provides the high electrical resistance and the low capacitance essential for a fast saltatory conduction of nerve impulses. Thanks to this close structural coupling, oligodendrocytes also contribute to axonal integrity and provide metabolic support necessary to axonal sustained firing. On average, every oligodendrocytes generates between 20 and 60 myelinating processes, enveloping as many axons with up to 100 membrane turns [Simons M. et al., 2016]. The correct myelination of neuronal axons is a crucial process in CNS development that requires a fine regulation driven by several molecular cues, susceptible of changing in the molecular microenvironment, thus easily perturbed by proinflammatory signals. This process continues through the entire lifetime, ensuring the continue renewal of myelin through a high metabolic expenditure required for the synthesis of new membrane lipids, resulting in a potential oxidative stress. Given their delicate role in maintaining CNS functionality, oligodendrocytes are considered one of the more vulnerable cell types to the inflammatory damage [Bradl M. et al., 2010]. Indeed, they express a wide range of receptors that make them susceptible to glutamate excitotoxicity, like AMPA, kainate, and NMDA receptors, which are needed to their functional coupling with neuronal activity, and the P2X7 receptors which predisposes them to the damaging action of sustained levels of eATP. Oligodendrocyte loss can also occur by direct inflammatory cytokines exposure. Particularly, TNF-α can induce apoptosis of oligodendrocytes by binding to its receptor and activation of caspase mediated pathway (see Fig. 18) [Zeis T. et al., 2015].

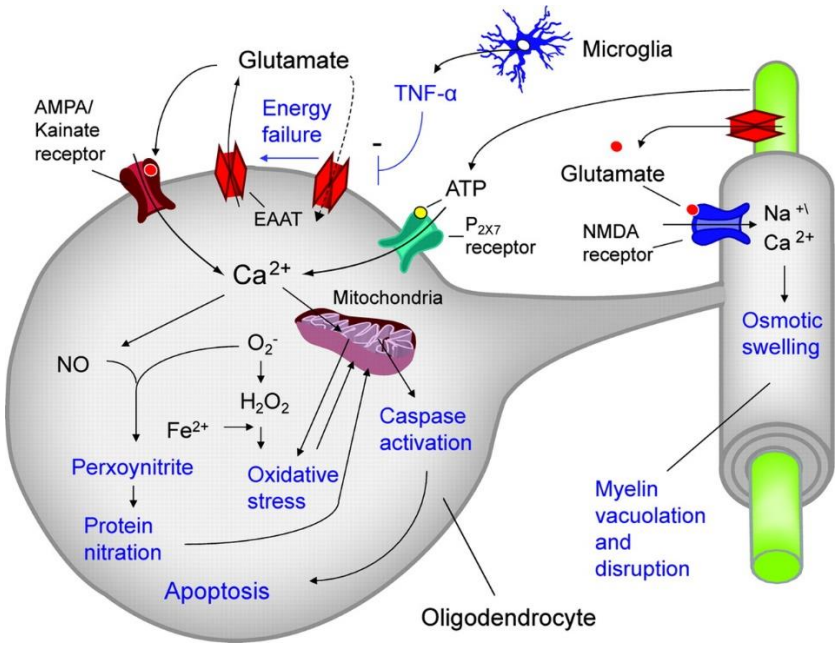


**Fig. 18: oligodendrocytes vulnerability factors [Benarroch E. E., 2009]**

Interestingly, far from being mere passive spectators in the neuroinflammatory microenvironment, oligodendrocytes are also able to produce immunomodulatory factors. Particularly, they express various cytokines and chemokines including IL-1β, IL-17, CCL2, CXCL10 and antigen presenting molecules (MHC class I and II) [Zeis T. et al., 2015; Kirby L. et al., 2021].

Furthermore, oligodendrocytes express different connexin types including Cx29, Cx32, and Cx47. They use to form homotypic GJs with other oligodendrocytes and heterotypic GJs composed of Cx47-Cx43 with astrocytic Cx43 hemichannels. Both types of junctions play a pivotal role in myelinating processes and in forming a functional glial syncytium supporting the buffering of extracellular $K^+$ and metabolic supply to axons [Papaneophytou C. et al., 2019].

# -3-
# The spinal cord neuroinflammation

The spinal cord is a fundamental component of the CNS which extends caudally from the brain stem, protected by the bony structures of the vertebral column and coated by the three meninges: the dura mater, the arachnoid and the innermost pia mater. It is a highly specialized structure evolved to relay signals between the periphery and the brain, transmitting sensory information and organizing complex motor behaviours and visceral functions [Watson C. et al., 2008]. Furthermore, far from being a mere passive gateway between the brain and the environment, the spinal cord may also manage autonomously reflex actions and rhythmic motor activity, thanks to its own complex neuronal circuitry and central pattern generators [Leung B. et al., 2019].

Given its complex role in coordinating visceral functions and mediating an efficient interaction with the environment, alteration in spinal cord functions, as seen in many disorders like spinal cord injury and ALS, are inevitably accompanied by a significant loss of quality of life for patients and by an enormous socio-economic burden for the society [James S. L. et al., 2019].

Neuroinflammation is a fundamental process accompanying the spinal cord neuropathologies, driving the evolution of diseases and often hampering a correct tissue healing and a complete recovery. As such, neuroinflammation has become rapidly a promising therapeutic target for treating CNS disorders, including spinal cord ones [Gilhus, N. E. et al., 2019].

## 3.1. Structural organization

From the point of view of the gross anatomy, the spinal cord is essentially organized in segments. Each segment (31 in humans) corresponds to a pair of spinal nerves connected to the cord by a series of dorsal and ventral rootlets. Dorsal rootlets are composed by afferent fibres constituted by sensory neurons, whose cell bodies form the dorsal roots ganglia (DRG). Ventral rootlets are composed by efferent fibres constituted by motoneurons and preganglionic autonomic neurons whose cell bodies are located in the ventral horns of the spinal grey matter (see Fig. 19). Each spinal nerve collects all the fibres that innervates a precise area of the body [Standring S., 2016].

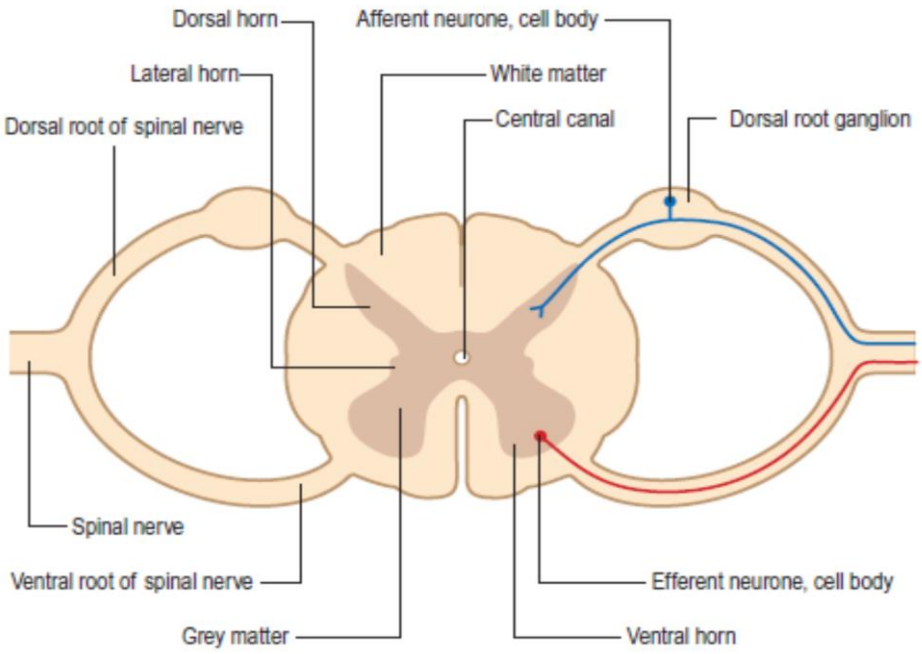


**Fig. 19: transverse section of the spinal cord [Standring S., 2016]**

The transverse section of the spinal cord reveals its internal organization consisting in a H shaped inner area of grey matter, surrounded by the white matter.

The grey matter is mainly composed by neuronal bodies which receive termination from primary afferent and efferent neurons as well as by interneurons. It is classically divided into ten zones called Rexed's laminae which are characterized by distinct cytoarchitectural features. Commonly, the laminae are further classified into three groups: the sensory dorsal horn (laminae I-VI), the intermediate grey (lamina VII), and the ventral horn (VII-IX) with motoneurons located in lamina IX (see Fig. 20) [Drake R. L. et al., 2020].

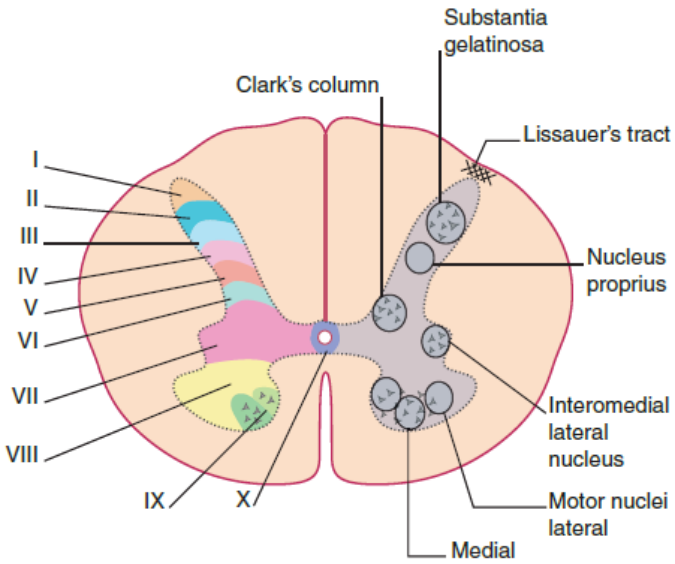


**Fig. 20: Rexed's laminae organization of the grey matter [Drake R. L. et al., 2020]**

The white matter is composed mainly by ascending and descending myelinated fibres organized in columns. Ascending spino-encephalic tracts are mainly located dorsally and laterally and convey sensory inputs associated with the sense of touch, pressure, proprioception and vibration, through large myelinated fibres from the periphery to the encephalic structures for superior elaboration processes. Descending cortico-spinal tracts are mainly located ventrolaterally and ventrally, and convey outputs from encephalic structures to effector organs and muscles. These tracts are also called pyramidal or extrapyramidal tracts, depending on their cortical or subcortical origin, and they are made of cortical motoneurons involved essentially in the regulation of fine movements and other types of complex motor behaviors such as postural control and locomotion (see Fig. 21) [Guertin P. A., 2013].

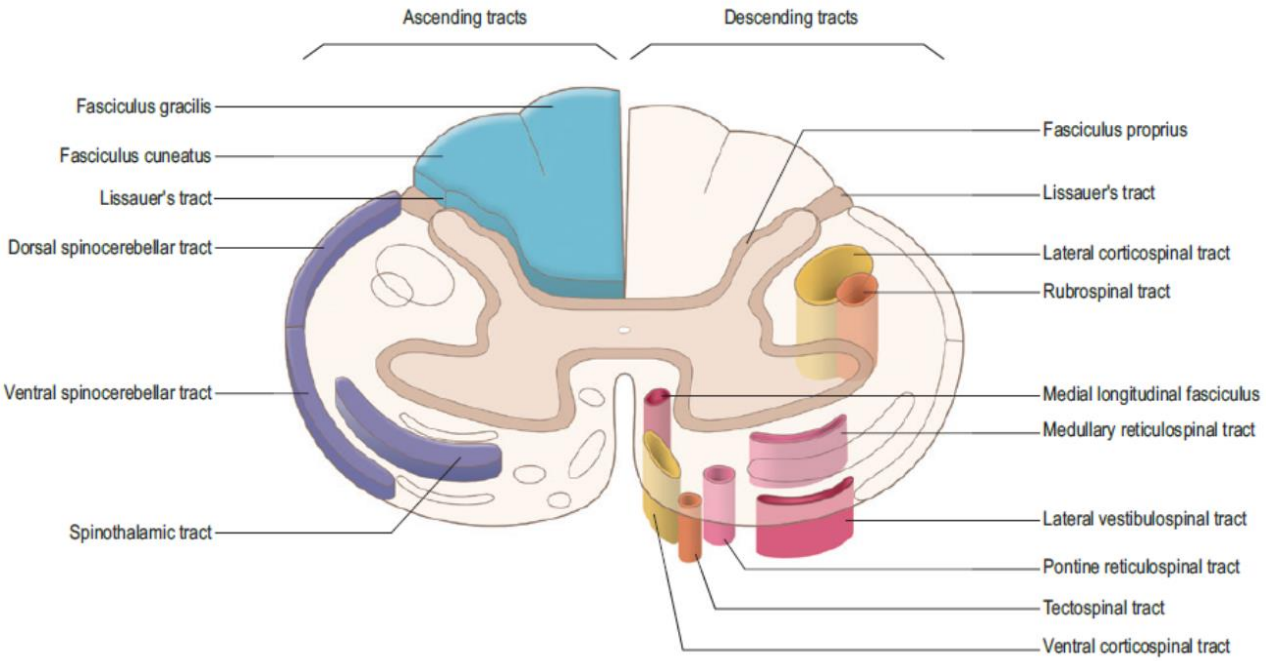


**Fig. 21: columnar organization of the white matter [Drake R. L. et al., 2020]**

## 3.2. Cellular organization and circuitry

The cellular organization of the mature spinal cord, emerges from a precise cell types patterning that is specified during early embryonic life. The complex spinal circuitry development requires a high spatial-temporal coordination aiming to orchestrate the correct positioning and wiring of a wide range of cellular identities. This complexity is well exemplified by the fact that various glial cell precursors and more than 20 distinct embryonic neuronal classes have been identify in the developing spinal cord. In mammals, those cells locate and differentiate during development along the three basic spatial axes of the embryonic body plan: rostro-caudal, dorsal-ventral and medio-lateral. The plan specification is mainly allowed by the action of specific growth factors [Lu D. C. et al., 2015]. Briefly:

- Rostro-caudal axis development is orchestrated by opposing gradients of fibroblast growth factor (FGF) whit caudalizing effect and retinoic acid (RA) with rostralizing effect
- Dorsal-ventral axis development is orchestrated mainly by the ventralizing effect of Sonic hedgehog (Shh) protein produced by the floorplate, and by the dorsalizing effect of bone morphogenetic proteins (BMPs) and by Wnt protein family produced from the roof plate
- Medio-lateral axis development is regulated by the division and migration plane of progenitor cells that are located adjacent to the lumen of the neural tube (medially), organized in a way that allow differentiating progeny migrate laterally

During this process, the so called neural progenitors cells (NPCs) and radial glia cells will then give rise to the various neural and glial population of the spinal cord, briefly described as follows:

***Neuronal spinal populations*:** the spinal cord hosts three neuronal macroclasses: the motoneurons, the interneurons and the sensory neurons, which are further classified in different subpopulation. Particularly, motoneurons are classified in somatic α motoneurons of the medial and lateral motor column, which provide the innervation of skeletal muscles, β motoneurons, a poorly characterized class which has been found to innervate both intrafusal and extrafusal muscle fibers, γ motoneurons, which innervate intrafusal fibers of the muscle spindles providing the structural basis of proprioception, and preganglionic motoneurons of the autonomic nervous system. These subtypes are further characterized by the expression of additional transcription factors which drive the guidance of axons to the target and the establishment of proper connectivity with sensory neurons and interneurons: a fundamental requirement for the precise anatomical organization of motor circuitry. Notably, motoneurons are basically excitatory and use acetylcholine as main neurotransmitter at their synapses [Lu D. C. et al., 2015]. Furthermore, seems that this neuronal class can arise from a peculiar precursor cell type, the so called motoneuron-oligodendrocyte precursors (MNOPs), which can be found exclusively in the developing spinal microenvironment and that can originate both oligodendrocytes and motoneurons [Martins-Macedo J. et al. 2021].
Interneurons are surely the most variegate neuronal population in the spinal cord, counting over 20 subtypes which have unique electrophysiological signature, behavioural output, expression of transcription proteins and types of neurotransmitter signalling. Their cell bodies and axons are located in the Rexed's laminae of the spinal grey matter, where they help in the integration of sensory-motor signals and form complex neural networks called central patter generators (CPGs) that can generate autonomously rhythmic motor activity in absence of descending afferent inputs to the spinal cord

[Côté M. P. et al., 2018]. Traditionally, they are broadly classified in ventral (V) interneurons, further subdivided in V0, V1 (also known as Renshaw cells), V2, and V3 subpopulations, mainly associated with motor function, and dorsal interneurons (dI), further subdivided in dI1-6, $dIL_A$ and $dIL_B$ subpopulations, mainly associated with sensory processing (see Fig. 22) [Stifani N. et al., 2014].
Notably, interneurons present a great variability in terms of used neurotransmitters. Indeed, given their modulatory function, they can establish both excitatory and inhibitory synapses with target cells. Generally, while excitatory interneuron use glutamate, in inhibitory synapses both GABA and glycine can be found. Interestingly, during embryonic development GABA and glycine act as excitatory neurotransmitters, able to depolarize the target cell and even trigger action potentials. The ratio between GABAergic and glycinergic neurons also changes during development. For example, mouse spinal interneurons express higher level of GABA, particularly in the ventral horn, during the first half of embryonic life while at E13, a higher number of glycinergic interneurons have been found [Sibilla S. et al., 2009]. This shift has been proven to take place through two main mechanisms: the loss of GABAergic synapses and the decrease in GABA synthesis in the synapses where both GABA and glycine are co-released. These mechanisms are thought to play a pivotal role in the activity-dependent development of synapses and also to promote the proper wiring by triggering spontaneous rhythmic activity in motor networks [Nabekura J. et al., 2004].

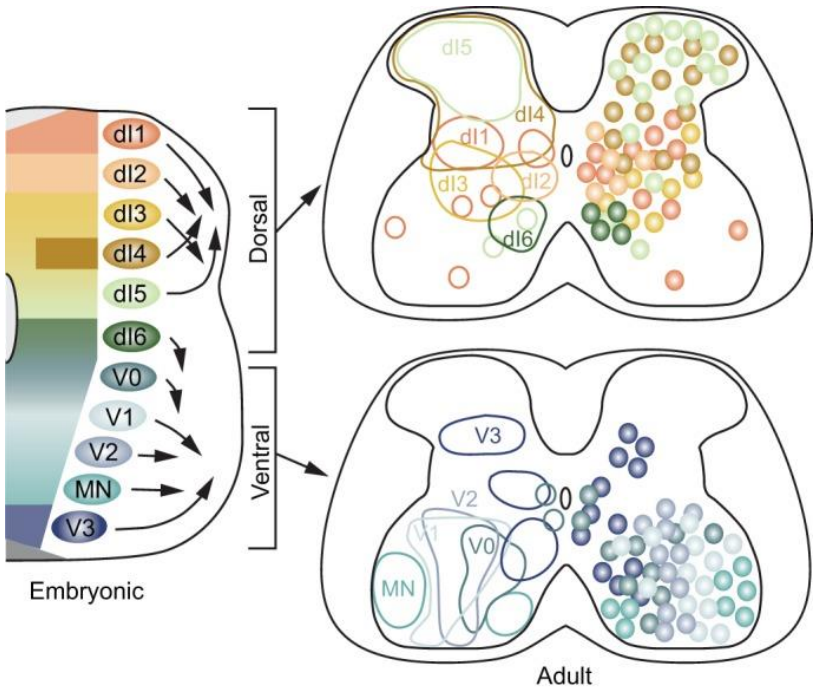


**Fig. 22: interneurons subpopulation and their distribution [Lai H. C. et al., 2016]**

Somatosensory neurons are pseudo-unipolar neurons characterized by cell bodies located in the dorsal root ganglia (DRGs) and a single bifurcated axon projecting in two directions: to the periphery and to the spinal cord. Somatosensory neurons can be classified in specific subpopulations. Historically they have been firstly classified in four general fibre types: Aα (mainly responsible for proprioception), Aβ (mainly responsible for mechanoception), Aδ and C (both responsible for nociception) based on cell body dimension, myelination degree, types of afferent endings and types of transmitters used [Lai H. C. et al., 2016]. However, the recent advent of more sophisticated molecular biology techniques revealed a higher diversity that highlights the specialization in the conduction of a particular sensory modality. From this point of view, the somatosensory neurons can be classified in chemoreceptors, thermoreceptors, mechanoreceptors and nociceptors, but further and more detailed classification systems based on specific genetic o protein signatures are now available [Le Pichon T. et al., 2014]. This neuronal type exhibits the greater variety of neurotransmitters among spinal neurons, including acetylcholine, monoamines, GABA, glycine, glutamate, endogenous cannabinoids and various neuropeptides like enkephalins and dynorphins, which allows the fine tuning required to discern precisely the environmental stimuli [Yam M. F. et al., 2018].

The precise control of motor and other effector functions to respond properly to such stimuli is performed by complex circuitry systems that involves the integration of the functions of all these neuronal types and often requires the superior elaboration of encephalic structures. Interestingly, the spinal cord is able to manage autonomously two main types of propriospinal neural circuits: reflexes and CPGs. Reflexes represent the simplest form of spinal circuit. They consist in relatively simple and local neural pathways (without cortical involvement) involving one (monosynaptic), two (disynaptic), or more (polysynaptic) synapses between neurons within one or two spinal segments. As an example, the basic monosynaptic reflex consists in a direct synapse between a somatosensory neuron and an α motorneuron, which allow a fast, involuntary and stereotyped response to a potentially noxious stimulus (see Fig. 23). Other reflexes involve autonomic neurons that generate visceral responses, like the aortic baroreflex for the regulation of blood pressure. On the other hand, CPGs represent the most complex intrinsic neuronal networks in the spinal cord. Although their structural and functional organizations is still not completely characterized, is known that they are composed by neurons with peculiar electrophysiological properties that enable them to generate a basic rhythmic electric activity, coordinating the firing pattern of multiple motoneuron pools, in order to produce rhythmic motor activities like walking, swimming, flying, micturing, breathing and chewing [Guertin P. A., 2013].

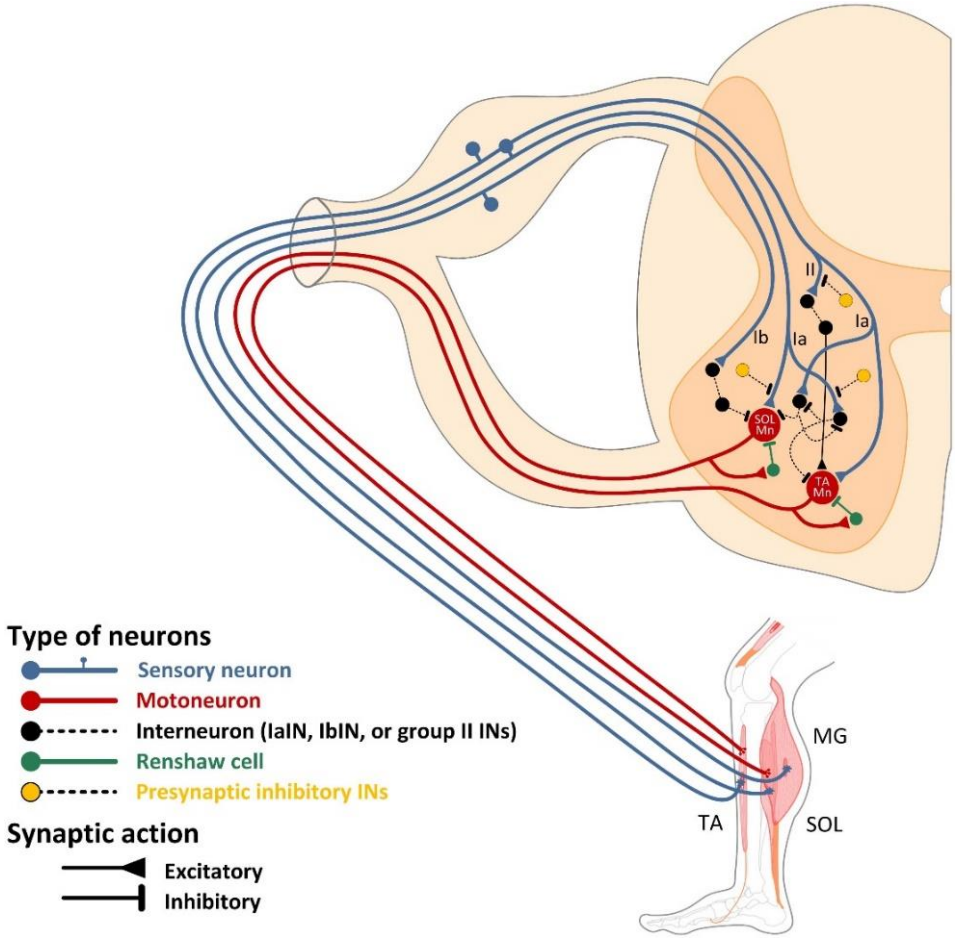


**Fig. 23: basic spinal cord circuitry [Côté M. P. et al., 2018]**

***Gliogenesis*:** since the neuron-glia crosstalk represents a fundamental feature for maintaining the normal function of the mature CNS, the establishment of fully functional neural circuitry requires also the correct spatial-temporal development of glial cells. In vertebrates, the generation and development of neuronal and glial cells arises sequentially. Particularly, while neuronal differentiation starts during early embryonic life, glial differentiation and axon myelination occurs later and continue also postnatally [Martins-Macedo J. et al. 2021]. Like neurons, glial cells are generated by two precursor cell types: NPCs and radial glia, which respond to appropriate biochemical stimuli that drive the specification of their differentiation path. In the spinal cord, the generation of glial cells is mainly driven by the generation of several intermediate precursors from NPCs, which have a restricted differentiation potential towards glia. Those cells, found both in rodents and humans, are commonly called glioblast or glial-restricted precursors (GRPs) and can differentiate into oligodendrocytes and two distinct astrocyte populations. Particularly, their exposure to precise sets of growth factors, induces their differentiation into type I (A2B5−/GFAP+) protoplasmic astrocytes, or in oligodendrocyte and Type-2 astrocyte precursors (O2A) that can

differentiate in myelinating oligodendrocytes or type II (A2B5+/GFAP+) fibrous astrocytes (see Fig. 24) [Rao M. S. et al., 1998].

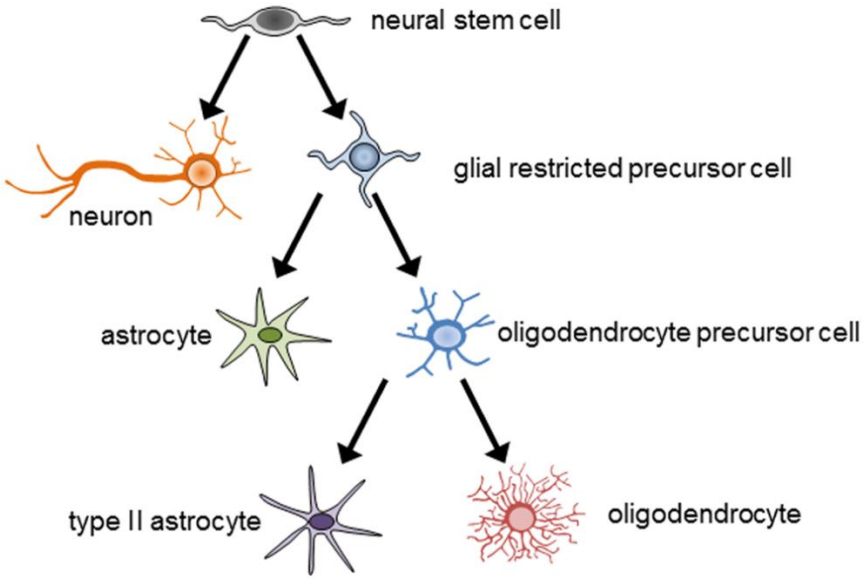


**Fig. 24: neural stem cells differentiation paths [Miller R. H., 2014]**

***Oligodendrocytes*:** during spinal cord development, the majority of oligodendrocytes are generated in a specialized area of the ventral ventricular zone, which first gives rise to motor neuron precursors, and then, to OPCs that finally differentiate into myelin-forming oligodendrocytes. In a later phase, an additional source of OPCs arises in the dorsal spinal cord, contributing to the myelination of the dorsal sensory area [Bradl et al., 2010].

***Astrocytes*:** despite a vast array of diverse neuronal subtypes been defined, less is known about astrocytes diversity. From an embryo-morphological point of view, two main types of astrocytes have been identified: protoplasmic astrocytes (type I), characterized by a bushy morphology and by their role in constituting the neurovascular unit (NVU), and fibrous astrocytes (type II), mainly located in the with matter and characterized by thinner and longer processes [Tabata H., 2015]. Apart from this broad distinction, the functional diversity and circuit specificity of astrocytes is poorly understood. However, recently, the advent of more sophisticated microscopy and molecular biology techniques are starting to dissect this topic. For example, a recent work from Mira Kronschläger and colleagues tried to uncover the astrocytes diversity in the rat spinal dorsal horn. Their data showed that astrocytes in the laminae L1 and L2 of were characterized by a peculiar electrophysiological activity and a higher expression of GFAP, Cx43 and GLAST, resulting in a better coupling strength compared to astrocytes in L3 [Kronschläger M. T. et al., 2021].

***Microglia*:** unlike the other glial cell types, microglia derive from primitive myeloid progenitors that originate from the extraembryonic yolk sac and start to colonize the neural tube after the beginning of the neurogenesis [Prinz M. et al., 2014]. While in the past has been speculated that microglial colonization of the CNS was stimulated by the physiological neuronal death during embryos development, subsequent studies performed using embryonic tissues, revealed that this event correspond with the beginning of spinal cord vascularization and it's promoted by the expression of ICAM adhesion proteins on endothelial cells membrane both in humans and in mice [Rezaie et al., 1999]. Particularly, in mice this process occurs at E9-E11 and continue until E14. This developmental period is characterized by the onset of functional spinal cord network synaptogenesis, supporting the idea that microglial cells are essential players in the development of spinal neuronal wiring [Rigato C. et al., 2011].

## 3.3. Spinal cord neuroinflammatory conditions

Physiological spinal cord development and function can be affected by diverse diseases during the lifespan. Despite the diversity of clinical presentation that characterize each disorder, made unique by peculiar dysfunctional neuron-glia crosstalk modalities, neuroinflammation remains their common pathologic hallmark. Following, a selection of major inflammatory spinal cord disorder and related physiopathological mechanisms with a particular focus on glial cells dysfunctions:

***Spinal cord injury (SCI)***: the term SCI refers to a damage to the spinal cord that occurs as a result of a traumatic event that temporarily or permanently causes changes in its function [Ahuja C. S. et al., 2017]. It affects between 250.000 and 500.000 every year causing a significant decrease in patient's quality of life, predispose to multiple comorbidities and rise an enormous socio-economic burden for the patients, its family and the healthcare system [who.int]. Despite the recent extraordinary advent of implanted epidural electrical stimulation devices have shown to restore basic walking functions in SCI patients [Rowald A. et al., 2022], the search of pharmacological interventions able to allow a complete physiological healing of the injured spinal tissue is still active.

From a pathophysiological point of view, SCI is characterized by the loss of synaptic connections, demyelination and axon damage that disrupt neural signal transmission. Mechanically injured neurons undergo cell death that cause the loss of spinal cord functions. Proinflammatory molecular signals derived from the primary injury promotes a secondary cascade of vascular and biochemical events that amplify the disruption of neuronal function. During these primary and secondary injury events, the reaction of glial cells is a pivotal event underlying endogenous both pathological and reparative processes [Orr M. B. et al., 2018]. During SCI acute phase, ischaemic processes and

excitotoxicity are the major contributors to the loss of intracellular and extracellular ionic homeostasis. Particularly, intracellular calcium dysregulation has shown to be a key mediator of cell death in both neurons and glia. Furthermore, the ongoing cell necrosis due to ischaemia, inflammation and excitotoxicity cause the massive release of DAMPs like ATP, nucleic acids and HSPs that activate microglial cells, stimulating the release of proinflammatory cytokines and promoting the infiltration [Ahuja C. S. et al., 2017]. Furthermore, the formation of the astrocytic scar is considered the critical event in interfering with axonal regeneration in SCI [Sofroniew M. V., 2014]. Interestingly, despite encouraging preclinical studies have suggested the possible efficacy of several small molecules targeting $Ca^{2+}$ mediated signalling (e.g. nimodipine), excitotoxicity (e.g. gacyclidine and riluzole) and microglial M1-M2 transition (e.g. minocycline), only methylprednisolone sodium succinate have later shown a good, even if not resolutive, neuroprotective activity in phase III clinical studies, further confirming the central role of non-cell autonomous neuroinflammation in SCI sequelae [Baptiste D. C. et al., 2008].

***Multiple sclerosis (MS)***: MS represents the prototypical chronic inflammatory spinal cord disorder, currently classified in two main subtypes based on clinical presentation: relapsing-remitting subtype and progressive subtypes. The pathological hallmark of MS is represented by the progressive accumulation of demyelinating lesions affecting the brain and the spinal cord functions, driving axonal degeneration phenomena and the consequent motor and cognitive symptomatology [Filippi M. et al., 2018]. It's based on well characterized Th-1/Th-17 autoimmune mechanisms, elicited by various environmental risk factors among which, past viral infections have recently shown to play a major role through a molecular mimicry mechanism [Bjornevik K et al., 2022]. Demyelinating processes are carried out by myelin-reactive T lymphocytes and are histologically characterized by an inflammatory microenvironment driven by the secretion of proinflammatory cytokines like TNF-α, IL-1β, IFN-γ, IL-17 and GM-CSF that heavily influence glial cells reactivity. Indeed, in the initial phases of the disease, microglia activation results essential in promoting remyelinating processes through the removal of myelin debris and the secretion of trophic factors, but the persistence of the inflammatory state due to the continuous oligodendrocytes loss, turns microglia in a neurotoxic phenotypes aggravating the course of the disease [Wilbanks B. et al., 2019]. Furthermore, recently, also astrocytes have been recognized as critical players in the development of MS lesions. Interestingly, reactive astrocytes found at the level of the lesions are characterized by myelin debris cytoplasmic inclusions, increased NF-κB signalling and increased expression of chemokines, cell adhesion molecules for immune cells recruitment, MHC II, CD80 and C86 suggesting that they may have a role in myelin antigen presentation to T lymphocytes [Ponath G. et al., 2018].

***Amyotrophic lateral sclerosis (ALS)***: ALS is the most common motorneuron disease, characterized by fast progression neurodegeneration and death upon 3-5 years upon diagnosis. Several genetic mutations have been correlated with hereditable as well as sporadic forms of ALS, of which TDP-43, SOD1, C9ORF72 and FUS are the most common [Ban J. et al., 2019]. Despite the heterogeneity of the genetic background, all these varieties are characterized by the progressive death of spino-bulbar and cortico-spinal motoneurons that causes the severe motor impairment that involves all the skeletal muscles, while some varieties (particularly those which carries C9ORF72 and TDP-43 mutations) are also associated with a form of frontotemporal dementia [van Es M. A. et al., 2017]. Neurodegeneration seems to be due to various cellular mechanisms that are implicated in a progressive loss of motorneuronal function, the involvement of reactive glial cells and, during the late stage of the disease, infiltrating peripheral lymphocytes. The main cellular mechanisms responsible for neuronal loss include oxidative stress, altered RNA metabolism, mitochondrial dysfunction, axoplasmatic transport impairment and excitotoxicity [Le Gall L. et al., 2020]. Furthermore, neuronal damage and the accumulation of toxic misfolded proteins in CNS resident cells are able to elicit neuroinflammatory processes that drive ALS progression. Indeed, the inflammation degree is strictly associated with ALS stages. During the initial phase, the slow progression of symptoms is allowed by the equilibrium between neuronal damage and microglia M2 phenotype activity that promotes neural tissue repair, while, as the disease progress, the accumulation of misfolded proteins and DAMPs from dying cells promotes the transition to M1 microglia phenotype, an event that correspond to the onset of a more aggressive symptomatic progress in patients. Microglia transition to M1 activation state in ALS have shown to be regulated mainly by the activation of CD14, TLR-2, TLR-4 and P2X7R [Liu J. et al., 2017].

## 3.4. Organotypic spinal cord cultures

Organotypic cultures is one of the most popular and attractive experimental model for neurobiological studies. Since their introduction in 1981, following the works of B. H. Gähwiler who first carried out explant cultures from different regions of the brain, they gain the attention of the scientific community due to the many advantages that they offer over other simpler model systems like dissociated cultures [Pandamooz S. et al., 2016]. Particularly, they maintain the original cellular organization and functionality of the tissue and they are long-lived systems able to reproduce the developmental feature of the original organism [Stoppini L. et al., 1991]. Several studies performed by our lab have uncover the advantages in using this type of culture that, despite the lacking of supraspinal inputs, maintains the correct ventral-dorsal orientation offering the possibility to focus on a specific tissue region,

displays the basic tissue architecture and neuronal circuitry comprising the DRGs thus reproducing the sensory-motor spinal organization, and preserves the cell diversity of the spinal tissue including microglia, astrocytes and oligodendrocytes, offering a unique opportunity to observe the crosstalk between cell types in a controlled microenvironment [Ballerini L. et al., 1999; Avossa D. et al., 2003]. From a functional point of view, we showed that organotypic spinal networks reproduce *in vivo* electrophysiological features during the *in vitro* maturation process, exhibiting a characteristic nerve fibers outgrowth accompanied by a progressive increase in spontaneous glycinergic postsynaptic currents frequency and peak amplitude (particularly evident after the second week *in vitro*), also displaying the physiological changes in glycinergic synapse function that typically occur during spinal development [Medelin M. et al. 2016; Usmani S. et al. 2016].

The conservation of the native tissue organization has proved to be important not only to preserve the spatial organization of cell-cell contacts but also to preserve cell molecular and functional diversity. As an example, Oleg Butovsky and colleagues demonstrated that cultured primary mouse microglia and microglia cell lines exhibit marked distinct molecular phenotypes when compared to the resident microglia in the brain tissue, highlighting the fact that cell behaviour is highly context-dependent [Butovsky O. et al., 2014]. In our case, we demonstrated that, in organotypic spinal slices, the specificity of interneurons subpopulations elecrophysiological signature is also preserved, allowing a better comprehension of spinal circuitry organization [Furlan F. et al. 2007]. Furthermore, recent experiments conducted in our lab using this model were able to:

- identify early alterations in the glycinergic inhibitory system as a contributing putative mechanism improving spinal cord excitability affecting motor outputs in a SOD1(G93A) ALS model [Medelin M. et al. 2016]
- characterize spinal GABAergic synaptic alterations induced by diverse inflammatory stimuli such as LPS and proinflammatory cytokines (IL-1β, TNF-α and GM-CSF) highlighting the ability of cytokines to modulates synaptic firing [Giacco V. et al. 2019]
- characterize the ability of graphene based nanomaterials (multiwalledcarbon nanotubes) to favour axonal regeneration and neuronal circuitry reorganization [Usmani S. et al. 2016]

Together, all these aspects contribute to make organotypic spinal slices an excellent model to investigate physiological as well as contributing to a more precise comprehension of pathological processes such as neuroinflammation, neurodegeneration and tissue damage.

# -4-
# Exosomes: unconventional players in neuroinflammation

Intercellular communication is a fundamental process for multicellular organisms, aiming the coordination of a correct developmental plan and to orchestrate the physiological adaptation to an ever-changing environment. Such a process often involves soluble factors like hormones, growth factors, cytokines and neurotransmitters which allow local or long distance information transfer through the binding of their cognate receptors, and specialized cell–cell contacts like electrical synapses and gap junctions which allow the direct interfacing between neighbouring cells [Mittelbrunn M. et al., 2012]. Within the past two decades, the intercellular communication landscape has been further enriched by the rise of a new class of biological messengers that have rapidly emerged as important mediators in health and disease: extracellular vesicles (EVs): cell-derived vesicles enclosed by a lipid bilayer, with diameter ranging from 30 nm to 2000 nm, secreted by cells into the extracellular space and contain a range of diverse signalling molecules which include cytokines and nucleic acids with the ability to modify the phenotype of the recipient cells [Doyle et al., 2019]. Despite a definitive classification is still lacking, due to some isolation and characterization drawbacks, it is now commonly accepted that EVs can be roughly classified in three main subtypes in respect to their release pathway: exosomes (or small EVs), microvesicles (or ectosomes) and apoptotic bodies. Particularly, exosomes derive from the endolysosomal pathway, microvesicles are generated by direct budding from the plasma membrane while apoptotic bodies are released by dying cells [EL Andaloussi S. et al., 2013].

I will focus on exosomes, since a growing body of scientific literature confirmed their pivotal role in physiological as well as pathological processes such as the regulation of the immune responses, viral pathogenicity, cardiovascular diseases, cancer progression to malignancy and, naturally, CNS disorders, offering new hints in the pathogenesis of these diseases. Furthermore, their lipidic nature and the particular cell-specific composition, makes them particularly attractive as potential drug delivery system and theranostic markers in liquid biopsy.

## 4.1. Exosomes: an introduction

Exosomes are a subclass of nano-sized extracellular vesicles, with a size range of ~40 to 160 nm, secreted by all kind of cells for specific intercellular communication. They are characterized by a variegated macromolecular cargo (including a set of proteins now accepted as specific exosomes biomarkers) able to modify the behavior of the recipient cells. Another exosomes unique feature is their biological origin: indeed, they are produced by the late endosomal multivesicular bodies (MVBs) pathway [Kalluri R. et al., 2020]. This exosome secretion pathway has been discovered

serendipitously in 1983 by two independent groups which were investigating the differentiation mechanisms of reticulocytes into mature erythrocytes [Harding C. et al., 1983; Pan B. T. et al., 1983]. Using transferrin-colloidal gold particles (AuTf) they tracked the transferrin receptor trafficking, a key step in the physiological recycling of iron ions and hemoglobin synthesis. Electron microscopy images revealed that, after the binding with transferrin receptor, AuTf particles were internalized through endocytosis, gathered into small vesicles collected in the so-called multivesicular bodies (MVB) and finally released into the extracellular environment through the fusion of the MBV with the plasma membrane (see Fig. 25). The small AuTf-decorated vesicles derived from the MBV-mediated exocytosis and isolated from the extracellular medium were then called exosomes, a term coined a few years later by the biologist Rose Johnstone [Harding C. V. et al., 2013].

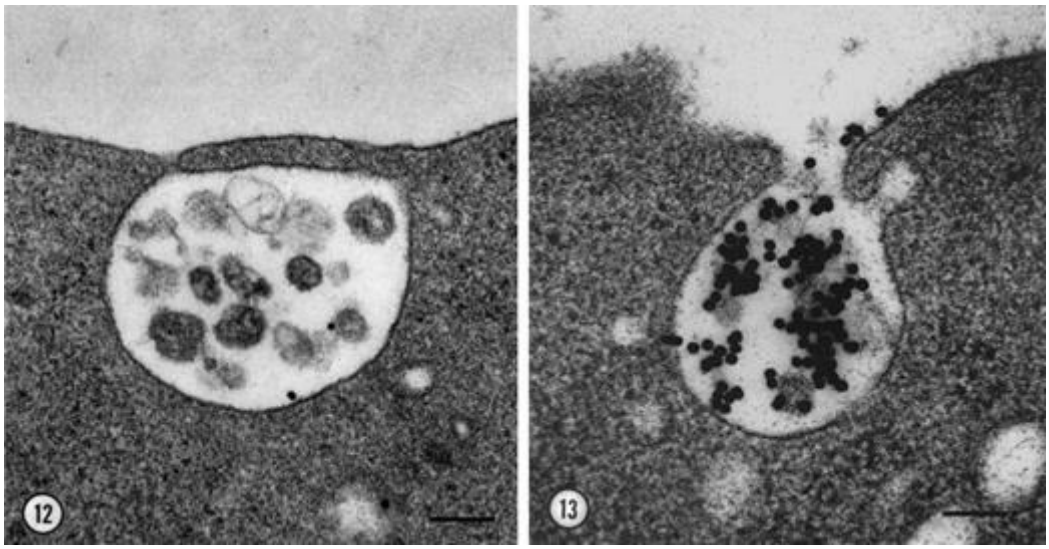


**Fig. 25: reticulocyte MVB containing exosomes labeled with AuTf [Harding C. V. et al., 1983]**

Since then, exosomes have gain considerable interest in the biomedical community and also contributed in inspiring new technological platforms. For example, in 1996 Graça Raposo and colleagues demonstrated that B lymphocytes are able to stimulate T cell response releasing exosomes bearing MHC-II–antigen complexes making them an attractive candidate immunization platform [Raposo G. et al., 1996], while in 2007 Hadi Valadi and colleagues demonstrated that exosomes contain and can transfer functional mRNA to recipient cells modifying their behaviour, expanding their potential applicability to gene transfer therapeutic platforms [Valadi H. et al., 2007].

***Origin, cargo sorting and release***: exosomes are a product of the endo-lysosomal pathway. While endosomes are commonly prone to be fused with lysosomes for the degradation of their content, a secretory variation of this pathway leads to multiple inward budding and pinching of vesicles into the late endosome lumen, finally giving rise to an exosomes-enriched MVB, ready to fuse with the plasma

membrane and release exosomes in the extracellular space [Raposo G. et al., 2013]. Despite the exact mechanism through which the cell determines the fate of the endosome has not been completely elucidated, recent studies suggest that a high cholesterol content of the endosome intraluminal vesicles' (ILVs, i.e. the forming exososmes) membranes seems to be the fundamental factor in determining if it will be addressed to the secretory pathway, while a high cholesterol content of the endosome limiting membrane seems to address this organelle to lysosomal degradation [Piper R. C. et al., 2007]. During this formation process, exosomes are enriched with several types of bioactive molecules including proteins and nucleic acids like RNA. The sorting of a specific cargo into luminal exosomes relies on the Endosomal Sorting Complex Required for Transport (ESCRT) machinery. ESCRT is composed of five protein complexes, which act synergistically to facilitate the movement of specific cargo molecules from the limiting membrane into vesicles that finally bud into the endosome lumen. Particularly, ESCRT-0 complex binds ubiquitinated cargo molecules, ESCRT-I/II/III contributes to vesicles inward budding and the vacuolar protein sorting-associated protein 4 (Vps4) complex ensures final membrane scission and ESCRT complexes recycling [Juan T. et al., 2018]. In addition to ESCRT complexes, several other proteins have been found to be important in cargo sorting and exosomes release. Among them, the best characterized are ALG-2-interacting protein X (ALIX), tumour susceptibility gene 101 protein (TSG101) and tetraspanins (particularly CD9, CD83 and CD61) which are also considered as valid exosomes biomarkers in characterization procedures (see Fig. 26) [Gurunathan S. et al., 2019].

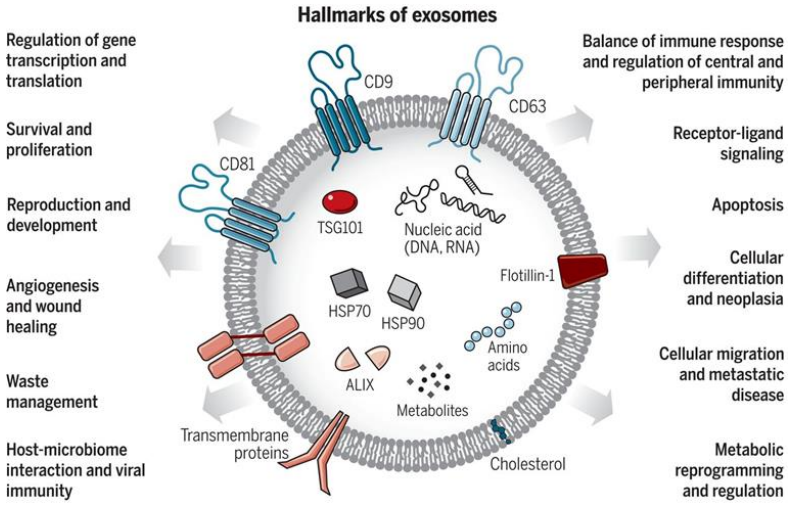


**Fig. 26: exosomes main components and functions [Kalluri R. et al., 2020]**

Exosomes can also be generated in an ESCRT-independent manner. This alternative pathway has been discovered by studies showing that MVB are still formed upon depletion of ESCRT complexes.

This process was shown to require the production of ceramide through the hydrolysis of sphingomyelin by neutral type II sphingomyelinase. The changing in MVB membrane lipidic composition may then allow the generation of ceramide subdomains, which impose a spontaneous negative curvature on the membranes allowing its inward budding. In addition, another ESCRT-independent endosomal sorting pathway is regulated by the tetraspanin proteins family. Despite the exact mechanism has not been completely elucidated, seems that these proteins can form clusters and dynamic membrane rafts with other transmembrane and cytosolic proteins probably acting in the formation of the inward budding microdomains [van Niel G. et al., 2018].

The release of exosomes in the extracellular space depends firstly on the motor-dependent transport of the MVB through the cytoplasm and its docking at the plasma membrane. The transport of the MVB is due to its interaction with cytoskeletal elements and seems to be promoted by some components of Rab protein family. The Rab family consists of small GTPases that plays a key role in the regulation of vesicle trafficking between different intracellular compartments [Gautreau A. et al., 2014]. In this context, many research groups found that Rab35, Rab27, Rab7 and Rab11 are preferentially recruited to favour the MBV docking at the plasma membrane mediating the interaction with microtubules and other cytoskeletal elements while the anchoring and fusion with the plasma membrane is mediated by the SNARE protein complexes (see Fig. 27) [Hessevik et al., 2018].

In 2005 Ariel Savina and colleagues showed that Rab11 activation is calcium dependent suggesting that elevation in cytoplasmic calcium may be in part correlated with exosomes release [Savina A. et al., 2005]. Furthermore, in 2018, Frederik Verweij and colleagues, studying the exosomes release mechanism using CD63-pHluorin reporter (a pH-sensitive GFP linked to the exosomal CD63 tetraspanin) expressed in HeLa cells, showed that the fusion of MVBs with the plasma membrane can be stimulated by the activation of various GPCRs and that this event largely lag behind the peak of intracellular calcium (10 s about). These authors also found that, combining intracellular calcium chelator BAPTA-AM and extracellular calcium chelator EGTA, did not significantly decrease the MVBs fusion events in HeLa cells suggesting that, at least in this cell model, exososomes release is not completely calcium dependent [Verweij, F. J. et al., 2018] differing substantially from the synaptic vesicles release mechanism.

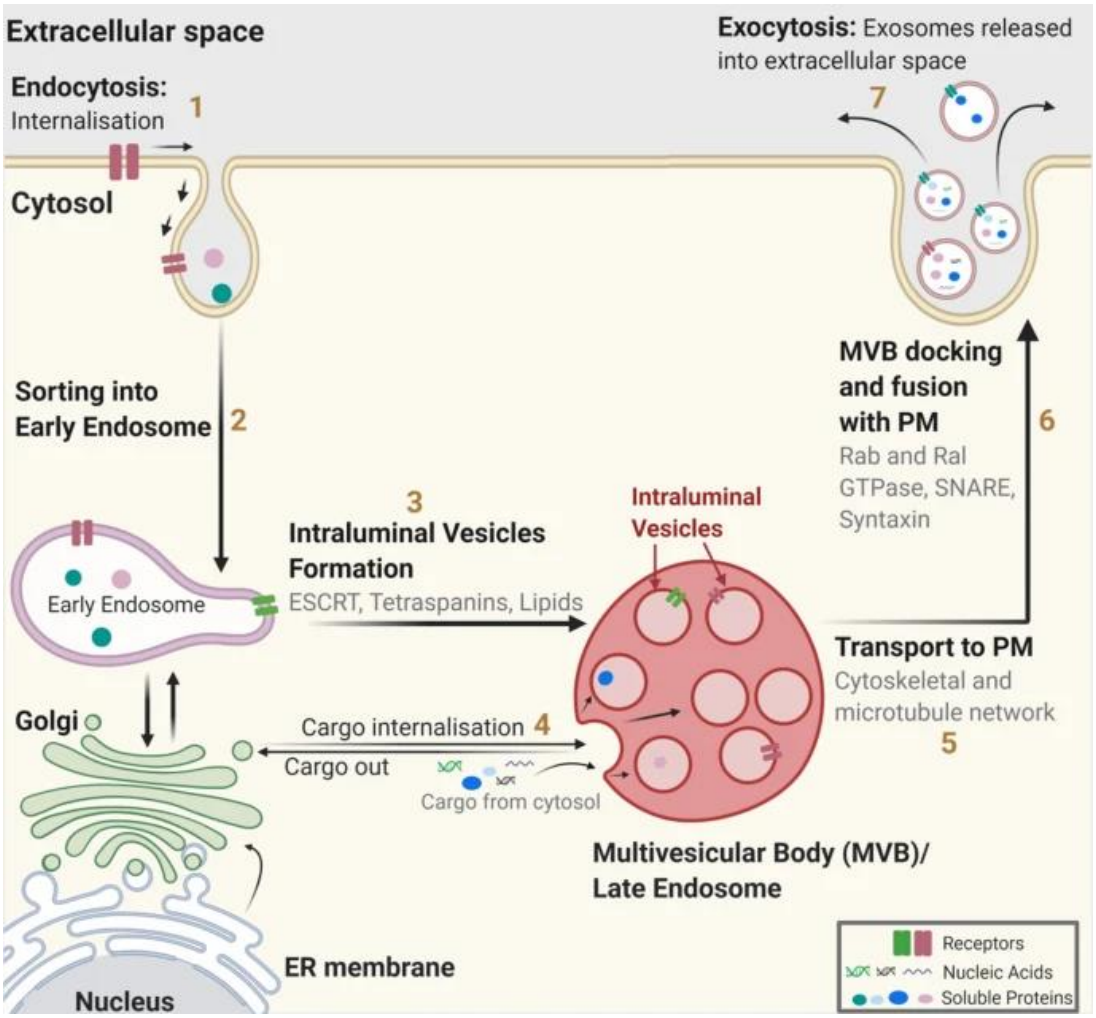


**Fig. 27: exosomes biogenesis and release pathways [Gurung S. et al., 2021]**

***Mechanisms of uptake and cargo delivery*:** exosomes ability to modify the behavior and phenotype of the recipient cell depends on three basic mechanisms: the direct interaction between exosomal membrane molecules and extracellular receptors, the fusion with the recipient plasma membrane, or the uptake by internalization [Gurung S. et al., 2021]. Interestingly, the direct interaction mechanism has been found to be particularly important for immune cells modulation and the induction of inflammatory events. As an example, in 2014, Andrea Sobo-Vujanovic and colleagues showed that exosomes secreted by dendritic cell can bind LPS and activate other immune cells through the interaction with TLR-4 [Sobo-Vujanovic A. et al., 2014], a mechanism probably due to the presence of CD14 (a TLR-4 co-receptor) on exosomal membrane [Chettimada S. et al., 2018]. In 2017, Mercedes Tkach and colleagues showed that exosomes derived from activated dendritic cells, carrying MHC proteins, were able to stimulate T lymphocytes by antigen presentation through the interaction with the TCR [Tkach M. et al., 2017].

The fusion with the plasma membrane of the recipient cell seems to be mediated by exosomes adhesion proteins belonging to the syncytin family through the interaction with Major Facilitator

Superfamily Domain 2a (MFSD2a) and Soluble Carrier Family 1 (ASCT-2) receptors expressed on the target cells, allowing the direct cytoplasmic release of the cargo [Prada I. et al., 2016].
Exosomes uptake by internalization can be instead mediated by all the major endocytic pathways including phagocytosis, micropinocytosis, and endocytosis mediated by caveolin proteins, clathrin and lipid rafts (see Fig.28) [Gurung S. et al., 2021].

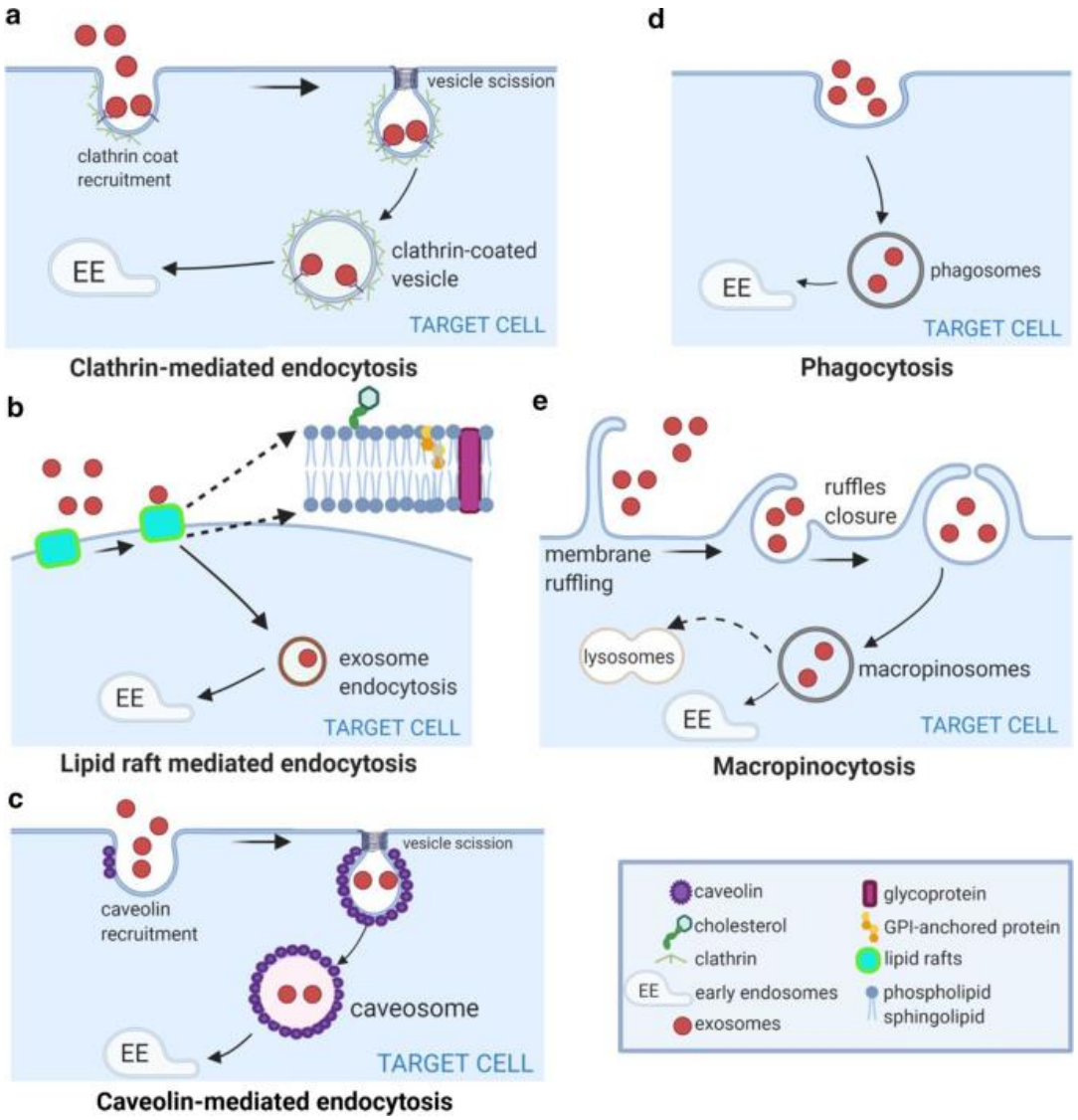


**Fig. 28: exosomes uptake and cargo delivery mechanisms [Gurung S. et al., 2021]**

The interactions between exosomes and the recipient cells are highly specific and vectorized by the expression of targeting proteins. In particular, beyond the more obvious targeted direct interaction mediated by exosomal membrane molecules that bind extracellular receptors acting by the activation of intracellular molecular cascades, also fusion and internalization events are orchestrated in a specific manner. Despite less is known about these processes, recent studies have uncovered the role of the phenotype-restricted expression of particular subset of integrin proteins [He J. et al., 2021]. As

an example, Eun Jeong Park and colleagues demonstrated that exosomes expressing integrin α4β7 secreted by T lymphocytes are able to target endothelial cells infected by hepatitis E virus [Park E. J. et al., 2019], while Ayuko Hoshino and colleagues showed that exosomes expressing integrin αvβ5 secreted by various tumors cell lines were able to target specifically target Kuppfer cells inducing immunodepression and promoting the hepatic seeding of tumor metastasis [Hoshino A. et al., 2015].

## 4.2. Isolation and characterization methods

Isolation and characterization are critical steps in exosomes research. Thus, given the increasing importance of this EV subclass in various biomedical fields, many isolation methods based on different principles have been developed in the attempt to ensure the quality and the efficiency of the extraction, which can largely vary depending on the source materials (e.g. culture medium and biological fluids). All these methods are characterized by respective advantages and drawbacks, and MISEV (Minimal Information for Studies of Extracellular Vesicles) 2018 Guidelines recommends only to choose the proper method in respect to the downstream applications and the scientific questions [Théry C. et al., 2018]. Thus, given the lack of a gold standard techniques, the quest of an efficient isolation method is still an active area of research.

The major issues are exosomes small diameter and their co-existence with other small biological objects (e.g. microvesicles, protein aggregates, plasma lipoproteins and others) characterized by consistent similarities in dimension range and other physical features. For these reasons, the presence of ‘contaminants’ it is a common finding in exosomes samples obtained with physical isolation methods based on particles size, which are the most commonly used in EVs research. On the other hand, despite chemical or immunochemical-based methods (like PEG-based precipitation or immunoaffinity capture respectively) allow a greater specificity, they are characterized by a lower isolation yield and are not easily employed in exosomes treatment studies due to the reagents residuals [Patel G. K. et al., 2019; Brennan K. et al., 2020; Sidhom K. et al., 2020].

One of the more used methods is based on differential ultracentrifugation and on the different sedimentation speed that characterize different particles suspended in a solution, according on their size. Briefly, it consists in various centrifugation steps at increased speed. Every step has the purpose of gradually eliminate larger particles like cell debris, apoptotic bodies and microvesicles. The last step consists in a high speed ultracentrifugation (at least 100.000 x g) necessary to obtain an exosomes enriched pellet. Despite this method is time consuming and cannot ensure the complete integrity of the isolated exosome (when compared to other physical methods like size exclusion chromatography), it appears a good compromise between the purity of the sample and the amount of vesicles obtained. Furthermore, even if it cannot be excluded that extracellular vesicles isolated with this method will

also include small vesicles derived from cell membrane budding, it is considered the best option for exosomes treatment-based study due to the lack of reagents residuals [Patel G. K. et al., 2019].
Exosomes characterization requires multiple complementary techniques in order to assess the quality and the efficiency of the used isolation method. Generally, international guidelines recommend the combination of a qualitative technique like electron microscopy (EM) or atomic force microscopy (AFM) imaging, which allow to assess the shape and the size of the isolated vesicles, a quantitative technique like dynamic light scattering (DLS), nanoparticle tracking analysis (NTA) or high-resolution flow cytometry (hrFC), which allow to assess the number of the isolated vesicles, and the identification of exosomal protein biomarker commonly carried out with western blot (WB) analysis, which allow to assess the specificity of the isolation process and the exclusion of other cellular components [Théry C. et al., 2018].

## 4.3. Exosomes in the CNS

In the last two decades, exosomes have emerged as fundamental intercellular communication mediators in health and disease in various biological systems including the CNS [Pascual M. et al., 2020]. In this context, they play the role of master regulators in neuron-glia crosstalk. Furthermore, given to their ability to freely cross the BBB in both directions, these nano-sized vesicles are now intensively studied for their potential as CNS specific theranostic system, offering an easily reachable window on neural cells physiological and pathological processes, as well as a CNS vectorised system for specific drug delivery [EL Andaloussi S. et al. 2013; Liu W. et al., 2019].
Exosomes have shown to be fine tuners in the normal CNS development, contributing to a well-orchestrated neurogenesis, myelination, synaptic differentiation and maturation, as a result of the specific vesicles-mediated targeted transfer of signalling proteins and miRNA [Bahram Sangani N. et al., 2021]. Furthermore, exosomes regulate, during the entire afterbirth life span, the neuron-glia crosstalk controlling homeostatic processes and disease, and their cell-specific roles in physiological and pathological events are resumed as follow:

***Neuronal exosomes***: neurons can secrete exosomes characterized by the specific neuronal derived markers L1CAM (a neuron-specific adhesion molecule) and glutamate receptor subunits GluR2/3 [Fauré J. et al., 2006]. The presence of the latter has suggested that neuronal exosomes are, not only involved in the crosstalk between neuronal and glial cells, but are also essential regulators in neuron-neuron interactions and widely involved in the regulation of the synaptic function. In support of this idea, electron microscopy studies showed that MVBs can be found in all the neuronal districts including the dendrites and the presynaptic membrane [Huo L. et al., 2021]. Furthermore, the release

of exosomes from mature neurons has shown to be stimulated by glutamate induced depolarization also at the synaptic level [Lachenal G. et al. 2011] and is involved in synapse maintenance. As an example, presynaptic exosomes release is involved in the postsynaptic transfer of synaptotagmin 4, a protein involved in synaptic plasticity, also at the level of the neuromuscular junction [Korkut C. et al., 2013]. Additionally, interneuronal communication mediated by exosomes can be highly neurotropic. Indeed, in 2014, Mathilde Chivet and colleagues demonstrated for the first time that, while exosomes secreted by neuroblastoma cells bound to and were endocytosed by neurons and glial cells indifferently, exosomes secreted from isolated cortical neurons stimulated with glutamate, bound to and were endocytosed by other neurons in an exclusive and specific manner [Chivet M. et al., 2014].

The molecular details of this specific targeting are still not entirely understood, probably due to the spatial localization of MVBs in neurons. In this regard, many studies have suggested that MVBs polarization on synaptic buttons can occur as a result of multiple factors such as the lipidic composition of plasma membrane domains that are prone to bind SNARE complex proteins, the location of specific cytoskeletal elements and molecular motors that participate to the MVBs translocation to the plasma membrane, and the position of phosphoinositides-rich plasma membrane domains able to recruit protein partners involved in the cytoskeletal regulation and vesicles secretion [Mittelbrunn M. et al., 2015].

Beside their physiological roles in supporting neuronal functions, exosomes have reported to actively participate to pathological processes such as the interneuronal transfer of misfolded proteins (i.e. $PrP^{Sc}$, amyloid precursors, mSOD1, phosphorylated tau or α-synuclein) during the course of neurodegenerative diseases [Chivet M. et al., 2013].

***Microglial exosomes***: microglia can secrete exosomes characterized by the specific markers aminopeptidase CD13 and the lactate transporter MCT-1 [Potolicchio I. et al., 2005]. The release of microglial exosomes is strictly related to its activation by the presence of noxious stimuli in the extracellular environment, through the activation of PRRs, becoming an efficient and long-range system to vehiculate cytokines, chemokines and non-coding RNA able to modulate recipient cells behaviours [Huo L. et al., 2021]. For instance, in experimental conditions, microglia stimulation with LPS, proinflammatory cytokines like IL-4 and ATP, have shown to significantly increase the secretion of exosomes, modifying their cargo composition [Bianco F. et al., 2005; Cunha C. et al., 2016; Tian Y. et al., 2019]. Particularly, in 2005, Fabio Bianco and colleagues demonstrated that eATP released by astrocytes is able to induce microglial cells to secrete vesicles containing IL-1β [Bianco F. et al., 2005]. Furthermore, Nhungoc Luong and Julie K. Olson recently demonstrated that

exosomes secreted by cultured microglia infected with Theiler's murine encephalomyelitis virus (TMEV) are loaded with viral RNA and are able to activate bystander microglia to secrete IFN-γ and pro-inflammatory cytokines and chemokines through the activation of viral RNA recognition receptor, tuning the cellular antiviral response [Luong N. et al., 2021].

Despite less is known about the role of microglial exososmes in non-pathological conditions, it seems that they may support and modulate neuronal activity. Indeed, in 2015, Konstantin Glebov and colleagues demonstrated that microglial cells secrete exosomes in response to neuronal serotoninergic activity through the activation of their 5-HT2a/b and 5-HT4 receptors in a calcium dependent manner [Glebov K. et al., 2015]. It was also demonstrated that microglia is able to modulate GABAergic neurotransmission by secreting exosomes loaded with membrane-linked N-arachidonoylethanolamine (AEA) capable of activating presynaptic type-1 cannabinoid receptors (CB1) [Gabrielli M. et al., 2015].

***Astroglial exosomes***: astrocytes can secrete exosomes characterized by the specific markers aminopeptidase GFAP, GLAST and GLUL [Goetzl E. J. et al., 2016]. Astroglial exosomes are involved in a plethora of homeostatic as well as pathogenic processes. They are able to vehiculate neurotrophic factors, promoting neurite growth and neuronal survival even after ischemic damage [Venturini A. et al., 2019]. For instance, Mikin Patel and Alissa Weaver have recently demonstrated that treating cortical neurons with exosomes derived from primary astrocytes cultures, enhance dendritic spine and synapses formation through the transfer of synaptogenic factors like fibulin-2 [Patel M. R. et al., 2021].

***Oligodendroglial exosomes***: oligodendrocytes can secrete exosomes characterized by the specific myelin markers PLP, MOG, MBP and CNP. Their secretion and functions are higly specialized since they can be internalized by neurons, microglia but apparently not by astrocytes [Krämer-Albers E. M., 2007; Krämer-Albers E. M., 2020; Ogaki A. et al., 2021]. Furthermore, as a consequence of oligodendrocyte physiological role and structure, exosomes secretion machineries in this cell type are characterized by a high degree of polarization. Indeed, at the level of the adaxonal membrane, oligodendrocytes transfer exosomes to neurons through the periaxonal space, while, at the level of the abaxonal membrane they release exosomes in the surrounding environment often targeting microglial cells.

Interestingly, adaxonal exosomes secretion apparently depends largely on neuronal electric activity and is stimulated during action potentials through the release of glutamate in the periaxonal space, which is able to activate oligodendrocyte AMPA and NMDA receptors allowing calcium influx that

promotes MVBs fusion with the plasma membrane (see Fig. 29) [Frühbeis C. et al., 2013]. Oligodendroglial exosomes are able to support neurons during their energy-consuming firing activity, promoting axonal transport and metabolic sustenance enhancing axonal mitochondria ATP production [Chamberlain K. A. et al., 2021] and transferring catalase and SOD1 enzymes that promote neuronal resistance to oxidative stress [Fröhlich D. et al., 2014].

On the other hand, oligodendroglial exosomes release through the abaxonal membrane are preferably taken up by microglial cells, a mechanism that seems to be involved in microglial mediated myelin recycling [Fitzner D. et al., 2011].

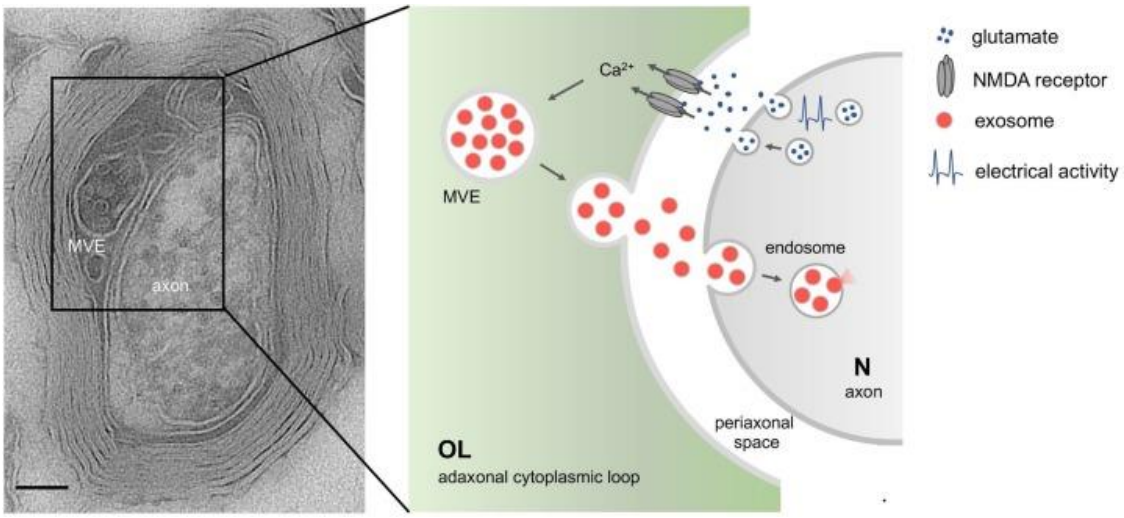


**Fig. 29: oligodendrocyte-axon exosomes delivery [Krämer-Albers E. M., 2020]**

## 4.4. Exosomes in the spinal neuroinflammatory processes

Neuroinflammation is a fundamental process in all CNS pathological processes including spinal cord disorders [Zhao S. et al., 2021]. Cytokines and chemokines released by glia and other immune-competent cells after SCI or during the progression of degenerative disorders like ALS or MS, have long been considered the major driver in perpetuating neuronal damage and impairing a complete functional recovery. This fact has inspired the search of treatments based on the modulation of the inflammatory phenomena. Despite that, the use of anti-inflammatory drugs in treating patients affected by those diseases have led to modest or none clinical benefits, suggesting an incomplete comprehension of the players involved in neuroinflammatory processes [Schiess M., 2003; Alexander J. K. et al., 2009]. Recently, exosomes have emerged as pivotal players in neuroinflammation. Indeed, their cargo can be enriched in proinflammatory cytokines, miRNA and pathological misfolded proteins that can be transmitted for long distances when packaged inside the exosomal membrane protected by enzymatic degradation [Gupta A et al., 2014]. For instance, exosomes have been

implicated in ALS progressive neuroanatomic propagation of pathology from the initial foci through the transmission of mSOD1 and TDP-43 [Grad L. I. et al., 2014; Iguichi Y. et al., 2016; Jo M. et al., 2020]. Oligodendrocytes exosomes loaded with the myelin protein MOG, isolated from the blood and the CSF of MS patients, have shown to activate peripheral T lymphocytes promoting the progression of the disease [Galazka G. et al., 2018]. Beside, their potential pathogenic role, exosomes are recently intensively investigated for their potential role as a therapeutic scaffold. Exosomal non-coding RNAs have shown promising results in the treatment of SCI dampening traumatic inflammation and promoting nerve regeneration in preclinical and clinical models, especially when exosomes are injected intrathecally [Romanelli P. et al., 2021; Yang Z. L. et al., 2022].

All these evidences pose exosomes at the centre of the contemporary debate in the field of neuroinflammation, providing novel approaches in the study of neuroinflammatory phenomena and inspiring the search of innovative therapeutic and theranostic platforms.

# Aims

Glial cells are well-recognized active players in neuropathology, actively influencing neuronal behaviour. Particularly, astrocytes are characterized by a close structural and functional relationship with neurons, and their signalling activity is able to modulate neuronal firing allowing the fine tuning of networks dynamics. Thus, the disruption of glial signalling activity, due to classical proinflammatory soluble mediators like cytokines and chemokines, can lead to neuronal dysfunction, and is a hallmark of CNS diseases. In the last two decades, exosomes have been intensively studied as an unconventional intercellular signalling system in health and disease. Furthermore, given the increase of their clinical relevance as potential therapeutic and theranostic platforms in neuroscience, a full characterization of their functions and effects is considered a must. Nevertheless, despite the great attention recently raised on this topic, exosomes' role in modulating glial cell function signalling is still poorly investigated.

The work of my thesis focused on the exploration of the role of exosomes in the context of spinal cord neuroinflammation, investigating their impact on glial cell functions and to uncover putative novel physiopathological mechanisms underlying CNS disorders. To this end, we used organotypic spinal cord slices, a 3-dimensional *in vitro* model characterized by the preservation of the native tissue cytoarchitecture that include neurons and glia, allowing high experimental manipulations but with a good approximation of the spinal microenvironment complexity. To achieve a more comprehensive view of these phenomena. we decided to proceed in a step-by-step fashion, first by exploring the dynamics of astrocyte EVs secretion in simplified *in vitro* setting, dissociated cortical astrocyte cultures, second by characterizing the glial calcium signal dynamics upon different inflammatory stimuli in a more complex biological model (organotypic spinal cord slices from mouse embryos) and third by assessing the impact of proinflammatory exosomes on the same system.

Since astrocytes are known to be one of the major EVs-producing cells in the CNS tissue, the first aim of this study was the characterization of astrocytic EVs secretion dynamics in a simple *in vitro* system: glial dissociated cultures from rat pups brain cortex. The ability of astrocytes to release EVs, has been assessed upon different stimulation protocols using pharmacological and nanotechnological tools. Particularly we used bzATP, for its agonist action on the well-known danger receptor $P_2X_7$, and small-size graphene oxide (s-GO), a graphene derivate with unique physical-chemical features able to interfere with cellular membrane dynamics.

Once assessed the dynamics of EVs release by astrocytes upon stimulation, we studied the effect of an inflammatory microenvironment on glial signalling behaviour. Since reactive astrocytes displaying altered signal activity are a key features in neuropathology, the second aim of this study was the characterization of glial calcium signalling dynamics, modelling neuroinflammation, using

organotypic spinal explants. In this model, where astrocytes are closely entangled with microglia and neurons, we induced inflammation using two different proinflammatory paradigms: LPS and a cytokines cocktail (TNF-α, IL-1β and GM-CSF), and we monitor live calcium signals dynamics in the spinal ventral area. Furthermore, in order to obtain more mechanistic insight about the observed alterations, we also investigated the role of intracellular calcium stores (ER and mitochondria) and connexin hemichannels.

My contribution to these two preliminary projects was instrumental to the characterization of the model used to achieve my conclusive aim: investigating exosomes ability to induce glial inflammatory phenotype and dysfunctional calcium dynamics in organotypic spinal slices. To achieve this aim I firstly establish an efficient protocol to isolate and characterize exosomes from spinal cultured slices conditioned media, induced upon inflammatory stimulation. Next step was to verify the ability of isolated exosomes to induce an inflammatory phenotype in glial cells. To do so, we measured morphological and functional changes in microglia and astrocytes through confocal images analysis and live calcium imaging. To conclude, we used pharmacological tools to explore the role of connexin hemichannels in mediating exosomes proinflammatory effects.

The results of this thesis are only in part published and are included as so in the following order:

Panattoni G., Amoriello R., **Memo C.**, Thalhammer A., Ballerini C., Ballerini L. “Diverse inflammatory threats modulate astrocytes Ca2+ signaling via connexin43 hemichannels in organotypic spinal slices.” Mol. Brain 14, 159 (2021)

Musto M., Parisse P., Pachetti M., **Memo C**., G. Di Mauro, Ballesteros B., Lozano N., Kostarelos K., Casalis L., Ballerini L. “Shedding plasma membrane vesicles induced by graphene oxide nanoflakes in brain cultured astrocytes” Carbon 176, 458-469 (2021)

**Memo C.**, Parisse P., Amoriello R., Di Mauro G., Ballerini C., Casalis L., Ballerini L. “Exosomes from LPS-stimulated spinal organotypic slices transfer neuroinflammation in naïve spinal explants via promoting aberrant calcium dynamics and hemichannels opening in astrocytes.” (Manuscript in preparation)

Panattoni *et al. Mol Brain* (2021) 14:159
https://doi.org/10.1186/s13041-021-00868-6

Molecular Brain

RESEARCH

Open Access

# Diverse inflammatory threats modulate astrocytes $Ca^{2+}$ signaling via connexin43 hemichannels in organotypic spinal slices

Giulia Panattoni[1], Roberta Amoriello[1,2], Christian Memo[1], Agnes Thalhammer[1], Clara Ballerini[2*] and Laura Ballerini[1*]

## Abstract

Neuroinflammation is an escalation factor shared by a vast range of central nervous system (CNS) pathologies, from neurodegenerative diseases to neuropsychiatric disorders. CNS immune status emerges by the integration of the responses of resident and not resident cells, leading to alterations in neural circuits functions. To explore spinal cord astrocyte reactivity to inflammatory threats we focused our study on the effects of local inflammation in a controlled micro-environment, the organotypic spinal slices, developed from the spinal cord of mouse embryos. These organ cultures represent a complex in vitro model where sensory-motor cytoarchitecture, synaptic properties and spinal cord resident cells, are retained in a 3D fashion and we recently exploit these cultures to model two diverse immune conditions in the CNS, involving different inflammatory networks and products. Here, we specifically focus on the tuning of calcium signaling in astrocytes by these diverse types of inflammation and we investigate the mechanisms which modulate intracellular calcium release and its spreading among astrocytes in the inflamed environment. Organotypic spinal cord slices are cultured for two or three weeks in vitro (WIV) and exposed for 6 h to a cocktail of cytokines (CKs), composed by tumor necrosis factor alpha (TNF-α), interleukin-1 beta (IL-1 β) and granulocyte macrophage-colony stimulating factor (GM-CSF), or to lipopolysaccharide (LPS). By live calcium imaging of the ventral horn, we document an increase in active astrocytes and in the occurrence of spontaneous calcium oscillations displayed by these cells when exposed to each inflammatory threat. Through several pharmacological treatments, we demonstrate that intracellular calcium sources and the activation of connexin 43 (Cx43) hemichannels have a pivotal role in increasing calcium intercellular communication in both CKs and LPS conditions, while the Cx43 gap junction communication is apparently reduced by the inflammatory treatments.

**Keywords:** Pro-inflammatory cytokines, LPS, Live imaging, Neuroinflammation, Gap junctions, Hemichannels, Spinal neurons, Immune resident cells

## Introduction

Neuroinflammation is a characterizing feature occurring in and contributing to CNS pathologies such as amyotrophic lateral sclerosis (ALS) and multiple sclerosis (MS) [1, 2]. In the CNS, successful inflammatory responses exert a protective homeostatic action, on the contrary, protracted tissue reactivity sustains unregulated cytokine/chemokine release and chronic inflammation, which has been proposed as a major cause of disease progression [3]. In the last decade, several studies documented, associated to neuroinflammatory processes, the appearance of synaptic dysfunction, i.e. synaptopathy [4, 5]. Indeed, the emergent activity of neural circuits may

*Correspondence: clara.ballerini@unifi.it; laura.ballerini@sissa.it
[1] International School for Advanced Studies (SISSA/ISAS), 34136 Trieste, Italy
[2] Dipartimento di Medicina Sperimentale e Clinica, University of Florence, 50139 Florence, Italy

be altered both acutely and chronically by inflammatory milieus activating intricate signaling pathways, orchestrated by various cell phenotypes, ultimately responsible for intercellular communication and contributing to the propagation of the inflammatory damage in the CNS. In this picture, astrocytes, the key cellular partners to neurons, play both beneficial roles, such as recovery of extracellular ionic homeostasis limiting inflammation [6] and deleterious ones, such as hypertrophy with increased astrogliosis [7, 8]. Knowing how astrocytes perform such signals might allow to selectively promote their beneficial functions and inhibit the adverse ones in diseased CNS.

We recently investigated the effects on spinal synaptic outputs of different inflammatory threats, focusing on the consequences of local inflammation in a controlled micro-environment: the organotypic slice cultures developed from the embryonic mouse spinal cord explants [9–11]. Core features of this in vitro model are the 3D organization of spinal cord resident cells and the preserved sensory-motor cytoarchitecture [11–13]. This model allows the study of spinal tissue alterations induced by inflammation, addressing the role of resident cells: neuronal and not neuronal populations. By the use of spinal cord explant cultures, we reported the ability of two diverse immune conditions to improve network excitability by specific synaptic mechanisms [11].

In the present study, we exploit spinal slice cultures to explore astrocyte recruitment upon exposure (6 h) to pro-inflammatory CKs cocktail (TNF-α, IL-1β and GM-CSF [4, 14, 15]) or to LPS, a potent trigger of cytokine release [16, 17] largely adopted to elucidate the mechanisms of brain inflammation. In our previous experiments, CKs and LPS treatments mediated an increase in cytokines and chemokines production, although differently regulating the morphology of resident neuroglia, suggestive of diverse activation states [11]. In reactive tissues, astrocytes can be neuroprotective or neurotoxic, depending on the context, and $Ca^{2+}$ signaling has a key role in these processes [18]. Reactive astrocytes are known to increase dynamic $Ca^{2+}$ signals, shown to be crucial to intracellular signaling and intercellular communication [19]. Such calcium dynamics were reported to vary in distinct pathological models and regions, indicating that aberrant $Ca^{2+}$ signals may depend on the context conditions [18].

To examine astrocytes responses to inflammation, we monitor live $Ca^{2+}$ signals within the spinal cord cultured microcircuits. We focus on astrocytes located in the ventral horn within pre-motor networks and we compared their calcium signaling when activated by CKs or LPS. We document the timing and appearance of intracellular calcium oscillations upon CKs or LPS exposure, such astrocyte episodes are generated by each treatment independently from the ongoing synaptic activity. We further show, by pharmacological treatments, that CKs and LPS induce calcium release from endoplasmic reticulum, mitochondria and that astrocyte pro-inflammatory activation as well as cytokines and chemokines production, are tuned by gap junctions (GJs) and hemichannels (HCs) regulation.

## Results

### Sulforhodamine-positive glial cells display slow spontaneous $Ca^{2+}$ activity

The presence of GFAP-positive astrocytes has long been described in cultured spinal explants ventral horns [11–13], as confirmed by Fig. 1A, where numerous astrocytes are visualized within the ventral area of a spinal organotypic culture after 2 WIV. We labeled by fluorescent dye Fluo-4 AM (see "Methods") cells in organotypic spinal cord and dorsal root ganglia (DRG) co-cultures to simultaneously visualize within the sampled area (visual field $330 \times 330$ μm$^2$, Fig. 1B) of the ventral horn pre-motor circuit [11], neuronal and glial cells calcium signaling. To reliably identify astrocytes for physiological measurements of calcium dynamics, we took advantage of a widely used astrocyte marker, sulforhodamine (SR101; 1 μM, Fig. 1C) [20–22] enabling the detection of living astrocytes during ex vivo calcium imaging experiments, in combination with the calcium dye Fluo-4 AM. As shown in Fig. 1C (top panels; white circles) and in the corresponding sample tracings of spontaneous fluorescent recordings in Fig. 1D (top traces), the imaging of visually identified small neurons close to the ventral fissure [23] resulted in SR101-negative cells highly active in control saline solution, with fast ($4.12 \pm 0.63$ s duration; $n = 14$ cells) calcium episodes which were silenced after application of tetrodotoxin (TTX, 1 μM; fast voltage-gated sodium channel blocker to remove action potentials [23]; Fig. 1D), confirming their neuronal identity. Differently, closely located SR101-positive cells (Fig. 1C, bottom panels; white circles) were spontaneously less active (Fig. 1D, bottom tracings) and typically displayed slow ($21.6 \pm 1.55$ s duration; $n = 42$ cells) and rare episodes of spontaneous activity, which were resistant to TTX application and allowed identifying glial cells calcium dynamics. In these conditions, we never detected short-lasting $Ca^{2+}$ transients (less than 8 s; Fig. 1D) [24, 25]. To further strengthen the astrocytic origin of the calcium events detected in TTX, in a separate set of experiments we used the genetically-encoded calcium dye GCaMP6f exclusively expressed in astrocytes [26] ($n = 4$) and we confirmed the occurrence of low-frequency and irregular calcium transients which were not affected by TTX (Additional file 1: Fig. S1A). In all subsequent

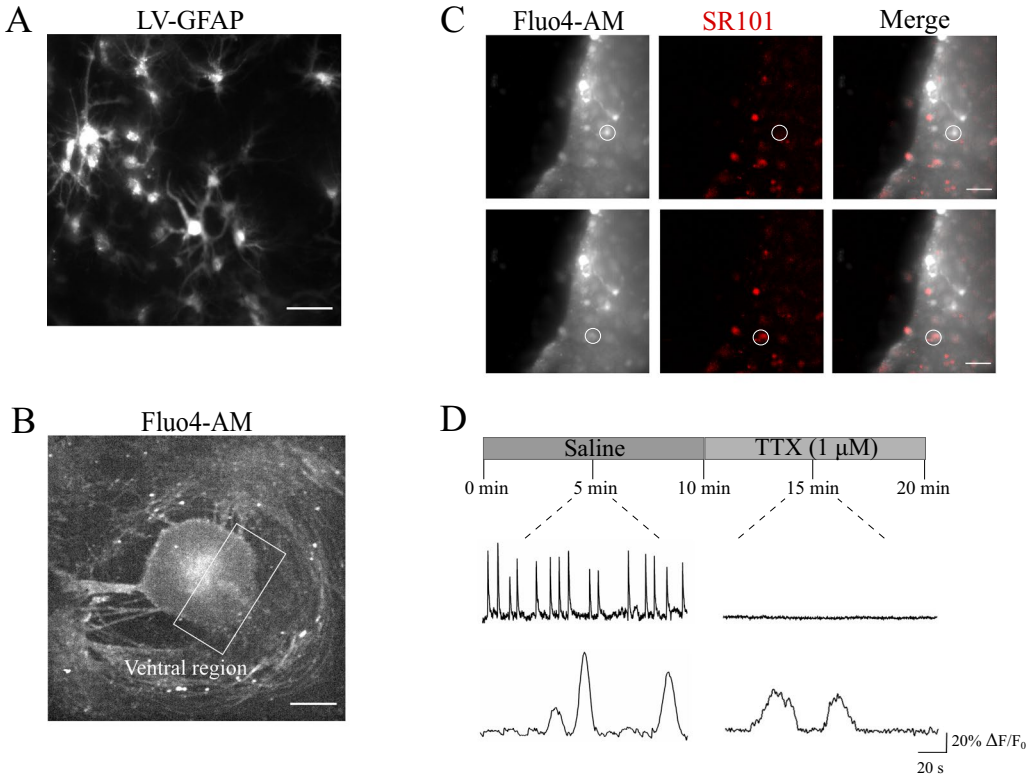


**Fig. 1** SR101-positive glial cells display spontaneous, slow $Ca^{2+}$ oscillations. **A** Representative images of GFAP-LV vectors visualizing astrocytes in the ventral-horn of the organotypic spinal slice. Scale bar 50 µm. **B** Representative fluorescent image at low magnification (4 ×) of a spinal organotypic slice loaded with the calcium dye Fluo4-AM (4 µM). The ventral region (white frame) is identified by the ventral fissure. Scale bar, 500 µm. **C** CCD-camera snapshots visualize cells located at the border of the ventral region and loaded with Fluo4-AM, in grey (left), and with SR101, in red (middle). Merged images on the right. Scale bars, 50 µm. **D** Top, representative fluorescent tracing of spontaneous neuronal $Ca^{2+}$ activity, prior and after 1 µM tetrodotoxin (TTX), recorded from SR101 negative cell (same as in **C**). Bottom, representative fluorescent tracing of astrocytes $Ca^{2+}$ oscillations, before and after the application of TTX, recorded from SR101 positive cell (same as in **C**)

experiments we used the spatial location, the slow kinetic and the TTX resistance to identify glial calcium signaling.

### CKs and LPS treatments affect $Ca^{2+}$ transients in organotypic spinal slices

To investigate the ability of inflammation to impact calcium dynamics in glial cells, organotypic spinal explants were treated (6H, see "Methods") with two danger signals triggering different, although well characterized, inflammatory states in these cultures [2, 3]: a pro-inflammatory cocktail of CK (10 ng/mL; TNF-α, IL-1 β and GM-CSF) [11, 13] and the LPS (1 µg/mL) [11, 17] stimuli. First, we monitored ventral neurons calcium signaling and we compared activity from neurons prior (Control; n = 8) and after CKs (n = 7) or LPS (n = 7) treatments. In the Additional file 1: Fig. S1B, snapshots of neurons stained with membrane permeable dye Fluo-4 AM are visualized in all conditions. Neurons, in CKs and LPS treated slices (Additional file 1: Fig. S1C) displayed a significant increase in the frequency of basal calcium oscillations, when compared to Control (0.24 ± 0.01 Hz Control, 0.31 ± 0.02 Hz CKs and 0.39 ± 0.03 Hz LPS; n = 7 each; $^{***}P < 0.001$ Control vs LPS and $^{**}P = 0.0052$ Control vs CKs, Kruskal–Wallis test; box plot in Additional file 1: Fig. S1C). This boost in activity was accompanied by high synchronization among correlated pairs of cells simultaneously recorded (see "Methods" and Additional file 2: Fig. S2A). Such an enhanced calcium dynamics probably reflect the high degree of spontaneous synaptic activity typical of spinal cord preparations when inflammatory states are activated [11, 13] and was not further examined. Calcium signaling due to synaptic activity was removed by TTX application, as shown in Fig. 1D, and we next explored glial cells activity and in particular how astrocytes respond to the localized inflammation, since it is known that also astrocytes display spontaneous calcium signaling [27–29]. Calcium dynamics in glial cells was measured always in the presence of TTX and in Control slices (n = 8) was characterized by the sporadic (on average 2.1 ± 0.29 active cells per recorded field)

appearance of slow oscillations, quantified by inter event intervals (IEIs) of 51.3 ± 5.4 s (Fig. 2 A-D). Upon CKs (n = 7) and LPS (n = 7) treatments, an increased number of active cells per recorded field was detected in respect to Control (4.5 ± 0.56 active cells in CKs and 5.8 ± 1.16 active cells in LPS; $^{**}P = 0.003$ Control vs LPS and $^{*}P = 0.04$ Control vs CKs, one-way ANOVA test; bar plot in Fig. 2C) displaying calcium oscillations characterized by a significant reduction in the IEIs when compared to the Control ones (36.5 ± 4.3 s in CKs and 31.1 ± 2.5 s in LPS; $^{***}P < 0.001$ Control vs LPS and $^{**}P = 0.005$ Control vs CKs, Kruskal–Wallis test; cumulative probability plot and box plot in Fig. 2 D). Glial cell calcium oscillations were also analyzed for their synchronicity among simultaneously recorded cells. To this aim we measured in each slice (n = 3 each, Control, CKs and LPS) the activity of distant (see "Methods"; Additional file 2: Fig. S2B) pairs of active glial cells (n = 6, 20 and 22 cell pairs in Control, CKs and LPS). Increase active cells during inflammatory threats, regardless the triggering by CKs or LPS, were significantly less synchronized when compared to Control ones (0.05 ± 0.01 pair p-value Control; 0.21 ± 0.02 pair p-value CKs 6H; 0.33 ± 0.02 pair p-value LPS 6H, $^{***}P < 0.001$ Control vs LPS and $^{**}P = 0.0025$ Control vs CKs, one-way ANOVA test; $\chi^2 = 7.73$, $^{*}P = 0.02$, Fisher's exact test; Additional file 2: Fig. S2B). Interestingly, in physiological states, GJs are usually responsible for the synchronization of glial calcium activity [30–32], which is often reduced by diverse pathological conditions [33].

Despite the similar response in terms of glial calcium dynamics, from the morphological point of view, CKs and LPS treatments differently affected the appearance of resident astrocytes and microglia, with opposite changes in Iba1 positive microglia dendritic arborizations (quantified by the transformation index; Additional file 1: Fig. S1D and box plot in E (bottom); with average index values 5.2 ± 2.4 Control, n = 4; 2.2 ± 1.7 CKs, n = 4; 13.2 ± 2.4 LPS, n = 4; $^{***}P < 0.001$ Control vs LPS 6H and $^{*}P = 0.03$ Control vs CKs, Kruskal–Wallis test), and in GFAP intensity enhancement, which was typically milder in LPS treatments in respect to CKs (Additional file 1: Fig. S1D and box plot in E, top; n = 10, 11, 10, Control,

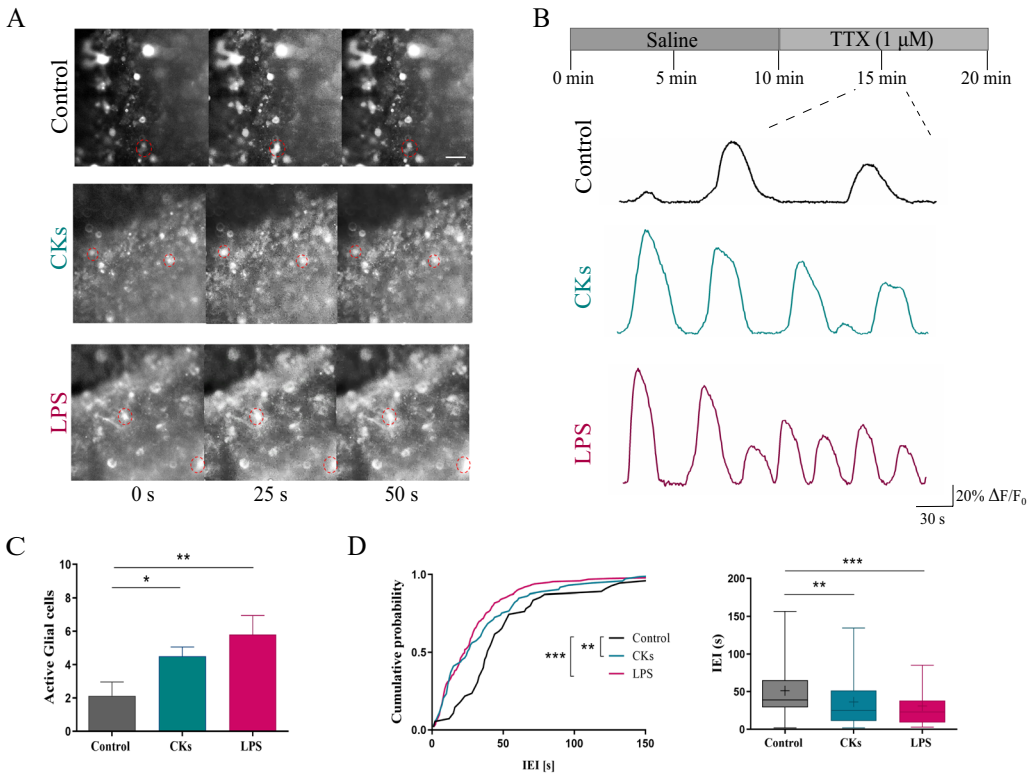


**Fig. 2** CKs and LPS enhance spinal astrocytes calcium dynamics. **A** Representative snapshots (40 × magnification) of the ventral area of organotypic spinal slices loaded with Fluo-4 AM (4 µM); frames were taken at variable time intervals (0, 25 and 50 s) in three different experimental conditions (Control, CKs and LPS). Scale bar 50 µm. **B** Representative fluorescent tracings depicting glial cells calcium oscillations in Control (black), CKs and LPS (6H, blue and purple, respectively), all recorded in the presence of TTX. **C** The bar plot summarizes the number of spontaneously active glial cells/field. $^{**}P < 0.01$ and $^{*}P < 0.05$, one-way ANOVA. **D** Cumulative distributions and box plot quantify the IEIs (s) of the recorded calcium activity in all conditions. $^{***}P < 0.001$ and $^{**}P < 0.01$, in the cumulative plot Kolmogorov–Smirnov test and in the Box plot, Kruskal–Wallis test

CKs and LPS respectively; in a.u. 799.9 ± 374.1 Control; 2312 ± 318.1 CKs and 1404 ± 586.5 LPS; **** $P \leq 0.0001$ Control vs CKs and CKs vs LPS, and * $P = 0.0112$ Control vs LPS, one way ANOVA). These results are in agreement and confirm our previous observations [11].

### Intracellular stores, gap-junction and hemi-channels dependence of glial calcium signals

In order to explore the nature of the observed oscillatory patterns, in Control as well as in CKs and LPS, we investigated the dependence on intracellular calcium stores of these activities. We assessed the contribution of internal $Ca^{2+}$ sources from the mitochondria and the endoplasmic reticulum (sketched in Fig. 3A). To explore the mitochondrial role, we used the protonophore carbonyl cyanide 3-chlorophenylhydrazone (CCCP, 2 μM) [23] to dissipate the proton gradient across the inner mitochondrial membrane and disrupt the $Ca^{2+}$ uptake. After CCCP application, $Ca^{2+}$ transients completely disappeared, this response did not differ among the three experimental conditions (n = 8, 7 and 5, Control, CKs and LPS, respectively; Fig. 3B). Next, we explored the contribution of intracellular $Ca^{2+}$ source, namely the endoplasmic reticulum, to the calcium events [23]. Application of the non-competitive inhibitor of the sarco/endoplasmic reticulum $Ca^{2+}$ ATPase (SERCA) thapsigargin (TG, 5 μM) blocked all calcium transients in the three conditions (n = 8, 9 and 5, Control, CKs and LPS, respectively; Fig. 3C). These results suggest that spontaneous intracellular $Ca^{2+}$ transients in single astrocytes in Control as well as in inflamed spinal tissues strongly rely on intracellular calcium sources.

In tissue cultures, $Ca^{2+}$ events can propagate among a network of astrocytes via GJs [34], allowing synchronization of the calcium activity. GJs are formed by the docking of two HCs and unapposed HCs, not assembled into GJs, are present in the plasma membrane. Non-junctional HCs may be activated in response to inflammation stimuli [35], thereby allowing ionic and molecular exchange between the intra- and extracellular environment. In the absence of neurotransmitter activation, cultured explant in CKs or LPS did not show propagated calcium signals or synchronization among astrocytes, however astroglial cells usually express connexins that support long-range communication. GJs and connexins are also known to have an enhanced turnover in the inflamed tissues [31, 32, 36] while HCs in non-junctional membrane and GJs are oppositely regulated by various conditions [37].

Since both GJs and HCs in astrocytes in culture are mainly composed by Cx43 protein [30, 38] to address potential changes in the expression of Cx43 we used immunoblotting analysis under the three different

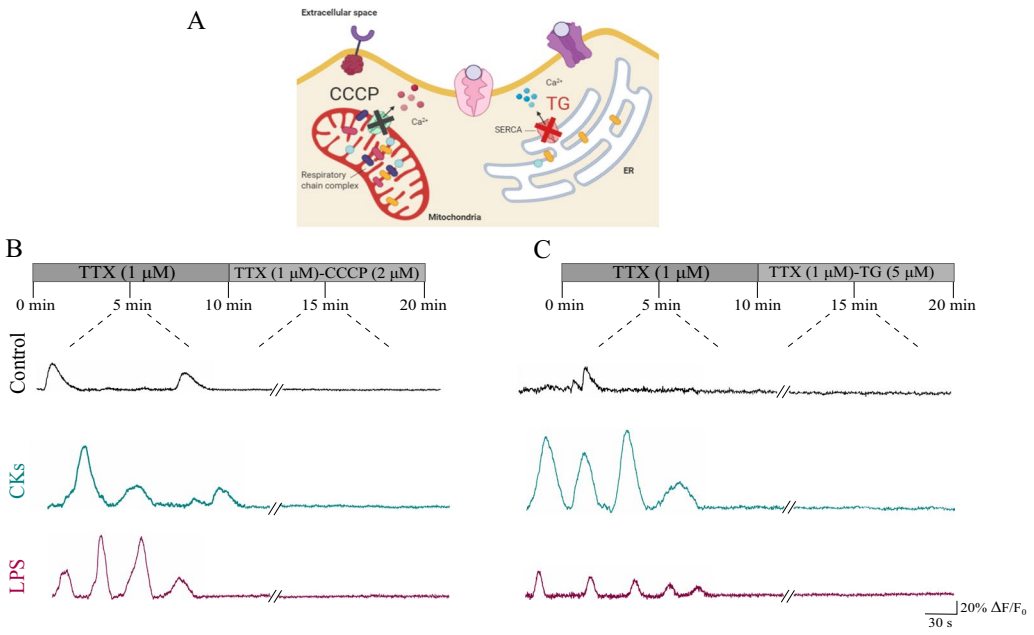


**Fig. 3** Intracellular calcium sources sustain calcium dynamics in astrocytes. **A** Sketch of the intracellular calcium sources targeted by the blockers used. **B** Fluorescent tracings from representative glial cells prior and after CCCP mitochondrial uncoupler administration in Control (black), CKs and LPS (blue and purple, respectively). **C** Fluorescent tracings from representative glial cells prior and after Thapsigargin (TG) administration in Control (black), CKs and LPS (blue and purple, respectively). All recordings were performed in the presence of TTX. Note the removal of calcium activity by each treatment in each condition

experimental conditions. The western blot (WB) in Fig. 4A shows the protein bands in the three culture groups (n = 8, 7 and 8, Control, CKs and LPS, respectively) and we observed that CKs and LPS treatments significantly (**$P = 0.004$ Control vs LPS and *$P = 0.03$ Control vs CKs, one-way ANOVA test; bar plot in Fig. 4A) reduced the expression of Cx43, in respect to Control, in agreement with previous works [36, 39]. It has been shown that proinflammatory CKs released by activated microglia, inhibit GJs mediated by Cx43, whereas opening HCs, a pathway enabling release of active molecules [39]. In the presence of reduced Cx43 expression, CKs and LPS might still enhance calcium activity in astrocytes by the opening of HCs.

The WB-blot analysis of Cx43 expression is in accordance with the functional evidence of desynchronization of calcium events in astrocytes detected upon inflammatory states, both results being supportive of a reduced GJ communication in the presence of pro-inflammatory stimuli, however HCs opening cannot be excluded [37]. We used the fluorescent dye ethidium bromide (EtBr), a tool adopted to investigate HCs permeability [39–41], to assess the presence of changes in HC activity upon CKs and LPS exposures. Control and treated slices (n = 5, 8, 7, control, CKs and LPS, respectively) were incubated (30 min) with EtBr (5 μM), as shown in Fig. 4B and EtBr positive glial cells were quantified in the bar plot (normalized to GFAP-positive cells: 0.41 ± 0.03 Control; 0.77 ± 0.02 CKs; 0.76 ± 0.04 LPS; *** $P < 0.0001$, one-way ANOVA test). We used carbenoxolone (CBX 200 μM, 30 min), a well-known GJs uncoupler [23, 41, 42] and a blocker of active HCs [43] to test the functional role of HCs in the observed dye uptake. When Control and treated slices were pre-incubated (n = 5, 9, 5, Control, CKs and LPS, respectively) with CBX, the astrocyte dye-uptake in treated slices was significantly reduced (0.36 ± 0.04 CKs + CBX; 0.36 ± 0.05 LPS + CBX; *** $P < 0.0001$, one-way ANOVA test) and did not differ from Control uptake (0.33 ± 0.03 Control + CBX).

Taken together these results apparently support an increase in the permeability of Cx43 HCs in parallel with GJs inhibition, upon CKs and LPS treatments. We decided to gain more insights on the role of activated HCs in astrocytes calcium dynamics. To this aim we pre-incubated Control and treated slices (n = 3 each group) with a distinct Cx43 peptide blocker, namely Gap27 (500 μM; 30 min), known to inhibit HCs opening triggered by chemical or electrical stimuli [44].

In TTX, upon Gap27 treatment, we did not observe any residual calcium activity in astrocytes in untreated or treated cultures (Fig. 5A). This result was strengthened by a separate set of experiments where CBX incubation also removed all calcium activity, thus recapitulating the findings of Gap27 (Additional file 3: Fig. S3; n = 4 each group). Thus, activated HCs are instrumental to the enhanced activity upon inflammation. To explore whether the increased calcium signaling was correlated to astrocyte reactivity and contributed to their inflammatory status we evaluated cytokines and chemokines produced in organotypic cultures after CKs (n = 6) or LPS (n = 6) stimulation [11, 13], compared to Control (n = 6), in the presence or not of the blocking factor Gap27 ("g" in Fig. 5B and C). Overall, in the absence of Gap27, the level of the analyzed soluble factors tends to increase after either CKs and LPS stimulation, compared to Control, confirming our previous observations [11]: this difference is statistically significant in IL-1β CKs-stimulated ($P < 0.0001$; Fig. 5B), TNFα CKs and LPS-stimulated ($P = 0.014$ and 0.003, respectively; Fig. 5B and C), IL6 and CXCL2 LPS-stimulated ($P = 0.033$ and 0.0002, respectively; Fig. 5C). Furthermore, our results show a trend towards a reduction of several cytokines and chemokines in the presence of Gap27, particularly after CKs + g stimulation. These differences become statistically significant in IL-1β, that decreases in CKs + g sample group

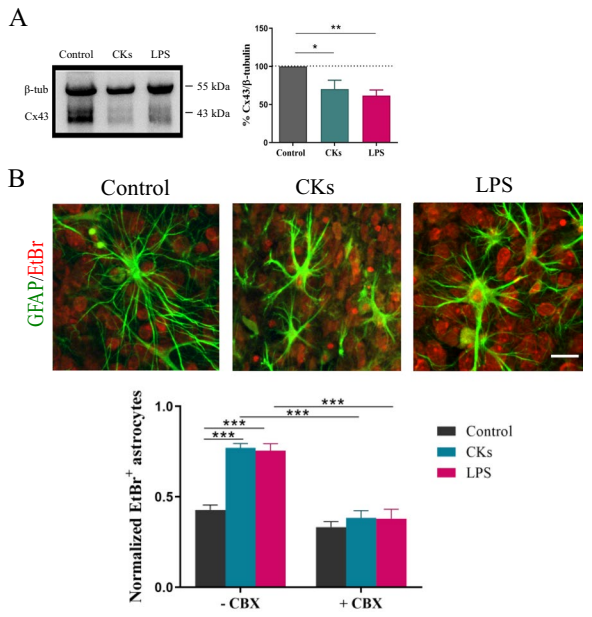


**Fig. 4** Cx43 GJs and HCs role in the increased calcium dynamics in CKs and LPS. **A** Western blot experiments (left) and analysis (bar plot, right) for the protein Cx43 in Control, CKs and LPS treated slices. Values are expressed as % of Control. **P < 0.01 and *P < 0.05, one-way ANOVA. **B** Representative high magnification (40 ×) confocal images of EtBr uptake (30 min, in red) in astrocytes (GFAP, in green) induced by CKs and LPS treatments, scale bar 25 μm. EtBr uptake is quantified in the bar plot, normalized to the total number of astrocytes/field, in the absence or in the presence of carbenoxolone (CBX, 200 μM) pre-incubation (30 min). ***P < 0.001, one-way ANOVA

compared to CKs alone (P = 0.018) and to Control groups (P = 0.029) (Fig. 5B); conversely, TNF-α (P = 0.016; Fig. 5B) and CXCL2 (P = 0.010; Fig. 5C) were still significantly increased in LPS + g group compared to controls, although to a lesser extent when compared to LPS alone. The release of soluble factors is activated by different pathways in CKs or LPS paradigms, thus the extent of cytokines and chemokines detected might be variably tuned by Gap27. We directly investigated whether Gap27 affected astrocyte reactivity induced by inflammatory threads (shown in Additional file 1: Fig. S1D and Fig. 5D top panels and box plot). Figure 5D fluorescence micrographs show that Gap27 (bottom panels) increased GFAP intensity in Control per se, which then remained unmodified in CKs and LPS in the presence of this blocking peptide (box plots in Fig. 5D; n = 4 each condition). This increase in GFAP intensity brought about by Gap27 was apparently unrelated to the inflammatory status but it prevents to fully clarify the relationship between Gap27, GFAP and astrocyte reactivity. To gain more insight on the nature of reactive astrocytes, we addressed the impact of Gap27 on the NFkB (nuclear factor kappa-light-chain-enhancer of activated B cells) pathway, which is strongly associated with neuroinflammation [45–47] and neuroinflammatory reactive astrocytes signaling [48, 49]. Figure 5E shows representative confocal micrographs of GFAP positive astrocytes marked for NFkB prior (top panels) and after (bottom panels) Gap27 incubation. In Control we rarely detected GFAP + astrocytes positive also for NFkB, which were instead present in all CKs and LPS fields (bar plot in Fig. 5E; n = 8 each condition; mean number of double positive cells/condition 1.44 ± 0.40 Control; 4.45 ± 1.12 CKs; 2.61 ± 0.46 LPS; **P = 0.0047 Control vs CKs, one-way ANOVA). In both CKs and LPS, double positive astrocytes were reduced by Gap27 (bar plot Fig. 5E; n = 8 each condition; mean number of double positive cells/condition 0.88 ± 0.34 CKs + GAP27; 0.94 ± 0.37 LPS + GAP27; ***P = 0.0004 CKs vs CKs + GAP27, **P = 0.0020 LPS vs LPS + GAP27; ***P = 0.0005 CKs vs LPS + GAP27; one-way ANOVA and Mann–Whitney non-parametric t-test). Thus, removing HC activity via Gap27 in astrocytes is associated to a block of calcium signaling, a reduction in cytokines and chemokines release and an attenuated NFkB pathway, both events being apparently dissociated to GFAP reactivity.

## Discussion

In the current study we strengthen the role of active HCs in the generation of inflammation-induced calcium dynamics in resident spinal cord astrocytes. We target spinal tissue reactivity, experimentally induced by pro-inflammatory treatments and involving local neuroglia. We imaged, in the spinal organotypic cultures, calcium signaling from glial cells located close to ventral interneurons, identified upon specific labeling [20], displaying calcium episodes resistant to synaptic activity removal and characterized by low pace kinetics [50]. We adopted the organotypic slice model, a well characterized cell system [11–13, 51], where the 3D-architecture of specific resident cells, neuronal and non-neuronal, can be directly investigated after pro-inflammatory treatments [11, 13]. We ignite inflammatory responses by adopting two different acute stresses known to alter synaptic transmission, to trigger different pro- and anti-inflammatory cytokine and chemokines network and to induce different changes in the morphology of GFAP-positive astrocytes and microglia, suggestive of different states of activation [11, 13]. A cytokines cocktail known to exert pro-inflammatory effects in the CNS of multiple sclerosis animal models [4, 11, 13] and LPS, a toll- like receptors (TLR) agonist, in particular of TLR4, expressed on the microglia surface, that influence cytokine production and immune cell function mimicking systemic inflammation [111317]. Despite the induction of alternative activation mechanisms by CKs and LPS [1113], these two functional conditions similarly enhanced both the number of active glial cells and their oscillatory activity, within the neuronal circuit. We focus on aberrant calcium signals when recorded from astrocytes in the absence of neuronal synaptic activity and restricted to a precise anatomical area, since to understand the functional implications of such signaling requires control of the heterogeneity of reactive cells and of CNS circuits. Apparently, although

(See figure on next page.)

**Fig. 5** Gap27 removed calcium activity in Control, CKs and LPS astrocytes. **A** Representative glial cells calcium oscillations in Control (black) and after CKs and LPS (blue and purple, respectively). Upon 30 min incubation in Gap27 (500 μM) glial cells activity was completely removed in all conditions. All were performed in TTX. **B** Production of cytokines (IL-1β; TNF-α; IL-6) and chemokine (CXCL2) determined by Milliplex assay of organotypic culture supernatants in CKs prior and after incubation with Gap27 (CKs + g). **C** Production of cytokines (IL-1β; TNF-α; IL-6) and chemokine (CXCL2) determined by Milliplex assay of organotypic culture supernatants in LPS prior and after incubation with Gap27 (LPS + g). Test *P < 0.05, **P < 0.01, ***P < 0.001, ****P < 0.0001, one-way ANOVA. **D** Representative high magnification (60 ×) confocal micrographs of organotypic slices immunolabeled with GFAP (in green) in Control, CKs and LPS prior before (top) or after (bottom) Gap27. GFAP intensity in all conditions is summarized in the box plot. *P < 0.05, Kruskal–Wallis test. **E** Representative high magnification (60 ×) confocal micrographs of organotypic slices co-immunolabeled with GFAP (in green) and NFκB p65 (in red) in Control, CKs and LPS prior (top) or after (bottom) Gap27. The bar plot summarizes the mean number of GFAP/NFκB p65 positive cells in all conditions. **P < 0.01, ***P < 0.001; one-way ANOVA and Mann–Whitney non parametric t-test

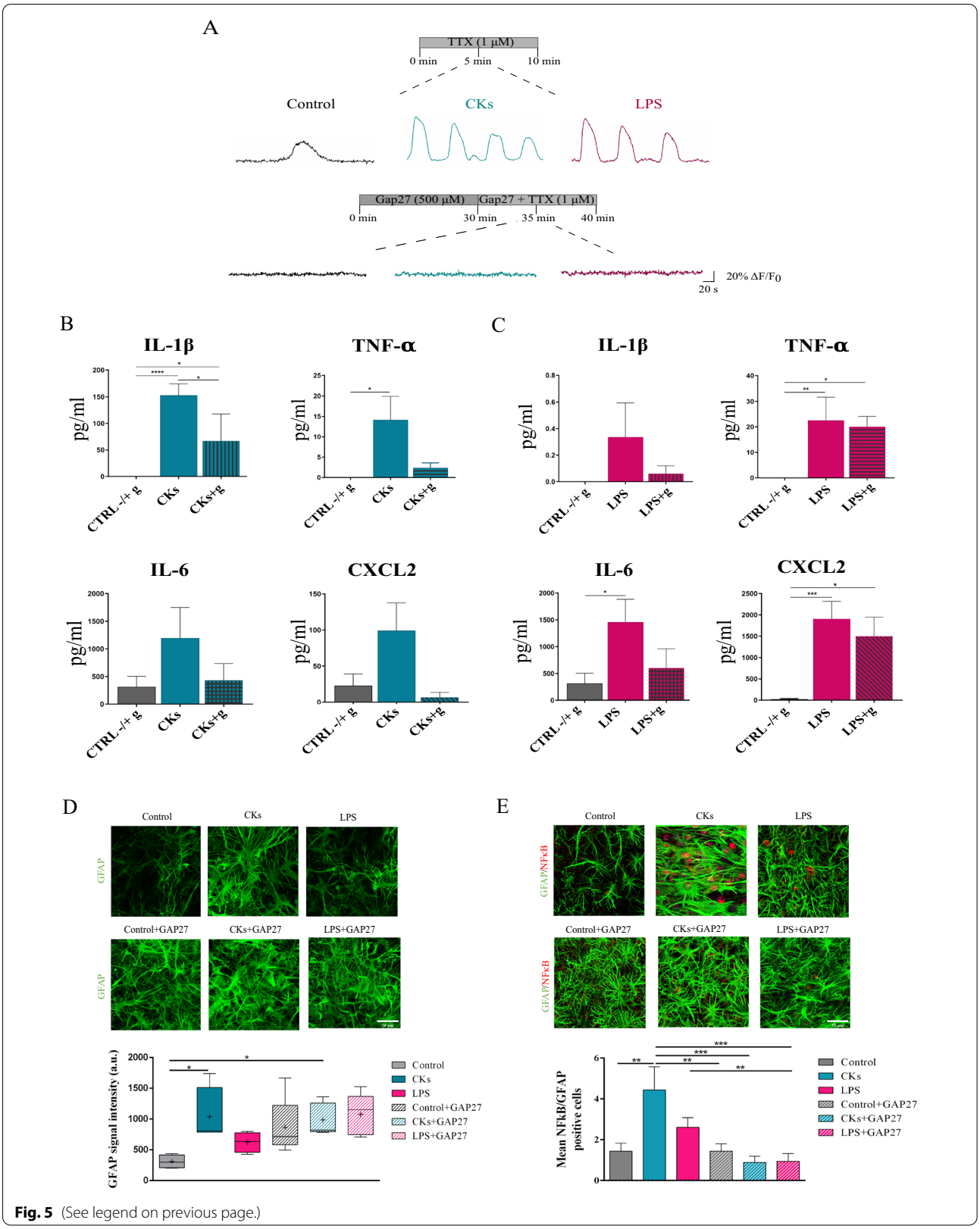


**Fig. 5** (See legend on previous page.)

representing distinct etiologies in the pathology of neuroinflammation, the used danger signals affect glia communication similarly and reactive astrocytes rapidly increase their calcium signals, in frequency and in terms of number of active cells, suggesting that both CKs and LPS promote a similar downstream signaling to translate inflammation into functional changes. It is important to note that we imaged astrocytes within a definite cell layer, and we recorded calcium activity in the cell body located within the focal plan, which prevent monitoring different spatial scales such as astrocyte's processes. Therefore, we cannot exclude that in CKs as well as in LPS treated slices we analyzed calcium activity limited to a subpopulation of astrocytes with defined phenotypic and functional features [52]. In both inflammatory conditions, aberrant calcium signals occurred spontaneously and relay on $Ca^{2+}$ release from the mitochondria and from the endoplasmic reticulum. In both CKs and LPS treated spinal slices, reactive astrocytes are less synchronized, and indeed WB analysis confirms a reduction in Cx43 protein detection, in accordance with a down regulation of GJs. Our results support the suggestion that Cx43 functions are regulated in an opposite manner by inflammatory stresses, namely with a reduction in GJs channel formation and an increase in permeable un-apposed HCs [39]. The increase cellular uptake of the non-fluorescent permeability tracer EtBr in CKs and LPS is reduced by CBX applications, thus indicating an increased activity of HC upon neuroinflammatory stresses. Indeed, cell death and plasma membrane rupture could influence this dye distribution, however our GFAP counterstaining confirm the presence of intact astrocytes, in addition we have previously shown that both treatments, despite inducing a clear inflammatory reaction, did not affect cell viability [1113]. HCs role as membrane pathways for signaling mechanisms and diffusion of small molecules or ions (including $Ca^{2+}$) can be regulated by pro-inflammatory CKs [3953] and further experiments are needed to clarify the relationship among intracellular stores and HCs when contributing to calcium signals. HCs might not be the exclusive membrane pathway contributing to the calcium response, however the use of a mimetic peptide which successfully inhibits abnormal opening of Cx43 HCs [4454] and displays a better selectivity than general inhibitors such as CBX [55] completely removed astrocyte calcium activity, suggesting that HCs opening is instrumental in such responses or is crucially recruiting other channels to allow gliotransmitters release and the activation of downstream pathways. Indeed, CBX recapitulated these findings. Since both Gap27 and CBX are also GJ blockers [404142], it is not surprising that even in Control calcium activity in astrocytes is removed by these agents.

In line with the hypothesis of HCs opening contributing to inflammation are the downregulation of cytokines and chemokines release upon inflammatory stimuli and the reduction in NFkB positive astrocytes both detected when HCs are blocked. It is relevant to outline that the activation of NFkB pathway is ubiquitous, making it difficult to evaluate its role as essential to initiate astrocyte reactivity. In all conditions, the HCs peptide blocker triggered an increase in GFAP expression, thus it is virtually impossible to assess the role, if any, of HC activation on GFAP increase following CKs or LPS inflammation. This increase in GFAP needs also to be addressed in future investigations, since connexin mimetic peptides have been reported to down regulate GFAP expression, yet after longer treatments [56] when compared to the current experiments. In addition, due to the impairment of astrocytes function due to Gap27, including glial spatial buffering ability of potassium ion excess [57] we cannot exclude that GFAP hypertrophy represent a transient homeostatic response.

Calcium-dependent glia signaling is a highly investigated and well characterized feature of astrocytes, nonetheless its key mechanisms and contribution to inflammatory pathology are still under debate [18, 58]. The finding that in spinal cord circuits local reactive astrocytes display similar calcium signals, but diverse hypertrophy [11, 13] may provide insight into the role of these functional changes. In both the pathological conditions, astrocytes Cx43 HC permeability, key to intracellular signaling including calcium oscillations [59, 60], is enhanced while apparently GJ intercellular trafficking is restricted.

## Conclusions

In this work we confirmed that the organotypic slice system represents an excellent setting, thanks to which it is possible to dissect how the inflammatory environment interferes with the spinal circuits function, due to the easy accessibility of the resident cells and to the long-lasting duration of the cultures. In fact, we exploited these cultures to investigate whole network changes of a precise region of interest under pathological conditions and we were able to mimic two different kinds of inflammation. The main finding of the current work is that local inflammation in organotypic spinal slices, induced by CKs and LPS, was able to regulate the astrocyte function, acting at the calcium signaling level, modulating the permeability of the HCs and altering the GJs communication, regardless GFAP hypertrophy. In conclusion, expanding our knowledge on the interplay between astrocytes and neurons in the spinal circuits and understanding the role of the occurring $Ca^{2+}$ oscillations during pathological conditions represent

the starting point for developing new therapies and strategies, essential for investigating the spinal neurodegenerative disorders.

## Methods

### Organotypic spinal cord cultures and pro-inflammatory treatments

All experiments were performed in accordance with the EU guidelines (2010/63/UE) and Italian law (Decree 26/14) and were approved by the local authority veterinary service and by our institution (SISSA) animal wellbeing committee (OBPA). All efforts were made to minimize animal suffering and to reduce the number of animals used. Animal use was approved by the Italian Ministry of Health (no. 22DABNQYA), in agreement with the EU Recommendation 2007/526/CE. Organotypic spinal cord and DRG slices were obtained from mouse embryos (C57BL/6 J) at E12–13 of gestation as previously described [11–13]. Briefly, pregnant mice were sacrificed by $CO_2$ overdose and fetuses delivered by caesarean section. Isolated fetuses were decapitated and their backs were isolated from low thoracic and high lumbar regions and transversely sliced (275 µm) with a tissue chopper. After dissecting the spinal cord and the DRG from the surrounding tissue, slices were embedded into a thick matrix obtained by chicken plasma (Sigma) and thrombin (Sigma) clot. Slices were cultured in plastic tubes with 1 mL medium. The tubes were kept in a roller drum rotating 120 times per hour in an incubator at 37 °C in the presence of humidified atmosphere, with 5% $CO_2$. Experiments were performed on spinal cultures at 2–3 weeks in vitro (WIV) treated for 6 h with two different inflammatory paradigms [11, 13]: (i) a cocktail of the mouse recombinant cytokines (10 ng/mL each) TNF-α (R&D Systems, #210-TA/CF), IL-1β (R&D Systems, #M15330), and granulocyte–macrophage colony stimulating factor (GM-CSF; R&D Systems, #P04141) [1, 11, 13]; (ii) lipopolysaccharide (LPS; 1 µg/mL, Sigma, O55:B5) [11]. CKs or LPS were removed after the incubation times, prior to live cell imaging recordings, immunoblotting analysis and immunostaining analysis.

### Lentiviruses preparations and organotypic slices infection

The lentiviruses were generated and titrated as previously described [62]. Lentiviral vectors employed in this study include: LV_pGfap-rtTA2S-M2, (built as previously shown [63]) and LV_TREt-mCherry, kindly provided by professor Antonello Mallamaci's lab. The slices were infected with 5 µL of lentiviral preparation, whose titres were $4 \times 106$ and $1 \times 107$ respectively. 2 µg/mL doxycycline were administered every two days (TetON system).

### Live cell $Ca^{2+}$ imaging

Organotypic spinal cord cultures were loaded with 4 µM Fluo-4 AM (Molecular Probes); 11.6 µL of DMSO (Sigma-Aldrich) were added to the stock 50 µg of the dye and cultures were incubated with a final concentration of 4 µM for 1 h in the roller drum at 37 °C, 5% $CO_2$. After dye loading, a de-esterification period followed, cultures were maintained in extracellular saline solution, also used as recording solution, composed of (mM): 150 NaCl, 4 KCl, 1 $MgCl_2$, 2 $CaCl_2$, 10 HEPES, 10 Glucose (pH adjusted to 7.35 with 2 M NaOH), in the same incubator for 30 min. The samples were mounted in a recording chamber placed on an inverted microscope (Nikon Eclipse Ti-U), where they were continuously perfused (5 mL/minute flow rate) at room temperature (RT) with the recording saline solution. The dye was excited at 488 nm with a mercury lamp and the emission was detected at 520 nm. Neurons and glial cells (the focus was set and maintained in a slice layer where both neurons and glial cells could be detected) at the premotor region in the ventral zone of the slice were observed with a 40× objective (PlanFluor, 0.60 NA) [23]. Images were constantly acquired at 6.67 fps every 150 ms using an ORCA-Flash4.0 V2 sCMOS camera (Hamamatsu) and the set-up was controlled by HCImage Live software. Basal activity was recorded for 10 min in the presence of saline solution to check for stability prior to adding the following drugs: 1 µM tetrodotoxin (TTX, fast voltage-gated $Na^+$ channel blocker, Latoxan); 2 µM carbonyl cyanide 3-chlorophenylhydrazone (CCCP, mitochondrial protonophore, Sigma); 5 µM thapsigargin (TG, SERCA inhibitor, Sigma); 200 µM carbenoxolone (CBX, gap junction uncoupler, Sigma). The kinetics of calcium events, to identify fast (neuronal) and slow (glial) events, was estimated by measuring the episode duration from $n = 14$ neurons and $n = 42$ glial cells in 3 cultures. For the Connexin43 mimetic Gap27 (500 µM) experiments, this peptide was dissolved in the saline solution and incubated for 30 min prior to recordings. The recorded images were analyzed selecting ROIs around dye positive cells with Fiji software. The corresponding traces were extracted with Clampfit software (pClamp suite, 10.6 version; Axon Instruments) and analyzed off-line. $Ca^{2+}$ transients were expressed as $\Delta F/F_0$, where $\Delta F$ is the fluorescence rise over baseline, and $F_0$ is the baseline fluorescence level, calculated as:

$$100 \times \frac{F - F_0}{F_0}$$

(F, fluorescence value; $F_0$, baseline fluorescence). $F_0$ was calculated as the median of the frame fluorescence values.

#### Sulforhodamine 101 (SR101) staining protocol

In order to confirm that the $Ca^{2+}$ activity detected in the presence of TTX was the one of glial cells and in particular of astrocytes, the slices were incubated for 20 min in the recording solution containing 1 µM SR101 at 37 °C, after the incubation with the calcium dye. The slices were then washed with the recording solution for 10 min at 37 °C, to allow the washout of excess dye from the extracellular space. The dye was excited at 594 nm with a mercury lamp.

#### Calcium imaging with GCaMP6f and analysis

pZac2.1 gfaABC1D-cyto-GCaMP6f was a gift from Baljit Khakh (Addgene viral prep # 52925-AAV5; http://n2t.net/addgene:52925; RRID:Addgene_52925). Organotypic slices at 1 WIV (n = 4) were infected with AAV5.gfaABC1D-cyto-GCaMP6f which leads to a selective expression of the genetically encoded calcium indicator GCaMP6f in astrocytes. Slices were placed at 2–3 WIV in a custom 3D-printed perfusion chamber mounted on a Nikon microscope (Nikon Eclipse Ti2 microscope endowed with a Nikon IntensiLight Hg lamp and an Andor Zyla sCMOS camera). GCaMP6f fluorescence was recorded with a 20 × S Plan Fluor ELWD NA 0.45 objective once an area within the ventral horn was identified that displayed fluorescence transient activity recognizable by eye. Images were taken at a rate of 1 per 150 ms, with an exposure time of 100 ms and 4 × 4 binning. The acquired time series of images were analysed in Fiji choosing ROIs of ~ Ø 20–30 µm and the obtained mean fluorescence traces were processed in ClampFit 10.7.

#### Western blotting analysis

Control and treated organotypic spinal cultures (n = 4 slices per condition) were scraped in 200 µL of Lysis buffer (10 mM Tris–HCl, 150 mM NaCl, 0.5% NP40, 0.5% DOC, protease inhibitor cocktail). Samples were triturated using 200-µL pipette and 1-mL syringe pass tissue suspension through a 26-gauge needle until all tissue were lysed. Subsequently lysates were subjected to 3 freeze–thaw cycles of 1 min each at − 80 °C, sonicated at 50% amplitude for 30 s and centrifuged at 100 × g at 4 °C for 5 min. Protein concentration of the lysate were determined using the bicinchoninic acid assay (Thermofisher Scientific). Samples were prepared adding 2 × Leammli buffer (10% SDS, 20% glycerol, 125 mM Tris–HCl, 0.01% bromophenol blue, 1 M DTT) to 20 µg of proteins and denatured boiling at 100 °C for 5 min. SDS-PAGE gels were prepared in relation to the molecular weight of the protein of interest (12% polyacrylamide separating gel). Samples were run at 120 V at RT and transferred onto Immun-Blot PVDF (Polyvinylidene difluoride) membrane (Millipore) by electroblotting at 100 V for 1 h and 30 min at 4 °C. Membranes were blocked in 5% BSA in TBS-T for 1 h and incubated overnight at 4 °C with anti-Cx43 (rabbit monoclonal, 1:8000, Abcam). The day after, the primary antibody was recovered, the washed membranes in TBS-T were incubated with secondary antibody (Alexa goat anti-rabbit horseradish peroxidase-conjugated, 1:1000, Invitrogen) at RT for 1 h and washed again. As housekeeping protein normalizer was used anti-β-Tubulin III (mouse monoclonal, 1:1000, Sigma) conjugated with the proper secondary antibody (Alexa goat anti-mouse horseradish peroxidase-conjugated, 1:1000, Invitrogen) at RT for 1 h. Subsequently, the membranes were washed with TBS-T and developed by enhanced chemiluminescence (ECL Western Blotting Substrate, Thermofisher) using the UViTEC Cambridge system. The quantified band intensity of three replicates were analyzed using Uviband Analysis, Image quantification Software.

#### Immunofluorescence imaging and analysis

For the tissue reactivity analysis, organotypic cultures were fixed with 4% formaldehyde (prepared from fresh paraformaldehyde; Sigma) in PBS (1 ×) for 1 h (RT) and washed in PBS. Free aldehyde groups were quenched in sodium borohydride ($NaBH_4$, Sigma) 1% in PBS for 5 min. Slices were permeabilized and blocked in PBS 1 ×, 5% FBS (Sigma), 1% BSA (Sigma), and 0.3% Triton X-100 (Sigma) at RT for 1 h and incubated overnight at 4 °C with anti-GFAP (mouse monoclonal, 1:400, Sigma), anti-Iba1 (rabbit polyclonal, 1:500, Wako) and anti-NFκB p65 (rabbit polyclonal, 1:500, Invitrogen) primary antibodies. Subsequently, the slices were PBS-washed and incubated with secondary antibodies diluted in blocking solution for 2 h (RT) in the dark. The secondary antibodies were Alexa 488 goat anti-mouse (1:500, Invitrogen), Alexa 594 goat anti-rabbit (1:500, Invitrogen) and we used DAPI (1:500, Thermo Fisher Scientific) to stain the nuclei. Samples were mounted on glass coverslips using Fluoromount-G aqueous mounting medium (Thermo Fisher Scientific). Images were acquired using Nikon A1 Confocal microscope with Ar/Kr, He/NE, and UV laser with 40 × objective (0.95 N.A.) and 60 × oil objectives (1.35 N.A.) using oil mounting medium (1.515 refractive index). Confocal sections were acquired up to a total Z-stack thickness of 5 to 15 µm (depending on the required analysis) in sequential mode with lasers (488 nm for GFAP and 561 nm for Iba1 and NFκB p65). For each experiment we performed ≥ 3 independent cultures; from each culture series, we used ≥ 3 slices for every condition, and from each slice, ≥ 5 fields were randomly acquired from the ventral region. Offline analysis of the image Z-stack was performed using the Volocity 3D Image Analysis Software. The offline analysis of the

Z-stacks for calculating the transformation index and the GFAP signal intensity were performed as previously reported [11]. Briefly, for microglia morphology, we measured the area and the perimeter, necessary to calculate the transformation index [11] as $\frac{[perimeterofcell(\mu m)]^2}{4\pi \bullet [areaofcell(\mu m^2)]}$ quantifying microglia ramifications. Astrocytes were quantified by measuring, in every acquired field, the intensity of the GFAP signal calculated by the software using a greyscale and expressed in the plot in arbitrary unit (a.u.). To quantify the astrocytes proinflammatory activation we evaluate the expression of the transcription factor NFκB p65 in GFAP positive cells. Double positive cells were identified by the Volocity tool "Intersect objects" to quantify only the objects where NFκB p65, GFAP, and DAPI signals are intersected. Furthermore, a size threshold limit was set to exclude all the objects with a dimension lower than 5 $\mu m^3$ in order to avoid background signal interference. The results were expressed as the mean number of NFκB p65/GFAP positive cells for each treatment condition.

#### Ethidium bromide uptake

For dye uptake experiments, cultures were exposed to 5 μM EtBr (Sigma) for 10 min at 37 °C. In order to investigate the contribution of GJs and HCs to the dye uptake, an independent experiment was performed where slices were incubated with CBX for 10–15 min prior to EtBr + CBX for additional 30 min. EtBr is permeable through membrane but can transit through HCs and becomes more fluorescent after binding to DNA. After 30 min exposure to EtBr, the slices were washed in extracellular saline solution for 15 min, fixed in 4% formaldehyde (prepared from fresh PFA, Sigma) in PBS 1 × for 1 h at RT and washed in PBS. Free aldehyde groups were quenched in 0.1 M glycine in PBS for 10 min. Slices were permeabilized and blocked in PBS 1 ×, 10% FBS (Sigma), 5% BSA (Sigma), and 0.3% Triton-X 100 (Sigma) at RT for 1 h, and then incubated over night at 4 °C with anti-GFAP primary antibody. Secondary antibodies were Alexa 488 goat anti-mouse (1:500, Invitrogen) and DAPI (1:500, Thermo Fisher Scientific) diluted in blocking solution for 2 h at RT, in the dark. Samples were mounted on glass coverslips using Fluoromount-G aqueous mounting medium (Thermo Fisher Scientific). Images were acquired using Nikon C2 Confocal microscopes with Ar/Kr, He/NE, and UV laser with 40 × oil objectives (1.4 N.A.) using oil mounting medium (1.515 refractive index). Confocal sections were acquired every 0.5 μm up to a total *Z*-stack thickness of 20 μm in sequential mode with lasers (488 nm for GFAP and 561 nm for EtBr). For each condition, we performed 3 independent cultures (3 slices/series), and from each slice ≥ 5 fields were randomly acquired. Offline analysis of the image Z-stack was performed using the Volocity3D Image Analysis Software. The "$GFAP^+$ objects" and the "$EtBr^+$ objects" were determined after thresholding images. With the Volocity tool "Intersect objects" we determined the number of "$EtBr^+$ astrocytes". EtBr uptake was expressed as the ratio between the "$EtBr^+$ astrocytes" over the total number of astrocytes ("$GFAP^+$ objects").

#### Cytokines and chemokines: Luminex assay and analysis

In organotypic culture supernatants 13 cytokines and chemokines were measured (IFN-γ, IL-1α, IL-1β, IL4, IL6, IL10, IL12p40, IL12p70, IL17, CXCL10, CCL2, CXCL2, TNF- α) by Milliplex assay (Merck Millipore, USA, #MCYTOMAG-70 K) using Bio-Plex device (Bio-Rad, USA), according to the manufacturer's protocol. For all the analyzed factors, the assay detection limit was below 1.1 pg/ml. Statistical analysis was performed by One-Way ANOVA followed by post-hoc Tukey's multiple comparisons test. Significance was considered when $P < 0.05$.

#### Statistical analysis and analysis of synchronization

All values from samples subjected to the same experimental protocols were pooled together and results are presented as mean ± S.E.M. with n = number of slices, if not stated otherwise. A statistically significant difference between three data sets was assessed by one-way ANOVA for parametric data or Kruskal–Wallis test for non-parametric ones and Mann–Whitney non parametric t-test. In addition, differences in the relative cumulative frequency distribution were obtained using the paired Kolmogorov–Smirnov test. Statistical significance was determined at $P < 0.05$.

In box-plots, the thick horizontal bar indicates the median value, the cross indicates the mean value, the boxed area extends from the 25$^{th}$ to 75$^{th}$ percentiles while whiskers from the 5$^{th}$ to the 95$^{th}$ percentiles.

The correlation between the oscillatory activities of two neighbor cells in the same slice was assessed by cross correlation analysis. The synchronization analysis was based on a bootstrapping method modified from Usmani et al. [64]. With this analysis, 200.000—time windows are generated from each pair of traces and used to obtain a "real CCF (cross-correlation factor)" distribution with its mean/median, then compared with the distribution of "randomly generated CCFs" obtained by shuffling the 200.000—time windows. The extent of the area of the "random CCFs" distribution that exceeded the mean/median of the "real CCFs" allowed the calculation of a p-value. Significantly ($^*P < 0.05$) correlated pairs were considered synchronized and their count over the total number of cell pairs analyzed was plotted as percentage of correlated pairs. The distribution of the *p*-values was

also plotted. For estimating significantly synchronous slices in the three groups, we performed a homogeneity test with the Fisher's exact test.

More in detail, we measured three slices per experimental condition and we obtained the measurements from non-overlapping neurons or glial cells. Here, we found that paired neurons (n = 135, 135 and 156 pairs in Control, CKs and LPS) in all the three different experimental conditions are synchronized (0.004 ± 0.001 pair *P*-value Control; 0.001 ± 0.0002 pair *P*-value CKs 6H; 0.001 ± 0.0002 pair *P*-value LPS 6H, Kruskal–Wallis test and Fisher's exact test; Additional file 2: Fig. S2), with no significant differences among the groups.

#### Abbreviations

ALS: Amyotrophic lateral sclerosis; CBX: Carbenoxolone; CCCP: 2 Carbonyl cyanide 3-chlorophenylhydrazone; CCF: Cross correlation coefficient; CKs: Cytokines; CNS: Central nervous system; Cx43: Connexin 43; DRG: Dorsal root ganglia; ER: Endoplasmic reticulum; EtBr: Ethidium bromide; GM-CSF: Granulocyte–macrophage colony-stimulating factor; GJs: Gap junctions; HCs: Hemichannels; IL-1β: Interleukin 1 beta; LPS: Lipopolysaccharide; MS: Multiple sclerosis; RT: Room temperature; SERCA: Sarco-endoplasmic reticulum; SR101: Sulforhodamine 101; TG: Thapsigargin; TLR: Toll-like receptor; TNF-α: Tumor necrosis factor alpha; TTX: Tetrodotoxin; WIV: Weeks in vitro; WB: Western blot.

## Supplementary Information

The online version contains supplementary material available at https://doi.org/10.1186/s13041-021-00868-6.

**Additional file 1: Figure S1.** Pro-inflammatory treatments boost neuronal calcium signaling and alter glial reactivity. A. Left, GCaMP6f fluorescence image, maximal projection of 3554 images acquired in 10 min of recording at 6.6 fps. Scale bar, 50 µm. Right, representative GCaMP6f fluorescence recordings from Control organotypic ventral horn before (in black) and after TTX (1 µM, in blue) application and (right) results are pooled together in the boxplot and cumulative distribution of interevent intervals (IEI, $n_{Control} = 32$ cells and $n_{TTX} = 46$ cells, P = 0.4539). B. Representative snapshots (40 × magnification) of the ventral area of organotypic spinal slices loaded with Fluo-4 AM; frames were taken at variable time intervals (0, 5 and 10 s) in three different experimental conditions (Control, CKs and LPS). Scale bar 50 µm. C. Representative fluorescent tracings depicting neuronal spontaneous activity as calcium transients in control (black) and after CKs and LPS (blue and purple, respectively). The box plot summarizes the frequency values of calcium events in all conditions. ***P < 0.001 and **P < 0.01, Kruskal–Wallis. D. Representative confocal images of organotypic spinal slices immunolabeled for Iba1 (red) and GFAP (green), visualizing microglia and astrocytes, respectively, prior and after CKs or LPS administration. Scale bar 25 µm. E. Box plot (top) summarizes GFAP signal intensity prior and after CKs or LPS treatments. Test ****P < 0.0001 Control vs CKs, ***P = 0.001 CKs vs LPS, P = 0.0112 Control vs LPS, one-way ANOVA. Box plot (bottom) summarizes transformation indices upon CKs and LPS administration. *P < 0.05 Control vs CKs and ****P < 0.0001 Control vs LPS, Kruskal–Wallis test.

**Additional file 2: Figure S2.** Pro-inflammatory treatments alter glial cells synchronization. A. Two example fluorescent tracings, obtained from two neurons (in red and blue) located in the same visual field in the ventral horn of organotypic slices in Control, CKs and LPS. The fluorescent recordings show calcium oscillations and the synchrony between recorded neurons was determined by computing their Pearson correlation coefficient in time windows that were randomly sampled from the all duration of the recording. The bar plot shows the % of correlated pairs in Control, CKs and LPS. Kruskal–Wallis test. The aligned dot plot shows the p values distributions obtained by the comparison of correlated pairs of traces. Fisher's exact test. B. Two example fluorescent tracings, obtained from two astrocytes (in red and blue) located in the same visual field in the ventral horn of organotypic slices in Control, CKs and LPS. The fluorescent recordings show calcium oscillations in the presence of TTX and the synchrony between recorded astrocytes was determined by computing their Pearson correlation coefficient in time windows that were randomly sampled from the all duration of the recording. The bar plot summarizes the % of correlated pairs detected in all conditions. ***P < 0.001 and **P < 0.01, one-way ANOVA. The aligned dot plot (right) shows the p values distribution obtained by the comparison of correlated pairs of traces. *p < 0.05 Fisher's exact.

**Additional file 3: Figure S3.** CBX removed calcium activity in Control, CKs and LPS astrocytes. A. The scatter plot shows the mean number of active glial cells/ slices in Control, CKs and LPS (in black, cyan and purple, respectively), before and after the administration of carbenoxolone (CBX, 200 µM). Each dot in the plot represents one different slice. B. Representative fluorescent tracings of glial cells calcium events, prior and after CBX, in Control (black) and after CKs and LPS administration (cyan and purple, respectively).

#### Acknowledgements

The authors would like to thank M. Grandolfo for providing technical support with immunofluorescence labelling, confocal microscopy and image analysis and M. Santo for assistance in lentivirus preparation and infections.

#### Authors' contributions

G.P. performed cell biology, live imaging, and together with C.M. immunofluorescence experiments and analysis; R.A. performed the Milliplex experiments and analysis. A.T. performed the GCaMP6f imaging experiments and analysis. L.B. and C.B. conceived the study, the experimental design and wrote the manuscript. All authors read and approved the final manuscript.

#### Funding

We acknowledge financial support from the European Union's Horizon 2020 research and innovation program under grant agreement no. 785219 and 881603 Graphene Flagship.

#### Availability of data and materials

The datasets supporting the conclusion of this article are included within the article (and its additional files). The datasets generated and/or analysed during the current study are stored in a public repository and are available from the corresponding author on reasonable request.

## Declarations

#### Ethics approval and consent to participate

All experiments were performed in accordance with the EU guidelines (2010/63/UE) and Italian law (Decree 26/14) and were approved by the local authority veterinary service and by our institution (SISSA) ethical committee. All efforts were made to minimize animal suffering and to reduce the number of animals used. Animal use was approved by the Italian Ministry of Health (no. 22DABNQYA), in agreement with the EU Recommendation 2007/526/CE.

#### Consent for publication

Not applicable.

#### Competing interests

The authors declare that they have no competing interests.

Received: 6 August 2021 Accepted: 15 October 2021
Published online: 25 October 2021

**References**


1. Kempuraj D, Thangavel R, Natteru PA, Selvakumar GP, Saeed D, Zahoor H, Zaheer S, Iyer SS, Zaheer A. neuroinflammation induces neurodegeneration. J Neurol Neurosurg Spine. 2016;1:1–15.
2. Puentes F, Malaspina A, Van Noort JM, Amor S. Non-neuronal cells in ALS: role of glial, immune cells and blood-CNS barriers. Brain Pathol. 2016;26:248–57.
3. Glass CK, Saijo K, Winner B, Marchetto MC, Gage H. Mechanisms underlying inflammation in neurodegeneration. Nih. 2010;140:918–34.
4. Centonze D, Muzio L, Rossi S, Cavasinni F, De Chiara V, Bergami A, Musella A, D'Amelio M, Cavallucci V, Martorana A, Bergamaschi A, Cencioni MT, Diamantini A, Butti E, Comi G, Bernardi G, Cecconi F, Battistini L, Furlan R, Martino G. Inflammation triggers synaptic alteration and degeneration in experimental autoimmune encephalomyelitis. J Neurosci. 2009;29:3442–52.
5. Mandolesi G, Gentile A, Musella A, Fresegna D, De Vito F, Bullitta S, Sepman H, Marfia GA, Centonze D. Synaptopathy connects inflammation and neurodegeneration in multiple sclerosis. Nat Rev Neurol. 2015;11:711–24.
6. Mader S, Brimberg L. Aquaporin-4 water channel in the brain and its implication for health and disease. Cells. 2019;8:90.
7. Farina C, Aloisi F, Meinl E. Astrocytes are active players in cerebral innate immunity. Trends Immunol. 2007;28:138–45.
8. Sofroniew MV. Molecular dissection of reactive astrogliosis and glial scar formation. Trends Neurosci. 2009;32:638–47.
9. Gähwiler BH. Organotypic monolayer cultures of nervous tissue. J Neurosci Methods. 1981;4:329–42.
10. Gähwiler BH, Capogna M, Debanne D, McKinney RA, Thompson SM. Organotypic slice cultures: a technique has come of age. Trends Neurosci. 1997;20:471–7.
11. Giacco V, Panattoni G, Medelin M, Bonechi E, Aldinucci A, Ballerini C, Ballerini L. Cytokine inflammatory threat, but not LPS one, shortens GABAergic synaptic currents in the mouse spinal cord organotypic cultures. J Neuroinflammation. 2019;16:127.
12. Avossa D, Rosato-Siri MD, Mazzarol F, Ballerini L. Spinal circuits formation: a study of developmentally regulated markers in organotypic cultures of embryonic mouse spinal cord. Neuroscience. 2003;122:391–405.
13. Medelin M, Giacco V, Aldinucci A, Castronovo G, Bonechi E, Sibilla A, Tanturli M, Torcia M, Ballerini L, Cozzolino F, Ballerini C. Bridging pro-inflammatory signals, synaptic transmission and protection in spinal explants in vitro. Mol Brain. 2018;11:1–14.
14. Pascual O, Achour SB, Rostaing P, Triller A, Bessis A. Microglia activation triggers astrocyte-mediated modulation of excitatory neurotransmission. Proc Natl Acad Sci U S A. 2012;109:197–205.
15. Rossi S, Furlan R, De Chiara V, Motta C, Studer V, Mori F. Interleukin-1β causes synaptic hyperexcitability in multiple sclerosis. Ann Neurol. 2012;71:76–83.
16. Vereker E, Campbell V, Roche E, McEntee E, Lynch MA. Lipopolysaccharide inhibits long-term potentiation in the rat dentate gyrus by activating caspase-1. J Biol Chem. 2000;275:26252–8.
17. Li X, Tupper JC, Bannerman DD, Winn RK, Rhodes CJ, Harlan JM. Phosphoinositide 3 kinase mediates toll-like receptor 4-induced activation of NF-kB in endothelial cells. Infect Immun. 2003;71(8):4414–20.
18. Shigetomi E, Saito K, Sano F, Koizumi SC. Aberrant calcium signals in reactive astrocytes: a key process in neurological disorders. Int J Mol Sci. 2019;20:996.
19. Araque A, Carmignoto G, Haydon PG, Oliet SHR, Robitaille R, Volterra A. Gliotransmitters travel in time and space. Neuron. 2014;81:728–39.
20. Rasmussen R, Nedergaard M, Petersen NC. Sulforhodamine 101, a widely used astrocyte marker, can induce cortical seizure-like activity at concentrations commonly used. Sci Rep. 2016;6:1–9.
21. Hülsmann S, Hagos L, Heuer H, Schnell C. Limitations of sulforhodamine 101 for brain imaging. Front Cell Neurosci. 2017;11:1–6.
22. Schnell C, Hagos Y, Hulsmann S. Active sulforhodamine 101 uptake into hippocampal astrocytes. PLoS ONE. 2012;7:1–13.
23. Fabbro A, Pastore B, Nistri A, Ballerini L. Activity-independent intracellular Ca2+ oscillations are spontaneously generated by ventral spinal neurons during development in vitro. Cell Calcium. 2007;41:317–29.
24. Garaschuk O, Linn J, Eilers J, Konnerth A. Large-scale oscillatory calcium waves in the immature cortex. Nat Neurosci. 2000;3:452–9.
25. Hirase H, Qian L, Barthó P, Buzsáki G. Calcium dynamics of cortical astrocytic networks in vivo. PLoS Biol. 2004;2:494–9.
26. Haustein MD, Kracun S, Lu X-H, Shih T, Jackson-Weaver O, Tong X, Xu J, Yang XW, O'Dell TJ, Marvin JS, Ellisman MH, Bushong EA, Looger LL, Khakh SB. Conditions and constraints for astrocyte calcium signaling in the hippocampal mossy fiber pathway. Neuron. 2014;82:413–29.
27. Petravicz J, Fiacco TA, McCarthy KD. Loss of IP3 receptor-dependent Ca2+ increases in hippocampal astrocytes does not affect baseline CA1 pyramidal neuron synaptic activity. J Neurosci Off J Soc Neurosci. 2008;28:4967–73.
28. Shigetomi E, Bushong EA, Haustein MD, Tong X, Jackson-Weaver O, Kracun S, Xu J, Sofroniew MV, Ellisman MH, Khakh BS. Imaging calcium microdomains within entire astrocyte territories and endfeet with GCaMPs expressed using adeno-associated viruses. J Gen Physiol. 2013;141:633-647.29.
29. Agarwal A, Wu P, Hughes EG, Fukaya M, Tischfield MA, Langseth AJ, Wirtz D, Bergles DE. Transient opening of the mitochondrial permeability transition pore induces microdomain calcium transients in astrocyte processes. Neuron. 2017;93:587-605.e7.
30. Giaume C, Fromaget C, Aoumari E, Cordier J, Clowinski J, Aoumari E. Gap junctions in cultured astrocytes: currents and characterization of protein single-channel. Neuron. 1991;6(1):133–43.
31. Ren J, Momose-Sato Y, Sato K, Greer JJ. Rhythmic neuronal discharge in the medulla and spinal cord of fetal rats in the absence of synaptic transmission. J Neurophysiol. 2006;95:527–34.
32. Hjorth J, Blackwell KT, Kotaleski JH. Gap junctions between striatal fast-spiking interneurons regulate spiking activity and synchronization as a function of cortical activity. J Neurosci. 2009;16:5276–86.
33. Yin J, VanDongen A. Enhanced neuronal activity and asynchronous calcium transients revealed in a 3D organoid model of Alzheimer's disease. 2020;7:254–264.
34. Cornell-Bell AH, Finkbeiner SM, Cooper MS, Smith SJ. Glutamate induces calcium waves in cultured astrocytes: long-range glial signaling. Science. 1990;247:470–3.
35. Orellana JA, Saez PJ, Shoji KF, Schalper KA, Palacios-Prado N, Velarde V, Giaume C, Bennett MVL, Saez JC. Modulation of brain hemichannels and gap junction channels by pro-inflammatory agents and their possible role in neuro-degeneration. Antioxid Redox Signal. 2009;11:369–99.
36. Liao CK, Jeng CJ, Wang HS, Wang SH, Wu JC. Lipopolysaccharide induces degradation of connexin43 in rat astrocytes via the ubiquitin-proteasome proteolytic pathway. PLoS ONE. 2013;8:1–11.
37. Sáez JC, Schalper KA, Retamal MA, Orellana JA, Shoji KF, Bennet MVL. Cell membrane permeabilization via connexin hemichannels in living and dying cells. Exp Cell Res. 2010;316:2377–89.
38. Giaume C, Venance L. Intercellular calcium signaling and gap junctional communication in astrocytes. Glia. 1998;64:50–64.
39. Retamal MA, Froger N, Palacios-Prado N, Ezan P, Saez PJ, Saez JC, Giaume C. Cx43 hemichannels and gap junction channels in astrocytes are regulated oppositely by proinflammatory cytokines released from activated microglia. J Neurosci. 2007;27:13781–92.
40. Contreras JE, Sanchez HA, Eugenin EA, Speidel D, Theis M, Willecke K, Bukauskas FF, Bennett MVL, Saez JC. Metabolic inhibition induces opening of unapposed connexin 43 gap junction hemichannels and reduces gap junctional communication in cortical astrocytes in culture. Proc Natl Acad Sci U S A. 2002;99:495–500.
41. Yin X, Feng L, Ma D, Yin P, Wang X, Hou S, Hao Y, Zhang J, Xin M, Feng J. Roles of astrocytic connexin-43, hemichannels, and gap junctions in oxygen-glucose deprivation/reperfusion injury induced neuroinflammation and the possible regulatory mechanisms of salvianolic acid B and carbenoxolone. J Neuroinflammation. 2018;15:1–24.
42. Wang N, De Bock M, Decrock E, Bol M, Gadicheria A, Bultynck G, Leybaert L. Connexin targeting peptides as inhibitors of voltage- and intracellular Ca2+-triggered Cx43 hemichannel opening. Neuropharmacology. 2013;75:506–16.
43. Chever O, Lee CY, Rouach N. Astroglial connexin43 hemichannels tune basal excitatory synaptic transmission. J Neurosci. 2014;34:11228–32.
44. Wang N, De Bock M, Antoon G, Gadicheria AK, Bol M, Decrock E, Evans WH, Sipido KR, Bukauskas FF, Leybaert L. Connexin mimetic peptides inhibit Cx43 hemichannel opening triggered by voltage and intracellular Ca2+ elevation. Basic Res Cardiol. 2012;107(6):17.

45. Mattson MP, Meffert MK. Roles for NF-kappaB in nerve cell survival, plasticity, and disease. Cell Death Differ. 2006;13:852–60.
46. Kaltschmidt B, Kaltschmidt C. NF-kappaB in the nervous system. Cold Spring Harb Perspect Biol. 2009;1: a001271.
47. Hsiao H-Y, Chen Y-C, Chen H-M, Tu P-H, Chern Y. A critical role of astrocyte-mediated nuclear factor-κB-dependent inflammation in Huntington's disease. Hum Mol Genet. 2013;22:1826–42.
48. Lian H, Yang L, Cole A, Sun L, Chiang ACA, Fowler SW, Shim DJ, Rodriguez-Rivera J, Tagliatela G, Jankowsky JL, Lu H-C, Zheng H. NFκB-activated astroglial release of complement C3 compromises neuronal morphology and function associated with Alzheimer's disease. Neuron. 2015;85:101–15.
49. Liddelow SA, Barres BA. Reactive astrocytes: production, function, and therapeutic potential. Immunity. 2017;46:957–67.
50. Deitmer JW, Verkhratsky A, Lohr C. Calcium signalling in glial cells. Pharmacogn Mag. 1998;24:405–16.
51. Furlan F, Taccola G, Grandolfo M, Guasti L, Arcangeli A, Nistri A, Ballerini L. ERG conductance expression modulates the excitability of ventral horn GABAergic interneurons that control rhythmic oscillations in the developing mouse spinal cord. J Neurosci. 2007;27:919–28.
52. Giovannoni F, Quintana FJ. The role of astrocytes in CNS inflammation. Trends Immunol. 2020;41(9):805–19.
53. Sáez PJ, Shoji KF, Aguirre A, Sáez JC. Regulation of hemichannels and gap junction channels by cytokines in antigen-presenting cells. Mediators Inflamm. 2014. https://doi.org/10.1155/2014/742734.
54. Evans WH, Leybaert L. Mimetic peptides as blockers of connexin channel-facilitated intercellular communication. Cell Commun Adhes. 2007;14:265–73.
55. Davidson JS, Baumgarten IM, Harley EH. Reversible inhibition of intercellular junctional communication by glycyrrhetinic acid. Biochem Biophys Res Commun. 1986;134:29–36.
56. O'Carroll SJ, Alkadhi M, Nicholson LFB, Green CR. Connexin43 mimetic peptides reduce swelling, astrogliosis, and neuronal cell death after spinal cord injury. Cell Commun Adhes. 2008;15:27–42.
57. Bazzigaluppi P, Weisspapir I, Stefanovic B, Leybaert L, Carlen PL. Astrocytic gap junction blockade markedly increases extracellular potassium without causing seizures in the mouse neocortex. Neurobiol Dis. 2017;101:1–7.
58. Nedergaard M, Rodríguez JJ, Verkhratsky A. Glial calcium and diseases of the nervous system. Cell Calcium. 2010;47:140–9.
59. Stout CE, Costantin JL, Naus CCG, Charles AC. Intercellular calcium signaling in astrocytes via ATP release through connexin hemichannels. J Biol Chem. 2002;277:10482–8.
60. Orellana JA, Sánchez HA, Schalper KA, Figueroa V, Sáez JC. Regulation of intercellular calcium signaling through calcium interactions with connexin-based channels BT—calcium signaling. 2012. 777–794.59.64.
61. Hanisch UK. Microglia as a source and target of cytokines. Glia 2002 40(2):140–55.
62. Brancaccio M, Pivetta C, Granzotto M, Filippis C, Mallamaci A. Emx2 and Foxg1 inhibit gliogenesis and promote neuronogenesis. Stem Cells. 2010;28:1206–18.
63. Tigani W, Rossi Pinzan M, Artimagnella O, Santo M, Rauti R, Sorbo T, Ulloa Severino FP, Provenzano G, Allegra M, Caleo M, Ballerini L, Bozzi Y, Mallamaci A. Foxg1 upregulation enhances neocortical activity. Cereb Cortex N Y N. 1991;2020(30):5147–65.
64. Usmani S, Aurand ER, Medelin M, Fabbro A, Scaini D, Laishram J, Rosselli FB, Ansuini A, Zoccolan D, Scarselli M, De Crescenzi M, Bosi S, Prato M, Ballerini L. 3D meshes of carbon nanotubes guide functional reconnection of segregated spinal explants. Sci Adv. 2016;2:1–10.


## Publisher's Note

# Exosomes from LPS-stimulated spinal organotypic slices transfer neuroinflammation in naïve spinal explants *via* promoting aberrant calcium dynamics and hemichannels opening in astrocytes

Christian Memo[1], Pietro Parisse[2], Roberta Amoriello[1,3], Giuseppe Di Mauro[1], Clara Ballerini[3*], Loredana Casalis[2*], Laura Ballerini[1*]

[1]International School for Advanced Studies (SISSA/ISAS), 34136 Trieste, Italy

[2]ELETTRA Synchrotron Light Source, 34149, Basovizza, Italy

[3]Dipartimento di Medicina Sperimentale e Clinica, University of Florence, 50139 Florence, Italy

Corresponding: clara.ballerini@unifi.it Loredana.casalis@elettra.eu laura.ballerini@sissa.it

## Abstract

Neuroinflammation processes contribute and exacerbate the genesis and progression of most Central Nervous System (CNS) pathologies and the understanding of the signaling crucial to propagate inflammatory responses is deemed as necessary to design treatments. In the CNS, glial cells are involved in inflammation signaling and represents crucial therapeutic targets to mitigate tissue reactivity. Glial inflammatory responses are also mediated by the release of extracellular vesicles, such as exosomes. Exosomes are well recognized key vectorized systems which mediate intercellular communication, actively transferring signaling molecules among different cell phenotypes and involved in tuning target CNS cells functions in physiology and pathology. Glial delivery of exosomes represents a powerful mechanism for spreading tissue inflammation associated with CNS diseases. We investigated by atomic force microscopy, nanoparticle tracking and immune blot analysis, CNS derived exosomes isolated by ultracentrifugation procedures from resting or immunereactive spinal cord organotypic cultures. By confocal microscopy and live calcium imaging we report the ability of exosomes *per se*, when isolated from LPS activated slices and used to treat naïve slices, to mediate glial inflammation reactivity mediated by astrocytes' hemichannels increased permeability.

## Keywords

## Introduction

Extracellular vesicles are increasingly investigated as key vectorized systems, released by any cell type, contributing to intercellular signaling [Dolcetti E. et al 2020]. The secretion of extracellular vesicles mediates communication among proximal and distant cells and is fundamental in several aspects of physiological as well as pathological conditions [Pan B. T. et al., 1983; Rashed H. et al., 2017]. Exosomes (EXOs) are a subset of extracellular vesicles that have been defined based on their size, biogenesis, and contents [reviewed in Doyle L. M. et al., 2019]. EXOs may contain microRNA (miRNA), messenger RNA (mRNA) or other bioactive molecules such as lipids and proteins, which, when taken up by target cells, modulate cellular signaling [Soria F. N. et al., 2017].

Glial cells, such as astrocytes, microglia, and oligodendrocytes, release EXOs to modulate intercellular communication in the Central Nervous System (CNS) and, depending on the physiological or pathological context of their release, might exert beneficial or detrimental effects on neurons [Zhao S. et al., 2021]. In neurodegenerative diseases, astrocytes derived EXOs are often associated with inflammation and have been indicated as contributors for disseminating neuronal damage [Oyarce K. et al., 2022]. Neuroinflammation comprises centralized inflammatory responses within the CNS which feature different properties depending on the triggering context: disease, injury/trauma, infection or stress. The understanding and treatment of the context, course, and duration of these inflammatory responses will impact their physiological, biochemical and behavioral consequences [Di Sabato D. et al., 2016]. Reactive glia contributes to neuroinflammation, and emerging evidence implicate glia EXOs release in favoring inflammatory escalation in the CNS [Marostica G. et al., 2021]. To what extent glia-derived EXOs are involved in spreading neuroinflammation and the molecular mechanisms adopted in such detrimental actions warrant further investigations and may lead to novel therapeutic targets aiming at mitigating the neuroinflammatory vicious cycle.

Glia EXOs release, isolation and characterization under controlled inflammatory conditions *in vitro* has opened the possibility to investigate the mechanistic aspects of EXOs in promoting or propagating neuroinflammation, however vesicles have been mostly collected from isolated glial cells in primary cultures or from cell lines [Musto M. et al., 2021]. Here we adopted a complex system *in vitro,* the organotypic spinal cord cultures, to isolate EXOs in control and neuroinflammatory conditions and, to further explore EXOs tuning of glial cell reactivity, we exposed naïve spinal cultures to the isolated vesicles.

Organ cultures allow to address local inflammation in a controlled microenvironment, which maintains the 3D organization of spinal cord resident cells and preserves the sensory-motor cytoarchitecture [Avossa D. et al., 2003; Furlan F. et al., 2007]. With this model we have characterized spinal tissue alterations induced by inflammation in response to danger signals, targeting the role of resident cells: neuronal and not neuronal populations [Medelin M. et al., 2018; Giacco V. et al., 2019;

Panattoni G. et al., 2021]. We adopted LPS treatments, reported to mediate an increase in cytokines and chemokines production [Panattoni G. et al., 2021], to mimic mild inflammatory conditions. We isolated and characterized by atomic force microscopy (AFM), nanoparticle tracking (NTA) and western blot analysis, EXOs released upon resting or LPS-reactive conditions. By immunolabelling, confocal microscopy and live calcium imaging we investigated naïve glial reactivity to EXOs isolated from LPS treated organ slices and we further show that EXOs, when released during neuroinflammation, trigger in naïve spinal astrocytes aberrant calcium dynamics *via* increased hemichannel (HC) permeability.

**Methods**

***Organotypic spinal cord cultures, benzoyl-ATP and LPS treatments and exosomes isolation***

All experiments were performed in accordance with the EU guidelines (2010/63/UE) and Italian law (Decree 26/14) and were approved by the local authority veterinary service and by our institution (SISSA) animal wellbeing committee (OBPA). All efforts were made to minimize animal suffering and to reduce the number of animals used. Animal use was approved by the Italian Ministry of Health (no. 22DABNQYA and 22DABN1WO), in agreement with the EU Recommendation 2007/526/CE. Organotypic spinal cord and dorsal root ganglia (DRG) slices (275 μm) were obtained from C57BL/6 J mouse embryos (embryonic days E12–13) and cultured in plastic tubes with 1 mL medium as previously described [Medelin M. et al., 2018; Giacco V. et al., 2019, Panattoni G. et al., 2021]. The tubes were kept in a roller drum rotating 120 times per hour in an incubator at 37 °C in the presence of humidified atmosphere, with 5 % $CO_2$. All the experiments were performed on spinal cultures at 2–3 weeks *in vitro* (WIV).

To isolate exosomes released from spinal cords in organ cultures, we collected the supernatant from 12 spinal cultured slices previously maintained for 24 hours in EXOs depleted medium, by adopting EXOs-free FBS. According to MISEV2018 [Théry C. et al., 2018], EXOs were removed from FBS by ultracentrifugation for 18 hours at 100000 × g at 4 °C. Incubations in EXO-depleted medium alone were used as basal control condition, with LPS (LPS 1 μg/mL 24 hours; Sigma, O55:B5) as inflammation condition [Giacco V. et al., 2019] and with benzoyl-ATP (bzATP 100 μM, 1 hour; Sigma) as positive secretion control [Musto M. et al., 2021]. To isolate EXOs from each group the harvested supernatants were subjected to differential centrifugation at 4 °C, first 15 min at 300 × g followed by 15 min at 3000 × g and then 70 min at 20000 × g in order to remove cell debris, apoptotic bodies, micro-vesicles and other larger particles. The resulting supernatant were finally filtered with 0.22 μm syringe filters (Merck Millipore) and ultracentrifuged in a Beckman Coulter Optima™ XE90 Ultracentrifuge for 70 minutes at 120000 × g using a SW 41 Ti rotor to pellet EXOs [adapted from

Théry C. et al., 2006; Musto M. et al., 2021]. The pellets were resuspended in 500 µL of PBS (isolated for further characterization) or in 500 µL EXO-free medium (isolated for slice treatments).

***Atomic force microscopy (AFM) analysis***

AFM characterization was performed as previously described [Musto M. et al., 2021]. Briefly, EXOs pellets were resuspended in PBS solution after isolation from spinal cultures and 15 µL of sample solution was placed and left to adsorb (30 min) onto a freshly peeled mica substrate. AFM analysis was performed in liquid at room temperature (RT), using the semicontact mode of a commercial instrument (Solver Pro, NT-MDT, RU). Silicon tips (NSC36/CR-AU, MikroMash, USA) with a typical force constant of 0.6 nN/nm and a resonance frequency of about 65 kHz were employed. Topographic height and phase images were recorded at 512 × 512 pixels at a scan rate of 0.5 Hz. Image processing was performed using Gwyddion freeware AFM analysis software, version 2.40. Diameter and height of each vesicle were evaluated from cross-line profiles, and results were statistically analyzed using Prism (*Graphpad* software).

***Nanoparticle tracking analysis (NTA)***

Measurement and analysis of EXOs size distribution by NTA was performed on a NanoSight LM10 system (Malvern) using 500 µL EXOs for each group (Control-derived, LPS-derived and bzATPderived) and diluted 1:100 in MilliQ $H_2O$. Individual videos of 60 seconds (recorded at 25 FPS; 3 videos/each group, Control, bzATP and LPS) were acquired at RT using the maximum camera gain, a detector threshold equal to 5 and analyzed by the NanoSight particle tracking software to calculate vesicles size and concentration.

***Western blot analysis***

Freshly isolated EXOs were resuspended in lysis buffer (50 mM Tris-HCl, pH 8.0, 150 mM NaCl, 1 % NP40, 0.1 % SDS) added with protease inhibitors cocktail (Sigma), sonicated for 30 seconds, and then boiled at 95 °C for 5 minutes [Shigetomi E. et al., 2019]. Samples were run on a 10 % polyacrylamide gel and blotted onto nitrocellulose membranes (Millipore, Italy). Membranes were then blocked in PBS-Tween-20 (0.1 %) plus 5 % BSA (Sigma) and, according with MISEV 2018 guidelines [Théry C. et al., 2018], incubated overnight at 4 °C with primary antibodies anti-flotillin1 (FLO-1, dilution 1:1000, BD Biosciences), anti- Tumor Susceptibility 101 (TSG101, dilution 1:1000, Invitrogen), anti- Golgi matrix protein 130 (GM130, dilution 1:1000, Invitrogen).

Membranes were then washed with PBS-Tween and incubated with peroxidase-conjugated antimouse and anti-rabbit secondary antibody (dilution 1:1000) for 2 hours at RT. Detection of immunolabeled ECL-exposed protein bands was measured with UVI-1D software over four independent experiments.

***Naïve organotypic slices treatments***

For experiments involving chronic treatments, organotypic cultures (>2 WIV) were incubated (24 hours) with EXO-depleted medium alone for control, with LPS (1 μg/mL, Sigma, O55:B5) [Giacco V. et al., 2019] as previously indicated for reference inflammation conditions and with EXO isolated from controls or from LPS treatments and resuspended. In the latter conditions, EXOs were resuspended in halved medium volume (i.e. EXOs extracted from 10 ml of medium were resuspended in 5 ml of treatment medium).

In a set of experiments, naïve slices were compared when incubated (24 hours) with the supernatant derived from LPS treatment medium (after EXOs removal) and with the fresh medium used to resuspend EXOs, after EXOs were re-isolated and removed.

All treatments (LPS or EXOs) were washed out prior to immunostaining analysis or live cell imaging recordings.

***Immunofluorescence imaging, Lucifer Yellow (LY) live uptake and analysis***

For immunostainings, organotypic cultures were fixed with 4 % formaldehyde (PFA, prepared from fresh paraformaldehyde; Sigma) in PBS (1 ×) for 1 h (RT) and washed in PBS. Free aldehyde groups were quenched in sodium borohydride (NaBH4, Sigma) 1 % in PBS for 5 minutes. Slices were permeabilized and blocked in PBS (1 ×), 5 % FBS (Sigma), 1 % BSA (Sigma), and 0.3 % Triton X100 (Sigma) at RT for 1 h and incubated overnight at 4 °C with anti-GFAP (mouse monoclonal, 1:200, Sigma), anti-Iba1 (rabbit polyclonal, 1:500, Wako) primary antibodies. Subsequently, the slices were PBS-washed and incubated with secondary antibodies diluted in blocking solution for 2 h (RT) in the dark. The secondary antibodies were Alexa 488 goat anti-mouse (1:500, Invitrogen), Alexa 594 goat anti-rabbit (1:500, Invitrogen) and we used DAPI (1:500, Thermo Fisher Scientific) to stain the nuclei. Samples were mounted on glass coverslips using Fluoromount-G aqueous mounting medium (Thermo Fisher Scientific). Images were acquired using Nikon A1 Confocal microscope with Ar/Kr, He/NE, and UV laser with 40 × objective (0.95 N.A.). Confocal sections were acquired up to a total Z-stack thickness of 5 - 15 μm (depending on the required analysis) in sequential mode with lasers (488 nm for GFAP and 561 nm for Iba1). For each experiment we performed $\geq 3$ independent culture series; from each culture series, we used $\geq 3$ slices for every condition, and from each slice $\geq 3$ fields were randomly acquired from the ventral region of the spinal slices. Offline analysis of the image Z-stack

was performed using the Volocity 3D Image Analysis Software. The offline analysis of the Z-stacks for calculating the Transformation Index (TI) and the GFAP signal volume were performed. Briefly, to quantify microglia ramifications degree as a correlate to changes in the activation state, we measured the area and the perimeter, necessary to calculate the transformation index [Fujita H. et al., 1996; Giacco V. et al., 2019]

$$\frac{[cell\ perim.\ (\mu m)]}{\cdot\ [cell\ area\ (\mu m^2)]}\ 24\pi$$

Astrocytes reactivity were quantified by measuring, in every acquired field, the volume occupied by the GFAP signal in the stack, calculated by the calibrated software and expressed in the plot in $\mu m^3$. To quantify the opening of connexin hemichannels (HCs) in astrocytes we quantify the Lucifer Yellow (LY; Sigma) uptake in GFAP positive cells. Cultures were incubated at 37 °C with 1 mM LY in standard physiological solution for 10 min and then washed three times with the same solution without LY [Chepied A. et al., 2020]. Cultures were fixed with 4 % PFA, subsequently astrocytes were labelled using anti-GFAP as described above. Images were acquired at the confocal microscope using 20× and 40× objectives. Confocal sections were acquired every 1 µm to a total Z-stack thickness of 5 µm. Analysis of LY-GFAP double positive astrocytes the Volocity [Giacco V. et al. 2019] tool "Intersect objects" to quantify only the objects where LY, GFAP, and DAPI signals are intersected. A size threshold limit was set to exclude all the objects with a dimension < 5 $\mu m^3$ in order to avoid background signal interference [Panattoni G. et al., 2021]. The results were expressed as the mean number of LY/GFAP positive cells for each treatment condition.

***Calcium imaging with GCaMP6f and analysis***

pZac2.1 gfaABC1D-cyto-GCaMP6f was a gift from Baljit Khakh (Addgene viral prep # 52925AAV5; http://n2t.net/addgene:52925; RRID:Addgene_52925). Organotypic slices at 1 WIV were infected with AAV5.gfaABC1D-cyto-GCaMP6f which leads to a selective expression of the genetically encoded calcium indicator GCaMP6f in astrocytes. At 2–3 WIV, before the recording procedures, cultures were maintained in extracellular saline solution, also used as recording solution, composed of (mM): 150 NaCl, 4 KCl, 1 MgCl2, 2 CaCl2, 10 HEPES, 10 Glucose (pH adjusted to 7.35 with 2 M NaOH), in the same incubator for 15 minutes for habituation. Slices were then placed in a custom 3D-printed perfusion chamber mounted on a Nikon microscope (Nikon Eclipse Ti2 microscope endowed with a Nikon IntensiLight Hg lamp and an Andor Zyla sCMOS camera) where they were continuously

perfused (5 mL/minute) at RT with the recording saline solution. GCaMP6f fluorescence was monitored with a 20 × S Plan Fluor ELWD (NA 0.45) objective from the ventral horn area. Images were taken at 1/ 150 ms rate, with an exposure time of 100 ms and 4 × 4 binning.

The acquired time series of images were analyzed in Fiji choosing ROIs of ~ Ø 20–30 µm and the fluorescence traces were processed in ClampFit 10.7 [Panattoni G. et al., 2021].
$Ca^{2+}$ transients were expressed as $\Delta F/F_0$, where $\Delta F$ is the fluorescence rise over baseline, calculated as:

$$100 \times \frac{F - F^0}{F_0}$$

(F, fluorescence value; F0, baseline fluorescence). F0 was calculated as the median of the frame fluorescence values.

***Gap27 treatment of EXOs***

Freshly isolated EXOs from LPS treated slices were incubated with the Cx43 inhibitor peptide gap27 (GeneCust; [Panattoni G. et al., 2021]) at a concentration of 500 µM for 1 hour at 4 °C under constant agitation using a rotating mixer. In order to eliminate the excess of gap27 peptide after the incubation period EXOs were resuspended in 10 mL of EXO-free medium, pelleted again for 70 minutes at 120,000 × g and resuspended in 500 µL of EXO-free medium ready to be used for treatments.

***Statistical analysis***

All the datasets underwent to the normality analysis to assess if data were as in a Gaussian distribution. On this basis, concerning the work on organotypic spinal cord slices the datasets were processed with ordinary one-way ANOVA test to measure statistic significant differences among the treatments (followed by Holm-Sidak comparisons as post-hoc test), otherwise the Kruskal-Wallis test was used (followed by Dunn's multiple comparison as post-hoc test). All the analysis of cumulative probability were performed using the Kolmogorov-Smirnov test among groups.
All the data are expressed as Mean ± SEM with n = number of slices unless stated otherwise.

**Results**

**Exosomes isolation from control and reactive organotypic spinal cord slices**

Organotypic spinal cord slices enable mimicking tissue responses to different inflammatory environments comprising the activation of resident cells, in particular astrocytes and microglia [Giacco V. et al., 2019; Panattoni G. et al., 2021]. We used 2-3 WIV explant cultures (□12 slices each treatment; □3 culture series) to explore the release of exosomes (EXOs) which were isolated for characterization upon three different conditions as sketched in Fig. 1a: basal EXOs release in saline control, evoked EXOs release by 1 hour incubation in bzATP (100 □M) [Doyle L. M. et al., 2019; Wang M. Z. et al., 2019], a well-known exosomes secretion booster (i.e. positive secretion control) and EXOs release upon 24 hours exposure to LPS (1□g/mL), a trigger of cytokine release [Vereker E. et al., 2000; Li X. et al., 2003] adopted to elucidate cellular and molecular signaling during brain inflammation, and shown to induce inflammatory conditions in spinal explants characterized by microglia morphological changes, the appearance of aberrant calcium signals in astrocytes displaying Cx43 hemi channels (HC) increased permeability [Panattoni G. et al., 2021].

EXOs were collected from the supernatant of control and treated slices maintained in EXOs-depleted medium (see Methods). The harvested supernatants underwent differential ultracentrifugation to isolate EXOs, avoiding contaminants [Théry C. et al., 2006; Musto M. et al., 2021; see Methods]. Figure 1c shows representative atomic force microscopy (AFM) images from a sample of EXOs isolated from LPS treated slices, appearing as vesicle-like objects on the mica surface ([Musto M. et al., 2021]; see Methods). EXOs mean height, measured by AFM, was similar among control and treated groups (CTR 51.57 ± 8.09 nm; bzATP 69.25 ± 6.73 nm; LPS 79.99 ± 18.61 nm; bar plot in Fig. 1d) and it was within the range of dimensions expected for EXOs [Parisse P. et al., 2017; Doyle L. M. et al., 2019; Pegtel D. M. et al., 2019]. The release and isolation of EXOs suggested by AFM measures were confirmed by immunoblot analysis (Fig. 1b) for the EXOs biomarkers TSG101 [Gurunathan S. et al., 2019] and flottilin-1(FLO1; [Musto M. et al., 2021]) while, the absence in EXO pellets of the Golgi membrane protein GM130 band [Sung, B.H. et al., 2020], present in the spinal culture lysates, supports the efficacy of the adopted isolation protocol. The increasing thickness (+38% and +48% bzATP and LPS, respectively; Fig. 1b) of TSG101 bands upon bzATP and LPS treatments suggests an enhanced EXOs release after these treatments. We further used nanoparticle tracking analysis (NTA) to compare control, bzATP and LPS resuspended EXOs. The bar plots in Fig. 1e summarise NTA quantification of EXO/mL (CTR 2.465e+009 ± 3.150e+008; LPS 3.245e+009 ± 9.500e+007; bzATP 3.755e+009 ± 3.500e+007; CTR vs LPS $*P = 0.0141$; CTR vs bzATP $*P = 0.0401$, Kruskal–Wallis test), confirming the suggested increase in vesicle secretion by bzATP and LPS. Figure 1f-g report the mean exosomes size calculated by NTA measures as hydrodynamic radius and the NTA size distribution. The combination of AFM, immunoblot and NTA analysis supported

the isolation and presence of EXOs in the different conditions, characterised by an enhanced EXOs release in bzATP and LPS treated slices.

**Fig.1**

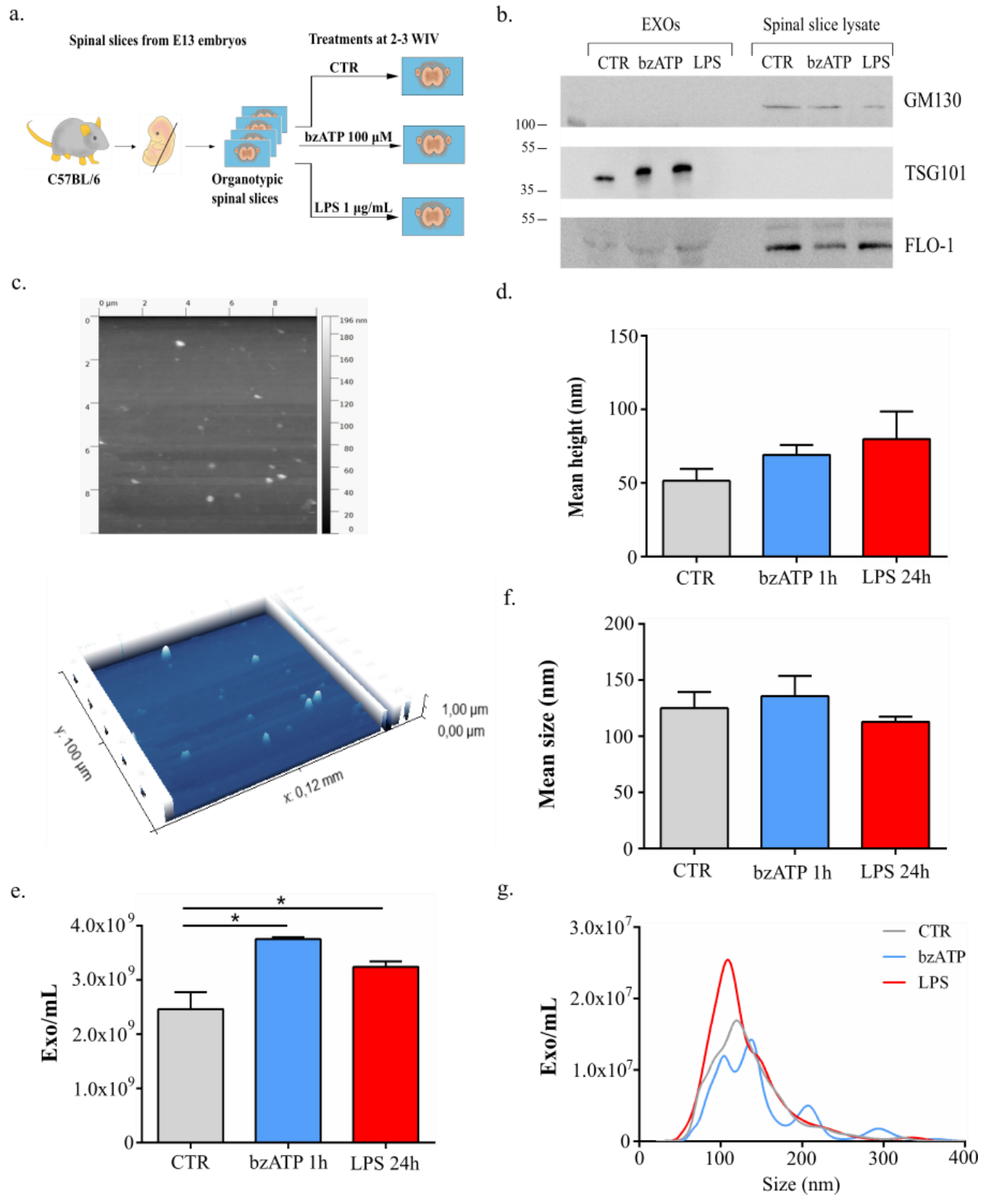

**Figure 1. Exosomes isolation and characterization from organotypic spinal cord slices: a**. Sketch of the experimental procedure and experimental groups to collect EXOs **b.** Western blotting of the pellets (left) and spinal slices lysate (right) for the Golgi apparatus protein GM130 and the exosomal markers TSG101 and FLO-1. Pellets were obtained from the medium of organotypic control slices (untreated) or stimulated with bzATP or LPS. **c.** Sample of AFM topographic reconstruction (2D and 3D top and bottom panel, respectively), of EXOs. **d.** EXOs mean height analysis by AFM. **e.** Exosomes quantification using NTA shows a significant increase in vesicles secretion in treated condition compared to control (CTR vs LPS *P = 0.0141; CTR vs bzATP *P = 0.0401, Kruskal–Wallis test). **f.** Mean exosomes size calculated as hydrodynamic radius by NTA. **g.** Size distribution of exosomes populations obtained with NTA appears quite homogeneous among all groups.

**Exposure to proinflammatory EXOs trigger tissue reactivity in naïve spinal slices**

To examine the ability of EXOs to transfer inflammation-related signalling we exploited and compared the vesicles isolated from resting control and reactive LPS slices, used as treatment to investigate resident glial cell reactivity in naïve organotypic cultures.

Resident glial cells can modify their phenotype in response to inflammatory cues that cause quantifiable changes in cell function, number and/or morphology [Refolo V. et al., 2019; Giacco V et al., 2019]. We used immunofluorescence labelling and confocal microscopy to visualize microglia and astrocytes in organotypic spinal explants by Iba1 and GFAP co-immunolabeling (Fig. 2a; [Panattoni G. et al., 2021]). We compared four conditions: control cultures (CTR; n=9), sister cultures incubated for 24 hours (see Methods) with EXOs isolated from control (untreated) slices ($EXO_{CTR}$; n=9), LPS treated slices (n=9) and slices incubated with EXOs isolated from LPS treated slices ($EXO_{LPS}$; n=9). All the treatments were performed using exosome-free resuspension medium. In Fig. 2a, confocal micrographs, depicting $Iba1^+$ (microglia, in red) and $GFAP^+$ (astrocytes, in green) cells in the ventral horn fields (318.20 □m □ 318.20 □m; see Methods), are shown for each condition. We further assessed the morphology of $Iba1^+$ microglia by measuring the transformation index (TI; see Methods; [Panattoni G. et al., 2021]) and the cell density. Bar plot in Fig. 2b quantifies the ability of LPS and of $EXO_{LPS}$ to induce a statistically significant increase in the TI in respect to control and $EXO_{CTR}$ (CTR 17.142 ± 0.933; $EXO_{CTR}$ 16.466 ± 0.688; LPS 44.276 ± 2.468; $EXO_{LPS}$ 44.476 ± 3.103; CTR vs LPS ****$P$ < 0.0001; CTR vs $EXO_{LPS}$ ****$P$ < 0.0001; $EXO_{CTR}$ vs LPS ****$P$ < 0.0001; $EXO_{CTR}$ vs $EXO_{LPS}$ ****$P$ < 0.0001, Kruskal–Wallis test); the bar plot in 2c reports a light microgliosis, expressed as number of Iba1+ cells/$mm^2$, induced by LPS (CTR 47.97 ± 4.326 ; $EXO_{CTR}$ 55.50 ± 4.336; LPS 74.31 ± 8.336; CTR vs LPS *$P$ = 0.033, One-way ANOVA) limited to an increased

trend in $EXO_{LPS}$ (66.02 ± 9.065). In all conditions we did not detect astrocytic proliferation by LPS [see also Panattoni G. et al., 2021] as well as in $EXO_{LPS}$, shown in the box plot of Fig. 2d where GFAP volume is quantified (see Methods).

LPS stress to spinal cultured slices is known to trigger different cytokines and chemokines network and to induce changes in the morphology of microglia, suggestive of activation states [Giacco V. et al., 2019] and apparently $EXO_{LPS}$ alone replicated such microglial activation. To rule out the influence of soluble mediators, or even of residual LPS *per se*, derived from the treatment medium used to induce EXOs release and collection and to exclude the presence of residues from vesicles damaged by the resuspension process, in a separate set of experiments we compared naïve slices in control (n=8) with those treated (24 hours; n=8 per condition) with the treatment medium *per se*, (usually discarded upon supernatant centrifugation to isolate $EXO_{LPS}$), with slices treated by $EXO_{LPS}$ (resuspended in fresh medium) and with slices treated with the resuspension medium deprived of $EXO_{LPS}$ (see Methods). Figure 2f confocal micrographs show the $Iba1^{+}$microglia morphological changes in these three conditions compared to control, and TI is quantified in the bar plot in Fig. 2g. As expected, isolated $EXO_{LPS}$ were reconfirmed capable to induce significant increase in the TI, and a similar result was obtained in slices exposed to the treatment medium alone, still retaining LPS and other proinflammatory soluble mediators, while no significant changes were measured in slices treated with resuspension medium once depleted of $EXO_{LPS}$, strengthening the absence of soluble proinflammatory mediators influencing $EXO_{LPS}$ treatments (TI: CTR 4.674 ± 0.408; Treat. medium 15.588 ± 1.109; Resusp. medium 3.952 ± 0.458; $EXO_{LPS}$ 17.477 ± 1.445; CTR vs Treat. medium $P^{****} < 0.0001$; CTR vs $EXO_{LPS}$ $P^{****} < 0.0001$; Treat. medium vs Resusp. medium $P^{****} < 0.0001$; Resusp. medium vs $EXO_{LPS}$ $P^{****} < 0.0001$, Kruskal–Wallis test).

**Fig. 2**

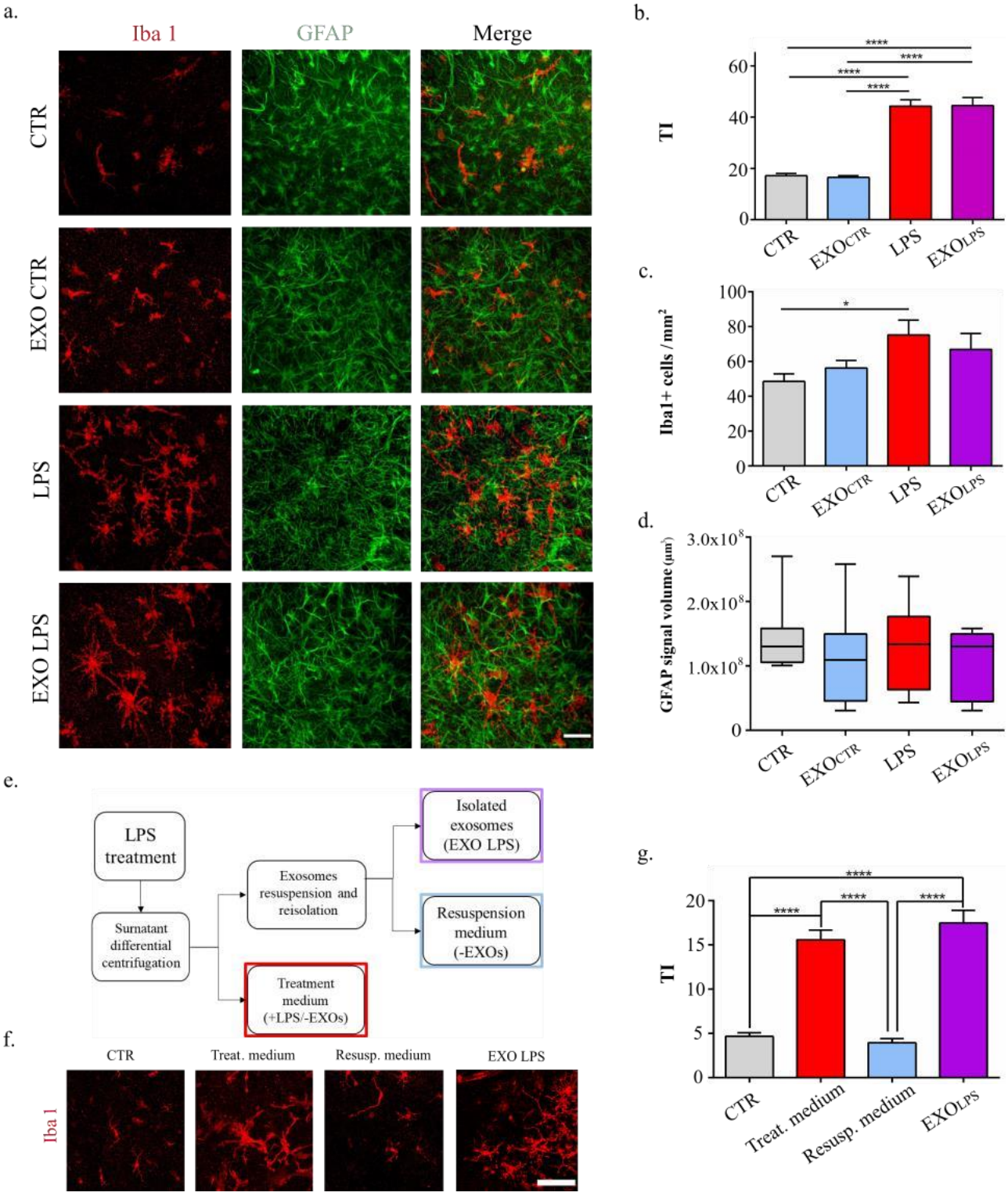


**Figure 2. Proinflammatory exosomes induce microglia activation in naïve spinal slices: a.** Representative confocal images (20 □) of microglia (Iba1, in red) and astrocytes (GFAP, in green) in the ventral horn of spinal slices (2-3 WIV) in control, in slices treated for 24 hours with LPS, with EXOs isolated from LPS-treated slices ($EXO_{LPS}$) and with EXOs isolated from untreated slices ($EXO_{CTR}$). Scale bar 50 µm **b.** The bar plot summarises the microglia Transformation Index (TI) in the different groups. (CTR vs LPS ****P < 0.0001; CTR vs $EXO_{LPS}$ ****$P$ < 0.0001; $EXO_{CTR}$ vs LPS

****$P$ < 0.0001; $EXO_{CTR}$ vs $EXO_{LPS}$ ****$P$ < 0.0001, Kruskal–Wallis test). **c.** The bar plot shows Iba1+ cells/mm$^2$ in all conditions (CTR vs LPS *P = 0.033, One-way ANOVA). **d.** Box-plot reports the volume occupied by GFAP signal in the slice Z-stack. **e.** Experimental flowchart for the assessment of EXOs-specific biological activity. **f.** Representative confocal images (20□) of microglia (Iba1, red; scale bar 100 µm). **g.** Microglia TI across the treatment conditions sketched in e and illustrated in f. (CTR vs Treat. medium $P$**** < 0.0001; CTR vs $EXO_{LPS}$ $P$**** < 0.0001; Treat. medium vs Resusp. medium $P$**** < 0.0001; Resusp. medium vs $EXO_{LPS}$ $P$**** < 0.0001, Kruskal– Wallis test).

These results strongly suggested that $EXO_{LPS}$ actively promoted resident glial cell reactivity, enabling spreading of neuroinflammation initiated in separated spinal cultures by LPS.

Cytoplasmic calcium signals in astrocytes are instrumental for the functioning of the CNS [Semyanov A. et al., 2020] and undergo to complex changes in response to a variety of external stimuli. A prominent feature of reactive astrocytes is the emergence of aberrant calcium signals [Shigetomi E. et al., 2019] which contribute to cytokines and chemokines release due to inflammation, and such enhanced calcium dynamics is replicated in spinal organotypic cultures when exposed to danger signals [Panattoni G. et al., 2021].

We design the next set of experiments to investigate $EXO_{LPS}$ ability to induce dysfunctional calcium dynamics in astrocytes. We recorded live calcium responses in control, LPS and $EXO_{LPS}$ cultured spinal explants (3 WIV) by expressing the latest generation of GCaMP6f genetically encoded calcium indicators (GECIs) based on green fluorescent protein fluorescence, whose expression is restricted to astrocytes (see Methods; [Haustein M. D. et al., 2014]; sketched in Fig. 3a). Figure 3b shows low magnifications images of organotypic culture (bright field) and the GCaMP6f signal from the same slice. In Fig. 2 c time-sequential snapshots are visualised and in d fluorescence tracings are shown depicting intracellular calcium dynamics in astrocytes recorded from the sampled area (680.42 □ 680.42 □m$^2$) of the ventral spinal horn in control (n=6), LPS (n=6) and $EXO_{LPS}$ (n=6) cultures. In control astrocyte population, calcium dynamics emerge as slow oscillations occurring at a low pace [Panattoni G. et al., 2021]. Upon LPS and $EXO_{LPS}$ exposures, an increased number of active astrocytes was detected in respect to control (active cell/recorded field in CTR 29.80 ± 4.89; LPS 41.40 ± 2.61; $EXO_{LPS}$ 42.00 ± 1.78; Fig. 2e) displaying calcium transients characterized by a higher pace, quantified by measuring the inter event interval (IEI), a correlate of calcium events frequency, significantly reduced by neuroinflammatory stimuli (IEI CTR 32.35 ± 5.96 s; IEI LPS 13.01 ± 1.19 s; IEI $EXO_{LPS}$ 9.31 ± 1.16 s; CTR vs LPS $P$** = 0.0012; CTR vs $EXO_{LPS}$ $P$**** < 0.0001; LPS vs $EXO_{LPS}$ $P$*** 0.0002, Kruskal–Wallis test; Fig. 2f-g).

**Fig. 3**

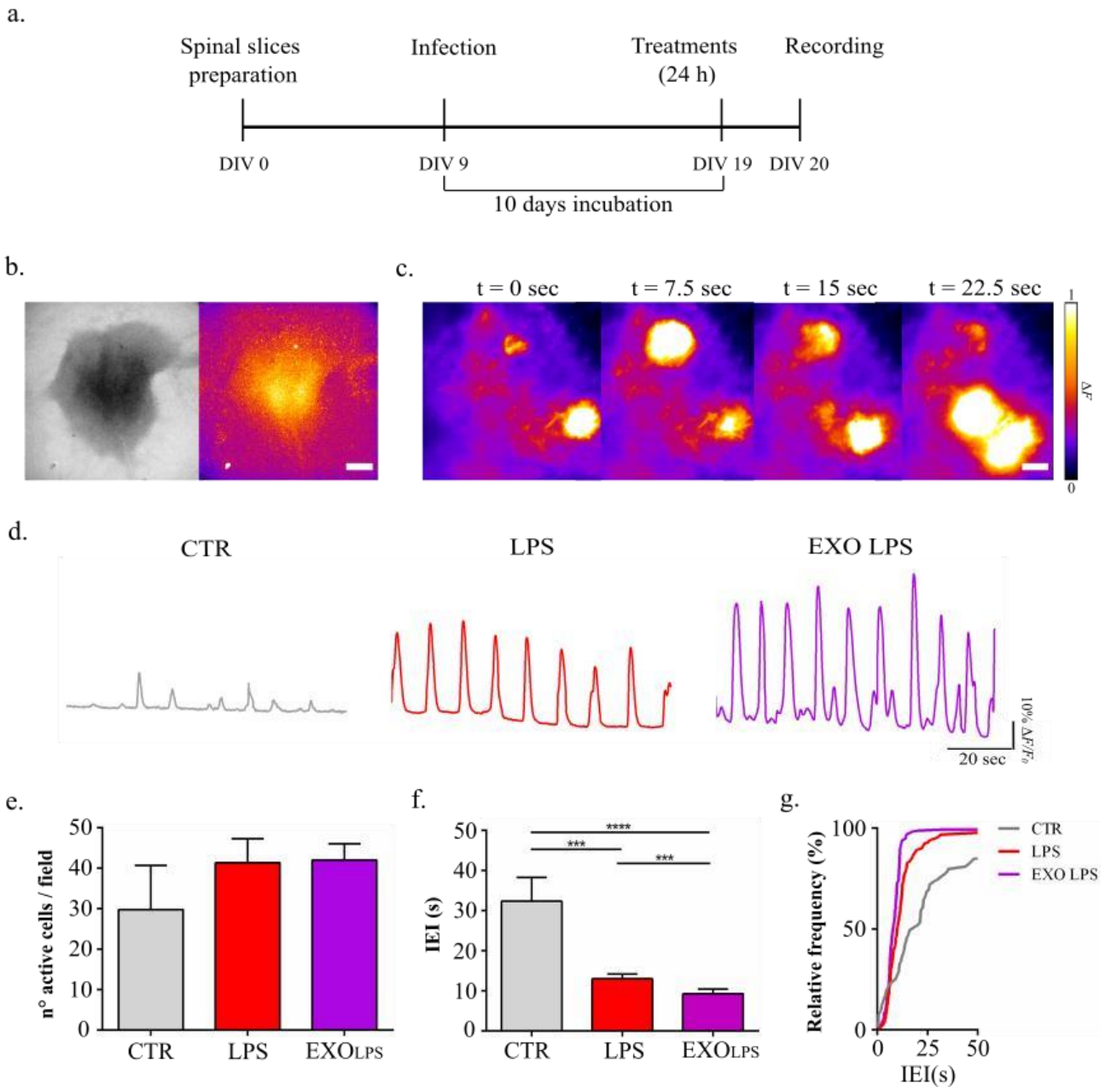


**Figure 3. Proinflammatory exosomes induce dysfunctional calcium dynamics in astrocytes: a.** Sketched experimental time line. **b.** representative brightfield (left) and fluorescence images (right) of the organotypic spinal slice infected by GCaMP6f (4 □; scale bar 500 µm). **c.** snapshots sequence of live calcium imaging recording of a control slice showing the characteristic astrocytic calcium bursts (20 □ magnification; scale bar 100 µm). **d.** representative calcium imaging traces. **e.** bar plot showing an increase in the mean number of active astrocytes/field in LPS and $EXO_{LPS}$ treated slices.
**f.** bar plot showing a significant decrease in the inter event intervals (IEI) in LPS and $EXO_{LPS}$ treated slices when compared to CTR (CTR vs $EXO_{LPS}$ P**** < 0.0001; LPS vs $EXO_{LPS}$ P*** 0.0002, Kruskal–Wallis test). **g.** cumulative probability plot of calcium events IEI.

**Proinflammatory EXOs induce altered calcium dynamics by increasing hemichannels opening**

In organotypic cultures, LPS *via* binding to Toll- like receptors (TLRs) [Giacco V. et al., 2019], induces glia production and release of cytokines, chemokines, and other inflammatory factors activating astrocytes aberrant calcium dynamics [Panattoni G. et al., 2021]. We recently show that inflammatory driven calcium signalling in $GFAP^+$ reactive cells rely on the increased permeability of Cx43 membrane hemichannels (HC; [Panattoni G. et al., 2021]), which provide an additional escalating pathway for diffusion of small molecules or ions contributing to inflammation spread [Peng B. et al., 2022]. At rest, connexin HCs can open in physiological conditions, under the control of multiple regulators [Saez J. C. et al., 2003], conversely, pathological conditions, such as inflammation, might be characterized by uncontrolled HCs opening [Orellana J. M. et al., 2016; Peng B. et al., 2022]. We used the low molecular-weight dye lucifer yellow (LY; 1 mM) to quantify HC permeability [Kanaporis G. et al., 2010] in $GFAP^+$ astrocytes in control, LPS and $EXO_{LPS}$ (n=8 each group). In Fig. 4a representative micrographs show LY and GFAP double positive cells, quantified in the bar plot in b. LPS and $EXO_{LPS}$ treatments resulted in a statistically significant increase in the number of double LY-GFAP positive cells (CTR 8.31 ± 1.76; LPS 27.00 ± 4.96; $EXO_{LPS}$ 27.64 ± 3.76; CTR vs LPS *P*** = 0.0094; CTR vs $EXO_{LPS}$ *P**** = 0.0005, Kruskal–Wallis test) when compared to control. The increased amount of LY positive astrocytes supports HCs opening in $EXO_{LPS}$ treated slices, strengthening the suggested ability of $EXO_{LPS}$ to transfer genuine inflammatory signalling. To ascertain whether the enhanced permeability of Cx43 HCs be an upstream key trigger in $EXO_{LPS}$ and needed to expand inflammation and activate astrocytes, we pre-incubated $EXO_{LPS}$ with a distinct Cx43 peptide blocker, namely Gap27 (500 μM; 30 min; $EXO_{LPS+gap27}$ n=6), known to block HCs opening triggered by chemical or electrical stimuli [Wang N. et al., 2012]. Upon washout the unbound peptide was removed and $EXO_{LPS+g}$ resuspended in fresh medium (sketched in Fig. 4c). We monitor astrocyte calcium signalling comparing control slices (n=6) with $EXO_{LPS}$ (n=6) and $EXO_{LPS+gap27}$ treated ones. Figure 4d shows fluorescence tracings where astrocytic calcium transients were significantly increased upon $EXO_{LPS}$ treatment when compared to control, conversely $EXO_{LPS+g}$ treated sample exhibit a near-physiologic calcium dynamic when compared to control astrocytes (IEI CTR 21.02 ± 4.48 s; IEI $EXO_{LPS}$ 11.68 ± 0.78 s; $EXO_{LPS+gap27}$ 26.38 ± 1.97 s; CTR *vs* $EXO_{LPS}$ *P*** = 0.0037; $EXO_{LPS}$ *vs* $EXO_{LPS+g}$ *P***** < 0.0001, Kruskal–Wallis test; Fig. 4 f -g). Accordingly, only $EXO_{LPS}$ enhanced the number of active cells (CTR 27.14 ± 2.53; $EXO_{LPS}$ 46.86 ± 2.26; $EXO_{LPS+gap27}$ 32.57 ± 2.91; CTR *vs* $EXO_{LPS}$ *P**** 0.0006; Kruskal–Wallis test; bar plot in Fig. 4e).

Fig.4

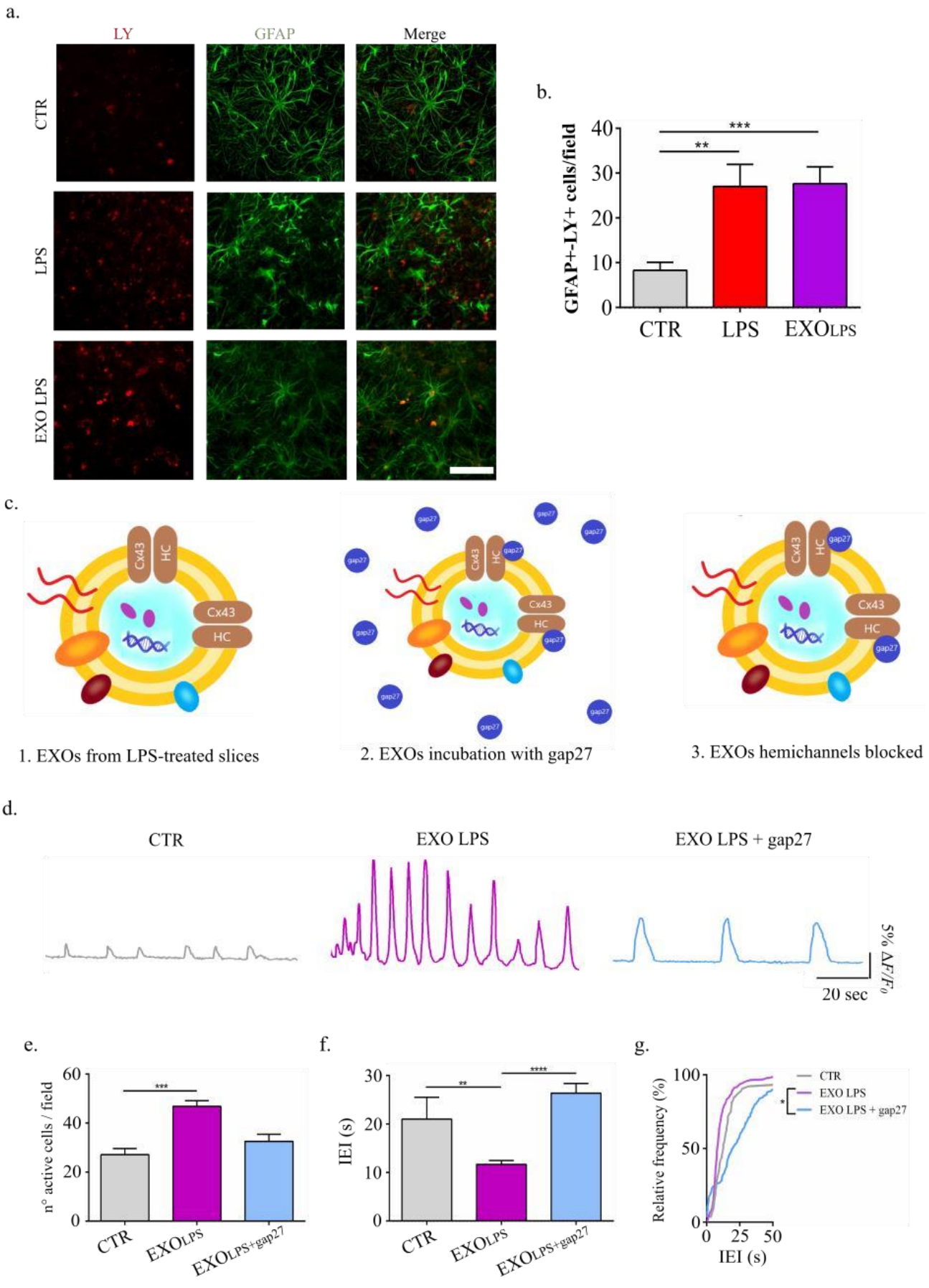
a.
LY
GFAP
Merge
CTR
LPS
EXO LPS
b.
GFAP+-LY+ cells/field
40
30
20
10
0
***
**
CTR
LPS
EXOLPS
c.
Cx43
HC
gap27
1. EXOs from LPS-treated slices
2. EXOs incubation with gap27
3. EXOs hemichannels blocked
d.
CTR
EXO LPS
EXO LPS + gap27
5% ΔF/F0
20 sec
e.
n° active cells / field
60
40
20
0
***
CTR
EXOLPS
EXOLPS+gap27
f.
IEI (s)
30
20
10
0
**
****
CTR
EXOLPS
EXOLPS+gap27
g.
Relative frequency (%)
100
50
0
0
25
50
IEI (s)
CTR
EXO LPS
EXO LPS + gap27
*

**Figure 4. Exosomes induced altered calcium dynamics is impaired by gap27 hemichannels blocker. a.** LY (in red) uptake visualised by confocal images depicting double positive LY and GFAP (in green) cells (40□; scale bar 100 µm). **b.** Bar plot quantifies the number of double positive GFAP/LY cells/field. (CTR vs LPS *P*** = 0.0094; CTR vs $EXO_{LPS}$ *P* *** = 0.0005, Kruskal–Wallis test). **c.** Sketched experimental protocol: $EXO_{LPS}$ were isolated and resuspended in 500 µl PBS in the presence of gap27 500 µM for 1 hour and then resuspended in 10 mL of EXO-free medium and reisolated. **d.** Representative calcium traces of astrocyte activity in control, $EXO_{LPS}$ and $EXO_{LPS+gap27}$. **e.** Bar plot showing an increase in the mean number of active astrocytes / field in treated slices. (CTR vs $EXO_{LPS}$ *P**** 0.0006; Kruskal–Wallis test). **f.** Bar plot showing a significant decrease in the IEI in $EXO_{LPS}$ treated slices. Strikingly, in sample treated with $EXO_{LPS+gap27}$ the calcium activity was significantly reduced when compared to $EXO_{LPS}$ (CTR vs $EXO_{LPS}$ *P*** = 0.0037; $EXO_{LPS}$ vs $EXO_{LPS + gap27}$ *P***** < 0.0001, Kruskal–Wallis test). **g.** Cumulative probability plot of calcium events IEI (Kolmogorov–Smirnov test).

**Discussion**

The main finding of the current work is the successful isolation of EXOs when released by tissue cultures under controlled resting or inflammatory reactive states. In addition, we report the ability of EXOs, delivered by activated cells, to spread inflammation in naïve tissues by triggering neuroinflammation morphological and functional features in exposed microglia and astrocytes.

The procedure to purify EXOs from multiple biological contexts (clinical or experimental) has been, and it is currently, a matter of debate. Indeed, the presence of vesicle subpopulations or contaminants (proteins, cell debris or others) might, in the case of our ultracentrifugation-based experiments, lead to reactive cells in a non-specific fashion, and EXOs isolation represents one of the major challenges in these types of studies and approaches [Patel G. K. et al 2019; Sidhom K. et al., 2020]. The important lack of standard procedures to purify EXOs has triggered the demand of new isolating technologies, in particular when EXOs are exploited as biomarkers of diseases [Chiriacò M. S. et al., 2018; Perissinotto F. et al., 2020]. Besides EXOs relevance as CNS biomarkers, we focused our attention on the role of CNS released EXOs in transferring signals related to their original microenvironment. In particular, we addressed EXOs as players in the biology and spreading of neuroinflammation. The protocol that we adopted to isolate EXOs from organotypic spinal cord slices cannot exclude the presence of contaminants or of heterogeneous vesicle subpopulations [Marostica G. et al., 2021]. However, our AFM, NTA and western blot results are in favour of a relatively homogenous EXOs population in terms of vesicle size, although we cannot exclude the presence of small vesicles released by membrane budding [Chen J. et al., 2022]. Being aware of EXOs potential mixed endosomal/nonendosomal origin, we are confident with their belonging to the small extracellular vesicle population, extracted in the absence of significant contaminations from the spinal cultured

tissue, the latter further strengthened by the control experiments adopting the re-suspended medium. In addition, the danger paradigm used (in terms of LPS concentration and exposure duration) is reported to lead to mild neuroinflammation, as confirmed in our histological and functional experiments, with negligible cell death [Panattoni G et al., 2021].

Organotypic slice cultures provide optimal experimental settings to reproduce inflammatory microenvironments which have been previously detailed [Giacco V. et al., 2019; Panattoni G. et al., 2021]. LPS treatments, similar to those adopted here, activate an immune condition where LPS binds to the TLRs expressed on the microglia surface resulting in the production and release of cytokines, chemokines, and other inflammatory factors [Panattoni G. et al., 2021]. Similarly, in the current results, the changes in microglia ramification status in the absence of clear GFAP hypertrophy [Giacco V. et al., 2019], but accompanied by the emergence of increased active astrocytes characterised by paroxysmal, aberrant calcium signalling [Panattoni G. et al., 2021], are good indicators of the emergence of local inflammation, triggered by LPS or re-vamped by $EXO_{LPS}$. We monitored astrocyte live calcium activity without the need of pharmacological neuronal firing removal [Panattoni G. et al., 2021], since GCaMP6f allows precise identification of active phenotypes while maintaining the background synaptic activity. Indeed, since inflammatory conditions enhance spinal synaptic activity [Medelin M. et al., 2018], and glial cells signaling also reflect neuronal electrical activity, our current experimental conditions may explain the higher amount of spontaneously active cells detected in each field, in resting or immune activated conditions, when compared to previous studies [Panattoni G. et al., 2021].

EXOs released and primed by inflammatory activated cells coordinate multicellular homeostatic reactivity and induce specific danger-associated changes in resident glial cells. In doing so, EXOs may interact with recipient cells in three major modalities [Zhao S. et al., 2021], they may be taken up by endocytic pathways (non-specific and receptor-mediated), alternatively EXOs may directly fuse with the plasma membrane or can remain attached to the plasma membrane, in all three cases manipulating downstream signalling pathways [Gurung S. et al., 2021]. It is interesting to note that the observed increase in opening of HCs upon $EXO_{LPS}$ treatment was prevented by the pre-treatment of EXOs with a HC blocker. In 2015 Soares and colleagues demonstrated that Cx43 HCs are present at the level of EXOs membrane and are essential for cargo transfer to recipient cells [Soares A. et al., 2015]. Although we cannot exclude the formation of a gap junctions by astrocytic and exosomal Cx43 allowing pro-inflammatory cargo transfer to the recipient cells [Soares A. et al., 2015], downstream activating inflammation and HC opening (in fact in LPS, increase in HC activity has been related to neuroinflammation expression; [Panattoni G. et al., 2021]), it is tempting to speculate that Cx43 HCs be involved in the transfer of EXOs inflammatory signals also by active transfer of open and functional

Cx43 HCs at the level of astrocytic plasma membrane. In fact, enhancing the permeability of the astrocyte HCs promotes the release of pro-inflammatory factors contributing to CNS damage progression [Makarenkova H. P. et al., 2014; Bernaus A. et al., 2020].

**Acknowledgments**

We thank F. Caponnetto and D.Cesselli for the NTA measures and analysis.

**References**

Avossa D., Rosato-Siri M. D., Mazzarol F., Ballerini L. **Spinal circuits formation: a study of developmentally regulated markers in organotypic cultures of embryonic mouse spinal cord.** Neuroscience. 2003;122:391–405.

Bernaus A., Blanco S., Sevilla A. **Glia Crosstalk in Neuroinflammatory Diseases**. Front Cell Neurosci. 2020 Jul 29;14:209.

Bindocci E., Savtchouk I., Liaudet N., Becker D., Carriero G, Volterra A. **Three-dimensional Ca2+ imaging advances understanding of astrocyte biology**. Science. 2017 May 19;356(6339)

Chen J., Li P., Zhang T., Xu Z., Huang X., Wang R., Du L. **Review on Strategies and Technologies for Exosome Isolation and Purification.** Front Bioeng Biotechnol. 2022 Jan 5;9:811971.

Chepied A., Daoud-Omar Z., Meunier-Balandre A. C., Laird D. W., Mesnil M., Defamie N. **Involvement of the Gap Junction Protein, Connexin43, in the Formation and Function of Invadopodia in the Human U251 Glioblastoma Cell Line**. Cells. 2020 Jan 3;9(1):117

Chiriacò M. S., Bianco M., Nigro A., Primiceri E., Ferrara F., Romano A., Quattrini A., Furlan R., Arima V., Maruccio G**. Lab-on-Chip for Exosomes and Microvesicles Detection and Characterization.** Sensors (Basel). 2018 Sep 20;18(10):3175.

Di Sabato D. J., Quan N., Godbout J. P. **Neuroinflammation: the devil is in the details.** J Neurochem. 2016 Oct;139 Suppl 2(Suppl 2):136-153.

Dolcetti E., Bruno A., Guadalupi L , Rizzo F. R., Musella A., Gentile A., De Vito F., Caioli S., Bullitta S., Fresegna D., Vanni V., Balletta S., Sanna K., Buttari F., Stampanoni Bassi M., Centonze D., Mandolesi G. **Emerging Role of Extracellular Vesicles in the Pathophysiology of Multiple Sclerosis**. Int J Mol Sci. 2020 Oct 4;21(19):7336

Doyle L. M., Wang M. Z. **Overview of Extracellular Vesicles, Their Origin, Composition, Purpose, and Methods for Exosome Isolation and Analysis**. Cells. 2019 Jul 15;8(7):727.

Fujita H., Tanaka J., Toku K., Tateishi N., Suzuki Y., Matsuda S., Sakanaka M., Maeda N. **Effects of GM-CSF and ordinary supplements on the ramification of microglia in culture: a morphometrical study.** Glia. 1996 Dec;18(4):269-81.

Furlan F., Taccola G., Grandolfo M., Guasti L., Arcangeli A., Nistri A., Ballerini L. **ERG conductance expression modulates the excitability of ventral horn GABAergic interneurons that control rhythmic oscillations in the developing mouse spinal cord.** J Neurosci. 2007 Jan 24;27(4):919-28

Giacco V., Panattoni G., Medelin M., Bonechi E., Aldinucci A., Ballerini C., Ballerini L. **Cytokine inflammatory threat, but not LPS one, shortens GABAergic synaptic currents in the mouse spinal cord organotypic cultures**. J Neuroinflammation. 2019;16:127.

Gurunathan S., Kang M. H., Jeyaraj M., Qasim M., Kim J. H. **Review of the Isolation, Characterization, Biological Function, and Multifarious Therapeutic Approaches of Exosomes**. Cells. 2019 Apr 3;8(4):307

Gurung S., Perocheau D., Touramanidou L., Baruteau J. **The exosome journey: from biogenesis to uptake and intracellular signalling.** Cell Commun Signal. 2021 Apr 23;19(1):47

Haustein M. D., Kracun S., Lu X. H., Shih T., Jackson-Weaver O., Tong X., Xu J., Yang X. W., O'Dell T. J., Marvin J. S., Ellisman M. H., Bushong E. A., Looger L. L., Khakh B. S. **Conditions and constraints for astrocyte calcium signaling in the hippocampal mossy fiber pathway.** Neuron. 2014 Apr 16;82(2):413-29.

Kanaporis G., Brink P. R., Valiunas V. **Gap junction permeability: selectivity for anionic and cationic probes.** Am J Physiol Cell Physiol. 2011 Mar;300(3):C600-9.

Li X., Tupper J. C., Bannerman D. D., Winn R. K., Rhodes C. J., Harlan J. M. **Phosphoinositide 3 kinase mediates Toll-like receptor 4-induced activation of NF-kappa B in endothelial cells.** Infect Immun. 2003 Aug;71(8):4414-20.

Makarenkova H. P., Shestopalov V. I. **The role of pannexin hemichannels in inflammation and regeneration.** Front Physiol. 2014 Feb 25;5:63

Marostica G., Gelibter S., Gironi M., Nigro A., Furlan R. **Extracellular Vesicles in Neuroinflammation.** Front Cell Dev Biol. 2021 Jan 21;8:623039

Medelin M., Giacco V., Aldinucci A., Castronovo G., Bonechi E., Sibilla A., Tanturli M., Torcia M., Ballerini L., Cozzolino F., Ballerini C.. **Bridging pro-inflammatory signals, synaptic transmission and protection in spinal explants in vitro**. Mol Brain. 2018;11:1–14.

Moon S., Shin D. W., Kim S., Lee Y. S., Mankhong S., Yang S. W., Lee P. H., Park D. H., Kwak H. B., Lee J. S., Kang J. H. **Enrichment of Exosome-Like Extracellular Vesicles from Plasma Suitable for Clinical Vesicular miRNA Biomarker Research**. J Clin Med. 2019 Nov 15;8(11):1995.

Musto M., Parisse P., Pachetti M., Memo C., Di Mauro G., Ballesteros B., Lozano N., Kostarelos K., Casalis L., Ballerini L. **Shedding plasma membrane vesicles induced by graphene oxide nanoflakes in brain cultured astrocytes** CARBON 176 (2021) 458–469

Orellana J. A., Retamal M. A., Moraga-Amaro R., Stehberg J. **Role of Astroglial Hemichannels and Pannexons in Memory and Neurodegenerative Diseases.** Front Integr Neurosci. 2016 Jul 20;10:26.

Oyarce K., Cepeda M. Y., Lagos R , Garrido C., Vega-Letter A. M., Garcia-Robles M., Luz-Crawford P., Elizondo-Vega R. **Neuroprotective and Neurotoxic Effects of Glial-Derived Exosomes.** Front Cell Neurosci. 2022 Jun 22;16:920686.

Pan B. T., Johnstone R. M. **Fate of the transferrin receptor during maturation of sheep reticulocytes in vitro: selective externalization of the receptor**. Cell. 1983 Jul;33(3):967-78.

Panattoni G., Amoriello R., Memo C., Thalhammer A., Ballerini C., Ballerini L. **Diverse inflammatory threats modulate astrocytes Ca2+ signaling via connexin43 hemichannels in organotypic spinal slices**. Mol Brain. 2021 Oct 25;14(1):159.

Parisse P., Rago I., Ulloa Severino L., Perissinotto F., Ambrosetti E., Paoletti P., Ricci M., Beltrami A. P., Cesselli D., Casalis L. **Atomic force microscopy analysis of extracellular vesicles.** Eur Biophys J. 2017 Dec;46(8):813-820.

Patel G. K., Khan M. A., Zubair H. et al. "**Comparative analysis of exosome isolation methods using culture supernatant for optimum yield, purity and downstream applications**." Sci. Rep. 9, 5335 (2019)

Pegtel D. M., Gould S. J. **Exosomes**. Annu Rev Biochem. 2019 Jun 20;88:487-514.

Peng B., Xu C., Wang S., Zhang Y., Li W. **The Role of Connexin Hemichannels in Inflammatory Diseases**. Biology (Basel). 2022 Feb 2;11(2):237.

Perissinotto F., Senigagliesi B., Vaccari L., Pachetti M., D'Amico F., Amenitsch H., Sartori B., Pachler K., Mayr M., Gimona M., Rohde E., Caponnetto F., Cesselli D., Casalis L., Parisse P. **Chapter Six - Multi-technique analysis of extracellular vesicles: not only size matters.** In Advances in Biomembranes and Lipid Self-Assembly, Volume 32, 2020, Pages 157-177

Rashed H. M., Bayraktar E., K Helal G., Abd-Ellah M. F., Amero P., Chavez-Reyes A., RodriguezAguayo C. **Exosomes: From Garbage Bins to Promising Therapeutic Targets.** Int J Mol Sci. 2017 Mar 2;18(3):538.

Rauti R., Lozano N., León V., Scaini D., Musto M., Rago I., Ulloa Severino F. P., Fabbro A., Casalis L., Vázquez E., Kostarelos K., Prato M., Ballerini L. **Graphene oxide nanosheets reshape synaptic function in cultured brain networks** ACS Nano, 10 (2016), pp. 4459-4471

Refolo V., Stefanova N. **Neuroinflammation and Glial Phenotypic Changes in AlphaSynucleinopathies**. Front Cell Neurosci. 2019 Jun 13;13:263.

Saez J. C., Berthoud V. M., Branes M. C., Martinez A. D., Beyer E. C. **Plasma membrane channels formed by connexins: their regulation and functions.** Physiol Rev. 2003 Oct;83(4):1359-400.

Semyanov A., Henneberger C., Agarwal A. **Making sense of astrocytic calcium signals - from acquisition to interpretation.** Nat Rev Neurosci. 2020 Oct;21(10):551-564

Shigetomi E., Saito K., Sano F., Koizumi S. **Aberrant Calcium Signals in Reactive Astrocytes: A Key Process in Neurological Disorders.** Int J Mol Sci. 2019 Feb 25;20(4):996

Sidhom K., Obi P. O., Saleem A. **A Review of Exosomal Isolation Methods: Is Size Exclusion Chromatography the Best Option?** Int J Mol Sci. 2020 Sep 4;21(18):6466

Soares A. R., Martins-Marques T., Ribeiro-Rodrigues T., Ferreira J. V., Catarino S., Pinho M. J., Zuzarte M., Anjo S. I., Manadas B., Sluijter J. P., Pereira P., Girao H. **Gap junctional protein Cx43 is involved in the communication between extracellular vesicles and mammalian cells**. Sci Rep. 2015 Oct 8;5:14888.

Soria F. N., Pampliega O., Bourdenx M., Meissner W. G., Bezard E., Dehay B. **Exosomes, an Unmasked Culprit in Neurodegenerative Diseases**. Front Neurosci. 2017 Jan 31;11:26.

Sung B. H., von Lersner A., Guerrero J. et al. **A live cell reporter of exosome secretion and uptake reveals pathfinding behavior of migrating cells.** Nat Commun 11, 2092 (2020).

Théry C., Clayton A., Amigorena S., Raposo G. **Isolation and Characterization of Exosomes from Cell Culture Supernatants and Biological Fluids**
Current Protocols in Cell Biology (2006) 3.22.1-3.22.29

Théry C., Witwer K. W., Aikawa E , et al. **Minimal information for studies of extracellular vesicles 2018 (MISEV2018): a position statement of the International Society for Extracellular Vesicles and update of the MISEV2014 guidelines.** J Extracell Vesicles. 2018 Nov 23;7(1):1535750

Vereker E., Campbell V., Roche E., McEntee E., Lynch M. A. **Lipopolysaccharide inhibits long term potentiation in the rat dentate gyrus by activating caspase-1.** J Biol Chem. 2000 Aug 25;275(34):26252-8

Wang N., De Bock M., Antoon G., Gadicheria A. K., Bol M., Decrock E., Evans W. H., Sipido KR, Bukauskas FF, Leybaert L. **Connexin mimetic peptides inhibit Cx43 hemichannel opening triggered by voltage and intracellular Ca2+ elevation**. Basic Res Cardiol. 2012;107(6):17

Zhao S., Sheng S., Wang Y., Ding L., Xu X., Xia X., Zheng J. C. **Astrocyte-derived extracellular vesicles: A double-edged sword in central nervous system disorders.** Neurosci Biobehav Rev. 2021 Jun;125:148-159.

Carbon 176 (2021) 458–469

Contents lists available at ScienceDirect

Carbon

journal homepage: www.elsevier.com/locate/carbon

# Shedding plasma membrane vesicles induced by graphene oxide nanoflakes in brain cultured astrocytes

Mattia Musto [a, 1], Pietro Parisse [b], Maria Pachetti [b], Christian Memo [a], Giuseppe Di Mauro [a], Belen Ballesteros [c], Neus Lozano [c], Kostas Kostarelos [c, d], Loredana Casalis [b, **], Laura Ballerini [a, *]

[a] International School for Advanced Studies (SISSA), 34136, Trieste, Italy
[b] ELETTRA Synchrotron Light Source, 34149, Basovizza, Italy
[c] Catalan Institute of Nanoscience and Nanotechnology (ICN2), Campus UAB, Bellaterra, 08193, Barcelona, Spain
[d] Nanomedicine Lab, National Graphene Institute and Faculty of Biology, Medicine & Health, The University of Manchester, Manchester, M13 9PT, United Kingdom

ARTICLE INFO

*Article history:*
Received 4 December 2020
Received in revised form
25 January 2021
Accepted 27 January 2021
Available online 8 February 2021

*Keywords:*
Graphene oxide
Extracellular vesicles
Atomic force microscopy and spectroscopy
FTIR-ATR and UVRR spectroscopy
Synaptic activity
Cortical neuronal cultures

ABSTRACT

Microvesicles (MVs) generated and released by astrocytes, the brain prevalent cells, crucially contribute to intercellular communication, representing key vectorized systems able to spread and actively transfer signaling molecules from astrocytes to neurons, ultimately modulating target cell functions. The increasing clinical relevance of these signaling systems requires a deeper understanding of MV features, currently limited by both their nanoscale dimensions and the low rate of their constituent release. Hence, to investigate the features of such glial signals, nanotechnology-based approaches and the applications of unconventional, cost-effective tools in generating MVs are needed. Here, small graphene oxide (s-GO) nanoflakes are used to boost MVs shedding from astrocytes in cultures and s-GO generated MVs are compared with those generated by a natural stimulant, namely ATP, by atomic force microscopy, light scattering, attenuated total reflection–fourier transform infra-red and ultraviolet resonance Raman spectroscopy. We also report the ability of both types of MVs, upon acute and transient exposure of patch clamped cultured neurons, to modulate basal synaptic transmission, inducing a stable increase in synaptic activity accompanied by changes in neuronal plasma membrane elastic features.


## 1. Introduction

In biology, newly described forms of intercellular communication comprise the release of vesicles, named extracellular vesicles, from virtually all cell types, including resident glial cells of the central nervous system (CNS), such as astrocytes and microglia [1,2]. In particular, the shedding of membrane vesicles is a recognized form of cross talk in the multidimensional signaling between astrocytes, (i.e. the majority of cells in the mammalian CNS), and neurons in physiology, but also in neurodegenerative and neuroinflammatory diseases as well as in brain tumors. Extracellular vesicle signaling molecules, either stored within their cargo or embedded in their plasma membrane, modulate relevant processes in the development, physiology and pathology of CNS target cells [3–6]. The signaling system based on release of extracellular vesicles comprises shedding microvesicles (MVs) and exosomes, characterized by different size, membrane composition, cargo and origin [7,8].

MVs are nanovesicles able to interact specifically with cells at local or distant sites [9]. In maintaining CNS functions, glial cells intensely communicate with neurons, also *via* the release of MVs, which represents a highly versatile tool to functionally impact the CNS [10–12]. MVs are considered a “vectorized” signaling system able to bind their target cells to transmit specific information. The

* Corresponding author.
** Corresponding author.
*E-mail addresses:* loredana.casalis@elettra.eu (L. Casalis), laura.ballerini@sissa.it (L. Ballerini).
[1] Present Addresses: Center for Synaptic Neuroscience, Istituto Italiano di Tecnologia (IIT), 16132, Genoa, Italy.

https://doi.org/10.1016/j.carbon.2021.01.142

reported spreading ability of MVs has suggested their potential exploitation as biomarkers or as engineered therapeutic carriers [13]. A comprehensive correlation between conditions used to release and harvest MVs from the same cell type, i.e. astrocytes, and their signaling ability, will impact our understanding of MVs physiology and the design of MV-based biomedical applications in the CNS [14,15]. Particular attention has to be conveyed to devise novel, cost-effective ways in generating MVs, in particular enhancing constitutive release.

Here, we concentrate on graphene oxide (GO), the most common derivative of graphene, whose properties can be tailored to adapt to new physical and biological applications [16,17]. GO flakes have been successfully designed for drug delivery applications in biomedicine [18]. In the CNS, small GO nano-flakes (s-GO) were shown to induce constitutive MV release from cultured astrocytes and to potentiate evoked MV release induced upon exposure to bzATP [19]. s-GO flakes, due to their physical features at the nanoscale, were reported to interfere with cellular membrane dynamics [19,20]. In addition, *via* adhesion to the plasma membrane, s-GO may alter the mechanical features of the lipid bilayer [21] triggering genuine biological responses, such as MVs signaling. Thus s-GOs may represent a tool to exploit mechanical signaling at the nanoscale to activate membrane release of MVs. Drug delivery applications where vesicle release from genetically engineered cells is required, may take advantage of the mechanical modulation of vesicle release brought about by graphene-based nanomaterials, representing a safer and cheaper alternative to pharmacological tools. Prolonged exposure to biomolecules able to induce MVs release, such as ATP, could in fact negatively affect cell physiology by promoting astrogliosis and inducing microglia-mediated neuroinflammatory responses [22].

We use the ability of s-GO to substantially increase the production of MVs from astrocytes to provide, for the first time, a robust and comparative vesicle characterization by means of ultramicroscopy, attenuated total reflection–fourier transform infra-red (FTIR-ATR) and UV Resonant Raman (UVRR) spectroscopy. We additionally explore by single cell patch-clamp recordings the impact of acute, local and transient delivery of MVs on neuronal basal synaptic activity and by atomic force microscopy (AFM) the accompanying changes in neuronal plasma membrane elastic features.

## 2. Material and Methods

### 2.1. Graphene oxide nanosheets synthesis

GO was manufactured under endotoxin-free conditions through our modified Hummers' method as previously described [19]. The complete characterization of the material used is shown and summarized in the Supplementary experimental section and Supplementary Figure S1 and Table S1.

### 2.2. Cell cultures

All experiments were performed in accordance with the EU guidelines (Directive 2010/63/EU) and Italian law (decree 26/14) and were approved by the local authority veterinary service and by our institution (SISSA-ISAS) ethical committee. All efforts were made to minimize animal suffering and to reduce the number of animals used. Animal use was approved by the Italian Ministry of Health, in agreement with the EU Recommendation 2007/526/EC.

Primary glial cultures were obtained from cortices isolated from neonatal rats (Wistar) at postnatal day 2–3 (P2–P3), as previously described [19,23]. Dissociated cells were plated into plastic 150 $cm^2$ flasks and incubated at 37 °C; 5% $CO_2$ in culture medium composed of DMEM (Invitrogen), supplemented with 10% fetal bovine serum (FBS; Thermo Fisher), 100 IU/mL penicillin, and 10 mg/mL streptomycin.

Cortical neurons were isolated from neonatal rat cortices (Wistar) at postnatal day 0–1 (P0–P1). Dissociated cells were then plated on poly-L-ornithine (Sigma) coated coverslips (Kindler, EU) at a concentration of 150000 cells in a volume of 200 μL and incubated at 37 °C; 5% $CO_2$ in a culture medium composed of Neurobasal-A (Thermo Fischer) containing 2% B27 (Gibco), 10 mM Glutamax and 0.5 μM Gentamycin (Gibco) for 8–10 *days in vitro* (DIV) before performing electrophysiological experiments.

### 2.3. MV isolation

MV shedding and isolation was performed as previously described [19]. One pool of MVs were collected from 21 to 24 DIV glial cultures previously treated with graphene oxide nanoflakes (s-GO) (10 μg/mL [19]), added to culture medium once and left for 6 days. At the end of 6-days exposure, the medium was removed and substituted with physiological saline solution, with the following composition: 152 mM NaCl, 4 mM KCl, 1 mM $MgCl_2$, 2 mM $CaCl_2$, 10 mM HEPES and 10 mM Glucose (pH adjusted to 7.4), at 37 °C and 5% $CO_2$ for 60 min prior to MVs collection and purification. The MVs pool was isolated from cultures treated (30 min) with benzoyl-ATP (bzATP; 100 μM) diluted in physiological saline solution. The 6-days exposure timepoint was chosen on the basis of previous Western blot experiments, and confirmed by our current experiments testing MVs release after 3 days of s-GO exposure (supplementary Figure S2) [19]. Negative controls were incubated with physiological solution without the presence of bzATP or s-GO. After the incubation period, cell medium was collected and centrifuged for 15 min at a speed of 300×*g* in order to remove cell debris. Supernatant was then collected and MVs were pelleted by centrifugation at 20000×*g* for 2 h. For $Ca^{2+}$ deprivation experiments, prior to supernatant collection and MVs pellet centrifugation, cultures were pre-incubated for 45 min in a saline solution identical to the physiological saline solution except for 0 mM $CaCl_2$, 3 mM $MgCl_2$ and 1 mM EGTA to allow the depletion of intracellular calcium storage. Upon this pre-treatment, we harvest the MVs from controls, s-GO treated and bzATP (30 min in $Ca^{2+}$ deprived solution; supplementary Figure S3).

### 2.4. Western blot analysis

MVs were prepared as previously reported, briefly they were resuspended in lysis buffer (50 mM Tris-HCl, pH 8.0, 150 mM NaCl, 1% NP40, 0.1% SDS), sonicated for 30 s, and then boiled at 95 °C for 5 min [19]. Samples were run on a 10% polyacrylamide gel and blotted onto nitrocellulose membranes (Millipore, Italy). Membranes were then blocked in PBS-Tween-20 (0.1%) plus 5% nonfat dry milk and incubated with the primary antibody antiflotillin-1 (dilution 1:1000) for 16 h at 4 °C. Membranes were then washed with PBS-Tween and incubated with peroxidase-conjugated anti-mouse secondary antibody (dilution 1:1000). Detection of immunolabeled ECL-exposed protein bands was measured with UVI-1D software over three independent experiments.

### 2.5. Immunofluorescence and confocal microscopy

Primary glial and cortical neurons cultures were fixed in 4% formaldehyde (PFA, prepared from fresh paraformaldehyde) in PBS for 20 min at room temperature (RT) and then washed in PBS. Free aldehyde groups were quenched in 0.1 M glycine solution for 5 min. The samples were permeabilized in 5% fetal bovine serum (FBS), 0.3% Triton-X 100 in phosphate buffer solution (PBS) for 30 min at

RT. Samples were then incubated with primary antibodies (mouse monoclonal anti-GFAP, Invitrogen, 1:500 dilution; rabbit polyclonal anti-β-tubulin III, Sigma-Aldrich, 1:500 dilution) diluted in PBS with 5% FBS at 4 °C for 1 h. Samples were then incubated with secondary antibodies (Alexa 488 goat anti-mouse, Invitrogen, 1:500 dilution; Alexa 594 goat anti-rabbit, Invitrogen, 1:500 dilution), and DAPI (Invitrogen, dilution 1:200) to stain the nuclei, for 45 min at RT and finally mounted on 1 mm thick glass coverslips using Fluoromount mounting medium (Sigma-Andrich). Images were acquired using a Nikon C2 Confocal, equipped with Ar/Kr, He/Ne and UV lasers with a 40 × or 60 × (1.4 NA) oil-objective (using oil mounting medium, 1.515 refractive index) to acquire glial cultures images and cortical neurons images respectively. 200 × 200 μm fields were acquired for cortical neurons images and 300 × 300 μm fields were acquired for glial cells images. Confocal sections were acquired every 0.25 μm for both the cultures.

### 2.6. Glial cell viability assay

Primary rat astrocytes (21–24 DIV) were exposed to s-GO 10 μg/mL or to equivalent volumes of the vehicle for 6 days. Cells were stained with propidium iodide (PI, 1 μg/mL; 15 min) for cell death quantification and subsequently fixed in PFA and labeled for DAPI for nuclei visualization and GFAP for visualizing astrocytes. The red (PI positive) fluorescent nuclei indicating dead cells were quantified at 40 × (1.4 NA) magnification using a Nikon C2 Confocal microscope, equipped with Ar/Kr, He/Ne and UV lasers, with random sampling of 10 fields per sample (n = 3 coverslips/sample, from 3 independent culture preparations). The average percentage of dead cells was calculated counting visual fields selected.

### 2.7. FM1-43 staining

Glial cells were incubated with the fluorescent styryl dye FM1-43 (2 μM) for 2 min in order to completely stain plasma membrane, then extensively washed with PBS and exposed for 30 min to bzATP (100 μM) or to standard saline solution [19]. Samples were placed in a recording chamber mounted on an inverted microscope (Nikon Eclipse Ti–U) and observed with a 40× objective (0.6 NA, PlanFluor, Nikon). Images (512 × 512 px) were acquired for 10 min with an exposure time of 150 ms (6.6 Hz) by a Hamamatsu Orca-Flash 4.0 digital camera controlled by an integrating imaging software package (HCImage, Hamamatsu). Recorded images were analyzed offline with the Clampfit software (pClamp suite, 10.2 version; Axon Instruments). Image time stacks were analyzed in selected regions of interest (ROI) to measure the variations in FM1-43 fluorescence intensity over time. Natural sample bleaching over time, due to prolonged light exposure, has the same time-course and intensity in all the three groups, as previously described [19].

### 2.8. Atomic force microscopy analysis

AFM characterization was performed as previously described [19]. Briefly, the pellet of MVs was re-suspended in PBS solution after isolation from cell cultures and a 15 μL drop of sample solution was placed and left to adsorb (30 min) onto a freshly peeled mica substrate. Vesicles were then fixed with 1% formaldehyde for 1 h (RT) in order to prevent their collapse during AFM acquisition. MVs were then washed with PBS and dried under a gentle stream of nitrogen. AFM analysis was performed in air at RT, using the semi-contact mode of a commercial instrument (Solver Pro, NT-MDT, RU). Silicon tips (NSC36/CR-AU, MikroMash, USA) with a typical force constant of 0.6 nN/nm and a resonance frequency of about 65 kHz were employed. Topographic height and phase images were recorded at 512 × 512 pixels at a scan rate of 0.5 Hz. Image processing was performed using Gwyddion freeware AFM analysis software, version 2.40. Diameter and height of each vesicle were evaluated from cross-line profiles, and results were statistically analyzed using Prism (Graphpad software).

### 2.9. Neuronal stiffness

9-10 DIV cortical neurons were exposed to MVs obtained by glial cultures treated with bzATP or s-GO and neuronal rigidity was assessed with AFM, 24 h after MVs exposure. Force spectroscopy measurements were performed with a commercial Smena AFM (NT-MDT, RU) mounted on an inverted microscope (Nikon Eclipse Ti–U). AFM cantilever deflection was measured when pushed against cortical neurons plated on a glass coverslip. Deflection values were subsequently converted into a force versus indentation curve based on cantilever spring constant and its displacement. Neuronal rigidity was evaluated in 50 randomly chosen neurons for each condition (from 3 independent experiments), acquiring three force spectroscopy curves in the center of each cell soma. The AFM tip was positioned by using an inverted microscope in bright field mode.

AFM micro-cantilevers with an elastic constant of about 0.03 nN/nm and a resonance frequency of about 10 kHz (CSG01 tipless cantilevers from NT-MDT, RU) were used. A borosilicate glass microsphere of about 18 μm in diameter (18.2 ± 1.0 mm from Duke Standards, CA, USA) was manually glued at the end of each cantilevers using a UV curable glue (Norland Optical Adhesive 61 from Norland Products Inc., NJ, USA). Force spectroscopy measurements were performed at a constant indentation speed of 1 mm/s with a maximum value of indentation deepness set at 500 nm. Elastic modulus values (E), expressed in kPa, were determined by fitting obtained force–indentation curves with a Hertzian model for the tip, using AtomicJ (v. 1.7.3) analysis software [24].

### 2.10. Nanoparticle tracking analysis (NTA)

Measurement and analysis of MVs size distribution by NTA was performed on a NanoSight LM10 system (Malvern) using approximately 500 μL of MVs of both conditions (bzATP-derived and s-GO-derived) diluited 1:20 in MilliQ $H_2O$. Individual videos of 60 s (recorded at 25 FPS; 3 videos per group) for each sample were acquired at RT using the maximum camera gain, a detector threshold equal to 8 and analyzed by the NanoSight particle tracking software to calculate size and vesicle concentration.

### 2.11. FTIR-ATR spectroscopy and UV Resonant Raman (UVRR) measurements

MVs were isolated from 21 to 24 DIV glial cultures by centrifugation as described above. MVs pellet was successively washed with NaCl solution (150 mM) and finally re-suspended in 50 μL of the same solution in order to avoid contribution of phosphate and sugar groups to the IR absorbance spectra. The IR measurements were carried out at the BL10.2-IUVS beamline at Elettra synchrotron Trieste. The spectra were collected in ATR mode using a MIR DLaTGS detector and a KBr-broadband beam-splitter. For each IR measurement, 2 μL of sample solution were spread over the whole area of a monolithic diamond ATR plate and left to dry forming a thin film. For each sample, 20 spectra were collected in the range 4000–800 $cm^{-1}$, accumulating 256 scans for each spectrum reaching a resolution of 4 $cm^{-1}$. Each spectrum was corrected for the background, aqueous vapor, $CO_2$ and not normalized to any absorbance band.

UVRR measurements were performed at the BL10.2-IUVS beamline at Elettra synchrotron Trieste using the experimental

set-up reported [25]. 5 μL of vesicles solution were drop-casted onto an aluminum foil, allowed to dry and kept under nitrogen purging. All the measurements were performed at RT, using an excitation wavelength of 244 nm and tuning the power of the incoming radiation to 50 μW. The outcoming radiation was collected in backscattering geometry by using a triple stage spectrometer (Trivista, Princeton Instrument) with a spectral resolution of 8 $cm^{-1}$. Samples were continuously oscillated horizontally in order to avoid photodamaging.

### 2.12. Electrophysiological recordings

Patch-clamp recordings (whole-cell, voltage clamp mode) were performed from visually identified (under differential interference contrast - DIC - microscopy) cortical neurons (DIV 8–10) placed in a recording chamber, mounted on an inverted microscope (Eclipse Ti–U, Nikon, Japan) and superfused with control physiological saline solution of the following composition (in mM): 152 NaCl, 4 KCl, 1 MgCl2, 2 CaCl2, 10 HEPES and 10 Glucose (pH adjusted to 7.4 by NaOH 1 M; osmolarity 300 mOsm). Cells were patched with glass pipettes (4–7 MΩ) containing (in mM): 120 K gluconate, 20 KCl, 10 HEPES, 10 EGTA, 2 $MgCl_2$ and 2 $Na_2ATP$ (pH adjusted to 7.35 by KOH; osmolarity 298 mOsm). All electrophysiological recordings were performed at RT and the spontaneous, basal synaptic activity was recorded by clamping the membrane voltage at −70 mV (corrected for liquid junction potential, which was −14 mV). To investigate the acute effect on synaptic activity of glia-derived MVs, an injection pipette (patch pipette with resistance of 1–4 MΩ) filled with MVs previously isolated glial cultures as described above and re-suspended in 100 μL of extracellular saline solution was positioned at 200 μm from the cell soma and connected to a pico-spritzer (PDES-02DX, npi Electronics) with 0.3 psi in-line pressure [19]. On the basis of MVs quantification obtained by NTA measurements, and considering that MVs isolation was performed using the same protocol in all the experiments described, we calculated that the concentration of MVs used for these tests was approximately of $6.64 \times 10^9$ for MVs obtained by bzATP stimulation and $1.64 \times 10^{10}$ for MVs isolated from s-GO treated cultures. Baseline spontaneous synaptic activity was recorded for the 10 min prior delivering the puff (500 ms duration) of MVs and followed up for 20 min to verify changes in post synaptic current (PSC) frequency and amplitude induced by the fusion of MVs with neuronal membranes.

Data were collected by Multiclamp 700B patch amplifier (Axon CNS, Molecular Devices) and digitized at 10 kHz with the pClamp 10.2 software (Molecular Devices LLC, USA). All recorded events were analyzed offline with the AxoGraph 1.4.4 (Axon Instrument) event detection software (Axon CNS, Molecular Devices).

### 2.13. Statistical analysis

Data sets found to follow a non-normal distribution, were represented as box plot. The central thick horizontal bar in the box plots indicates the median value, while the boxed area extends from the 25th to 75th percentiles with the whiskers ranging from the 2.5th to the 97.5th percentiles. Statistically significant differences between two non-parametric data sets were assessed by Mann-Whitney's test, while to assess statistically significant differences among three data-set we used the Kruskal-Wallis test and Dunn's post hoc test. $P < 0.05$ was considered at a statistically significant.

## 3. Results and discussion

Astrocytes were isolated from postnatal (2–3 days) rat (Wistar) cortices, as previously described [19,20,23]. We used visually homogenous s-GO dispersions containing s-GO nanosheets with lateral dimensions predominantly between 50 and 500 nm [19,20]. We treated pure glial cell cultures with s-GO (10 μg/mL) for 6 days [19]. Immunofluorescence labeling by antigen against glial-fibrillary acidic protein (GFAP), an intermediate filament protein that is highly specific for cells of the astroglial lineage, was used to visualize control and s-GO-treated neuroglial cultures (GFAP, in green; Fig. 1a) [26]. At the low concentrations used, s-GO treatment did not impair astrocyte morphology and cell density when compared with matched control cultures (box-plot in Fig. 1b) [19,27]. Viability of glial cells was confirmed by propidium iodide (PI) cell death assay. Control and s-GO treated cultures were incubated with PI, which stain dead cells nuclei (Fig. 1c, in red) and the percentage of PI-positive nuclei was calculated (bar plot in Fig. 1d). Graphene nanosheets cytotoxicity is a largely debated issue, due to the variable impact on cell toxicity of several material's features, related either on the GO physical-chemical properties (thickness, size, surface functionalization, aggregation state and concentration) or on the synthesis method [28,29], the experimental conditions adopted here and in our previous works [19,20] exclude any cytotoxic effect on glial cells or neurons, both *in vitro* and *in vivo*.

MVs are released into the extracellular space by direct budding from the plasma membrane of astrocytes [30]. To explore the dynamics of MVs release in control, in s-GO treated and in ATP treated (see below) astrocytes, we measured the presence of changes in membrane trafficking by briefly incubating cultures with the fluorescent styryl dye FM1-43 and then quantifying the astrocyte-membrane fluorescence decay to provide a cumulative measure of exocytosis in the different growth conditions [19,30].

FM dyes are fluorescent probes that reversibly stain membranes, and are largely used for optical real-time measurements of membrane dynamics and secretory processes [31–33]. Incubation with the FM dye (2 μM, 2 min) resulted in clear surface membrane staining of control, bzATP, an agent known to evoke massive MVs release (100 μM, 30 min) and s-GO treated cultures (10 μg/mL, 6 days), highlighted in Fig. 1e (left panels) [30]. Brighter spots were considered as adherent debris and were excluded from the analysis. Besides these, both bright and weak FM-stained plasma membrane domains were present along the whole cytoplasmic surface and became visible within 2 min incubation (Fig. 1e). Due to this initial variability in the intensity of the membrane staining, all FM de-staining measures were normalized to the relative time 0. Once astrocyte membranes were labeled by the fluorescent dye FM1-43 we measured the plasma membrane de-staining over a fixed time (10 min) in control, in s-GO treated cultures, or during acute exposure to bzATP, under the same culturing conditions [19]. Representative fluorescence intensity traces are shown in Fig. 1f (top plot); the dynamic of the fluorescence decay observed in control cultures, indicates the presence of physiological bleaching of fluorophore over the acquisition time course, however s-GO and bzATP groups, despite the same bleaching-induced loss of fluorescence, showed a faster de-staining rate in respect to controls. This is also visualized by the time-lapse images framed at time 0 s, 300 s and 600 s of the crude recordings (Fig. 1e middle and right panels). We quantified the fluorescence decay time constant ($\tau$) values (box plot of Fig. 1f) and detected shorter decay values in both bzATP and s-GO groups ($median_{control} = 219$ s; $median_{bzATP} = 184.2$ s; $median_{s\text{-}GO} = 163.9$ s). This result suggested that the membrane de-staining was actually related to MVs release, as expected in bzATP treated cells, more than to other membrane turnover activities. Such a release was comparable between bzATP and s-GO, both significantly faster than controls ($P_{bzATP} < 0.001$; $P_{s\text{-}GO} < 0.001$).

The release of MVs suggested by FM1-43 measures, was confirmed by immunoblot analysis for the biomarker flotillin-1 of

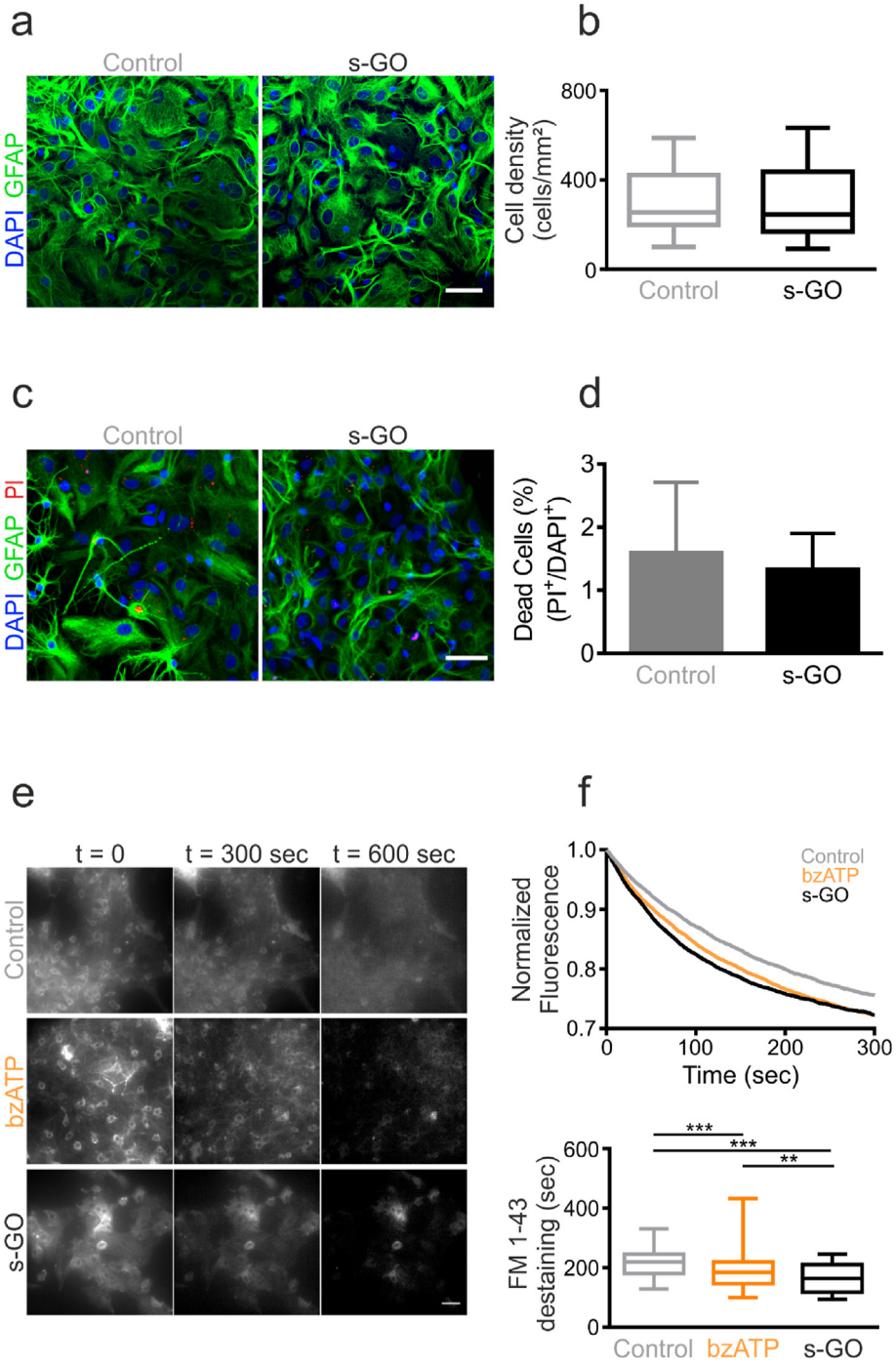


**Fig. 1. Graphene oxide nanosheets does not affect astrocytes vitality.** Cultured astrocytes release microvesicles (MVs) upon ATP or s-GO stimulation. a) Confocal images visualize cultured astrocytes in control and after s-GO (10 μg/mL; 6 days) treatment; anti-GFAP, in green, and DAPI (to visualize nuclei), in blue; scale bar 50 μm. b) Box plot summarizes the cell density measures; note the similar values in both groups. c) Confocal images visualize cultured astrocytes in control and after s-GO (10 μg/mL; 6 days) treatment. Cultures were treated with propidium iodide (PI) to visualize death cells. Anti-GFAP, in green, DAPI (to visualize nuclei), in blue and PI in red; scale bar 50 μm. d) Histogram summarizes the percentage of death cells followed the s-GO exposure and in control condition; note that there are no significant difference between two groups e) Surface membrane staining and activity dependent de-staining of FM1-43 in cultured astrocytes, scale bar 25 μm. f) Normalized FM1-43 de-staining traces (top) in control astrocytes (light grey), in bzATP treated once (orange) and in s-GO treated once (black). The box plot (bottom) summarizes the decay time constant $\tau$ of FM1-43 de-staining in the three conditions ($median_{control}$ = 219.2 s; $median_{bzATP}$ = 184.2 s; $median_{s\text{-}GO}$ = 163.9 s). Thick horizontal bars in the box plots indicate median value; boxed area extends from the 25th to 75th percentiles, whiskers from 2.5th to the 97.5th percentiles. Significance: **P < 0.01 ***P < 0.001, Kruskal-Wallis test, Dunn's post hoc test). (A colour version of this figure can be viewed online.)

the supernatant collected from control and treated cultures (Fig. 2a). As expected, bzATP stimulation and s-GO incubation induced the appearance of a thick band corresponding to flotillin-1 (Fig. 2a), a signature of MVs release by astrocytes, with an additive effect between s-GO exposure and pharmacological stimulation with bzATP ($s\text{-}GO_{Ringer}$ is quantified as 100% more than $Control_{Ringer}$; $bzATP_{Ringer}$ is quantified as 360% more than $Control_{Ringer}$; $bzATP_{s\text{-}GO}$ is quantified as 2900% more than $Control_{Ringer}$. Calculated over three independent experiments) [19,30,34]. In control conditions only a weak band was perceived, indicating that MVs

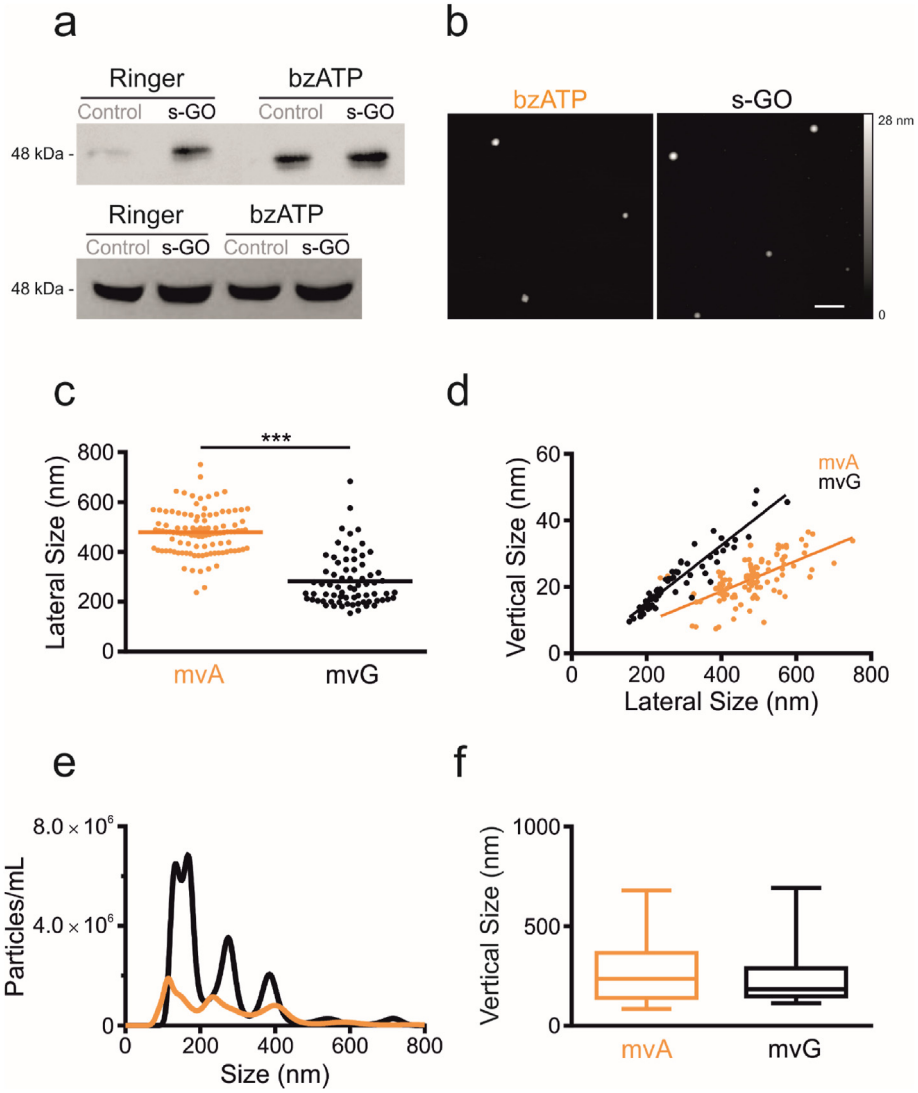


**Fig. 2. Graphene oxide nanosheets and bzATP induce MVs release in Astrocytes.** Microvesicle released by glial cells *via* bzATP or s-GO stimulations characterized by ultra-resolution approaches. a) Western blotting of the pellets (top row) and cell lysates (bottom row) for the MV marker flotillin-1 (N = 3). Pellets were obtained from the medium of glial cultures treated or untreated (control) with s-GO under two different conditions: not stimulated (ringer) or stimulated (bzATP) by 100 μM bzATP. $s\text{-}GO_{Ringer}$ is quantified as 100% more than $Control_{Ringer}$; $bzATP_{Ringer}$ is quantified as 360% more than $Control_{Ringer}$; $bzATP_{s\text{-}GO}$ is quantified as 2900% more than $Control_{Ringer}$. Calculated over three independent experiments. b) AFM topographic reconstruction of MVs isolated from cultured primary astrocytes treated with bzATP (100 μM) and s-GO (10 μg/mL) and performed in air (semi-contact mode). Scale bar 500 nm. c) Lateral size values distribution and median values for both groups, note that mvG lateral size is significantly smaller than that of mvA ($median_{mvA}$ = 479 nm; $median_{mvA}$ = 244.1 nm; ***P > 0.001, Mann-Whitney test). d) AFM measures of lateral size are plotted against AFM measures of height of MVs isolated from glial cells treated by bzATP (100 μM; mvA; in orange) or by s-GO (10 μg/mL; mvG; in black). e) Size distribution of MVs isolated from glial cells treated by bzATP (100 μM; in orange) or by s-GO (10 μg/mL; in black) measured by nanoparticle tracking analysis (NTA). Values of the peaks are expressed in nm. f) Lateral size values distribution and median values for both groups, obtained by NTA measurement. (A colour version of this figure can be viewed online.)

constitutive release in culture was poorly detectable. Atomic force microscopy (AFM) topographic reconstruction of re-suspended MVs pellet (Fig. 2b) confirmed the presence of MVs detected by the immunoblot in both bzATP (mvA) and s-GO (mvG) groups. When investigating the effect of shorter (3 days) exposure to s-GO, Western blot experiments (supplementary Fig. S2) showed the absence of a significant increase in MVs constitutive release when compared to control. Yet, bzATP release of MVs was potentiated by 3 days s-GO (supplementary Fig. S2) suggesting that s-GO already modulated MVs release, but longer time of s-GO exposure are needed to enhance basal release in the absence of additional stimuli. In an additional set of Western blot experiments, we tested the sensitivity of bzATP and s-GO MVs release to extracellular calcium deprivation (supplementary Fig. S3). Differently from bzATP, s-GO release was apparently not affected by calcium removal. In control condition, a thick band appeared upon calcium removal, suggestive of an increase in constitutive release (supplementary Fig. S3). These preliminary results hint at release mechanisms differently tuned by calcium among control, bzATP and s-GO and require further studies.

We systematically investigated and compared the MV size distribution by means of AFM and nanoparticle tracking analysis (NTA) measurements. AFM images show the presence of roundish protrusions of dimensions compatible with the size of MVs. No other kind of contaminant was present, to indicate that the procedure for isolating and collecting MVs from the medium was clean and effective. When analyzed by AFM (Fig. 2c) s-GO-derived MVs (mvG) lateral size were significantly smaller (n = 72, $median_{mvG}$ = 244 nm) than bzATP-derived ones (mvA; n = 107, $median_{mvA}$ = 479 nm) (P < 0.001). Conversely, we detected no

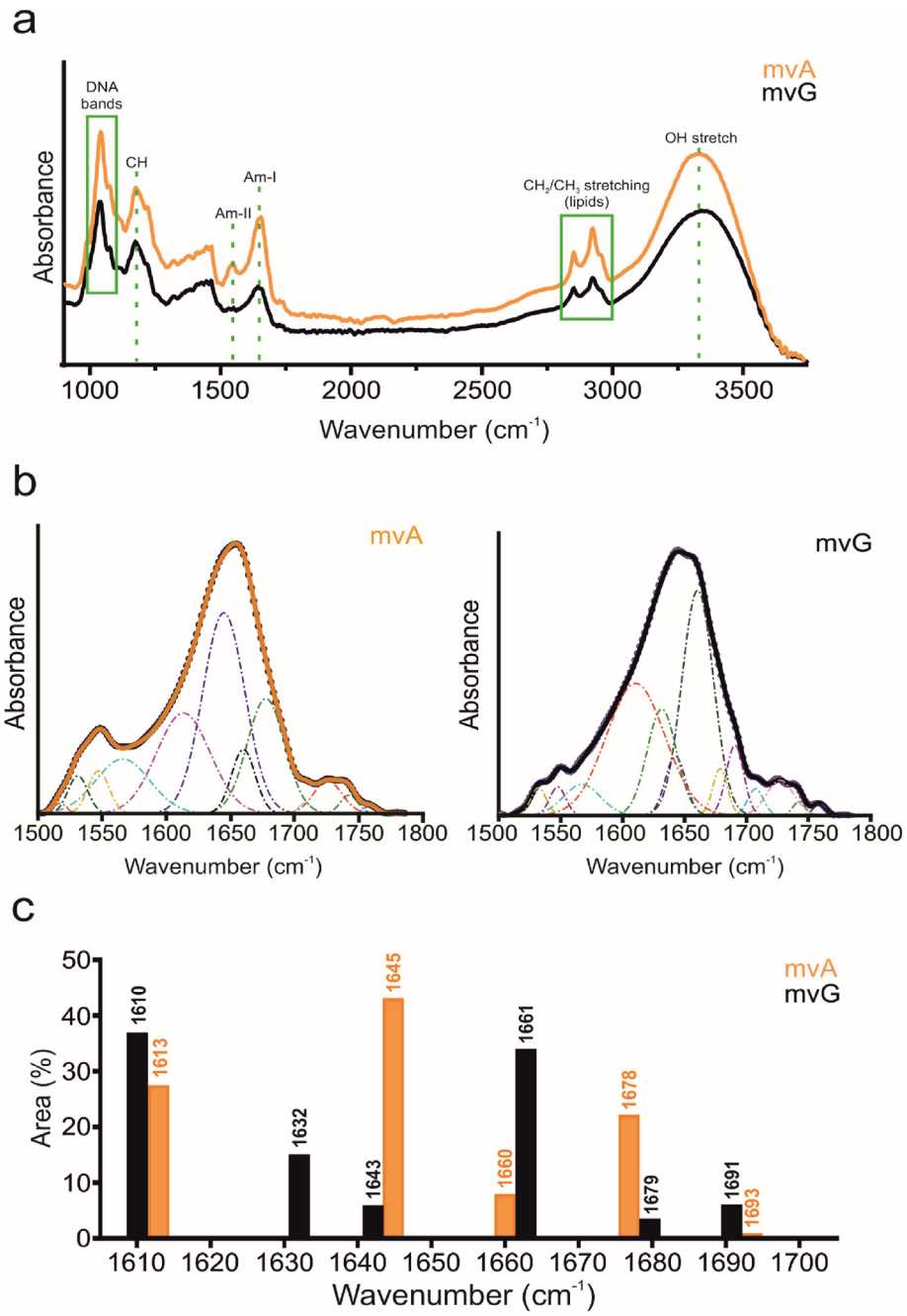


**Fig. 3. MVs characterization by infrared spectroscopy.** Microvesicles produced by glial cells *via* bzATP or s-GO stimulation and characterized by infrared spectroscopy. a) Infrared spectra of microvesicles obtained by bzATP stimulation (mvA, in orange) or by s-GO exposure (mvG, in black) in the region 950-3600 $cm^{-1}$. Contributions arisen from nucleic acids, proteins and lipids characterize the spectra. The two boxes in green and the green dashed lines are used as eye-guides to highlight nucleic acids, $CH_2$–$CH_3$ stretching of lipids and protein amide bands, respectively. b) Fitting procedure applied to mvA (on the left) and mvG (on the right) amide bands spectra. Multicomponent Gaussian curves were used to actually reproduce the experimental data. The centres of the Gaussian curves were chosen as the minimum of the 2nd derivative of the spectrum and kept free to variate within 4 $cm^{-1}$ around its maximum. c) Histograms representing the areas of the Gaussian curves used to reproduce the experimental data of mvA (in orange) and mvG (in black) in the region 1500-1785 $cm^{-1}$. The areas of each band has been weighted respect to the total amide band area which they belongs to (i.e. 1640 $cm^{-1}$ band has been weighted with respect to the total Am–I band area). (A colour version of this figure can be viewed online.)

differences in MV height values ($median_{mvG}$ = 19 nm; $median_{mvA}$ = 22 nm; P = 0.17). Within each group, the distribution of size values detected was not negatively correlated to the height, as shown in Fig. 2d (left; $r_{mvG}$ = 0.8808 and $r_{mvA}$ = 0.4039; P < 0.001). However, AFM experiments were performed in air, thus a not specific flattening of MVs caused by vesicle collapsing might have influenced these measurements. In principle differences in MV elastic properties, potentially related to diverse membrane components, might lead to a variable collapsing of MVs when measured in air.

Since AFM measurements are affected by the reduced size of the analyzed samples, and might not reflect the entire MVs population, we decided to use nanoparticle tracking analysis (NTA) to perform bulk analysis of vesicles in aqueous suspension. NTA tracks single particle Brownian motion within a dark field microscope, derives mean square vesicles velocity and translates them into size distribution [35]. NTA revealed a more complex pattern of size

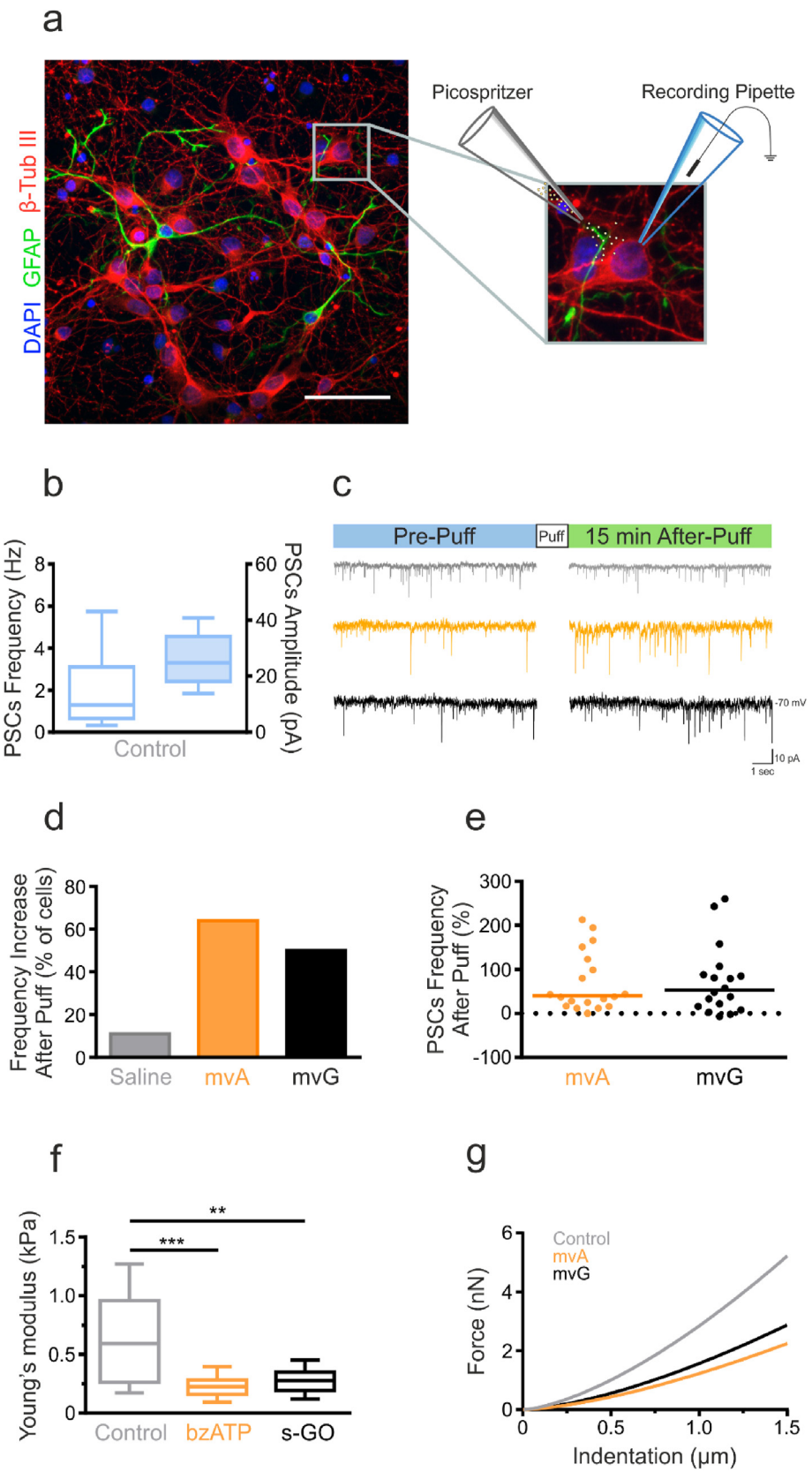


**Fig. 4. MVs released by astrocytes affect cortical neuron post-synaptic activity and mechanical properties.** Potentiation of synaptic activity upon local applications of MVs in cortical neurons. a) Confocal micrograph visualizing cortical primary cultures at 8 days *in vitro*; anti-class III β-tubulin is used to visualize neurons (in red), anti-GFAP for astrocytes (in green) and DAPI (in blue) to visualize neurons. Scale bar 50 μm. On the right, a representation of the experimental setting for the simultaneous MVs pressure-release (*puff*) and the cell patch-clamp recording from cultured neurons. b) Box plot summarizes the PSCs frequency and amplitude values in control cortical neurons. c) Top: diagram of the experimental protocol. Bottom: representative current tracings of the spontaneous synaptic activity detected prior and after puff applications of control saline (in light grey) or mvA

distribution (Fig. 2e): in the case of mvA we observed three subpopulations of vesicles at 115 nm, 235 nm and 400 nm respectively while in the case of mvG we found two partially overlapping peaks at 135 nm and 168 nm, plus two distinct peaks at 275 nm and 385 nm (Fig. 2e). The diameter analysis revealed a slight, but not significant, difference between the two populations with the diameter of mvG smaller and less distributed, compared to those of mvA ($median_{mvA}$ = 235.4 nm; $median_{mvG}$ = 183.6 nm) (Fig. 2f). These results convincingly suggested a comparable size distribution in both MV populations and subpopulations. However, we detected a significant difference in the number of vesicles released within the same time window (Fig. 2e) to indicate that cultures treated with s-GO produced more MVs when compared to cultures stimulated with bzATP (mvA = $3.32 \times 10^8$ vesicle/mL; mvG = $8.19 \times 10^8$ vesicles/mL), consistently with our results obtained by MV release analysis and immunoblot (but see also Visnovitz et al., 2019 [36]). Therefore, even though the overall size of the MV population produced did not change, s-GO was more efficient in generating MVs from astrocytes.

In order to analyze the macromolecular composition of MVs we took advantage of two complementary techniques: FTIR-ATR and UVRR spectroscopy. For these measurements, MVs were isolated by differential centrifugation as described before (see Material and Methods). To avoid any spurious effect due to the absorption of phosphate groups from the buffer, we washed and re-suspended the MVs pellet with a NaCl solution (150 mM). The infrared (IR) absorbance spectra (Fig. 3a) revealed a clear contribution of the CH and the phosphate bands linked to DNA in both samples, mvA and mvG, as well as the lipid signatures at 2900-3000 $cm^{-1}$, arisen from the $CH_2$ and $CH_3$ stretching mode. The amide I and amide II bands between 1500 and 1785 $cm^{-1}$, the two major protein bands in the IR spectrum, show more pronounced differences between the two populations of vesicles. The amide I band, which is primarily related to the C═O stretching in the peptide bonds and modulated by the proteins' secondary structures, displayed similar shapes for mvA and mvG. The amide II band, primarily due to C–N stretching and N–H in plane bending vibrations, also reflecting the protein secondary structure, was instead clearly depleted in the case of mvG. To gain insights into the contribution of different protein secondary structures in the two families of vesicles, we analyzed the second derivative of the IR signal in the amide I + amide II region (Fig. 3b) and used the position of the minima to guide a multicomponent gaussian fit of the bands in the region 1500 and 1785 $cm^{-1}$. The % area contributions obtained by the fit are reported in Fig. 3c. The low-energy flank of amide I of both mvA and mvG is characterized by the presence of the 1610-1613 $cm^{-1}$ vibrational peak which could be addressed to a mixed contribution arisen from β-sheets and side-chains vibrations. Additionally, the band at 1660 $cm^{-1}$ might also be derived from the presence of RNA in the vesicles [37]. Noteworthy, the relative populations of the peaks at approximately 1645 $cm^{-1}$, 1660 $cm^{-1}$ and 1678 $cm^{-1}$ are inverted between mvA and mvG. According to the literature [37], the 1645 $cm^{-1}$ peak (depleted in mvG) might be assigned to random structures and/or helices; the 1660 $cm^{-1}$ peak (depleted in mvA) to flexible helices (as $3_{10}$ helices); the 1678 $cm^{-1}$ peak (depleted in mvG) to beta structures such as b-turns. The bands at 1632 $cm^{-1}$ and at 1693 $cm^{-1}$, both present in the mvG only, are ascribed to antiparallel beta sheet, as found in aggregates in tissues [37,38]. We can conclude that mvGs contain proteins with perturbed secondary structure, characterized by beta structure-based aggregates and flexible helices. No significant variations in the DNA phosphate bands were measured as well as the nature or localization of the DNA signature detected. It is interesting to note that in previous measures the DNA delivered by EVs has been reported to be stocked either inside the vesicles or on their surface [39].

UV Resonant Raman (UVRR) measurements taken using an excitation wavelength of 244 nm (see experimental section and supplementary Fig. S4) confirmed the amide I signal depression in mvG absorption spectrum. Due to an overlap between the UVRR s-GO band, we could not confirm or discard the presence of s-GO inside the vesicles. Thus, we cannot exclude that the changes in protein native structure might be due to s-GO altering the MV micro(nano)environment or the possibility of a general interference with the measurements. The absence of astrocytes cytotoxicity, even upon prolonged exposure to s-GO, together with the functional measures of increased MVs release kinetic obtained by live imaging, are against a mere alteration in protein integrity due to denaturation of membrane proteins in the presence of s-GO [40–42]. FTIR-ATR spectroscopy is a powerful tool to assess the disordered character of proteins, and the absence of a well-defined structure under native conditions is a peculiar property of intrinsically disordered proteins (IDP) [43,44]. In this framework, IDPs might represent a specific signal vehiculated by mvG and the lack of protein structural constraints could facilitate several, yet unknown, biological processes [44].

It is clearly visible that mvA and mvG vesicles have a different secondary structure: the former is mainly characterized by an intense peak at 1645 $cm^{-1}$ (43%), which can be assigned to random structures/a-helix structure, and at 1678 $cm^{-1}$ (22%) usually assigned to b-turn and at 1613 $cm^{-1}$ (27%), which could be assigned to side chains vibrations; in contrast, mvG are mainly characterized by anti-parallel b-sheets structure (1632 (15%) and 1693 $cm^{-1}$ (3%) bands) with a strong contribution of flexible 3–10 helix (1661 $cm^{-1}$ peak (34%)) and of side chain band at 1610 $cm^{-1}$ (37%).

Finally, we set up a functional test to compare the impact of mvG delivery with that of mvA on synaptic activity, when neuronal networks are acutely and transiently exposed to MVs. To this aim, we isolated cortical neurons and glial cells from postnatal rat cortices and cultured them for 10 days. Fig. 4a shows confocal high magnification microscopy images of cortical cultures where neurons were visualized by labeling class III β-tubulin (in red), a microtubule component expressed exclusively by neurons, while astrocytes were visualized by GFAP labeling (in green) [45]. We patch-clamped visually identified cortical neurons (in voltage clamp configuration, holding potential − 70 mV), while a second pipette for the local delivery of saline solution was positioned at a distance of 200 μm (under microscopy visual control) from the recorded cell (sketched in Fig. 4a, right). We estimated that, at this distance, the application of a brief (500 ms) pulse of pressure should result in a local (i.e. on the recorded neuron) and transient delivery of standard saline solution alone or containing mvG or mvA (re-suspended in saline). A typical feature of these cultures is the prominent expression of spontaneous synaptic activity, represented by heterogeneous postsynaptic currents (PSCs) of variable frequency and amplitude (box plots in Fig. 4b). Baseline PSCs were recorded before (10 min) and after (15 min) the local saline, mvG or

(in orange) or mvG (in black). d) Bar plots of pooled data summarize the % of cells displaying PSCs frequency increase upon delivery of pressure ejected saline (light grey), mvA (orange) and mvG (black). Note that in control (saline) the large majority (88%) of neurons did not increase their basal activity. e) The plot summarizes the distribution of the % of increase in PCSs frequency detected within the three groups. f) Elastic moduli of cortical neurons, grown on glass, and exposed to MVs isolated from glial cells previously treated with bzATP (orange) or s-GO flakes (black). Neurons treated with mvA and mvG are significantly less rigid if compared with control ($P_{mvA} < 0.001$; $P_{mvG} < 0.01$). Thick horizontal bars in the box plots indicate median value; boxed area extends from the 25th to 75th percentiles, whiskers from 5th to the 95th percentiles. Significance: **P < 0.01 ***P < 0.001, Kruskal-Wallis test, Dunn's post hoc test) **g.** Indentation curves of cortical neurons previously treated with mvA or mvG. (A colour version of this figure can be viewed online.)

mvA ejection. Fig. 4c shows representative current tracings where standard saline was pressure ejected (light grey, top), or where mvA solution (orange, middle) and mvG (black, bottom) were administered.

Since spontaneous fluctuations in PSCs frequency ≤15% of baseline values were frequently detected, we took this as the threshold value to estimate changes when comparing PSCs before and after pressure ejections of saline. In the large majority (88%, n = 16/18 neurons; histograms in Fig. 4d) of neurons exposed to saline solution alone, spontaneous PSCs frequency did not change. On the contrary, within 5–8 min from the acute mvA and mvG ejections, PSCs frequency was stably increased in 64% (n = 16/25 neurons, mvA) and 54% (n = 13/24 neurons, mvG; summarized in the histograms of Fig. 4d) of recorded neurons. Fig. 4e shows the increases in PSCs frequency in individual experiments and highlights the variability of such changes when administering MVs, with increased frequencies ranging from 25% to 200%. Since we could not experimentally control the amount of MVs collected by primary astrocytes and delivered by pressure ejection, neurons were exposed to different amounts of MVs and this can in part explain the detected variability. PSCs frequency increases due to MVs exposures were not reversible upon 20 min washout. From such functional investigation, glial-signaling generated by ATP or s-GO affected similarly neuronal synapses upon transient, direct exposure.

To our knowledge, this is the first time that the functional effects of MVs generated by astrocytes on synaptic activity upon local delivery have been electrophysiologically documented. Neuroglia extracellular vesicles have been described to provide support on synaptic activity, with the majority of studies focused on microglia and inflammation, apparently regulating neural transmission at the pre-synaptic level [5,46–48]. Astrocytic MVs have been proposed to exert neuroprotective effects in neuropathology and in physiology, however the role of astrocytes or of discrete astrocyte populations in delivering different messages *via* MV release has yet to be elucidated [49,50].

After assessment of the ability of MVs released by glial cells to affect cortical neuron physiology within min after their interaction with the targeted neuron, we asked if the presumed fusion of vesicles with neuronal plasma membrane could also affect their mechanical properties. To investigate this aspect, we delivered MVs obtained from glial cultures previously treated with bzATP or s-GO to cortical neurons by re-suspending the isolated MVs in 100 μL of neuronal culture medium and adding them to neuronal cultures. 24 h after the exposure, force spectroscopy measurement on treated neuronal cultures were performed with AFM by positioning the tipless cantilever with a borosilicate glass bead previously glued on it [51], at the center of randomly chosen neurons. As showed by the boxplot in Fig. 4f, the exposure to mvA caused a significant softening of neuronal soma, when compared to controls ($median_{mvA} = 0.22$ kPa, $median_{control} = 0.59$ kPa; $P_{mvA} < 0.001$). A similar result was observed also in the case of mvG exposure even if the effect exerted on neuronal stiffness is less pronounced than that induced by mvA ($median_{mvG} = 0.28$ kPa, $median_{control} = 0.59$ kPa; $P_{mvG} < 0.01$). The reported effect of mvA and mvG on neuronal cell mechanical properties is presumably a consequence of vesicular fusion with the cellular plasma membrane, which may affect its lipid composition. Since the mechanical properties of a cell are mostly defined by plasma membrane features and the ones of the underlying cytoskeleton, a change in neuronal plasma membrane lipid composition can partially justify the observed reduction in mvA and mvG-treated neurons stiffness [52]. In particular, glia-derived MVs are able to transport the enzyme Acid sphingomyelinase (A-SMase) involved in the metabolism of sphingomyelin (SM), a precursor of the phospholipid sphingosine (sph). Sph and its metabolites have been already reported to play a fundamental role in facilitating synaptic vesicles release by changing the membrane composition at pre-synaptic level [48,53]. This intrinsic capacity of MVs to participate in membrane lipid metabolism may therefore modulate the contribution of plasma membrane to neuronal rigidity. In this context, the slight difference of stiffness values reported among mvA and mvG-treated neurons, although not statistically significant ($P_{mvA\text{-}mvG} > 0.05$) should not be underestimated [54,55]. It is tempting to speculate that this difference can be explained by the presence of specific proteins in the vesicles, that are unstable in mvG. Based on our measures, we cannot exclude the presence of residual s-GO flakes either inside or on the vesicle surface. It is known that GO is reportedly able to interact with the hydrophobic region of biological and model lipid membranes, even though the nature of the interaction is strictly dependent to its size and degree of surface oxygenation [56,57]. Assuming that the GO nanosheets, once added to the culture medium, can adsorb on plasma membrane or pierce it and being embedded in the lipid bilayer, there is a concrete possibility that MVs, which directly originate from plasma membrane, can include those flakes in their structure [30]. The horizontal transfer of s-GO from glial cells to cortical neurons, mediated by MVs, may therefore affect plasma membrane rigidity of targeted neurons. Regardless of this, we can exclude a direct effect of s-GO in synaptic transmission, reported to be transient and reversible upon acute exposure, in view of the persistent modulation of synaptic current frequency brought about by MVs [19,20].

## 4. Conclusion

Astrocyte-derived MVs may play significant roles in propagating signaling molecules, in CNS physiology and disease. Despite the increasing knowledge on extracellular vesicles (in particular exosomes) ability to promote inflammation or contribute in spreading of pathogenic proteins in neurodegenerative disorders (from Amyotrophic Lateral Sclerosis to Alzheimer disease [58,59]) little is currently known on their properties (mechanical, biochemical, lipid membrane composition, cargo nature etc.), in particular when focusing on the smaller class of such natural vectors, the MVs. Nevertheless, MVs emerge as key players in neuronal and synaptic physiology, able to influence neurotransmission, or to support neurons [48,60–62]. In our study, we report the ability of artificially generating MVs by s-GO transient exposure. MVs generated by s-GO were apparently characterized by altered protein content when compared to the ATP-driven ones. Intriguingly, the tuning of synaptic activity by mvG or mvA was similar, supposedly being related to features diverse from MV protein content. The ability of s-GO to interfere with exo-endocytotic membrane dynamics is not surprising, indeed we have described the ability of s-GO nanoflakes to interfere with presynaptic vesicle release *in vitro* and *in vivo* [19,20]. In the current work, we describe the direct interference of MVs with synaptic activity, presumably due to MVs fusion with the target neuron plasma membrane. Such an approach holds the potential to open new opportunities in engineering MVs for synaptic targeting. In this framework, it is tempting to speculate that s-GO interactions with the cell membrane mimic extracellular mechanical signaling at the nanoscale sufficient to enable the release of MVs, thus representing unconventional tools to exploit the physics governing vesicle release. We feel pertinent here to consider the fact, that the enormous potentiality of graphene-based materials in nanomedicine has already promoted the development of new generation-nanocarriers for either gene or drug delivery [17,63]. In this framework, we may speculate on future developments where engineered cells are mechanically induced to release MVs, carrying GO nanoflakes properly functionalized to deliver genes or drugs of interest and thus representing either the trigger and the cargo.

## Author contributions

M.M. performed cell biology, electrophysiology, and immunofluorescence experiments and analysis; M.M. and P.P. designed and performed AFM experiments; M.P. performed IR and UVRR experiments and analysis. CM and GDM performed biology and WB experiments; N.L. and K.K. contributed to the synthesis and characterization of thin graphene oxide of biological grade. BB performed SEM micrographs of GO. L.B. and L.C. conceived the study; L.B. conceived the experimental design and contributed to the analysis of data; L.B. wrote the manuscript.

## CRediT authorship contribution statement

**Mattia Musto:** Formal analysis, performed cell biology, electrophysiology, and immunofluorescence experiments and analysis, designed and performed AFM experiments. **Pietro Parisse:** designed and performed AFM experiments. **Maria Pachetti:** Formal analysis, performed IR and UVRR experiments and analysis. **Christian Memo:** performed biology and WB experiments. **Giuseppe Di Mauro:** performed biology and WB experiments. **Belen Ballesteros:** performed SEM micrographs of GO. **Neus Lozano:** contributed to the synthesis and characterization of thin graphene oxide of biological grade. **Kostas Kostarelos:** contributed to the synthesis and characterization of thin graphene oxide of biological grade. **Loredana Casalis:** conceived the study. **Laura Ballerini:** Writing - original draft, conceived the experimental design and contributed to the analysis of data, wrote the manuscript.

## Declaration of competing interest

The authors declare no competing financial interest.

## Acknowledgment

We acknowledge the financial support from the European Union's Horizon 2020 Research and Innovation Programme under grant agreement no. 785219 and no. 881603 Graphene Flagship. MM, PP and LC acknowledge CERIC-ERIC proposal grant n. 20167063 for the IR measurements, performed at the SISSI-Bio beamline of Elettra Sincrotrone Trieste. PP and LC acknowledge also the European Regional Development Fund and Interreg V-A Italia-Austria 2014–2020 project EXOTHERA (ITAT1036).

## Appendix A. Supplementary data

Supplementary data to this article can be found online at https://doi.org/10.1016/j.carbon.2021.01.142.

## References

[1] D.A. Shifrin, M.D. Beckler, R.J. Coffey, M.J. Tyska, Extracellular vesicles: communication, coercion, and conditioning, Mol. Biol. Cell 24 (2013) 1253–1259, https://doi.org/10.1091/mbc.e12-08-0572.
[2] Y.J. Yoon, O.Y. Kim, Y.S. Gho, Extracellular vesicles as emerging intercellular communicasomes, BMB Rep 47 (2014) 531–539, https://doi.org/10.5483/BMBREP.2014.47.10.164.
[3] V. Zappulli, K.P. Friis, Z. Fitzpatrick, C.A. Maguire, X.O. Breakefield, Extracellular vesicles and intercellular communication within the nervous system, J. Clin. Invest. 126 (2016) 1198–1207, https://doi.org/10.1172/JCI81134.
[4] C.P.-K. Lai, X.O. Breakefield, Role of exosomes/microvesicles in the nervous system and use in emerging therapies, Front. Physiol. 3 (2012) 228, https://doi.org/10.3389/fphys.2012.00228.
[5] V. Budnik, C. Ruiz-Cañada, F. Wendler, Extracellular vesicles round off communication in the nervous system, Nat. Rev. Neurosci. 17 (2016) 160–172, https://doi.org/10.1038/nrn.2015.29.
[6] A. Grimaldi, C. Serpe, G. Chece, V. Nigro, A. Sarra, B. Ruzicka, M. Relucenti, G. Familiari, G. Ruocco, G.R. Pascucci, F. Guerrieri, C. Limatola, M. Catalano, Microglia-derived microvesicles affect microglia phenotype in glioma, Front. Cell. Neurosci. 13 (2019) 41, https://doi.org/10.3389/fncel.2019.00041.
[7] E. Cocucci, J. Meldolesi, Ectosomes and exosomes: shedding the confusion between extracellular vesicles, Trends Cell Biol. 25 (2015) 364–372, https://doi.org/10.1016/j.tcb.2015.01.004.
[8] G. Raposo, W. Stoorvogel, Extracellular vesicles: exosomes, microvesicles, and friends, J. Cell Biol. 200 (2013) 373–383, https://doi.org/10.1083/jcb.201211138.
[9] S.L.N. Maas, X.O. Breakefield, A.M. Weaver, Extracellular vesicles: unique intercellular delivery vehicles, Trends Cell Biol. 27 (2017) 172–188, https://doi.org/10.1016/j.tcb.2016.11.003.
[10] C. Frühbeis, D. Fröhlich, E.-M. Krämer-Albers, Emerging roles of exosomes in neuron–glia communication, Front. Physiol. 3 (2012) 119, https://doi.org/10.3389/fphys.2012.00119.
[11] G. Lachenal, K. Pernet-Gallay, M. Chivet, F.J. Hemming, A. Belly, G. Bodon, B. Blot, G. Haase, Y. Goldberg, R. Sadoul, Release of exosomes from differentiated neurons and its regulation by synaptic glutamatergic activity, Mol. Cell. Neurosci. 46 (2011) 409–418, https://doi.org/10.1016/j.mcn.2010.11.004.
[12] K.E. van der Vos, L. Balaj, J. Skog, X.O. Breakefield, Brain tumor microvesicles: insights into intercellular communication in the nervous system, Cell. Mol. Neurobiol. 31 (2011) 949–959, https://doi.org/10.1007/s10571-011-9697-y.
[13] D. Ha, N. Yang, V. Nadithe, Exosomes as therapeutic drug carriers and delivery vehicles across biological membranes: current perspectives and future challenges, Acta Pharm. Sin. B. 6 (2016) 287–296, https://doi.org/10.1016/J.APSB.2016.02.001.
[14] C. Verderio, L. Muzio, E. Turola, A. Bergami, L. Novellino, F. Ruffini, L. Riganti, I. Corradini, M. Francolini, L. Garzetti, C. Maiorino, F. Servida, A. Vercelli, M. Rocca, D.D. Libera, V. Martinelli, G. Comi, G. Martino, M. Matteoli, R. Furlan, Myeloid microvesicles are a marker and therapeutic target for neuroinflammation, Ann. Neurol. 72 (2012) 610–624, https://doi.org/10.1002/ana.23627.
[15] S. EL Andaloussi, I. Mäger, X.O. Breakefield, M.J.A. Wood, Extracellular vesicles: biology and emerging therapeutic opportunities, Nat. Rev. Drug Discov. 12 (2013) 347–357, https://doi.org/10.1038/nrd3978.
[16] K.P. Loh, Q. Bao, G. Eda, M. Chhowalla, Graphene oxide as a chemically tunable platform for optical applications, Nat. Chem. 2 (2010) 1015–1024, https://doi.org/10.1038/nchem.907.
[17] G. Reina, J.M. González-Domínguez, A. Criado, E. Vázquez, A. Bianco, M. Prato, Promises, facts and challenges for graphene in biomedical applications, Chem. Soc. Rev. 46 (2017) 4400–4416, https://doi.org/10.1039/c7cs00363c.
[18] M. Baldrighi, M. Trusel, R. Tonini, S. Giordani, Carbon nanomaterials interfacing with neurons: an in vivo perspective, Front. Neurosci. 10 (2016) 250, https://doi.org/10.3389/fnins.2016.00250.
[19] R. Rauti, N. Lozano, V. León, D. Scaini, M. Musto, I. Rago, F.P. Ulloa Severino, A. Fabbro, L. Casalis, E. Vázquez, K. Kostarelos, M. Prato, L. Ballerini, Graphene oxide nanosheets reshape synaptic function in cultured brain networks, ACS Nano 10 (2016) 4459–4471, https://doi.org/10.1021/acsnano.6b00130.
[20] R. Rauti, M. Medelin, L. Newman, S. Vranic, G. Reina, A. Bianco, M. Prato, K. Kostarelos, L. Ballerini, Graphene oxide flakes tune excitatory neurotransmission in vivo by targeting hippocampal synapses, Nano Lett. 19 (2019) 2858–2870, https://doi.org/10.1021/acs.nanolett.8b04903.
[21] Z. Song, Y. Wang, Z. Xu, Mechanical responses of the bio-nano interface: a molecular dynamics study of graphene-coated lipid membrane, Theor. Appl. Mech. Lett. 5 (2015) 231–235, https://doi.org/10.1016/j.taml.2015.11.003.
[22] R.J. Rodrigues, A.R. Tomé, R.A. Cunha, ATP as a multi-target danger signal in the brain, Front. Neurosci. 9 (2015) 148, https://doi.org/10.3389/fnins.2015.00148.
[23] F. Calegari, S. Coco, E. Taverna, M. Bassetti, C. Verderio, N. Corradi, M. Matteoli, P. Rosa, A regulated secretory pathway in cultured hippocampal astrocytes, J. Biol. Chem. 274 (1999) 22539–22547.
[24] P. Hermanowicz, M. Sarna, K. Burda, H. Gabryś, AtomicJ: an open source software for analysis of force curves, Rev. Sci. Instrum. 85 (2014), 063703, https://doi.org/10.1063/1.4881683.
[25] F. D'Amico, M. Saito, F. Bencivenga, M. Marsi, A. Gessini, G. Camisasca, E. Principi, R. Cucini, S. Di Fonzo, A. Battistoni, E. Giangrisostomi, C. Masciovecchio, UV resonant Raman scattering facility at Elettra, Nucl. Instruments Methods Phys. Res. Sect. A Accel. Spectrometers, Detect. Assoc. Equip. 703 (2013) 33–37, https://doi.org/10.1016/J.NIMA.2012.11.037.
[26] A. Bignami, L.F. Eng, D. Dahl, C.T. Uyeda, Localization of the glial fibrillary acidic protein in astrocytes by immunofluorescence, Brain Res. 43 (1972) 429–435, https://doi.org/10.1016/0006-8993(72)90398-8.
[27] M. Musto, R. Rauti, A.F. Rodrigues, E. Bonechi, C. Ballerini, K. Kostarelos, L. Ballerini, 3D organotypic spinal cultures: exploring neuron and neuroglia responses upon prolonged exposure to graphene oxide, Front. Syst. Neurosci. 13 (2019) 1, https://doi.org/10.3389/fnsys.2019.00001.
[28] M. Bramini, G. Alberini, E. Colombo, M. Chiacchiaretta, M.L. DiFrancesco, J.F. Maya-Vetencourt, L. Maragliano, F. Benfenati, F. Cesca, Interfacing graphene-based materials with neural cells, Front. Syst. Neurosci. 12 (2018) 12, https://doi.org/10.3389/fnsys.2018.00012.
[29] A.B. Seabra, A.J. Paula, R. De Lima, O.L. Alves, N. Durán, Nanotoxicity of graphene and graphene oxide, Chem. Res. Toxicol. 27 (2014) 159–168, https://doi.org/10.1021/tx400385x.
[30] F. Bianco, C. Perrotta, L. Novellino, M. Francolini, L. Riganti, E. Menna, L. Saglietti, E.H. Schuchman, R. Furlan, E. Clementi, M. Matteoli, C. Verderio, Acid sphingomyelinase activity triggers microparticle release from glial cells, EMBO J. 28 (2009) 1043–1054, https://doi.org/10.1038/emboj.2009.45.

[31] E. Amaral, S. Guatimosim, C. Guatimosim, Using the fluorescent styryl dye FM1-43 to visualize synaptic vesicles exocytosis and endocytosis in motor nerve terminals, Methods Mol. Biol. (2011) 137–148, https://doi.org/10.1007/978-1-60761-950-5_8.
[32] W.J. Betz, F. Mao, C.B. Smith, Imaging exocytosis and endocytosis, Curr. Opin. Neurobiol. 6 (1996) 365–371, https://doi.org/10.1016/S0959-4388(96)80121-8.
[33] A. Brumback, J.L. Lieber, J.K. Angleson, W.J. Betz, Using FM1-43 to study neuropeptide granule dynamics and exocytosis, Methods 33 (2004) 287–294, https://doi.org/10.1016/j.ymeth.2004.01.002.
[34] Y. Yoshioka, Y. Konishi, N. Kosaka, T. Katsuda, T. Kato, T. Ochiya, Comparative marker analysis of extracellular vesicles in different human cancer types, J. Extracell. Vesicles 2 (2013), https://doi.org/10.3402/jev.v2i0.20424.
[35] R.A. Dragovic, C. Gardiner, A.S. Brooks, D.S. Tannetta, D.J.P. Ferguson, P. Hole, B. Carr, C.W.G. Redman, A.L. Harris, P.J. Dobson, P. Harrison, I.L. Sargent, Sizing and phenotyping of cellular vesicles using Nanoparticle Tracking Analysis, Nanomedicine 7 (2011) 780–788, https://doi.org/10.1016/j.nano.2011.04.003.
[36] T. Visnovitz, X. Osteikoetxea, B.W. Sódar, J. Mihály, P. Lőrincz, K.V. Vukman, E.Á. Tóth, A. Koncz, I. Székács, R. Horváth, Z. Varga, E.I. Buzás, An improved 96 well plate format lipid quantification assay for standardisation of experiments with extracellular vesicles, J. Extracell. Vesicles 8 (2019), 1565263, https://doi.org/10.1080/20013078.2019.1565263.
[37] J. Mihály, R. Deák, I.C. Szigyártó, A. Bóta, T. Beke-Somfai, Z. Varga, Characterization of extracellular vesicles by IR spectroscopy: fast and simple classification based on amide and C H stretching vibrations, Biochim. Biophys. Acta Biomembr. 1859 (2017) 459–466, https://doi.org/10.1016/j.bbamem.2016.12.005.
[38] D. Ami, F. Lavatelli, P. Rognoni, G. Palladini, S. Raimondi, S. Giorgetti, L. Monti, S.M. Doglia, A. Natalello, G. Merlini, In situ characterization of protein aggregates in human tissues affected by light chain amyloidosis: a FTIR microspectroscopy study, Sci. Rep. 6 (2016) 29096, https://doi.org/10.1038/srep29096.
[39] A. Németh, N. Orgovan, B.W. Sódar, X. Osteikoetxea, K. Pálóczi, K. Szabó-Taylor, K.V. Vukman, Á. Kittel, L. Turiák, Z. Wiener, S. Tóth, L. Drahos, K. Vékey, R. Horvath, E.I. Buzás, Antibiotic-induced release of small extracellular vesicles (exosomes) with surface-associated DNA, Sci. Rep. 7 (2017) 1–16, https://doi.org/10.1038/s41598-017-08392-1.
[40] M.Y. Sherman, A.L. Goldberg, Cellular defenses against unfolded proteins: a cell biologist thinks about neurodegenerative diseases, Neuron 29 (2001) 15–32, https://doi.org/10.1016/s0896-6273(01)00177-5.
[41] R. V Rao, D.E. Bredesen, Misfolded proteins, endoplasmic reticulum stress and neurodegeneration, Curr. Opin. Cell Biol. 16 (2004) 653–662, https://doi.org/10.1016/j.ceb.2004.09.012.
[42] D.J. Selkoe, Folding proteins in fatal ways, Nature 426 (2003) 900–904, https://doi.org/10.1038/nature02264.
[43] A. Natalello, D. Ami, S.M. Doglia, Fourier transform infrared spectroscopy of intrinsically disordered proteins: measurement procedures and data analyses, Methods Mol. Biol. (2012) 229–244, https://doi.org/10.1007/978-1-61779-927-3_16.
[44] C.J. Oldfield, A.K. Dunker, Intrinsically disordered proteins and intrinsically disordered protein regions, Annu. Rev. Biochem. 83 (2014) 553–584, https://doi.org/10.1146/annurev-biochem-072711-164947.
[45] D. V Caccamo, M.M. Herman, A. Frankfurter, C.D. Katsetos, V.P. Collins, L.J. Rubinstein, An immunohistochemical study of neuropeptides and neuronal cytoskeletal proteins in the neuroepithelial component of a spontaneous murine ovarian teratoma. Primitive neuroepithelium displays immunoreactivity for neuropeptides and neuron-associated beta-tu, Am. J. Pathol. 135 (1989) 801–813.
[46] R.C. Paolicelli, G. Bergamini, L. Rajendran, Cell-to-cell communication by extracellular vesicles: focus on microglia, Neuroscience 405 (2019) 148–157, https://doi.org/10.1016/j.neuroscience.2018.04.003.
[47] Y. Yang, A. Boza-Serrano, C.J.R. Dunning, B.H. Clausen, K.L. Lambertsen, T. Deierborg, Inflammation leads to distinct populations of extracellular vesicles from microglia, J. Neuroinflammation 15 (2018) 168, https://doi.org/10.1186/s12974-018-1204-7.
[48] F. Antonucci, E. Turola, L. Riganti, M. Caleo, M. Gabrielli, C. Perrotta, L. Novellino, E. Clementi, P. Giussani, P. Viani, M. Matteoli, C. Verderio, Microvesicles released from microglia stimulate synaptic activity via enhanced sphingolipid metabolism, EMBO J. 31 (2012) 1231–1240, https://doi.org/10.1038/emboj.2011.489.
[49] M.J. Carson, J.C. Thrash, B. Walter, The cellular response in neuroinflammation: the role of leukocytes, microglia and astrocytes in neuronal death and survival, Clin. Neurosci. Res. 6 (2006) 237–245, https://doi.org/10.1016/j.cnr.2006.09.004.
[50] M.M. Holm, J. Kaiser, M.E. Schwab, Extracellular vesicles: multimodal envoys in neural maintenance and repair, Trends Neurosci. 41 (2018) 360–372, https://doi.org/10.1016/j.tins.2018.03.006.
[51] T. Gerecsei, I. Erdődi, B. Peter, C. Hős, S. Kurunczi, I. Derényi, B. Szabó, R. Horvath, Adhesion force measurements on functionalized microbeads: an in-depth comparison of computer controlled micropipette and fluidic force microscopy, J. Colloid Interface Sci. 555 (2019) 245–253, https://doi.org/10.1016/j.jcis.2019.07.102.
[52] S. Kasas, X. Wang, H. Hirling, R. Marsault, B. Huni, A. Yersin, R. Regazzi, G. Grenningloh, B. Riederer, L. Forrò, G. Dietler, S. Catsicas, Superficial and deep changes of cellular mechanical properties following cytoskeleton disassembly, Cell Motil Cytoskeleton 62 (2005) 124–132, https://doi.org/10.1002/cm.20086.
[53] E. Norman, R.G. Cutler, R. Flannery, Y. Wang, M.P. Mattson, Plasma membrane sphingomyelin hydrolysis increases hippocampal neuron excitability by sphingosine-1-phosphate mediated mechanisms, J. Neurochem. 114 (2010) 430–439, https://doi.org/10.1111/j.1471-4159.2010.06779.x.
[54] V. Amrhein, S. Greenland, B. McShane, Scientists rise up against statistical significance, Nature 567 (2019) 305–307, https://doi.org/10.1038/d41586-019-00857-9.
[55] It's time to talk about ditching statistical significance, Nature 567 (2019), https://doi.org/10.1038/d41586-019-00874-8, 283–283.
[56] R. Frost, S. Svedhem, C. Langhammer, B. Kasemo, Graphene oxide and lipid membranes: size-dependent interactions, Langmuir 32 (2016) 2708–2717, https://doi.org/10.1021/acs.langmuir.5b03239.
[57] N. Li, Q. Zhang, S. Gao, Q. Song, R. Huang, L. Wang, L. Liu, J. Dai, M. Tang, G. Cheng, Three-dimensional graphene foam as a biocompatible and conductive scaffold for neural stem cells, Sci. Rep. 3 (2013) 1604, https://doi.org/10.1038/srep01604.
[58] M. Basso, S. Pozzi, M. Tortarolo, F. Fiordaliso, C. Bisighini, L. Pasetto, G. Spaltro, D. Lidonnici, F. Gensano, E. Battaglia, C. Bendotti, V. Bonetto, Mutant copper-zinc superoxide dismutase (SOD1) induces protein secretion pathway alterations and exosome release in astrocytes: implications for disease spreading and motor neuron pathology in amyotrophic lateral sclerosis, J. Biol. Chem. 288 (2013) 15699–15711, https://doi.org/10.1074/jbc.M112.425066.
[59] G. Wang, M. Dinkins, Q. He, G. Zhu, C. Poirier, A. Campbell, M. Mayer-Proschel, E. Bieberich, Astrocytes secrete exosomes enriched with proapoptotic ceramide and prostate apoptosis response 4 (PAR-4), J. Biol. Chem. 287 (2012) 21384–21395, https://doi.org/10.1074/jbc.M112.340513.
[60] R.-D. Gosselin, P. Meylan, I. Decosterd, Extracellular microvesicles from astrocytes contain functional glutamate transporters: regulation by protein kinase C and cell activation, Front. Cell. Neurosci. 7 (2013) 251, https://doi.org/10.3389/fncel.2013.00251.
[61] A.R. Taylor, M.B. Robinson, D.J. Gifondorwa, M. Tytell, C.E. Milligan, Regulation of heat shock protein 70 release in astrocytes: role of signaling kinases, Dev. Neurobiol. 67 (2007) 1815–1829, https://doi.org/10.1002/dneu.20559.
[62] S. Wang, F. Cesca, G. Loers, M. Schweizer, F. Buck, F. Benfenati, M. Schachner, R. Kleene, Synapsin I is an oligomannose-carrying glycoprotein, acts as an oligomannose-binding lectin, and promotes neurite outgrowth and neuronal survival when released via glia-derived exosomes, J. Neurosci. 31 (2011) 7275–7290, https://doi.org/10.1523/JNEUROSCI.6476-10.2011.
[63] H. Zhao, R. Ding, X. Zhao, Y. Li, L. Qu, H. Pei, L. Yildirimer, Z. Wu, W. Zhang, Graphene-based nanomaterials for drug and/or gene delivery, bioimaging, and tissue engineering, Drug Discov. Today 22 (2017) 1302–1317, https://doi.org/10.1016/j.drudis.2017.04.002.

# Update


## Carbon

**Volume 178, Issue , 30 June 2021, Page 824**

**DOI: https://doi.org/10.1016/j.carbon.2021.04.026**

Carbon 178 (2021) 824

Contents lists available at ScienceDirect

Carbon

journal homepage: www.elsevier.com/locate/carbon

Corrigendum

# Corrigendum to Shedding plasma membrane vesicles induced by graphene oxide nanoflakes in brain cultured astrocytes [CARBON 176 (2021) 458–469]

Mattia Musto [a], Pietro Parisse [b], Maria Pachetti [b], Christian Memo [a], Giuseppe Di Mauro [a], Belen Ballesteros [c], Neus Lozano [c], Kostas Kostarelos [c, d], Loredana Casalis [b, **], Laura Ballerini [a, *]

[a] International School for Advanced Studies (SISSA), 34136, Trieste, Italy
[b] ELETTRA Synchrotron Light Source, 34149, Basovizza, Italy
[c] Catalan Institute of Nanoscience and Nanotechnology (ICN2), Campus UAB, Bellaterra, 08193, Barcelona, Spain
[d] Nanomedicine Lab, National Graphene Institute and Faculty of Biology, Medicine & Health, The University of Manchester, Manchester, M13 9PT, United Kingdom

The authors regret that the printed version of the above article contained a number of errors. The correct and final version follows. The authors would like to apologise for any inconvenience caused.

The authors would like to make the following addition to the Acknowledgment section of the article:

The authors are grateful to Dr. Gesmi Milcovich for contributing to the recording and analyses in the AFM biomechanics measurements and related fruitful discussions.

DOI of original article: https://doi.org/10.1016/j.carbon.2021.01.142.
* Corresponding author.
** Corresponding author.
*E-mail addresses:* loredana.casalis@elettra.eu (L. Casalis), laura.ballerini@sissa.it, ballerin@sissa.it (L. Ballerini).

https://doi.org/10.1016/j.carbon.2021.04.026

# Conclusions

EVs have recently surge as an unconventional but crucial intercellular communication vectorised system among CNS cell types. Their dimension, in the order of the nanoscale, and their multicellular origin, makes their functional characterization, at the level of cell-specific EVs subpopulation, very hard to be performed in complex model systems. However, recent experiments uncovered the role of astrocytes as major EVs-producing cells in the context of CNS tissue. For this reason, in the first part of this work, we decide to initially explore the dynamics of EVs secretion from a simple *in vitro* model: dissociated glial cell culture from rat cerebral cortex, focusing on microvesicles (MVs), the larger subclass of EVs that originate from the outward budding of the plasma membrane. To this end, we used small graphene oxide (s-GO), a graphene derivate known for its ability to interfere with cell membrane dynamics at the nanoscale level, and bzATP, a semisynthetic danger signal with a great affinity for the $P_2X_7$ purinergic receptor, whose activation can boost MVs secretion.

To asses glial MVs ability to mediate neuron-glia crosstalk, we challenged cultured rat cortical neurons with isolated MVs using a picospritzer, acutely monitoring neuron electrical activity. Interestingly, using patch-clamp recordings, we detect an increase in postsynaptic currents frequency in MVs challenged neurons.

In order to further explore the EVs ability of modulate physiopathological events in a more complex system, we move to the organotypic spinal cord model of neuroinflammation. We focused, in particular, on the role of exosomes (the smaller class of extracellular vesicles) in modifying astrocytic signalling behaviour. First, we characterized astrocytic $Ca^{2+}$ signals dynamics upon different inflammatory treats. Particularly, we found that inflammation induced by LPS or by a cytokines cocktail (namely IL-1β, TNF-α, GM-CSF) were able to increase the frequency of astrocytic calcium events that also appear to be more desynchronized. In order to obtain more mechanistic cues explaining the observed phenomena, we investigated hemichannels (HCs) dynamics during the induced inflammation. HCs are known to be transmembrane pathways for signalling, allowing the diffusion of small molecules and ions (including $Ca^{2+}$) that can influence cells behaviour. HCs activity can be regulated by proinflammatory cytokines. In astrocytes, Cx43 is the major component of HCs and GJs. Using WB analysis, we observed a reduction in Cx43 protein detection in both CKs and LPS treated slices, which suggests a down regulation of GJs expression and function, in part explaining the glial calcium events desynchronization. To address the role HCs in modulating neuroinflammatory events in our model, we decided to treat cultures with the selective Cx43 inhibitor peptide gap27 that completely abolished glial calcium signalling activity in LPS or CKs treated slices. More interestingly, Cx43 inhibition led to a significant reduction in proinflammatory cytokines

.

secretion (namely IL-1α, IL-1β, TNF-α, IL-6 and CXCL2) and a significant reduction in NF-κB expression in GFAP+ cells, suggesting an important role for HCs in promoting the expression and maturation of proinflammatory mediators.

Since exosomes have a major role in intercellular communication in health and disease we moved to assess their role in mediating neuroinflammatory events in organotypic spinal slices. Classical EVs studies isolate exosomes secreted by cells cultured in culture flasks, collecting large amounts of medium. From this point of view, one of the major challange in isolating exosomes form the organotypic model is the small amount of media (1 mL per slice) that can be collected and thus affect the efficiency of the isolation process. We establish a clean and effective protocol to isolate exosomes from slices conditioned media, based on simple differential ultracentrifugation. This method is commonly associated with the presence of impurity (mainly proteic aggregates) in the isolated sample, nevertheless is considered one of the best choice when isolated exosomes will be used as a treatment because the use of commercial isolation kits is often affected by unwanted reagents residuals that can interfere with vesicles biological activity. In our experiments, exosomes were isolated from control slices and from slices treated with LPS and with bzATP. We chose LPS as inflammatory stimulus, for its agonist action on TLR-4, an innate immunity receptor involved in multiple CNS disorders, and again bzATP as a positive secretion control. Despite the above mentioned concerns about random proteic aggregates contamination, AFM imaging, performed in liquid phase on a functionalized mica surface, showed only the presence of roundish vesicles-like object in our exosomes samples, suggesting the absence of proteic aggregates. Furthermore, western blot analysis detected the typical exosome markers TSG101, FLO1 and the absence of the Golgi apparatus protein GM130, confirming also the absence of cell debris. Interestingly, TSG101 WB bands were thicker than the control one, suggesting an increase in exosomes secretion in treated slices. Once assessed the efficacy of our isolation method, we ask whether inflammatory treats could quantitatively affect exosomes secretion dynamics in organotypic spinal slices. Exosomes samples isolated from control, LPS treated and bzATP treated slices were analysed using Nanoparticle Tracking Analysis to detect quantitative changes. As expected, bzATP treatment increased significantly exosomes secretion when compared to control, further confirming data obtained from cortex glial dissociated cultures. Interestingly, comparable results were obtained after LPS treatments and reflect the thickening in TSG101 bands detected by WB analysis. These findings are consistent with data that showed how the increase in intracellular Ca2+ concentration caused by P2X7 channel opening and TLR-4 activation via IP3 mediated pathway, is associated with the development of multivesicular bodies (MVBs) and increase in EVs release [Lombardi M et al., 2021; Xia L. et al.,

2022]. Exosomes are well-known conveyors of a wide range of molecular messages in health and disease, thus, we hypothesised that the increase in vesicles secretion by LPS treatment may have a functional role in spreading and sustaining inflammation also in the context of spinal microenvironment. To test this hypothesis, we decided to treat naïve slices with exosomes isolated from LPS treated slices (EXOLPS) looking at phenotypic and functional changes in glial cells. Interestingly, confocal images analysis showed that EXOLPS treatments increased Iba1+ cells branching and number (a marker of microglia activation) comparably to LPS treatment, while exosomes isolated from untreated slices (EXOCTR) showed no significant activity, excluding an intrinsic exosomal immunogenicity. In order to assess the impact of exosomes on glial calcium dynamics, we performed live calcium imaging on spinal slices after EXOLPS treatment. The data obtained clearly show that, similarly to LPS, exosomes isolated from an inflammatory microenvironment are able to induce a dysfunctional signalling behaviour in astrocytes, characterized by an increase in calcium events. Furthermore, we also demonstrate that EXOLPS treatment, comparably to LPS, is also increasing the opening of HCs in astrocytes as resulted from Lucifer Yellow permeability assay. This phenomenon may be partly due to cytokines secreted by activated microglia, but we also explored new putative mechanisms. In 2015 Soares and colleagues demonstrated that Cx43 HCs are present at the level of exosomal membrane and that they are essential for cargo transfer to recipient cells [Soares A. et al., 2015]. Thus, we investigated if functional Cx43 HCs are involved inthe transfer of inflammatory signals, contributing in modifying glial cells functions. To address this issue, we incubated EXOLPS with gap27 to selectively and specifically inhibit Cx43 HC in exosomes. Glial live calcium imaging showed that calcium fluctuations in slices treated with EXOLPS pre-treated with gap27 (unbound gap27 was washed out) display nearphysiological features similarly to control samples. This result suggests that Cx43 HCs can modulate astrocytic calcium activity acting at medium-long distance when shuttled by exosomes. If this function is solely based on the formation of a GJs by astrocytic and exosomal Cx43 allowing proinflammatory cargo transfer to the recipient cell [Soares A. et al., 2015] or if exosomes can actively transfer opened and functional Cx43 HCs at the level of astrocytic plasma membrane remains an open question.

# References


1. Abe N., Nishihara T., Yorozuya T. et al. “Microglia and Macrophages in the Pathological Central and Peripheral Nervous Systems.” Cells **9**, 1-21 (2020)
2. Aleph Prieto G. and Cotman G. W. “Cytokines and cytokine networks target neurons to modulate long-term potentiation.” Cytokine Growth Factor Rev. **34**, 27-33 (2017)
3. Alexander J. K. and Popovich P. G. “Neuroinflammation in spinal cord injury: therapeutic targets for neuroprotection and regeneration.” Prog. Brain Res. **175**, 125-137 (2009)
4. Allan S. and Rothwel, N. “Cytokines and acute neurodegeneration.” Nat. Rev. Neurosci. **2**, 734744 (2001)
5. Allen N. J. and Eroglu C. “Cell Biology of Astrocyte-Synapse Interactions.” Neuron **96**, 697-708 (2017)
6. Almad A., Maragakis N. J. “A stocked toolbox for understanding the role of astrocytes in disease.” Nat. Rev. Neurol. **14**, 351-362 (2018)
7. Amarante-Mendes G. P., Adjemian S., Migliari Branco L. et al. “Pattern Recognition Receptors and the Host Cell Death Molecular Machinery.” Front. Immunol. **9**, 1-19 (2018)
8. Anderson K. V., Jurgens G. and Nüsslein-Volhard C., “Establishment of dorso-ventral polarity in the Drosophila embryo: genetic studies on the role of the Toll gene product.” Cell **42**, 779-789 (1985)
9. Antel J. P., Becher B., Ludwin S. K. et al. “Glial Cells as Regulators of Neuroimmune Interactions in the Central Nervous System.” J. Immunol. **204**, 251-255 (2020)
10. Appel S. H., Zhao W., Beers D. R., et al. “The Microglial-Motorneuron dialogue in ALS.” Acta Myol. **30**, 4-8 (2011)
11. Ashley N. T., Weil Z. M. and Nelson R. J. “Inflammation: Mechanisms, Costs, and Natural Variation.” Annu. Rev. Ecol. Evol. Syst. **43**, 385-406 (2012)
12. Aspelund A., Antila S., Proulx S. T. et al. “A dural lymphatic vascular system that drains brain interstitial fluid and macromolecules.” J. Exp. Med. **212**, 991–999 (2015)
13. Avossa D., Rosato-Siri M. D., Mazzarol F. et al. “Spinal circuits formation: a study of developmentally regulated markers in organotypic cultures of embryonic mouse spinal cord.” Neuroscience **122**, 391-405 (2003)
14. Ban J., Sámano C., Mladinic M. et al. “Glia in amyotrophic lateral sclerosis and spinal cord injury: common therapeutic targets.” Croat. Med. J. 60, 109-120 (2019)

15. Bahram Sangani N., Gomes A. R., Curfs L. M. G. et al. “The role of Extracellular Vesicles during CNS development.” Prog. Neurobiol. **205**, 102124 (2021)

16. Ballerini L., Galante M., Grandolfo M. et al. “Generation of rhythmic patterns of activity by ventral interneurones in rat organotypic spinal slice culture.” J. Physiol. **517** (Pt 2) 459-475 (1999)

17. Baptiste D. C. and Fehlings M. G. “Emerging drugs for spinal cord injury.” Expert Opin. Emerg.

Drugs **13**, 63-80 (2008)

18. Becher, B., Spath, S. & Goverman, J. “Cytokine networks in neuroinflammation.” Nat. Rev. Immunol. **17**, 49–59 (2017)

19. Benarroch E. E. “Oligodendrocytes: susceptibility to injury and involvement in neurologic disease.” Neurology **72**, 1779-1785 (2009)

20. Berghoff S. A., Spieth L., Sun T. et al. “Microglia facilitate repair of demyelinated lesions via post-squalene sterol synthesis.” Nat. Neurosci. **24**, 47–60 (2021)

21. Bernaus A., Blanco S. and Sevilla A. “Glia Crosstalk in Neuroinflammatory Diseases.” Front. Cell. Neurosci. **14**, 1-17 (2020)

22. Bianco F., Pravettoni E., Colombo A. et al. “Astrocyte-derived ATP induces vesicle shedding and IL-1 beta release from microglia.” J. Immunol. **174**, 7268–7277 (2005)

23. Bjornevik K., Cortese M., Healy B. C. et al. “Longitudinal analysis reveals high prevalence of Epstein-Barr virus associated with multiple sclerosis.” Science **375**, 296-301 (2022)

24. Bodnar C. N., Morganti J. M. and Bachstetter A. D. “Depression following a traumatic brain injury: uncovering cytokine dysregulation as a pathogenic mechanism.” Neural Regen. Res. **13**,

1693-1704 (2018)

25. Bradl M. and Lassmann H. “Oligodendrocytes: biology and pathology.” Acta Neuropathol. **119**, 37-53 (2010)

26. Brennan K., Martin K., FitzGerald, S. P. et al. “A comparison of methods for the isolation and separation of extracellular vesicles from protein and lipid particles in human serum.” Sci. Rep. **10**, 1039 (2020)

27. Bsibsi M., Ravid R., Gveric D et al. “Broad expression of Toll-like receptors in the human central nervous system.” J. Neuropathol. Exp. Neurol. **61**, 1013-1021 (2002)

28. Burnstock G. “Purinergic receptors.” J. Theor. Biol. **62**, 491-503 (1976)

29. Burnstock G. “P2X ion channel receptors and inflammation.” Purinergic Signal. **12**, 59-67 (2016)

30. Burnstock G. “Purine and purinergic receptors.” Brain Neurosci. Adv. **2**, 1-10 (2018)
31. Butovsky O., Jedrychowski M., Moore C. et al. “Identification of a unique TGF-β–dependent molecular and functional signature in microglia.” Nat. Neurosci. **17**, 131-143 (2014)
32. Calvo-Rodriguez M., García-Rodríguez C., Villalobos C. et al. “Role of Toll Like Receptor 4 in Alzheimer’s Disease.” Front. Immunol. **11**, 1-6 (2020)
33. Campolo M., Paterniti I., Siracusa R. et al. “TLR4 absence reduces neuroinflammation and inflammasome activation in Parkinson's diseases in vivo model.” Brain Behav. Immun. **76**, 236247 (2019)
34. Carpentier P. A. and Palmer T. D. “Immune influence on adult neural stem cell regulation and function.” Neuron **64**, 79-92 (2009)
35. Carson M. J., Doose J. M, Melchior B. et al. “CNS immune privilege: hiding in plain sight.” Immunol. Rev. **213**, 48–65 (2006)
36. Casula M., Iyer A. M., Spliet W. G. M et al. “Toll-like receptor signaling in amyotrophic lateral sclerosis spinal cord tissue.” Neuroscience **179**, 233-243 (2011)
37. Chai M. and Kohyama J. “Non-Cell-Autonomous Neurotoxicity in Parkinson’s Disease Mediated by Astroglial α-Synuclein.” Stem Cell Reports **12**, 183–185 (2019)
38. Chamberlain K. A., Huang N., Xie Y. et al. “Oligodendrocytes enhance axonal energy metabolism by deacetylation of mitochondrial proteins through transcellular delivery of SIRT2.” Neuron **109**, 3456-3472 (2021)
39. Chavan S. S., Pavlov V.A. and Tracey K. J. “Mechanisms and Therapeutic Relevance of Neuroimmune Communication.” Immunity **46**, 927-942 (2017)
40. Chettimada S., Lorenz D. R., Misra V. et al. “Exosome markers associated with immune activation and oxidative stress in HIV patients on antiretroviral therapy.” Sci. Rep. **8**, 7227 (2018)
41. Chivet M., Javalet C., Hemming F. et al. “Exosomes as a novel way of interneuronal communication.” Biochem. Soc. Trans. **41**, 241-244 (2013)
42. Chivet M., Javalet C., Laulagnier K. et al. “Exosomes secreted by cortical neurons upon glutamatergic synapse activation specifically interact with neurons.” J. Extracell. Vesicles **3**, 24722 (2014)
43. Choi S. S., Lee H. J., Lim I. et al. “Human astrocytes: secretome profiles of cytokines and chemokines.” PLoS One **9**, 1-7 (2014)
44. Cornell-Bell A. H, Finkbeiner S. M., Cooper M. S. et al. “Glutamate induces calcium waves in cultured astrocytes: long-range glial signaling.” Science **247**, 470-473 (1990)

45. Côté M. P., Murray L. M. and Knikou M. “Spinal Control of Locomotion: Individual Neurons, Their Circuits and Functions.” Front. Physiol. **9**, 1-27 (2018)

46. Crotti A. and Glass C. K. “The choreography of neuroinflammation in Huntington’s disease.” Trends Immunol. **36**, 364–373 (2015)

47. Cunha C., Gomes C., Vaz A. R. et al. “Exploring new inflammatory biomarkers and pathways during LPS-induced M1 polarization.” Mediators Inflamm. 6986175 (2016)

48. Cui W., Sun C., Ma Y. et al. “Inhibition of TLR4 Induces M2 Microglial Polarization and Provides Neuroprotection via the NLRP3 Inflammasome in Alzheimer's Disease.” Front. Neurosci. **20**, 1-16 (2020)

49. De Marchi E., Orioli E., Dal Ben D., et al. “P2X7 Receptor as a Therapeutic Target.” Adv. Protein Chem. Struct. Biol. **104**, 39-79 (2016)

50. De Paola M., Mariani A., Bigini P. et al. “Neuroprotective Effects of Toll-Like Receptor 4 Antagonism in Spinal Cord Cultures and in a Mouse Model of Motor Neuron Degeneration.” Mol. Med. **18**, 971–981 (2012)

51. De Paola M., Sestito S. E., Mariani A., Memo C. et al. “Synthetic and natural small molecule TLR4 antagonists inhibit motoneuron death in cultures from ALS mouse model.” Pharmacol. Res. **103**, 180-187 (2016)

52. De Vuyst E., Decrock E., De Bock M., et al. “Connexin Hemichannels and Gap Junction Channels Are Differentially Influenced by Lipopolysaccharide and Basic Fibroblast Growth Factor.” Mol. Biol. Cell. **18**, 34–46 (2007)

53. Deverman B. E. and Patterson P. H. “Cytokines and CNS Development.” Neuron **64**, 61-78 (2009)

54. Dong Y. and Benveniste E. N. “Immune function of astrocytes.” Glia **36**, 180-90 (2001)

55. Doyle L. M. and Wang M. Z. “Overview of Extracellular Vesicles, Their Origin, Composition, Purpose, and Methods for Exosome Isolation and Analysis.” Cells **8**, 1-24 (2019)

56. Dong Y and Benveniste E. N. “Immune function of astrocytes.” Glia **36**, 180-190 (2001)

57. Drake R. L., Vogl A. W. and Mitchell A. W. M. “Gray’s anatomy for students.” Elsevier, 4th ed. (2020)

58. Durkee C. A. and Araque A. “Diversity and Specificity of Astrocyte-neuron Communication.” Neuroscience **396**, 73-78 (2019)

59. EL Andaloussi S., Mäger I., Breakefield X. et al. “Extracellular vesicles: biology and emerging therapeutic opportunities.” Nat. Rev. Drug Discov. **12**, 347–357 (2013)

60. Engelhardt B., Vajkoczy P. and Weller R. “The movers and shapers in immune privilege of the CNS.” Nat. Immunol. **18**, 123–131 (2017)

61. Esposito E., Di Matteo V., Benigno A. et al. “Non-steroidal anti-inflammatory drugs in Parkinson's disease.” Exp. Neurol. **205**, 295-312 (2007)

62. Farina C., Aloisi F. and Meinl E. “Astrocytes are active players in cerebral innate immunity.” Trends Immunol. **28**, 138-145 (2007)

63. Fauré J., Lachenal G., Court M. et al. “Exosomes are released by cultured cortical neurones.” Mol. Cell. Neurosci. **31**, 642-648 (2006)

64. Ferrari D., Chiozzi P., Falzoni S. et al. “Purinergic modulation of IL-1β release from microglial cells stimulated with bacterial endotoxin.” J. Exp. Med. **185**, 579-582 (1997)

65. Ferro A., Auguste Y. S. S. and Cheadle L. “Microglia, Cytokines, and Neural Activity: Unexpected Interactions in Brain Development and Function.” Front. Immunol. **12**, 1 – 14 (2021)

66. Fiebich B. L., Akter S. and Akundi R. S. “The two-hit hypothesis for neuroinflammation: role of exogenous ATP in modulating inflammation in the brain.” Front. Cell. Neurosci. **8**, 1-11 (2014)

67. Fitzner D., Schnaars M., van Rossum D. et al. “Selective transfer of exosomes from oligodendrocytes to microglia by macropinocytosis.” J. Cell Sci. **124**, 447-458 (2011)

68. Fodstad H. “The Neuron Theory.” Stereotact. Funct. Neurosurg. **77**, 20-24 (2001)

69. Franchi L., Eigenbrod T., Muñoz-Planillo R. et al. “The inflammasome: a caspase-1-activation platform that regulates immune responses and disease pathogenesis.” Nat. Immunol. **10**, 241–247 (2009).

70. Freeman L. C. and Ting J. P. “The pathogenic role of the inflammasome in neurodegenerative diseases.” J. Neurochem. **136**, 29-38 (2016)

71. Fröhlich D., Kuo W. P., Frühbeis C. et al. “Multifaceted effects of oligodendroglial exosomes on neurons: impact on neuronal firing rate, signal transduction and gene regulation.” Philos. Trans. R. Soc. Lond. B Biol. Sci. **369**, 20130510 (2014)

72. Frühbeis C., Fröhlich D., Kuo W. P. et al. “Neurotransmitter-triggered transfer of exosomes mediates oligodendrocyte-neuron communication.” PLoS Biol. **11**, e1001604 (2013)

73. Fujii Y., Maekawa S. and Morita M. “Astrocyte calcium waves propagate proximally by gap junction and distally by extracellular diffusion of ATP released from volume-regulated anion channels.” Sci. Rep. **7**, 13115 (2017)

74. Furlan F., Taccola G., Grandolfo M. et al. “ERG conductance expression modulates the excitability of ventral horn GABAergic interneurons that control rhythmic oscillations in the developing mouse spinal cord.” J. Neurosci. 27, 919-928 (2007)

75. Gabrielli M., Battista N., Riganti L. et al. “Active endocannabinoids are secreted on extracellular membrane vesicles.” EMBO Rep. **16**, 213-220 (2015)

76. Gadani S. P., Walsh J. T., Lukens J. R. et al. “Dealing with Danger in the CNS: The Response of the Immune System to Injury.” Neuron **87**, 47-62 (2015)

77. Galazka G., Mycko M. P., Selmaj I. et al. “Multiple sclerosis: Serum-derived exosomes express myelin proteins.” Mult. Scler. **24**, 449-458 (2018)

78. Galea, I. “The blood–brain barrier in systemic infection and inflammation.” Cell. Mol. Immunol. **18**, 2489–2501 (2021)

79. Gao W., Xiong Y., Li Q. et al. “Inhibition of Toll-Like Receptor Signaling as a Promising Therapy for Inflammatory Diseases: A Journey from Molecular to Nano Therapeutics.” Front. Physiol. **8**, 1-20 (2017)

80. Garcia-Bonilla L., Benakis C., Moore J. et al. “Immune mechanisms in cerebral ischemic tolerance.” Front. Neurosci. **8**, 1-19 (2014)

81. Gautreau A., Oguievetskaia K. and Ungermann C. “Function and Regulation of the Endosomal

Fusion and Fission Machineries.” Cold Spring Harb. Perspect. Biol. **6**, 1-16 (2014)

82. Giacco V., Panattoni G., Medelin M. et al. “Cytokine inflammatory threat, but not LPS one, shortens GABAergic synaptic currents in the mouse spinal cord organotypic cultures.” J. Neuroinflamm. **16**, 127 (2019)

83. Gilhus, N. E., and Deuschl, G. “Neuroinflammation - a common thread in neurological disorders.” Nat. Rev. Neurol. **15**, 429–430 (2019)

84. Ginhoux F., Greter M., Leboeuf M. et al. “Fate mapping analysis reveals that adult microglia derive from primitive macrophages.” Science **330**, 841–845 (2010)

85. Glass C. K., Saijo K., Winner B., et al. “Mechanisms underlying inflammation in neurodegeneration.” Cell **140**, 918–934 (2010)

86. Glebov K., Löchner M., Jabs R. et al. “Serotonin stimulates secretion of exosomes from microglia cells.” Glia **63**, 626-634 (2015)

87. Goetzl E. J., Mustapic M., Kapogiannis D. et al. “Cargo proteins of plasma astrocyte-derived exosomes in Alzheimer's disease.” FASEB J. **30**, 3853-3859 (2016)

88. Grad L. I., Yerbury J. J., Turner B. J. et al. “Intercellular propagated misfolding of wild-type Cu/Zn superoxide dismutase occurs via exosome-dependent and -independent mechanisms.” Proc. Natl. Acad. Sci. U S A. **111**, 3620-3625 (2014)

89. Guertin P. A. “Central pattern generator for locomotion: anatomical, physiological, and pathophysiological considerations.” Front. Neurol. **3**, 1-15 (2013)

90. Guo S., Wang H. and Yin Y. “Microglia Polarization From M1 to M2 in Neurodegenerative Diseases.” Front. Aging Neurosci. **14**, 1-8 (2022)

91. Gupta, A., Pulliam, L. Exosomes as mediators of neuroinflammation. J Neuroinflammation **11**, 68 (2014)

92. Gurunathan S., Kang M. H., Jeyaraj M. et al. “Review of the Isolation, Characterization, Biological Function, and Multifarious Therapeutic Approaches of Exosomes.” Cells. **307**, 1-36 (2019)

93. Gurung S., Perocheau D., Touramanidou L. et al. “The exosome journey: from biogenesis to uptake and intracellular signalling.” Cell Commun. Signal. **19**, 47 (2021)

94. Harding C. V., Heuser J. E. and Stahl P. D. “Receptor-mediated endocytosis of transferrin and recycling of the transferrin receptor in rat reticulocytes.” J. Cell Biol. **97**, 329–339 (1983)

95. Harding C. V., Heuser J. E. and Stahl P. D. “Exosomes: Looking back three decades and into the future.” J. Cell Biol. **200**, 367–371 (2013)

96. He J., Ren W., Wang W. et al. “Exosomal targeting and its potential clinical application.” Drug Deliv. and Transl. Res. (2021)

97. Heneka M. T., Kummer M. and Latz E. “Innate immune activation in neurodegenerative disease.” Nat. Rev. Immunol. **14**, 463–477 (2014)

98. Heneka M. T., McManus R. M. and Latz E. “Inflammasome signalling in brain function and neurodegenerative disease.” Nat. Rev. Neurosci. **19**, 610–621 (2018)

99. Hessvik N. P. and Llorente A. “Current knowledge on exosome biogenesis and release.” Cell. Mol. Life Sci. **75**, 193-208 (2018)

100. Hof P. R., Kidd G., DeFelipe J. et al. “Cellular Components of Nervous Tissue.” cap. 1, pp. 3-21, in Byrne J. H., Heidelberger R. and Waxham M. N. “From Molecules to Networks. An Introduction to Cellular and Molecular Neuroscience” 3rd ed., Academic Press (2014)

101. Hoshino A., Costa-Silva B., Shen T. L. et al. “Tumour exosome integrins determine organotropic metastasis.” Nature **527**, 329-335 (2015)

102. Howard R., Zubko O., Bradley R. et al. “Minocycline in Alzheimer Disease Efficacy (MADE) Trialist Group. Minocycline at 2 Different Dosages vs Placebo for Patients With Mild Alzheimer
Disease: A Randomized Clinical Trial.” JAMA Neurol. **77**, 164-174 (2020)

103. Hristovska I. and Pascual O. “Deciphering Resting Microglial Morphology and Process Motility from a Synaptic Prospect.” Front. Integr. Neurosci. **9**, 1-12 (2016)

104. Hughes C., Choi M. L., Yi J. H. et al. “Beta amyloid aggregates induce sensitised TLR4 signalling causing long-term potentiation deficit and rat neuronal cell death.” Commun. Biol. **3**, 1-7 (2020)

105. Huo L., Du X., Li X. et al. “The Emerging Role of Neural Cell-Derived Exosomes in Intercellular Communication in Health and Neurodegenerative Diseases.” Front. Neurosci. **15**, 738442 (2021)

106. Iguchi Y., Eid L., Parent M. et al. “Exosome secretion is a key pathway for clearance of pathological TDP-43.” Brain **139**, 3187-3201 (2016)

107. Ilieva H., Polymenidou M., Cleveland D. W. “Non-cell autonomous toxicity in neurodegenerative disorders: ALS and beyond.” J. Cell Biol. **187**, 761-772 (2009)

108. Jäkel S. and Dimou L. “Glial Cells and Their Function in the Adult Brain: A Journey through the History of Their Ablation.” Front. Cell. Neurosci. **11**, 1-17 (2017)

109. James S. L., Theadom A., Ellenbogen L. G. et al. “Global, regional, and national burden of traumatic brain injury and spinal cord injury, 1990–2016: a systematic analysis for the Global Burden of Disease Study 2016.” Lancet Neurol. **18**, 56-87 (2019)

110. Janeway C. A. Jr. “Approaching the Asymptote? Evolution and Revolution in Immunology.” Cold. Spring. Harb. Symp. Quant. Biol. 54, 1-13 (1989)

111. Jo M., Lee S., Jeon Y. M. et al. “The role of TDP-43 propagation in neurodegenerative diseases: integrating insights from clinical and experimental studies.” Exp. Mol. Med. **52**, 16521662 (2020)

112. Juan T. and Fürthauer M. “Biogenesis and function of ESCRT-dependent extracellular vesicles.” Semin. Cell Dev. Biol. **74**, 66-77 (2018)

113. Kaebisch C., Schipper D., Babczyk P. et al., “The role of purinergic receptors in stem cell differentiation.” Comput. Struct. Biotechnol. J. **13**, 75-84 (2015)

114. Kalluri R. and Lebleu V. S. “The biology, function, and biomedical applications of exosomes.” Science **367**, 1-24 (2020)

115. Kettenmann H., Verkhratsky A. “Neuroglia: the 150 years after.” Trends Neurosci. **31**, 653659 (2008)

116. Kiehn, O. “Decoding the organization of spinal circuits that control locomotion.” Nat. Rev. Neurosci. **17**, 224-238 (2016)

117. Kielian T. “Glial connexins and gap junctions in CNS inflammation and disease.” J. Neuorchem. **106**, 1000-1016 (2008)

118. Kigerl K. A., de Rivero Vaccari J. P., Dietrich W. D. et al. “Pattern recognition receptors and central nervous system repair.” Exp. Neurol. **258**, 5–16 (2014)

119. Kigerl K. A., Lai W., Rivest S. et a. “Toll-like receptor (TLR)-2 and TLR-4 regulate inflammation, gliosis, and myelin sparing after spinal cord injury.” J. Neurochem. **102**, 37-50 (2007)

120. Kim C., Yousefian-Jazi A., Choi S. “Non-Cell Autonomous and Epigenetic Mechanisms of Huntington’s Disease.” Int. J. Mol. Sci. **22**, 1-25 (2021)

121. Kölliker-Frers R., Udovin L., Otero-Losada M. et al. “Neuroinflammation: An Integrating Overview of Reactive-Neuroimmune Cell Interactions in Health and Disease.” Mediators Inflamm. **2021**, 1-20 (2021)

122. Korkut C., Li Y., Koles K. et al. “Regulation of postsynaptic retrograde signaling by presynaptic exosome release.” Neuron **77**, 1039-1046 (2013)

123. Krämer-Albers E. M. “Extracellular vesicles in the oligodendrocyte microenvironment.” Neurosci. Lett. **725**, 134915 (2020)

124. Krämer-Albers E. M., Bretz N., Tenzer S. et al. “Oligodendrocytes secrete exosomes containing major myelin and stress-protective proteins: trophic support for axons?” Proteomics Clin. Appl. **1**, 1446–1461 (2007)

125. Kronschläger M. T., Siegert A. S. M., Resch F. J. et al. “Lamina-specific properties of spinal astrocytes.” Glia **69**, 1749-1766 (2021)

126. Lachenal G., Pernet-Gallay K., Chivet M. et al. “Release of exosomes from differentiated neurons and its regulation by synaptic glutamatergic activity.” Mol. Cell. Neurosci. **46**, 409-418 (2011)

127. Lai H. C., Seal R. P. and Johnson J. E. “Making sense out of spinal cord somatosensory development.” Development. **143**, 3434-3448 (2016)

128. Le Gall L., Anakor E., Connolly O. et al. “Molecular and Cellular Mechanisms Affected in ALS.” J. Pers. Med. **10**, 101 (2020)

129. Le Pichon C. E. and Chesler A. T. “The functional and anatomical dissection of somatosensory subpopulations using mouse genetics.” Front. Neuroanat. **8**, 1-18 (2014)

130. Lee S. J. “Toll-like Receptors and Neuroinflammation”, cap. 9, pp. 135-156, in Suzumara A., Ikenaka K. (eds) “Neuron-Glia Interaction in Neuroinflammation”, Advances in Neurobiology vol. 7, Springer (2013)

131. Lee J. Y., Lee J. D., Phipps S. et al. “Absence of toll-like receptor 4 (TLR4) extends survival in the hSOD1G93A mouse model of amyotrophic lateral sclerosis.” J. Neuroinflammation **12**, 18 (2015)

132. Lehnardt S., Lachance C., Patrizi S., et al. “The Toll-Like Receptor TLR4 Is Necessary for Lipopolysaccharide-Induced Oligodendrocyte Injury in the CNS.” J. Neurosci. **22**, 2478-2486 (2002)

133. Lenhardt S., Massillon L., Follet P., et al. “Activation of innate immunity in the CNS triggers neurodegeneration through a Toll-like receptor 4-dependent pathway.” Proc. Natl. Acad. Sci. USA **100**, 8514-8519 (2003)

134. Lemaitre, B., Nicolas, E., Michaut, L. et al. “The dorsoventral regulatory gene cassette spätzle/Toll/cactus controls the potent antifungal response in Drosophila adults.” Cell **86**, 973– 983 (1996)

135. Leow-Dyke S., Allen C., Denes A. et al. “Neuronal toll-like receptor 4 signaling induces brain endothelial activation and neutrophil transmigration in vitro.” J. Neuroinflamm. **9**, 230 (2012)

136. Leung B. and Shimeld S. M. “Evolution of vertebrate spinal cord patterning.” Dev. Dyn. **248**, 1028–1043 (2019)

137. Liddelow S. A., Guttenplan K. A., Clarke L. E. et al. “Neurotoxic reactive astrocytes are induced by activated microglia.” Nature **541**, 481-487 (2017)

138. Liu H., Leak R. K. and Hu X. “Neurotransmitter receptors on microglia.” Stroke Vasc, Neurol. **1**, 52-58 (2016)

139. Liu J. and Wang F. “Role of Neuroinflammation in Amyotrophic Lateral Sclerosis: Cellular Mechanisms and Therapeutic Implications.” Front. immunol. **8**, 1005 (2017)

140. Liu W., Bai X., Zhang A. et al. “Role of Exosomes in Central Nervous System Diseases.” Front. Mol. Neurosci. **12**, 240 (2019)

141. Lobsiger C. and Cleveland D. “Glial cells as intrinsic components of non-cell-autonomous neurodegenerative disease.” Nat. Neurosci. **10**, 1355–1360 (2007)

142. Lombardi M., Gabrielli M., Adinolfi E. et al. “Role of ATP in Extracellular Vesicle Biogenesis and Dynamics.” Front. Pharmacol. 12, 654023 (2021)

143. Lopez-Castejon G., Brough D. “Understanding the mechanism of IL-1β secretion.” Cytokine Growth Factor Rev. **22**, 189-195 (2011)

144. Louveau A., Harris T. H. and Kipnis J. “Revisiting the concept of CNS immune privilege.” Trends Immunol. **36**, 569–577 (2015)

145. Louveau A., Herz J., Alme M.N. et al. “CNS lymphatic drainage and neuroinflammation are regulated by meningeal lymphatic vasculature.” Nat. Neurosci **21**, 1380–1391 (2018)

146. Louveau A., Smirnov I., Keyes T. et al. “Structural and functional features of central nervous system lymphatic vessels.” Nature **523**, 337–341 (2015)

147. Lu D. C., Niu T. and Alaynick W. A. “Molecular and cellular development of spinal cord locomotor circuitry.” Front. Mol. Neurosci. **8**, 1-18 (2015)

148. Luong N. and Olson J. K. “Exosomes Secreted by Microglia During Virus Infection in the Central Nervous System Activate an Inflammatory Response in Bystander Cells.” Front. Cell Dev. Biol. **9**, 661935 (2021)

149. Martins-Macedo J., Lepore A. C., Domingues H. S. et al. “Glial restricted precursor cells in central nervous system disorders: Current applications and future perspectives.” Glia **69**, 513-531 (2021)

150. McCoy M. K., Tansey M. G. “TNF signaling inhibition in the CNS: implications for normal brain function and neurodegenerative disease.” J. Neuroinflamm. **5**, 45 (2008)

151. Medawar P. B. “Immunity to homologous grafted skin; the fate of skin homografts transplanted to the brain, to subcutaneous tissue, and to the anterior chamber of the eye.” Br. J. Exp. Pathol. **29**, 58-69 (1948)

152. Medelin M., Rancic V., Cellot G. et al. “Altered development in GABA co-release shapes glycinergic synaptic currents in cultured spinal slices of the SOD1(G93A) mouse model of amyotrophic lateral sclerosis.” J. Physiol. 594, 3827-3840 (2016)

153. Medzhitov R., Preston-Hurlburt P. and Janeway C. A. Jr. “A human homologue of the Drosophila Toll protein signals activation of adaptive immunity.” Nature **388**, 394–397 (1997)

154. Miller L. G., Galpern W. R., Dunlap K. et al. “Interleukin-1 augments gamma-aminobutyric acid A receptor function in brain.” Mol. Pharmacol. **39**, 105-108 (1991)

155. Miller R. H. “Glial development and axon regeneration.” In “Textbook of Neural Repair and Rehabilitation”, pp. 367-375, Cambridge University Press (2014)

156. Miras-Portugal M. T., Sebastián-Serrano Á., de Diego García L. et al. “Neuronal P2X7 Receptor: Involvement in Neuronal Physiology and Pathology.” J. Neurosci. **37**, 7063-7072 (2017)

157. Mittelbrunn M. and Sánchez-Madrid F. “Intercellular communication: diverse structures for exchange of genetic information.” Nat. Rev. Mol. Cell. Biol. **13**, 328–335 (2012)

158. Mittelbrunn M., Vicente Manzanares M. and Sánchez-Madrid F. “Organizing polarized delivery of exosomes at synapses.” Traffic. **16**, 327-337 (2015)

159. Mizuno T. “Factors from intact and damaged neurons”, cap. 3, pp. 49-62, in Suzumara A., Ikenaka K. (eds) “Neuron-Glia Interaction in Neuroinflammation”, Advances in Neurobiology vol. 7, Springer (2013)

160. Mogensen T. H. “Pathogen Recognition and Inflammatory Signaling in Innate Immune Defenses.” Clin. Microbiol. Rev. **22**, 240–273 (2009)

161. Moresco, E. M., LaVine, D., and Beutler, B. “Toll-like receptors.” Curr. Biol. **21**, 488–493 (2011)

162. Mundt S., Greter M., Flügel A. et al. “The CNS Immune Landscape from the Viewpoint of a T Cell.” Trends Neurosci. **42**, 667-679 (2019)

163. Murphy J. B., Sturm E. “Conditions determining the transplantability of tissues in the brain.” J. Exp. Med. **38**, 183-197 (1923)

164. Najjar S., Pearlman D. M., Alper K. et al. “Neuroinflammation and psychiatric illness.” J. Neuroinflam. **10**, 1-24 (2013)

165. Nie L., Cai S. Y., Shao J. Z. et al. “Toll-Like Receptors, Associated Biological Roles, and Signaling Networks in Non-Mammals.” Front. Immunol. **9**, 1-19 (2018)

166. Nabekura J., Katsurabayashi S., Kakazu Y. et al. “Developmental switch from GABA to glycine release in single central synaptic terminals.” Nat. Neurosci. **7**, 17–23 (2004)

167. Nishida K., Nakatani T., Ohishi A. et al. “Mitochondrial dysfunction is involved in P2X7 receptor-mediated neuronal cell death.” J. Neurochem. **122**, 1118-1128 (2012)

168. Nógrádi A. and Vrbová G. “Anatomy and Physiology of the Spinal Cord.” In: Madame Curie Bioscience Database (2000-2013)

169. North R. A. “P2X receptors.” Philos. Trans. R. Soc. Lond. B Biol. Sci. **371**, 1-7 (2016)

170. Ogaki A., Ikegaya Y. and Koyama R. “Extracellular Vesicles Taken up by Astrocytes.” Int. J. Mol. Sci. **22**, 10553 (2021)

171. Ohashi K., Burkart V., Flohé S. et al. “Cutting edge: heat shock protein 60 is a putative endogenous ligand of the toll-like receptor-4 complex.” J. Immunol. **164**, 558-561 (2000)

172. Okun E., Griffioen K. J. and Mattson M. P. “Toll-like receptor signaling in neural plasticity and disease.” Trends Neurosci. **34**, 269-281 (2011)

173. Orr M. B. and Gensel J. C. “Spinal Cord Injury Scarring and Inflammation: Therapies Targeting Glial and Inflammatory Responses.” Neurotherapeutics **3**, 541-553 (2018)

174. Pan B. T. and Johnstone R. M. “Fate of the transferrin receptor during maturation of sheep reticulocytes in vitro: selective externalization of the receptor.” Cell **33**, 967–978 (1983)

175. Panaro M. A., Lofrumento D. D., Saponaro C. et al. “Expression of TLR4 and CD14 in the Central Nervous System (CNS) in a MPTP Mouse Model of Parkinson's-Like Disease.” Immunopharmacol. Immunotoxicol. **30**, 729-740 (2008)

176. Panattoni G., Amoriello R., Memo C. et al. “Diverse inflammatory threats modulate astrocytes Ca2+ signaling via connexin43 hemichannels in organotypic spinal slices.” Mol. Brain **14**, 159 (2021)

177. Pandamooz S., Nabiuni M., Miyan J. et al. “Organotypic Spinal Cord Culture: a Proper Platform for the Functional Screening.” Mol. Neurobiol. **53**, 4659-4674 (2016)

178. Papaneophytou C., Georgiou E. and Kleopa K. A. “The role of oligodendrocyte gap junctions in neuroinflammation.” Channels **13**, 247-263 (2019)

179. Park E. J., Prajuabjinda O., Soe, Z. Y. et al. “Exosomal regulation of lymphocyte homing to the gut.” Blood adv. **3**, 1-11 (2019)

180. Pascual M., Ibáñez F. and Guerri C. “Exosomes as mediators of neuron-glia communication in neuroinflammation.” Neural Regen. Res. **15**, 796-801 (2020)

181. Patel G. K., Khan M. A., Zubair H. et al. “Comparative analysis of exosome isolation methods using culture supernatant for optimum yield, purity and downstream applications.” Sci. Rep. **9**, 5335 (2019)

182. Patel M. R. and Weaver A. M. “Astrocyte-derived small extracellular vesicles promote synapse formation via fibulin-2-mediated TGF-β signaling.” Cell Rep. **34**, 108829 (2021)

183. Piccinini A. M. and Midwood K. S. “DAMPening Inflammation by Modulating TLR Signalling.” Mediators Inflamm. **10**, 1-21 (2010)

184. Piper R. C. and Katzmann D. J. “Biogenesis and function of multivesicular bodies.” Annu. Rev. Cell. Dev. Biol. **23**, 519-547 (2007)

185. Poltorak A., He X., Liu M. Y., et al. “Defective LPS signaling in C3H/HeJ and C57BL/10ScCr mice: mutation in Tlr4 gene.” Science **282**, 2085-2088 (1998)

186. Potolicchio I., Carven G. J., Xu X. et al. “Proteomic analysis of microglia-derived exosomes: metabolic role of the aminopeptidase CD13 in neuropeptide catabolism.” J. Immunol. **175**, 22372243 (2005)

187. Prada I. and Meldolesi J. “Binding and Fusion of Extracellular Vesicles to the Plasma Membrane of Their Cell Targets.” Int. J. Mol. Sci. **17**, 1296 (2016)

188. Prinz M., Priller J. “The role of peripheral immune cells in the CNS in steady state and disease.” Nat. Neurosci. **20**, 136–144 (2017)

189. Probert L. “TNF and its receptors in the CNS: The essential, the desirable and the deleterious effects.” Neuroscience **302**, 2-22 (2015)

190. Probert L., Akassoglou K., Kassiotis G. et al. “TNF-alpha transgenic and knockout models of CNS inflammation and degeneration.” J. Neuroimmunol. **72**,137-141 (1997)

191. Proell M., Riedl S. J., Fritz J. H. et al. “The Nod-Like Receptor (NLR) Family: A Tale of Similarities and Differences.” PLoS One **3**, 1-11 (2008)

192. Quincozes-Santos A., Santos C. L., de Souza Almeida R. R. et al. “Gliotoxicity and Glioprotection: the Dual Role of Glial Cells.” Mol. neurobiol. **58**, 6577–6592 (2021)

193. Ramesh G., MacLean A. G. and Philipp M. T. “Cytokines and Chemokines at the Crossroads of Neuroinflammation, Neurodegeneration, and Neuropathic Pain.” Mediators Inflamm. **2013**, 120 (2013)

194. Ranshoff R. M. “How neuroinflammation contributes to neurodegeneration.” Science **353**, 777-783 (2016)

195. Rao M. S., Noble M., Mayer-Pröschel M. et al. “A tripotential glial precursor cell is present in the developing spinal cord.” Proc. Natl. Acad. Sci. USA **95**, 3996-4001 (1998)

196. Raposo G., Nijman H. W., Stoorvogel W. et al. “B lymphocytes secrete antigen-presenting vesicles.” J. Exp. Med. **183**, 1161-1172 (1996)

197. Raposo G. and Stoorvogel W. “Extracellular vesicles: Exosomes, microvesicles, and friends.” J. Cell Biol. **200**, 373–383 (2013)

198. Ratsimandresey R. A., Rappaport J.and Zagury J.-F. “Anti-Cytokine Therapeutics: History and Update.” Curr. Pharm. Des. **15**, 1998 – 2025 (2009)

199. Retamal M. A., Froger N., Palacios-Prado N. et al. “Cx43 hemichannels and gap junction channels in astrocytes are regulated oppositely by proinflammatory cytokines released from activated microglia.” J. Neurosci. **27**, 13781–13792 (2007)

200. Rezaie P., Patel K. and Male D. K. “Microglia in the human fetal spinal cord patterns of distribution, morphology and phenotype.” Brain Res. Dev. Brain Res. **8**, 71-81 (1999)

201. Ribeiro Alvares Batista C., Freitas Gomes G., Candelario-Jalil E.et al. "LipopolysaccharideInduced Neuroinflammation as a Bridge to Understand Neurodegeneration.” Int. J. Mol. Sci. **20**, 1-31 (2019)

202. Rigato C., Buckinx R., Le-Corronc H. et al. “Pattern of invasion of the embryonic mouse spinal cord by microglial cells at the time of the onset of functional neuronal networks.” Glia **59**, 675-695 (2011)

203. Rodrigues R. J., Tomé A. R. and Cunha R. A. “ATP as a multi-target danger signal in the brain.” Front. Neurosci. **9**, 1-11 (2015)

204. Rolls A., Shechter R., London A. et al. “Toll-like receptors modulate adult hippocampal neurogenesis.” Nat. Cell Biol. **9**, 1081–1088 (2007)

205. Romanelli P., Bieler L., Heimel P. et al. “Enhancing Functional Recovery Through Intralesional Application of Extracellular Vesicles in a Rat Model of Traumatic Spinal Cord Injury.” Front. Cell Neurosci. **15**, 795008 (2022)

206. Rothwell N. I., Luheshi G., and Toulmond S. “Cytokines and Their Receptors in the Central Nervous System: Physiology, Pharmacology, and Pathology.” Pharmacol. Ther. **69**, 85-95 (1996)

207. Rowald A., Komi S., Demesmaeker R. et al. “Activity-dependent spinal cord neuromodulation rapidly restores trunk and leg motor functions after complete paralysis.” Nat. Med. **28**, 260-271 (2022)

208. Sankowski R., Mader S. and Valdés-Ferrer S. I. “Systemic inflammation and the brain: novel roles of genetic, molecular, and environmental cues as drivers of neurodegeneration.” Front. Cell. Neurosci. **9**, 1-20 (2015)

209. Savina A., Fader C. M., Damiani M. T. et al. “Rab11 promotes docking and fusion of multivesicular bodies in a calcium-dependent manner.” Traffic **6**, 131-143 (2005)

210. Scemes E., Suadicani S. I. and Spray D. C. “Intercellular Communication in Spinal Cord Astrocytes: Fine Tuning between Gap Junctions and P2 Nucleotide Receptors in Calcium Wave Propagation.” J. Neurosci. **20**, 1435-1445 (2000)

211. Schaefer L. “Complexity of Danger: The Diverse Nature of Damage-associated Molecular Patterns.” J. Biol. Chem. **289**, 35237–35245 (2014)

212. Schiess M. “Nonsteroidal Anti-inflammatory Drugs Protect Against Parkinson Neurodegeneration.” Arch. Neurol. **60**, 1043-1044 (2003)

213. Sibilla S. and Ballerini L. “GABAergic and glycinergic interneuron expression during spinal cord development: dynamic interplay between inhibition and excitation in the control of ventral network outputs.” Prog. Neurobiol. **89**, 46-60 (2009)

214. Sidhom K., Obi P. O., Saleem A. “A Review of Exosomal Isolation Methods: Is Size Exclusion Chromatography the Best Option?” Int. J. Mol. Sci. **21**, 6466 (2020)

215. Shechter R., London A. and Schwartz M. “Orchestrated leukocyte recruitment to immuneprivileged sites: absolute barriers versus educational gates.” Nat. Rev. Immunol. **13**, 206–218

(2013)

216. Shirai Y. “Transplantation of the rat sarcoma in adult heterogenous animals.” Japan Med. World. **1**, 14–15 (1921)

217. Sobo-Vujanovic A., Munich S. and Vujanovic N. L. “Dendritic-cell exosomes cross-present Toll-like receptor-ligands and activate bystander dendritic cells.” Cell. Immunol. **289**, 119–127 (2014)

218. Sofroniew M. V. “Astrogliosis.” Cold Spring Harb. Perspect. Biol. **7**, 1-16 (2014)

219. Somjen G. G. “Nervenkitt: Notes on the History of the Concept of Neuroglia.” Glia **1**, 2-9 (1988)

220. Standring S. “Gray’s Anatomy: The Anatomical Basis of Clinical Practice.” Elsevier 41st ed. (2016)

221. Stifani N. “Motor neurons and the generation of spinal motor neuron diversity.” Front. Cell. Neurosci. **8**, 1-22 (2014)

222. Stoppini L., Buchs P. A. and Muller D. “A simple method for organotypic cultures of nervous tissue.” J. Neurosci. Methods **37**, 173-182 (1991)

223. Szelenyi J. “Cytokines and the central nervous system.” Brain Res. Bull. **54**, 329–338 (2001)

224. Tabata H. “Diverse subtypes of astrocytes and their development during corticogenesis.” Front. Neurosci. **9**, 1-7 (2015)

225. Takeuchi H. and Suzumura A. “Gap junctions and hemichannels composed of connexins: potential therapeutic targets for neurodegenerative diseases.” Front. Cell. Neurosci. **8**, 1-12 (2014)

226. Takeuchi O. and Akira S. “Pattern Recognition Receptors and Inflammation.” Cell **140**, 805–820, (2010)

227. Tauber A. I. “Moving beyond the immune self?.” Semin. Immunol. 12, 241-248 (2000)

228. Théry C., Witwer K. W., Aikawa E. “Minimal information for studies of extracellular vesicles 2018 (MISEV2018): a position statement of the International Society for Extracellular Vesicles and update of the MISEV2014 guidelines.” J. Extracell. Vesicles **7**, 1535750 (2018)

229. Tian Y., Zhu P., Liu S. et al. “IL-4-polarized BV2 microglia cells promote angiogenesis by secreting exosomes.” Adv. Clin. Exp. Med. **28**, 421-430 (2019)

230. Tkach M., Kowal J., Zucchetti A. E. et al. “Qualitative differences in T-cell activation by dendritic cell-derived extracellular vesicle subtypes.” EMBO J. **36**, 3012–3028 (2017)

231. TNF neutralization in MS: results of a randomized, placebo-controlled multicenter study. The Lenercept Multiple Sclerosis Study Group and The University of British Columbia MS/MRI Analysis Group. Neurology. **53**, 457-465 (1999)

232. Tropepe V., Hitoshi S., Sirard C. et al. “Direct Neural Fate Specification from Embryonic Stem Cells: A Primitive Mammalian Neural Stem Cell Stage Acquired through a Default Mechanism.” Neuron **30**, 65-78 (2001)

233. Usmani S., Aurand E. R., Medelin M. et al. “3D meshes of carbon nanotubes guide functional reconnection of segregated spinal explants.” Sci. Adv. 2(7), 1-10 (2016)

234. Van Den Bosch L., Van Damme P., Bogaert E. et al. “The role of excitotoxicity in the pathogenesis of amyotrophic lateral sclerosis.” Biochim. Biophys. Acta **1762**, 1068-1082 (2006)

235. Van Harten A. C. M., Phatnani H. and Przedborski S. “Non-cell-autonomous pathogenic mechanisms in amyotrophic lateral sclerosis.” Trends Neurosci. **44**, 658-668 (2021)

236. van Niel G., D'Angelo G. and Raposo G. “Shedding light on the cell biology of extracellular vesicles.” Nat. Rev. Mol. Cell Biol. 19, 213–228 (2018)

237. Valadi H., Ekström K., Bossios A. et al. “Exosome-mediated transfer of mRNAs and microRNAs is a novel mechanism of genetic exchange between cells.” Nat. Cell Biol. **9,** 654–659 (2007)

238. van Es M. A., Hardiman O., Chio A. et al. “Amyotrophic lateral sclerosis.” Lancet **390**, 20842098 (2017)

239. Venturini A., Passalacqua M., Pelassa S., et al. “Exosomes From Astrocyte Processes: Signaling to Neurons.” Front. Pharmacol. **10**, 1452 (2019)

240. Verkhratsky A., Matteoli M., Parpura V. et al. “Astrocytes as secretory cells of the central nervous system: idiosyncrasies of vesicular secretion.” EMBO J. **35**, 239-257 (2016)

241. Verweij F. J., Bebelman M. P., Jimenez C. R. et al. “Quantifying exosome secretion from single cells reveals a modulatory role for GPCR signaling.” J. cell boil., **217**, 1129-1142 (2018)

242. Vezzani A.and Viviani B. “Neuromodulatory properties of inflammatory cytokines and their impact on neuronal excitability.” Neuropharmacology **96**, 70-82 (2015)

243. Wake H., Moorhouse A. J., Jinno S. et al. “Resting microglia directly monitor the functional state of synapses in vivo and determine the fate of ischemic terminals.” J. Neurosci. **29**, 39743980 (2009)

244. Wang J. and Yu Y. “Insights into the channel gating of P2X receptors from structures, dynamics and small molecules.” Acta Pharmacol. Sin. **37**, 44–55 (2016)

245. Watson C. and Kayalioglu G. “The Organization of the Spinal Cord.” Cap. 1, 1-7 in Watson C., Paxinos G. and Kayalioglu G. “The spinal cord – a Christopher and Dana Reeve Foundation text and atlas.” Elsevier Science Publishing Co. Inc. (2008)

246. Wilbanks B., Maher L. J. 3rd and Rodriguez M. “Glial cells as therapeutic targets in progressive multiple sclerosis.” Expert Rev. Neurother. **19**, 481-494 (2019)

247. Willebrords J., Crespo Yanguas S., Maes M., et al. “Connexins and their channels in inflammation.” Crit. Rev. Biochem. Mol. Biol. **51**, 413-439 (2016)

248. Wolf S. A., Boddeke H. W. and Kettenmann H. “Microglia in Physiology and Disease.” Annu. Rev. Physiol. **79**, 619-643 (2017)

249. Xia L., Wang X., Yao W. et al. “Lipopolysaccharide increases exosomes secretion from endothelial progenitor cells by toll-like receptor 4 dependent mechanism.” Biol. Cell. **114**, 127137 (2022)

250. Yam M. F., Loh Y. C., Tan C. S. et al. “General Pathways of Pain Sensation and the Major Neurotransmitters Involved in Pain Regulation.” Int. J. Mol. Sci. **19**, 1-23 (2018)

251. Yang T., Dai Y., Chen G. et al. “Dissecting the Dual Role of the Glial Scar and Scar-Forming Astrocytes in Spinal Cord Injury.” Front. Cell. Neurosci. **14**, 1-7 (2020)

252. Yang Z. L., Rao J., Lin F. B. et al. “The Role of Exosomes and Exosomal Noncoding RNAs From Different Cell Sources in Spinal Cord Injury.” Front. Cell. Neurosci. **16**, 882306 (2022)

253. Yazawa, I., Giasson B. I., Sasaki R. et al. “Mouse model of multiple system atrophy αsynuclein expression in oligodendrocytes causes glial and neuronal degeneration.” Neuron **45**, 847–859 (2005).

254. Yin X., Feng L., Ma D. et al. “Roles of astrocytic connexin-43, hemichannels, and gap junctions in oxygen-glucose deprivation/reperfusion injury induced neuroinflammation and the possible regulatory mechanisms of salvianolic acid B and carbenoxolone.” J. Neuroinflamm. **15**, 1-24 (2018)

255. Yune T. Y., Chang M. J., Kim S. J. et al. “Increased production of tumor necrosis factor-alpha induces apoptosis after traumatic spinal cord injury in rats.” J. Neurotrauma **20**, 207-219 (2003)

256. Zhang Y. K., Liu J. T., Peng Z. W. et al. “Different TLR4 expression and microglia/macrophage activation induced by hemorrhage in the rat spinal cord after compressive injury.” J. Neuroinflammation **10**, 1-15 (2013)

257. Zhao S., Sheng S., Wang Y. “Astrocyte-derived extracellular vesicles: A double-edged sword in central nervous system disorders.” Neurosci. Biobehav. Rev. **125**, 148-159 (2021)

258. Zhou L., Cao X., Fang J., et al. “Macrophages polarization is mediated by the combination of PRR ligands and distinct inflammatory cytokines.” Int. J. Clin. Exp. Pathol. **8**, 10964-10974 (2015)